

2-9-2022

o-Sulfonamidophenol Ligands and Derivatives for f-Element Sensing, Complexation, and Extraction from Alkaline High-Level Waste

Oluwaseun William Adedoyin
Florida International University, oaded004@fiu.edu

Follow this and additional works at: <https://digitalcommons.fiu.edu/etd>

 Part of the [Inorganic Chemistry Commons](#), and the [Radiochemistry Commons](#)

Recommended Citation

Adedoyin, Oluwaseun William, "o-Sulfonamidophenol Ligands and Derivatives for f-Element Sensing, Complexation, and Extraction from Alkaline High-Level Waste" (2022). *FIU Electronic Theses and Dissertations*. 4998.

<https://digitalcommons.fiu.edu/etd/4998>

This work is brought to you for free and open access by the University Graduate School at FIU Digital Commons. It has been accepted for inclusion in FIU Electronic Theses and Dissertations by an authorized administrator of FIU Digital Commons. For more information, please contact dcc@fiu.edu.

FLORIDA INTERNATIONAL UNIVERSITY

Miami, Florida

o-SULFONAMIDOPHENOL LIGANDS AND DERIVATIVES FOR F-ELEMENT
SENSING, COMPLEXATION, AND EXTRACTION FROM ALKALINE
HIGH-LEVEL WASTE

A dissertation submitted in partial fulfillment of

the requirements for the degree of

DOCTOR OF PHILOSOPHY

in

CHEMISTRY

by

Oluwaseun W. Adedoyin

2022

To: Dean Michael R. Heithaus
College of Arts, Sciences, and Education

This dissertation, written by Oluwaseun W. Adedoyin, and entitled *o*-Sulfonamidophenol Ligands and Derivatives for f-Element Sensing, Complexation, and Extraction from Alkaline High-level Waste, having been approved in respect to style and intellectual content, is referred to you for judgment.

We have read this dissertation and recommend that it be approved.

Joerg Reinhold

Raphael Raptis

Stanislaw Wnuk

Christopher Dares

Konstantinos Kavallieratos, Major Professor

Date of Defense: February 9, 2022

The dissertation of Oluwaseun W. Adedoyin is approved.

Dean Michael R. Heithaus
College of Arts, Sciences, and Education

Andres G. Gil
Vice President for Research and Economic Development
and Dean of the University Graduate School

Florida International University, 2022

© Copyright 2022 by Oluwaseun W. Adedoyin
All rights reserved.

DEDICATION

I dedicate this work to my parents Dr. Abiose Adedoyin and Mrs. Grace Odeyemi for their love support and prayers. To my amazing wife Jane, for being the backbone of my family during my studies and research, and to my children Sewa and Fola, for teaching me how to be a child again.

ACKNOWLEDGMENTS

I am grateful to my supervisor, Dr. Konstantinos Kavallieratos for his guidance and support regarding both academic and non-academic matters. I am also thankful for his encouragement over the years, which has helped me get to this point in my academic pursuit. To my dissertation committee members: Dr. Raphael Raptis, Dr. Stanislaw Wnuk, Dr. Christopher Dares, and Dr. Joerg Reinhold: I appreciate all your constructive criticism which has helped me become a better scientist.

I acknowledge the support my group received through several research contracts (BOA 541, TOAs 0000217393, 0000403071, and 0000525181) to FIU by the US Department of Energy Office of Environmental Management MSIPP program managed by the Savannah River National Laboratory. I also acknowledge the support I received from Florida International University as a Dissertation Year Fellowship (DYF for Summer and Fall 2021).

Special thanks go to Mrs. Magali Autie for her help in administrative matters, Dr. Indranil Chakraborty for his help and collaboration with X-ray crystallography and for being the nicest person I know, Dr. Ievgen Govor and Dr. Tosin Jonah for being my first scientific mentors at FIU, Dr. René Panzer, Dr. Ingrid Lehman-Andino, Dr. Joshua Silverman, Dr. Xinrui Zhang and Dr. Setareh Sakhdari for being always ready to help me with scientific problems. Special thanks to Cristian Gonzalez who helped me with several titrations and Job plots among other experiments, Cristian, you were my one-man army, your dedication and commitment to duty are truly unmatched and exemplary. I also especially acknowledge Dr. Adenike Fasiku and her family for advice and assistance

during the writing of this dissertation, for the moral support all through these past years, and for being an extended family to my family. To my friend and “brother” Gabriel Flores for being always witty, smart, and kind.

Lastly, I appreciate my wife Jane Adedoyin, and my wonderful children Sewa and Fola. You all mean the world to me and, you are the best gift a man could ever wish for. Thank you!!

ABSTRACT OF THE DISSERTATION

o-SULFONAMIDOPHENOL LIGANDS AND DERIVATIVES FOR F-ELEMENT SENSING, COMPLEXATION, AND EXTRACTION FROM ALKALINE HIGH- LEVEL WASTE

by

Oluwaseun W. Adedoyin

Florida International University, 2022

Miami, Florida

Professor Konstantinos Kavallieratos, Major Professor

The accumulated (>100 Mgal) alkaline high-level waste (HLW), which is a legacy of nuclear weapons manufacturing during the cold war era, is an issue of environmental concern that has presented reprocessing challenges, due to its complex physicochemical properties and the presence of ^{137}Cs , ^{90}Sr , and long-lived actinides.

This study is focused on *o*-sulfonamidophenol derivatives bearing electron-rich O- and N- donor sites (when deprotonated in alkaline conditions) for effective complexation, sensing, and extraction of f-elements from highly alkaline solutions. Using Ln(III) as experimental surrogates for An(III), a family of *o*-sulfonamidophenol ligands (L1H₂ – L4H₂) bearing *tert*-butyl and/or isopropyl groups gave high extraction for Sm(III), with recoveries as high as 96.1 (±4.4)% and 93.3 (±5.2)% at pH 13.0 and 14.0, respectively, after just one extraction/stripping contact using CH₂Cl₂ as a diluent (Chapter 2). With a diluent similar to those used in the waste reprocessing industry

(*n*-dodecane:octanol (80:20, v/v)), extraction as high as 82.6 (± 9.3)% and 53.9 (± 4.0)% was achieved at pH 12.5 and 14.0 respectively as well as a binding constant range of $\beta_2 = 3.98 (\pm 0.01) \times 10^{10} - 1.26 (\pm 0.04) \times 10^{12} \text{ M}^{-2}$. DFT studies further suggested the likely formation of close ion pairs of type $\{\text{Na}[\text{Sm}(\text{III})\text{L}_2(\text{H}_2\text{O})_x]\}_{\text{org}}$ as the extracted species. This work was expanded to even more lipophilic analogs (Chapter 3) that showed extraction even in *n*-dodecane with recoveries as high as 50.7 (± 1.2)%. Sensing for Ln(III) in alkaline conditions was explored using dansyl (Chapter 4) and *p*-nitro (Chapter 5) derivatives of our *o*-sulfonamidophenol framework. The dansyl derivative (Chapter 4) demonstrated fluorescent sensing along with Sm(III) recovered after extraction in CH_2Cl_2 , as high as 92.2 (± 13.5)% at pH 13.0. The *p*-nitro derivative demonstrated μM optical sensing for Lu(III) (in CH_3CN) in the presence of competing metals which are predominant in HLW, with color change from yellow to colorless observed only in the presence of Lu(III). Lu(III) complexation was further confirmed with the isolation and X-ray characterization of two unique complexes, a monomeric $(\text{Et}_3\text{NH})_3[\text{Lu}(\text{LH})_6]$ and a trimeric $(\text{Et}_3\text{NH})_5[\text{Lu}_3(\mu_3\text{-OH})_2(\text{LH})_6(\text{L})_3]$. These results, overall, point to the potential application of easily synthesized and affordable *o*-sulfonamidophenol ligands for large-scale actinide extraction and sensing from alkaline HLW.

TABLE OF CONTENTS

CHAPTER	PAGE
Chapter I: Introduction to f-Element Separation and Sensing.....	1
1.1 Introduction	1
1.2 Metal speciation in alkaline HLW - liquid phases (supernates).....	6
1.3 Pretreatment techniques for alkaline HLW	11
1.3.1 General	11
1.3.2 Solid-liquid separations	12
1.3.3 Liquid-liquid separations.....	15
1.3.4 HLW processing at the Savannah River Site	24
1.4 Ligand design criteria.....	31
1.5 Sulfonamides for metal complexation, extraction, and sensing (including f- elements).....	32
1.6 Methods for quantification of Metal – Ligand interactions	37
1.6.1 General	37
1.6.2 Binding constant determination by UV-Vis and fluorescence spectroscopy ¹¹⁸	38
1.6.3 Solvent extraction studies ¹¹⁹	39
1.7 Dissertation scope and overall summary.....	40
1.8 References	41
 Chapter II: Lanthanide Coordination and Extraction from Alkaline Media by <i>o</i> -Sulfonamidophenol Derivatives.	 53
2.1 Abstract	53
2.2 Introduction	54
2.3 Experimental section	57
2.3.1 Materials and methods.....	57
2.3.2 Synthesis of 4-(<i>tert</i> -butyl)-N-(5-(<i>tert</i> -butyl)-2-hydroxyphenyl)benzene sulfonamide (L2H ₂).....	58
2.3.3 Synthesis of N-(2-hydroxyphenyl)-2,4,6- triiisopropylbenzenesulfonamide (L3H ₂).....	59
2.3.4 Synthesis of N-(5-(<i>tert</i> -butyl)-2-hydroxyphenyl)-2,4,6- triiisopropylbenzenesulfonamide (L4H ₂).....	59
2.3.5 UV-Vis Titrations.....	60
2.3.6 Continuous variation method (Job Plots) ^{26,27}	61

2.3.7	pH-dependent extraction and stripping of Sm(III) with CH ₂ Cl ₂ as a diluent and spectrophotometric determination of [Sm(III)] _t .	61
2.3.8	pH-dependent extraction and stripping of Ln(III) with CH ₂ Cl ₂ as a diluent and ICP-MS determination of [Ln(III)] _t .	63
2.3.9	pH-dependent extraction and stripping of Sm(III) with <i>n</i> -dodecane:octanol (80:20, v/v) as a diluent and spectrophotometric determination of [Sm(III)] _t .	64
2.3.10	Extraction and stripping of Sm(III) with CH ₂ Cl ₂ as a diluent with various concentration of L ₂ H ₂ .	64
2.3.11	Theoretical Studies of Ln(III) complexation – DFT calculations.	64
2.3.12	X-ray crystallography for L ₁ H ₂ , L ₂ H ₂ , L ₃ H ₂ , and L ₄ H ₂ .	65
2.4	Results and discussion.	66
2.4.1	Synthesis and general characteristics of studied <i>o</i> -sulfonamidophenol ligand family.	66
2.4.2	UV-Vis titrations.	67
2.4.3	Continuous variation method for determination of binding stoichiometry (Job Plots).	69
2.4.4	Extraction and recovery of Sm(III) and other Ln(III) with CH ₂ Cl ₂ as a diluent.	70
2.4.5	Extraction and recovery of Sm(III) with <i>n</i> -dodecane:octanol (80:20, v/v) as diluent.	78
2.4.6	Density Functional Theory (DFT) calculations.	80
2.4.7	X-ray crystallography.	88
2.5	Conclusions.	119
2.6	Acknowledgement.	119
2.7	References.	120
Chapter III: Highly-Lipophilic Alkylated Sulfonamides for Ln(III) Extraction from Alkaline Solutions into Organic Diluents.		125
3.1	Abstract.	125
3.2	Introduction.	126
3.3	Experimental section.	130
3.3.1	Materials and methods.	130
3.3.2	Synthesis of 4-(dodecane-3-yl)benzenesulfonyl chloride (1).	130
3.3.3	Synthesis of N-(5-(<i>tert</i> -butyl)-2-hydroxyphenyl)-4-(dodecan-3-yl)benzenesulfonamide (msa).	131

3.3.4	Synthesis of N,N'-(1,2-phenylene)bis(4-(dodecan-3-yl)benzenesulfonamide) (dsa).....	132
3.3.5	UV-Vis titrations.....	133
3.3.6	Determination of complex stoichiometry by the continuous variation method (Job plot).....	134
3.3.7	pH-dependent experiments for extraction & recovery of Sm(III) into <i>n</i> -dodecane by dsa or msa in the presence or absence of trioctylamine with spectrophotometric quantification of Sm(III).....	134
3.3.8	pH-dependent experiments for extraction & recovery of Ln(III) into <i>n</i> -dodecane with quantification of Ln(III) by ICP-MS.....	136
3.3.9	Determination of complex stoichiometry in extraction by slope analysis ⁴⁷	137
3.4	Results and discussion.....	137
3.4.1	Synthesis.....	137
3.4.2	UV-Vis spectroscopic study of Ln(III) complexation.....	138
3.4.3	Extraction studies.....	141
3.4.3.1	pH-dependent experiments for extraction and recovery of Sm(III) into <i>n</i> -dodecane by dsa or msa in the presence or absence of trioctylamine with spectrophotometric quantification of Sm(III).....	141
3.4.3.2	pH-dependent experiments for extraction and recovery of Ln(III) into <i>n</i> -dodecane by msa with quantification of Ln(III) by ICP-MS.	145
3.5	Conclusion.....	146
3.6	Acknowledgement.....	147
3.7	References.....	148
Chapter IV: Fluorescence Sensing and Extraction of Ln(III) from Alkaline Solutions with a Dansyl <i>o</i> -Sulfonamidophenol Ligand.....		153
4.1	Abstract.....	153
4.2	Introduction.....	154
4.3	Experimental section.....	157
4.3.1	Materials and methods.....	157
4.3.2	Synthesis of N-(5-(<i>tert</i> -butyl)-2-hydroxyphenyl)-5-(dimethylamino)naphthalene-1-sulfonamide (1).....	157
4.3.3	Selectivity studies.....	159
4.3.4	Fluorescence titrations.....	159
4.3.5	Job plots.....	160

4.3.6	UV-Vis titrations	160
4.3.7	pH-dependent extraction and stripping of Sm(III) with CH ₂ Cl ₂ as diluent and spectrophotometric determination of [Sm(III)] _t	161
4.3.8	X-ray crystallography studies.....	163
4.4	Results and discussion.....	163
4.4.1	Synthesis.....	163
4.4.2	Selectivity studies.....	164
4.4.3	Fluorescence titrations.....	166
4.4.4	Job plots.....	169
4.4.5	UV-Vis titrations	171
4.4.6	Extraction and recovery of Sm(III) with CH ₂ Cl ₂ as diluent.....	174
4.4.8	X-ray crystallography studies.....	177
4.5	Conclusions	184
4.6	Acknowledgement.....	184
4.7	References	185
Chapter V: A <i>p</i> -Nitrophenol-sulfonamide Lu(III) Optical Sensor Forms a Unique Lu(III)- μ -hydroxo Trimer in the Solid State.....		188
5.1	Abstract	188
5.2	Introduction	189
5.3	Experimental section	191
5.3.1	Materials and methods.....	191
5.3.2	UV-visible spectroscopic studies	192
5.3.3	DFT calculations	194
5.3.4	Electrochemistry.....	195
5.3.5	X-ray crystallography.....	195
5.4	Results and discussion.....	196
5.4.1	UV-Visible spectroscopic studies	196
5.4.2	DFT calculations	203
5.4.3	Electrochemistry.....	206
5.4.4	X-ray crystallography for LH ₂ , (Et ₃ NH) ₅ [Lu ₃ (μ ₃ -OH) ₂ (LH) ₆ (μ -L) ₃] and (Et ₃ NH) ₃ [Lu(LH) ₆].....	211
5.5	Conclusions	245
5.6	Acknowledgments	246

5.7 References 246

Chapter VI: General Conclusions 253

APPENDICES 258

VITA 299

LIST OF TABLES

TABLES	PAGE
Table 1.1. NEA-TDB data on hydroxides based on most stable redox states for Th, U, Np, Pu, and Am. ²⁰	9
Table 1.2. CSSX components and concentrations for Cs extraction during CSSX (Image obtained from Moyer et al. ⁴⁵).	28
Table 1.3. NG-CSSX components and concentrations for Cs extraction from HLW (Image obtained from Moyer et al. ⁴⁵)	30
Table 2.1. Stability constants for formation of [Sm(III)L ₂] ⁻ 1:2 complexes from UV-Vis titrations in CH ₃ CN:CH ₃ OH (96:4, v/v).	69
Table 2.2. Selected bond lengths (Å) and coordination number for the calculated L2/Sm/OH ⁻ /H ₂ O for the 1:2 complexes in dichloromethane. ‘*’ denotes the N-deprotonated L2H ⁻ ligand form.	83
Table 2.3. Selected bond lengths (Å) coordination number (CN), and free energies (kcal/mol) for the calculated L2/Sm/OH ⁻ /NO ₃ ⁻ /H ₂ O 1:1 complexes in dichloromethane.	87
Table 2.4. Experimental details, crystal data, and structural refinement parameters for L1H ₂	89
Table 2.5. Fractional atomic coordinates and isotropic or equivalent isotropic displacement parameters (Å ²) for L1H ₂	91
Table 2.6: Atomic displacement parameters (Å ²).....	93
Table 2.7: Geometric parameters (Å, °)	94
Table 2.8: Experimental details, crystal data, and structural refinement parameters for L2H ₂	98
Table 2.9: Fractional atomic coordinates and isotropic or equivalent isotropic displacement parameters (Å ²).....	99
Table 2.10: Atomic displacement parameters (Å ²).....	101
Table 2.11. Geometric parameters (Å, °)	102
Table 2.12: Experimental details, crystal data, and structural refinement parameters for L3H ₂	106
Table 2.13: Fractional atomic coordinates and isotropic or equivalent isotropic displacement parameters (Å ²).....	107
Table 2.14: Geometric parameters (Å, °).....	109
Table 2.15: Experimental details, crystal data, and structural refinement parameters for L4H ₂	112
Table 2.16: Fractional atomic coordinates and isotropic or equivalent isotropic displacement parameters (Å ²)	113
Table 2.17: Atomic displacement parameters (Å ²).....	116

Table 2.18: Geometric parameters (\AA , $^\circ$)	117
Table 4.1: Experimental details for 1	178
Table 4.2: Fractional atomic coordinates and isotropic or equivalent isotropic displacement parameters (\AA^2) for 1	180
Table 4.3: Atomic displacement parameters (\AA^2) for 1	181
Table 4.4: Geometric parameters (\AA , $^\circ$) for 1	181
Table 5.1: Crystal data and structure refinement for LH_2	211
Table 5.2: Fractional atomic coordinates and isotropic or equivalent isotropic displacement parameters (\AA^2) for LH_2	213
Table 5.3: X-ray Crystallography data for $(\text{Et}_3\text{NH})_5[\text{Lu}_3(\mu_3\text{-OH})_2(\text{LH})_6(\mu\text{-L})_3]$	218
Table 5.4: X-ray crystallography data for $(\text{Et}_3\text{N})_3[\text{Lu}(\text{LH})_6]$	231
Table 5.5: Fractional atomic coordinates and isotropic or equivalent isotropic displacement parameters (\AA^2)	232
Table A.1: Crystal data for 1	267
Table A.2: Crystal data for 2	269
Table B.1: Crystal data of $(\text{Et}_3\text{NH})_2[\text{ZnL}_2]$	280

LIST OF FIGURES

FIGURE	PAGE
Figure 1.1. Composition of tank waste at the Savannah River Site as reported by Chew et al. ⁸	4
Figure 1.2. Liquid waste treatment flowsheet at the Savannah River Site (Image obtained from Chew et al. ⁸).	6
Figure 1.3. Solubility of Aged Am(OH) ₃ (s) in increasing alkalinity (0 – 10 M KOH) (Image obtained from Neck et al.). ^{22,23}	10
Figure 1.4. Solubility of Nd(III) and Cm(III) under the prevailing alkalinity (a) Solubility of Nd(OH) ₃ in 5.0 M NaCl solution. (b) Solubility of Nd(OH) ₃ in 3.5 M MgCl ₂ and CaCl ₂ solution (Image obtained from Neck et al.). ²²	10
Figure 1.5. Schematic representation of the Integrated Salt Waste Processing Facility at the Savannah River Site. ²⁷	12
Figure 1.6. Commonly used solid-liquid separation methods at the SRS.	13
Figure 1.7. A crossflow filter showing the separation of permeate flow from the concentrated slurry. (Wilmarth et al. ⁶).	14
Figure 1.8. Co-ligands used alongside CSSX system for joint Cs(I) and Sr(II) extraction under alkaline conditions ⁵⁰	16
Figure 1.9. TAM derivative upon deprotonation at high alkalinity bound to Pu(IV) via the catecholate oxygens.	17
Figure 1.10. Catecholamide ligands studied for actinide removal. ⁵³	18
Figure 1.11. (a) 2-hydroxy-5-alkylbenzyl diethanolamine (DEAP) (b) 4-(α,α -dioctylethyl) pyrocatechol (DOP). ^{64,65}	20
Figure 1.12. Alkylphenol Oligomers: (a) YaRB (b) Oktofor 10S (c) Oktofor 101K ⁶⁷	22
Figure 1.13. (left) <i>p-tert</i> -butylcalix[4]arene bearing pendant pyridine groups. (right) <i>p-tert</i> -butylcalix[4]arene. ⁶⁸	22
Figure 1.14. (a) <i>p</i> -Alkylcalix[8]arenes with a combination of <i>tert</i> -butyl and isononyl substituents, n = number of <i>tert</i> -butyl groups present, m = number of isononyl groups present. (b) isononylcalix[8]arene (c) <i>p-tert</i> -butylcalix[8]arene.....	24
Figure 1.15. Scanning electron microscopy image of monosodium titanate. (Image obtained from Wilmarth et al. ⁶).	26
Figure 1.16. Sorption time for strontium, plutonium, and neptunium using 0.4 g/L of MST (Image obtained from Wilmarth et al. ⁶).	27
Figure 1.17. Schematic flowsheet for ¹³⁷ Cs removal using CSSX at SRS. ⁶	29
Figure 1.18. Schematic representation of the sulfonamide moiety.....	33
Figure 1.19. Complexation reaction of <i>o</i> -phenylenediamine derivatives with Pb(NO ₃) ₂ in the presence of organic base diisopropylethylamine and co-ligand	

bipyridine to give a ternary complex (a) or without the co-ligand giving the binary complex (b). ⁹⁷	34
Figure 1.20. Sulfonamide ligands for f-element extraction from alkaline medium (a) 4- <i>ipr</i> -tsa ¹⁰⁰ (b) dsa ⁸⁹	35
Figure 1.21. (a) Dansylamide derivative of <i>o</i> -phenylenediamine for Pb(II) sensing and complexation. ⁹⁴ (b) A bis-dansylamide sensor for Hg(II) ¹¹⁷ (c) Dansylamide sensor for Zn(II). ¹¹⁴	37
Figure 2.1. <i>o</i> -Sulfonamidophenol ligands studied for complexation and extraction of f-elements.....	66
Figure 2.2. UV-Vis titration plots show change in absorbance at 250 nm plotted against concentration of Sm(III). Inset: Changes in UV-Vis spectra of ligands upon titration with Sm(NO ₃) ₃ ·6H ₂ O (4.0 × 10 ⁻⁴ M) (a) L1H ₂ (b) L2H ₂ (c) L3H ₂ , or (d) L4H ₂ in CH ₃ CN:CH ₃ OH (96:4, v/v) at constant concentrations of LH ₂ (4.0 × 10 ⁻⁵ M) and NaOH (8.8 × 10 ⁻⁵ M).....	68
Figure 2.3. Job plots for ligands (2.0 × 10 ⁻⁵ M) and NaOH (5.0 × 10 ⁻⁵ M), with Sm(III) (2.0 × 10 ⁻⁵ M) in CH ₃ CN:CH ₃ OH (96:4, v/v). Absorbance taken at 250 nm.	70
Figure 2.4. Percent Sm(III) recovered after extraction and stripping (0.1 M HNO ₃) with L1H ₂ -L4H ₂ (30.0 mM in CH ₂ Cl ₂) for pH 10.0 – 14.0. Initial Sm(III) concentration was 2.0 mM. Sm(III) recovered was quantified using the Arsenazo-III spectrophotometric method (for L1H ₂ and L2H ₂) and ICP-MS (for L3H ₂ and L4H ₂).	74
Figure 2.5. Mass balance for Sm(III) recovered after extraction and stripping (0.1 M HNO ₃) by L2H ₂ (30.0 mM) in CH ₂ Cl ₂ [Sm(III)] _t = 2.0 mM. Sm(III) recovered and measured in the acidic aqueous phase after extraction and consecutive stripping is noted by the red circles, while soluble leftover Sm(III) in the aqueous phase is noted by the black squares. Sm(III) recovered was quantified by the Arsenazo-III spectrophotometric method. ...	75
Figure 2.6. Percent Sm(III) recovered after extraction and stripping (0.1 M HNO ₃) as a function of increased concentration of L2H ₂ at pH 13.0. Aqueous phase: [Sm(III)] _t = 1.0 mM in 0.1 M NaOH. Organic phase: [L2H ₂] _t = 0 – 20.0 mM). Sm(III) recovered was quantified using ICP-MS.	76
Figure 2.7. Percent La(III), Nd(III), Sm(III), and Eu(III) recovered after extraction and stripping (0.1 M HNO ₃) by L2H ₂ (30.0 mM) in CH ₂ Cl ₂ [Ln(III)] _t = 2.0 mM, Ln(III) recovered was quantified using ICP-MS.....	78
Figure 2.8. Percent Sm(III) recovered after extraction and stripping (0.1 M HNO ₃) by L2H ₂ (left) and L4H ₂ (right) (30.0 mM respectively) in <i>n</i> -dodecane:octanol (80:20, v/v) [Sm(III)] _t = 2.0 mM. Sm(III) recovered was quantified using the Arsenazo-III spectrophotometric method.	79

Figure 2.9. Structure of a 1:2 Sm(III) complex with L2H ₂ , Sm(L2)(L2H).2H ₂ O. L2H indicates a mono-deprotonated ligand on the phenolic O-atom.....	81
Figure 2.10. Structure of a 1:2 Sm(III) complex with L2H ₂ , Sm(L2)(L2H)*.2H ₂ O. (L2H* indicates a mono-deprotonated ligand on the sulfonamide N-atom).....	82
Figure 2.11. Structure of a 1:2 complex of Sm(III) with L2H ₂ , Na[Sm(L2) ₂ .H ₂ O] showing close ion-pair formation.....	83
Figure 2.12. Structure of a 1:1 complex of Sm(III) and L2H ₂ with structure Sm(L2)(NO ₃)(H ₂ O) ₆	84
Figure 2.13. Structure of a 1:1 complex of Sm(III) and L2H ₂ with structure Sm(L2)(NO ₃)(H ₂ O) ₅	85
Figure 2.14. Structure of a 1:1 complex of Sm(III) and L2H ₂ with structure Sm(L2)(OH)(H ₂ O) ₅	86
Figure 2.15. ORTEP representation of the crystal structure of L1H ₂ (50 % probability ellipsoids).	89
Figure 2.16: ORTEP representation of the crystal structure of L2H ₂ showing intermolecular hydrogen bonding with a molecule of methanol (50% probability ellipsoids).....	97
Figure 2.17: ORTEP representation of the crystal structure of L3H ₂ (50% probability ellipsoids).	105
Figure 2.18: ORTEP representation of the crystal structure of L4H ₂ (50% probability ellipsoids), showing intramolecular hydrogen bonding.	112
Figure 3.1. Schematic drawing of sulfonamide extractants msa and dsa.	138
Figure 3.2. (left) UV-Vis spectra for titration of msa (4.0×10^{-5} M) and NaOH (8.8×10^{-5} M) with Sm(III) (4.0×10^{-4} M) in CH ₃ CN:CH ₃ OH (96:4, v/v). Inset: Expanded spectra for 0.0 – 0.5 absorbance range, and 220 – 350 nm wavelength range. (right): Titration plot showing the absorbance change at 250 nm plotted against the concentration of Sm(III). The solid line shows the actual nonlinear regression fitting to the 1:1 binding isotherm.	139
Figure 3.3. (left) UV-Vis spectra for titration of dsa (4.0×10^{-5} M) and NaOH (8.0×10^{-5} M) with Sm(III) (8.0×10^{-4} M) in CH ₃ CN:CH ₃ OH (96:4, v/v). (right): Titration plot showing the absorbance change at 260 nm plotted against the concentration of Sm(III). The solid line shows the actual nonlinear regression fitting to the 1:1 binding isotherm.....	140
Figure 3.4. Job plots ($A_{250 \text{ nm}}$) for msa (left) and ($A_{260 \text{ nm}}$) for dsa (right). Solution A: $[L]_t = 2.0 \times 10^{-5}$ M, $[\text{NaOH}] = 5.0 \times 10^{-5}$ M in CH ₃ CN:CH ₃ OH (96:4, v/v). Solution B: $[\text{Sm(III)}]_t = 2.0 \times 10^{-5}$ M in CH ₃ CN:CH ₃ OH (96:4, v/v).	141
Figure 3.5. Percent Sm(III) recovered after extraction and subsequent stripping (0.1M HNO ₃) using msa (20.0 mM) (left) or dsa (20.0 mM) (right) with or without the presence of trioctylamine (40.0 mM). $[\text{Sm(III)}]_t = 2.0$ mM.	143

Figure 3.6. Log-log Plot of D_{Sm} vs. $[dsa]_t$ (20.0 mM – 40.0 mM) in <i>n</i> -dodecane at pH 12.0. $[Sm(III)]_t = 2.0 \times 10^{-4}$ M).	144
Figure 3.7. Percent recovered for La(III), Nd(III), Sm(III), and Eu(III) after extraction and subsequent stripping (0.1M HNO ₃) using msa (20.0 mM) in <i>n</i> -dodecane in absence of trioctylamine. $[Ln(III)]_t = 2.0$ mM.....	146
Figure 4.1. (a) Visual fluorescent changes of 1 (4.0×10^{-6} M) and 2.2 equivalents of NaOH in the presence of equimolar concentration of several metals. Fluorescence changes from left: 1, Na(I), Sr(II), Sm(III) K(I) and Cs(I) in CH ₃ CN:CH ₃ OH (96:4, v/v) ($\lambda_{exc}=360$ nm). (b) Fluorescence spectra of 1 (4.0×10^{-6} M) and 2.2 equivalents of NaOH in the presence of equimolar concentrations of Na(I), K(I), Cs(I), Sr(II) and Sm(III) in CH ₃ CN:CH ₃ OH (96:4, v/v) ($\lambda_{exc}=360$ nm).	165
Figure 4.2. Fluorescence emission spectra showing response of 1 (4.0×10^{-6} M) and 4 equivalents of NaOH in the presence of equimolar concentration Na(I), K(I), Cs(I), Ag(I), Ba(II), Hg(II), Sr(II), Pb(II), Co(II), Ru(III), Cr(III), Yb(III) and Sm(III) in CH ₃ CN:H ₂ O (99:1 v/v) ($\lambda_{exc}=360$ nm).	166
Figure 4.3. (a) Changes in fluorescence emission spectra of 1 due to titration of 1 (4.0×10^{-6} M) and 2.2 equivalents of NaOH with Sm(III) (4.0×10^{-5} M, 0 – 0.88 mL) in CH ₃ CN:CH ₃ OH (96:4, v/v) ($\lambda_{exc}=360$ nm). (b) Changes in intensity of 1 with increasing concentration of Sm(III).	168
Figure 4.4. (a): Fluorescence titration spectra of 1 (5.0×10^{-6} M) after addition of NaOH (5.0×10^{-2} M) (no metal present) in CH ₃ CN:CH ₃ OH (96:4 v/v). $\lambda_{exc} = 360$ nm. (b) Fluorescence titration spectra of 1 (5.0×10^{-6} M) after titration with Sm(III) (5.0×10^{-3} M) (no base present) in CH ₃ CN:CH ₃ OH 96:4 v/v. $\lambda_{exc} = 360$ nm.	168
Figure 4.5. (a) Changes in fluorescence emission spectra of 1 due to titration of 1 (5.0×10^{-6} M) and 2.2 equivalent of NaOH with Yb(III) (5.0×10^{-5} M, 0 – 0.88 mL) in CH ₃ CN:CH ₃ OH (96:4, v/v) ($\lambda_{exc}=360$ nm). (b) Changes in intensity of 1 with increasing concentration of Yb(III).	169
Figure 4.6. Job plot of 1 (2.0×10^{-5} M) with 2.2 equivalents of NaOH and Sm(III) (2.0×10^{-5} M) using changes in absorbance on UV-Vis spectra in CH ₃ CN:CH ₃ OH (96:4, v/v). Absorbance taken at 250 nm.	170
Figure 4.7. Job plot of 1 (2.0×10^{-5} M) with 2.2 equivalents of NaOH and Yb(III) (2.0×10^{-5} M) using changes in absorbance on UV-Vis spectra in CH ₃ CN:CH ₃ OH (96:4, v/v). Absorbance taken at 250 nm.	171
Figure 4.8. (a) Spectral changes of 1 due to titration of 1 (4.0×10^{-5} M) and 2.2 equivalents of NaOH with Sm(III) (4.0×10^{-4} M, 0 – 0.88 mL) in CH ₃ CN:CH ₃ OH (96:4, v/v) (b) Titration curve showing change in absorbance of 1 as a result of added Sm(III) at 303 nm.	172

- Figure 4.9. (a) Spectral changes of **1** due to titration of **1** (4.0×10^{-5} M) and 2.2 equivalent of NaOH with Yb(III) (4.0×10^{-4} M, 0 – 0.88 mL) in CH₃CN:CH₃OH (96:4, v/v). (b) Titration curve showing the change in absorbance of **1** as a result of added Yb(III) at 303 nm..... 173
- Figure 4.10. Percent Sm(III) recovered after extraction and consecutive stripping using **1** for pHs 10.0 – 14.0. Initial Sm(III) concentration in the aqueous phase was 2.0 mM and in the organic phase was 20.0 mM in dichloromethane. Quantification of Sm(III) was done using ICP-MS. 175
- Figure 4.11. Mass balance for extraction experiment, showing Sm(III) recovered and measured in the acidic aqueous phase after extraction with the ligand solution (20.0 mM) and consecutive stripping (0.1 M HNO₃) (black squares) and unextracted Sm(III) in the alkaline aqueous phase after contact with ligand solution (20.0 mM) (red circles) for pH 10.0 – 14.0. Initial Sm(III) concentration in the alkaline aqueous phase was 2.0 mM. Quantification of Sm(III) was done using the Arsenazo-III spectrophotometric method..... 176
- Figure 4.12. Comparison of ICP-MS and the Arsenazo-III method for quantification of Sm(III) recovered for pH 10.0 – 14.0 after stripping of the loaded organic phase with 0.1 M nitric acid..... 177
- Figure 4.13. ORTEP representation of the crystal structure of **1** showing intramolecular hydrogen bonding (50% probability ellipsoids). 178
-
- Figure 5.1. Visible color changes of LH₂ (50.0 μM) and DIPEA (125.0 μM) in CH₃CN before and after the addition of various metals (50.0 μM) - La(NO₃)₃·6H₂O, Sm(NO₃)₃·6H₂O, Lu(NO₃)₃·6H₂O, Co(NO₃)₂·6H₂O, Pb(NO₃)₂, Sr(NO₃)₂, Ag(NO₃), NaNO₃, KNO₃ in CH₃CN..... 197
- Figure 5.2. UV-Vis spectra for LH₂ (50.0 μM) and DIPEA (125.0 μM) in CH₃CN before and after addition of various metals (50.0 μM). Left: Spectra before and after addition of Ag(NO₃), Co(NO₃)₂·6H₂O, La(NO₃)₃·6H₂O, Pb(NO₃)₂, Sm(NO₃)₃·6H₂O, Sr(NO₃)₂, Lu(NO₃)₃·6H₂O, KNO₃, and NaNO₃. Right: Spectra before and after addition of Ca(NO₃)₂·4H₂O, Lu(NO₃)₃·6H₂O, and CsNO₃..... 198
- Figure 5.3. UV-Vis titration spectra for LH₂ (1.0×10^{-5} M) / DIPEA (2.5×10^{-5} M) with Ln(NO₃)₃·6H₂O (1.0×10^{-4} M) in CH₃CN (top), and fitted titration plots of $\Delta A_{432\text{nm}}$ vs. $[M]_t$ (bottom) for (a) La(III) (b) Sm(III) (c) Lu(III). 200
- Figure 5.4. Control titrations of (a) LH₂ (1.0×10^{-5} M) without DIPEA in CH₃CN with Lu(NO₃)₃·6H₂O (0 – 1.7×10^{-5} added) M (b) DIPEA (2.5×10^{-5} M) without LH₂ in CH₃CN with Lu(NO₃)₃·6H₂O (0 – 1.7×10^{-5} M added). 200

Figure 5.5. (a) Plots of $A_{432\text{nm}}$ vs $[M]_t$ for titrations of LH_2 (1.0×10^{-5} M) and DIPEA (2.5×10^{-5} M) with Na(I), K(I), Sr(II) or Lu(III) (each 1.0×10^{-4} M) when titrated independently in CH_3CN	202
Figure 5.6. Competitive titration of LH_2 (1.0×10^{-5} M) with Lu(III) ($0 - 1.2 \times 10^{-5}$ M added) in excess concentration of the other metals (Na(I) = 5.0×10^{-3} M, K(I) = 1.0×10^{-3} M, Sr(II) = 2.0×10^{-4} M) in CH_3CN (black). Titration of LH_2 with Lu(III) in absence of other metals (red).	203
Figure 5.7. DFT optimization of the Lu(III) complex in CH_3CN , minimized as $\text{Lu(III)L(NO}_3\text{)}_3(\text{H}_2\text{O})_5$	204
Figure 5.8. HOMO – LUMO energy transitions for L^{2-} (left) and $\text{Lu(III)L(NO}_3\text{)}_3(\text{H}_2\text{O})_5$ (right).	205
Figure 5.9. HOMO – LUMO (left) and HOMO-1 – LUMO (right) transitions in the ligand LH_2	205
Figure 5.10. (a) Experimental UV-Vis Spectra of LH_2 (1.0×10^{-5} M) and DIPEA (2.5×10^{-5} M) upon titration with Lu(III) (1.0×10^{-4} M) showing wavelength maxima for L^{2-} at 432 nm and the Lu(III)-L complex at 398 nm. (b) Absorption spectra from TD-DFT calculations showing calculated wavelengths and oscillator strengths for LH_2 , L^{2-} and the Lu(III)-L complex $\text{Lu(III)L(NO}_3\text{)}_3(\text{H}_2\text{O})_5$	206
Figure 5.11. Left: CVs of 1.0 mM of free ligand LH_2 with 2.5 equivalents of DIPEA with scan rates varying from 400 mV/s (black), to 10 mV/s (green); Right: associated peak currents at each acquired scan rate.	208
Figure 5.12. CV of a 1.0 mM Lu(III) solution acquired at 100 mV/s, showing no redox events.	208
Figure 5.13. Left: Comparisons of CVs at 100 mV/s containing solutions of 1.0 mM LH_2 and 2.5 equivalents of DIPEA without Lu(III) (black), and with 1.0 mM Lu(III) (red). Right: CV at 20 mV/s of a solution containing 1.0 mM $\text{Lu(NO}_3\text{)}_3 \cdot \text{H}_2\text{O}$ and 1.0 mM LH_2 (with 2.5 equivalents of DIPEA) after mixing for 30 min.	209
Figure 5.14. CV cycles of a solution containing 1.0 mM Lu(III) and 1.0 mM LH_2 (with 2.5 added equivalents of DIPEA). The first scan (black) reverses direction after the first oxidation event (+0.7 V), while the second scan (red) features both ligand-based oxidation events.	209
Figure 5.15. Left: CVs of a solution containing 1.0 mM of Lu(III), 1.0 mM LH_2 , and 2.5 equivalents of DIPEA with scan rates varying from 200 mV/s (black) to 20 mV/s (green); Right: associated peak currents at each acquired scan rate for the first oxidation event at 0.65 V (black), the second oxidation event at 0.85 V (red), and the reduction event at 0.14 V (blue).	210
Figure 5.16. CVs of a solution containing 1.0 mM of Lu(III) and 1.0 mM LH_2 (red), 2.0 mM LH_2 (blue), 3.0 mM LH_2 (black), without any DIPEA. The	

	scan rate in all cases is 100 mVs/, and the potential is referenced to Ag/AgCl.	210
Figure 5.17.	X-ray crystal structure of LH ₂ (ORTEP plot – 50% probability ellipsoids).	211
Figure 5.18.	X-ray structure of the anionic [Lu ₃ (μ ₃ -OH) ₂ (LH) ₆ (L) ₃] ⁵⁻ (ball-and-stick diagram - five Et ₃ NH ⁺ are not shown). (a) view down the threefold axis, showing three equatorial L ²⁻ bridging three Lu(III) (b) Projected view perpendicular to the 3-fold axis with hydrogens omitted for clarity. Color code: teal = Lu, red = O, yellow = S, blue = N, and black = C.	217
Figure 5.19.	ORTEP representation of the anionic [Lu ₃ (μ ₃ -OH) ₂ (LH) ₆ (L) ₃] ⁵⁻ (30% probability ellipsoids) Projected view perpendicular to the 3-fold axis (five Et ₃ NH ⁺ are not shown).	217
Figure 5.20.	Ball and stick representation of (Et ₃ NH) ₃ [Lu(LH ₆)] showing three triethylammonium counteranions and an O---H intermolecular hydrogen bond interaction.	230
Figure 5.21.	Packing pattern of (Et ₃ NH) ₃ [Lu(LH ₆)].....	230
Figure A.1.	Synthesis of sulfonamide (1) and sulfonic ester (2)	263
Figure A.2.	Synthetic scheme for N-(5-(<i>tert</i> -butyl)-2-hydroxyphenyl)-4-methylbenzenesulfonamide (1)	264
Figure A.3.	Synthetic scheme for 2-amino-4-(<i>tert</i> -butyl)phenyl-4-methylbenzenesulfonate (2)	264
Figure A.4.	UV-Vis spectra showing absorbance changes due to addition of Sm(NO ₃) ₃ ·6H ₂ O (1.0 × 10 ⁻³ M) to (a) 2 (1.0 × 10 ⁻⁵ M) with 2 equivalents of DIPEA in acetonitrile, (b) DIPEA in acetonitrile (2.0 × 10 ⁻⁵ M).....	265
Figure A.5.	ORTEP representation of the X-ray crystal structure of 1 (50% probability ellipsoids).....	266
Figure A.6.	Ball and stick representation of 1 showing π-π stacking interaction and C-H···O intermolecular hydrogen bonding interactions of 1.	266
Figure A.7.	ORTEP representation of the X-ray crystal structure of 2 (50% probability ellipsoids).....	268
Figure A.8.	Ball and stick representation of 2, showing slipped π - π stacking interaction and weak nonclassical C-H···O intermolecular hydrogen bonding interactions	268
Figure B.1.	Synthesis of (Et ₃ NH) ₂ [ZnL ₂]	275
Figure B.2.	FT-IR spectra of LH ₂ and (Et ₃ NH) ₂ [ZnL ₂] (2000 - 600 cm ⁻¹ range).....	276
Figure B.3.	¹ H-NMR in CDCl ₃ of (i) LH ₂ (ii) LH ₂ in presence of triethylamine, (iii) Isolated (Et ₃ NH) ₂ [ZnL ₂].....	278

Figure B.4. ORTEP representation of the structure of $[\text{ZnL}_2]^{2-}$ (showing 50% probability ellipsoids). Hydrogens and triethylammonium counteranions have been omitted for clarity.....	279
Figure C.1. Structure of synthesized ligands 1, 2, 3	291
Figure C.2. UV-Vis titration of a solution of 1 (1.0×10^{-5} M) and 2.5 eq. of DIPEA in CH_3CN with Sm(III) (1.0×10^{-4} M).....	292
Figure C.3. UV-Vis titration of a solution of 2 (1.0×10^{-5} M) and 2.5 eq. of DIPEA in CH_3CN with Sm(III) (1.0×10^{-4} M)	293
Figure C.4. UV-Vis titration of a solution of 3 (1.0×10^{-5} M) and 2.5 eq. of DIPEA in CH_3CN with Sm(III) (1.0×10^{-4} M).....	293
Figure C.5. Comparison of ^1H -NMR spectra in deuterated chloroform of (a) 3, (b) 3 with 3.2 eq. of py, (c) 3 with 3.2 eq. of DIPEA.	295
Figure C.6. Percent unextracted Sm(III) in the alkaline aqueous phase when using 3 (30.0 mM) in CH_2Cl_2 . $[\text{Sm(III)}]_t = 2.0$ mM	296

LIST OF ABBREVIATIONS

AIE	Aggregation Induced Emission
ARP	Actinide Removal Process
CAM	Cathecholamide
CHEF	Chelation Enhanced Fluorescence
CHEQ	Chelation Enhanced Quenching
CSSX	Caustic Side Solvent Extraction
CST	Crystalline silicotitanate
DEAP	2-hydroxy-5-alkylbenzyl diethanolamine
DF	Decontamination Factor
DFT	Density Functional Theory
D_m	Distribution Coefficient
DOE	Department of Energy
DOP	4-(α,α -dioctylethyl)pyrocatechol
DTPA	Diethylenetriaminepentamethylphosphonic Acid
DWPF	Defence Waste Processing Facility
FP	Fission Products
FRET	Forster Resonance Energy Transfer
FT-IR	Fourier Transform Infrared
HLW	High-Level Waste
HS	Hanford Site
ICP-MS	Inductively Coupled Plasma Mass Spectrometry

ISWPF	Integrated Salt Waste Processing Facility
ISWPF	Integrated Saltstone Processing Facility
LAW	Low Activity Waste
LLW	Low Level Waste
LMCT	Ligand to Metal Charge Transfer
LOD	Limit of Detection
MA	Minor Actinides
MCU	Modular CSSX Unit
MCU	Modular Caustic Side Solvent Extraction Unit
MLCT	Metal to Ligand Charge Transfer
MST	Monosodium Titanate
NEA	Nuclear Energy Agency
NG-CSSX	Next Generation Caustic Side Solvent Extraction
NMR	Nuclear Magnetic Resonance
PEI	Polyethyleneimine
PET	Photoinduced Electron Transfer
PPM	Parts Per Million
PUREX	Plutonium Uranium Redox eXtraction
QAB	Quaternary Ammonium Bases
REE	Rare Earth Elements
SF	Separation Factor
SNF	Spent Nuclear Fuel

SPF	Saltstone Processing Facility
SRS	Savannah River Site
TAM	2,3-dihydroxyterephthalamide
TBP	Tributyl Phosphate
TCE	Tetrachloroethylene
TDB	Thermochemical Energy database
TD-DFT	Time-Dependent Density Functional Theory
TICT	Twisted Intermolecular Charge Transfer
TRLFS	Time-Resolved Laser Fluorescence Spectroscopy
UV-Vis	UV-Visible

Chapter I: Introduction to f-Element Separation and Sensing

1.1 Introduction

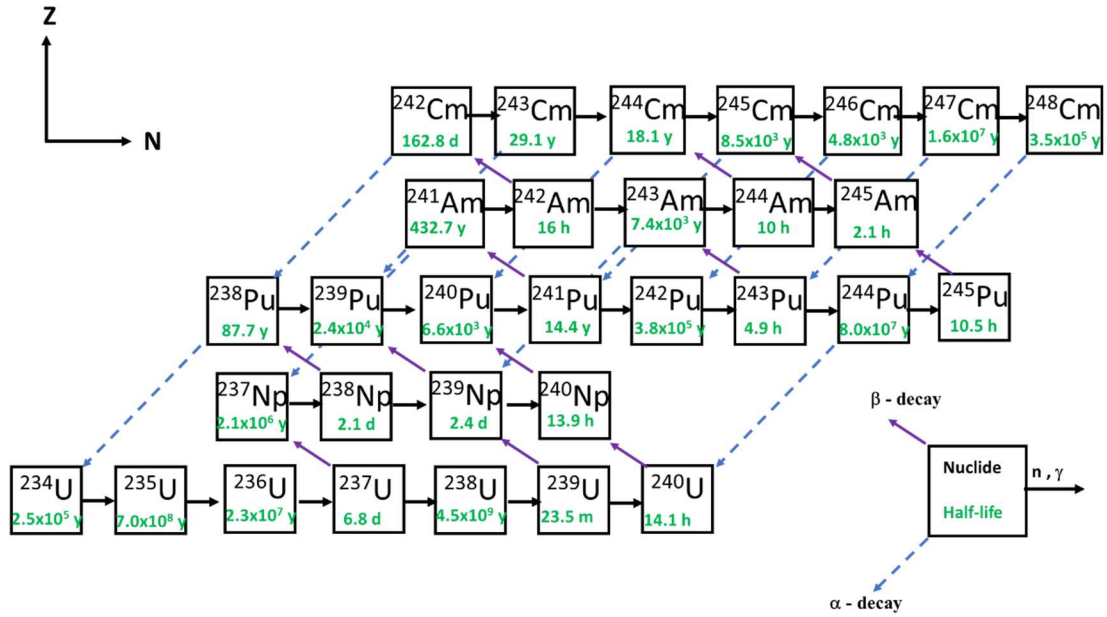
High-Level Waste (HLW), which is also often referred to as “Legacy Waste” or “Tank Waste” is defined as the highly radioactive material that has been generated and accumulated from the early 1950s during the nuclear arms race between the USA and the former USSR.^{1,2} As uranium and plutonium were valuable materials for weapons production, they were separated from spent nuclear fuel (SNF) and other irradiated materials using the established PUREX (Plutonium Uranium Redox Extraction) process.³ In the PUREX process SNF is dissolved in concentrated nitric acid, and plutonium/uranium are extracted together from the acidic aqueous phase into a paraffin-based organic phase using tributyl phosphate (TBP), with a subsequent redox step leading to a separate plutonium stream, which is especially valuable for production and maintenance of nuclear arsenals. The acidic raffinates from years of PUREX processing were made highly alkaline by adding concentrated NaOH and stored in underground carbon steel tanks, mainly at the Hanford and Savannah River DOE reservations.⁴ The NaOH addition was considered critical at that time for two reasons: i) It immobilized several components as insoluble hydroxides, including the highly radiotoxic long-lived actinides, thus reducing environmental risks, and ii) It maintained tank integrity for prolonged storage, especially for carbon-steel tanks, considering stainless steel was in short supply during the immediate post-WWII era.⁵ Addition of NaOH led to phase separation within the tanks, including a soluble supernatant, which is often referred to as

“supernate” (mainly containing alkali and alkaline earth metals) and an insoluble sludge at the bottom (mainly transition and post-transition metals and actinides), leading to complex physicochemical phenomena through years of storage under substantial heat and radioactivity.⁶

Production and modification of nuclear materials in the US throughout the cold war occurred mainly at the Oak Ridge Reservation (Tennessee), the Savannah River Site (South Carolina), the Idaho National Laboratory, the Hanford Reservation (Washington), and the Rocky Flats Site (Colorado).¹ In the former USSR, nuclear materials were produced at the Mayak Production Association, and therefore this is currently the main Russian HLW storage site.⁵ In the US, the overwhelming majority of HLW are stored in underground tanks at two sites; the Savannah River Site (SRS) and the Hanford Site (HS).^{1,6} The HS contains 177 waste tanks with about 56 million gallons^{6,7} of HLW while the SRS contains 43 active tanks⁸ with about 35 million gallons.⁶ Although the HS has more tanks, the total radioactivity is about 176 MCi while the total radioactivity at the SRS is 248 MCi.⁸ As these tanks are alkaline, the different components are separated based on their solubility in the basic aqueous phase (Figure 1.1). Components that are soluble at high pH, such as alkali and alkaline earth metals, are found in the supernatant and the saltcake, which is an intermediate layer between supernatant and sludge formed due to evaporation in the supernatant. These components account for over 50% of the radioactivity of the SRS tanks.⁶ Alkali and alkaline earth metals are predominant in the supernatant as salts of NO_3^- , NO_2^- , OH^- , CO_3^- , SO_4^- , and $\text{Al}(\text{OH})_4^-$ alongside other metals, including technetium, and actinides found in high alkalinity and ionic strength where they form soluble complexes.^{2,9} Metals responsible for the bulk of the radioactivity in the

supernate⁶ include mainly ¹³⁷Cs, ⁹⁰Sr, and ⁹⁹Tc, along with actinides and other fission products (FP), including lanthanides, to a lesser degree. Presently, as a result of increased evaporation, the concentration of OH⁻ and NO₃⁻ in the supernatant has increased significantly, giving rise to a saltcake which is composed of 22% (by volume) of ⁹⁰Sr and some transuranic salts⁶ alongside 78% of NaNO₃, Na₂CO₃ and Na₂SO₄.^{2,10} The sludge has the highest density of the three HLW phases, lying at the bottom of the tanks as a gel-like solid consisting of insoluble oxides and hydroxides of metals like aluminum, manganese, chromium, cerium, and actinides.¹¹ The origin of some of the radionuclides found in HLW can be traced to the bombardment of uranium dioxide nuclear fuel by thermal neutrons (eq. 1.1, 1.2, and Scheme 1.1).





Scheme 1.1 Transuranic element formation as a result of successive neutron capture.

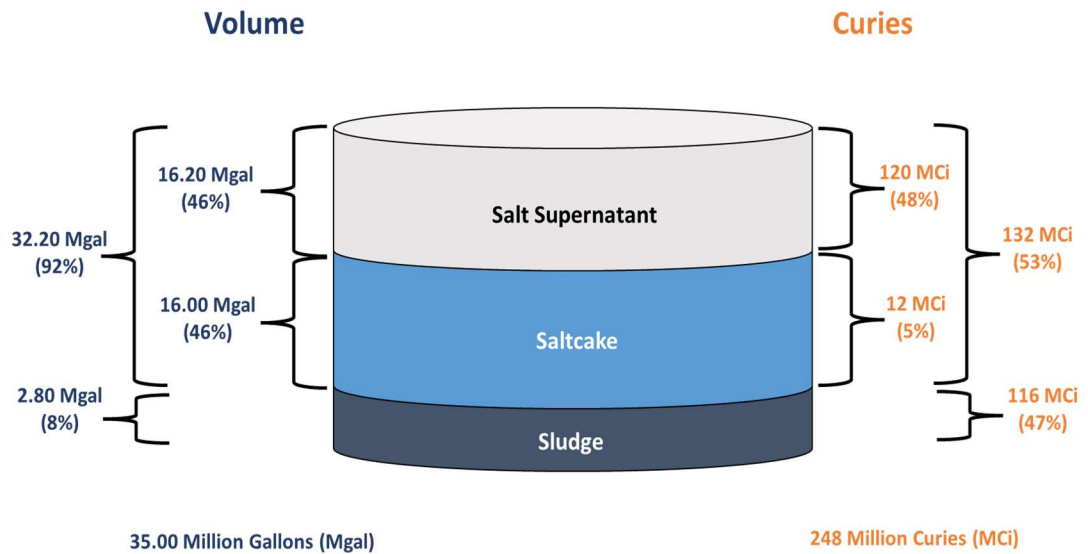


Figure 1.1. Composition of tank waste at the Savannah River Site as reported by Chew et al.⁸

Prolonged storage of HLW in tanks has been deemed unsustainable due to the very large volume and the magnitude of environmental hazard by an accidental release.¹²

As underscored by previous events, some tanks have experienced leaks into secondary containments,² and the immediate environment,^{13,14} and because of this, the Environmental Management Program under the US Department of Energy (DOE) was mandated to immobilize legacy waste in solid form, thus facilitating safe long term storage in geological repositories.¹² The cornerstone of this overall strategy entails a separation (often referred to as “pre-treatment”) into a small volume of very high activity for geological disposal and large volumes of much less hazardous Low-Activity Waste (LAW) fractions stored in separated waste forms and with different standards of treatment and storage. LAW in the SRS is stored in sandstone onsite, while HLW is immobilized into a borosilicate glass matrix at the Defense Waste Processing Facility (DWPF) and is also currently temporarily stored on-site in Glass Waste Storage Buildings (GWSB), with future storage plans at designated geological repositories. Figure 1.2 gives a brief schematic summary of integrated HLW waste processing at SRS.

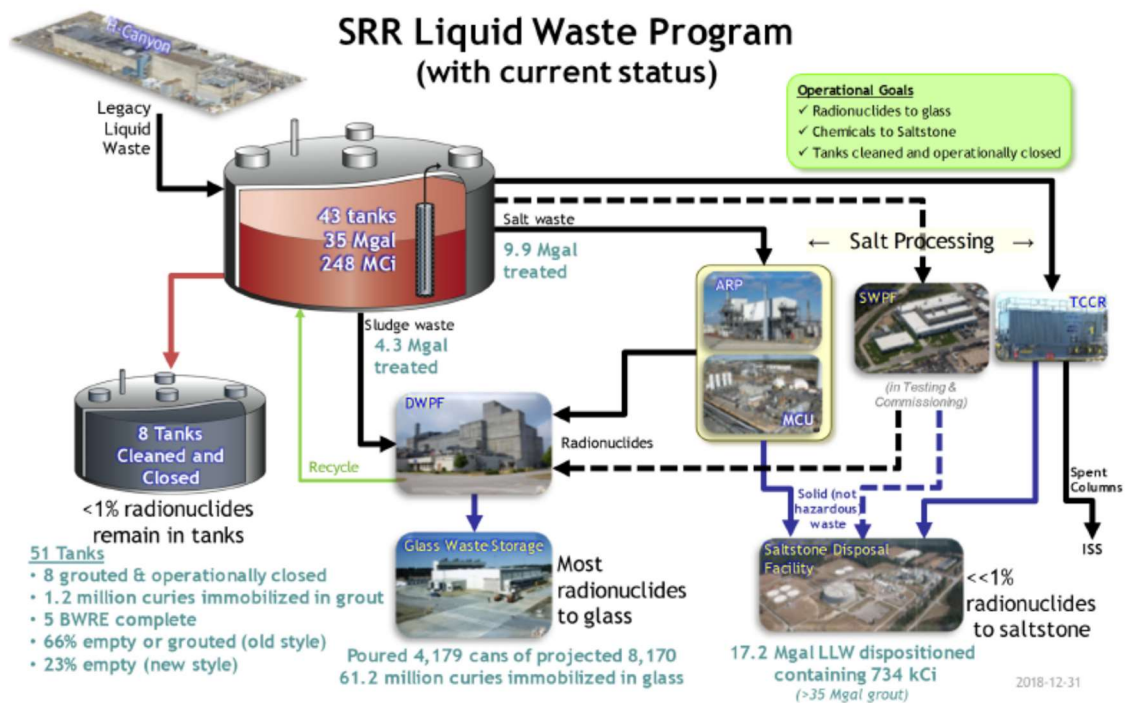
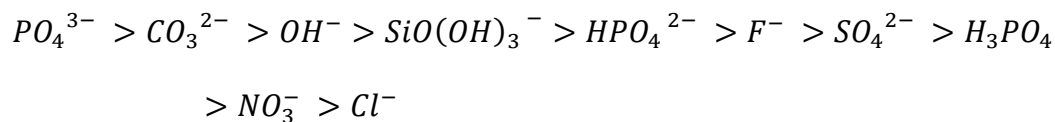


Figure 1.2. Liquid waste treatment flowsheet at the Savannah River Site (Image obtained from Chew et al.⁸).

1.2 Metal speciation in alkaline HLW - liquid phases (supernates)

The subject of metal speciation (including actinides) as it pertains to pH considerations and ionic strength in alkaline and near alkaline conditions, is of great interest because it explains their presence in HLW supernates and can facilitate

strategies for their effective separation.¹⁵⁻¹⁹ In alkaline media, f-elements, including actinides, can coordinate with inorganic coordinating anions present, and by extension become soluble, especially at conditions of high ionic strength. These coordinating anions include hydroxides, carbonates, and nitrates, all present at HLW supernates at various concentrations (dependent on tanks).²⁰ The overall stability series of actinide complexes with common inorganic anions are shown below:²¹



Actinides have variable oxidation states (OS) in solution, and depending on the alkalinity, which OS is predominant may vary. Their complex redox chemistry often results in more than one OS coexisting in solution,^{20,21} with some oxidation states being able to result in more soluble actinide species than others. The chemical thermodynamic series published by the Nuclear Energy Agency (NEA) Thermochemical Energy Database (TDB) project gives a summary of prominent aqueous actinide species likely present in solution along with their redox states (Table 1.1).²⁰ In neutral to alkaline media, trivalent actinides and lanthanides are expected to be hydrolyzed. In the case of Am(III), for instance, the NEA-TDB reviews primarily considered the $AmOH^{2+}$, $Am(OH)_2^+$ and $Am(OH)_3$ (aq.) as prevalent species (Table 1.1) based on time-resolved laser fluorescence spectroscopic (TRLFS) studies, and did not include data from very high alkalinity (>3.0 M $[OH^-]$) due to the high and variable ionic strength.^{22,23} However, this information was updated based on the work of Neck et al.,²² whose data reevaluated previously held beliefs that Am(III) is almost exclusively precipitated as $Am(OH)_3$.

Under higher alkalinity (0 – 10.0 M KOH), and in the presence of NaCl, MgCl₂, and CaCl₂, which increase ionic strength, it was proposed that the presence of soluble Am(OH)₄⁻ was very likely, especially at >3M KOH (Figure 1.3), with very high estimated stability ($\log \beta_4 = -40.7 \pm 0.7$).²² Similarly, the solubility of An(III) in alkaline CaCl₂ solution was investigated by Rabung et al.²⁴ TRLFS data revealed the presence of a ternary Ca-An^(III)-OH complexation state for Cm(III) in > 2.5 M CaCl₂. The species present were identified as Ca[An(III)(OH)₃]²⁺, Ca₂[An(III)(OH)₄]³⁺ and Ca₃[An(III)(OH)₆]³⁺. Data obtained using the Pitzer model calculations are shown in Figure 1.4 along with analogous studies with NaCl and MgCl₂. Moving forward, Neck and coworkers²² also investigated the solubility and speciation of Ln(III) at 0.25 – 3.50 M concentration of CaCl₂ in solutions of pH 7.0 to pH 12.0, and they found an increase in Nd(III) solubility at pH > 10.0. As a result, while the majority of actinide radioactivity is present in the sludge, a significant amount of radioactive actinide component is still present in soluble form in the supernatant due to the presence of highly-coordinating anions and high ionic strength and alkalinity. This presence of soluble actinides in the aqueous phase forms the impetus of this study, which emphasizes the design of ligands for extraction of soluble actinides from alkaline aqueous phases into select organic phases. In this study, trivalent lanthanides, such as Sm(III), Eu(III), and Nd(III) have been used as surrogates for trivalent minor actinides, especially Am(III), and we hope that some of the ligand designs we have introduced will find application for Am(III) separation in the future.

Table 1.1. NEA-TDB data on hydroxides based on most stable redox states for Th, U, Np, Pu, and Am at pH = 14.²⁰

Hydroxides					
	Th	U	Np	Pu	Am
Oxidation state					
3+	-	-	NpOH ²⁺	PuOH ²⁺	AmOH ²⁺ Am(OH) ₂ ⁺ Am(OH) ₃ (aq)
4+	ThOH ³⁺ Th(OH) ₂ ²⁻ Th(OH) ₄ (aq) Th ₂ (OH) ₂ ⁶⁺ Th ₂ (OH) ₃ ⁵⁺ Th ₄ (OH) ₈ ⁸⁺ Th ₄ (OH) ₁₂ ⁴⁺ Th ₆ (OH) ₁₄ ¹⁰⁺ Th ₆ (OH) ₁₅ ⁹⁺	UOH ³⁺ U(OH) ₄ (aq)	NpOH ³⁺ Np(OH) ₂ ²⁺ Np(OH) ₄ (aq)	PuOH ³⁺ Pu(OH) ₂ ²⁺ Pu(OH) ₃ ⁺ Pu(OH) ₄ (aq)	-
5+	-	-	NpO ₂ OH (aq) NpO ₂ (OH) ₂ ⁻	PuO ₂ OH (aq)	-
6+	-	UO ₂ OH ⁺ UO ₂ (OH) ₂ (aq) UO ₂ (OH) ₃ ⁻ UO ₂ (OH) ₄ ²⁻ (UO ₂) ₂ OH ₃ ⁺ (UO ₂) ₂ (OH) ₂ ²⁺ (UO ₂) ₃ (OH) ₄ ²⁺ (UO ₂) ₃ (OH) ₅ ⁺ (UO ₂) ₃ (OH) ₇ ⁻ (UO ₂) ₄ (OH) ₇ ⁺	NpO ₂ OH ⁺ (NpO ₂) ₂ (OH) ₂ ²⁺ (NpO ₂) ₃ (OH) ₅ ⁻	PuO ₂ OH ⁺ PuO ₂ (OH) ₂ (aq) (PuO ₂) ₂ (OH) ₂ ²⁺	-

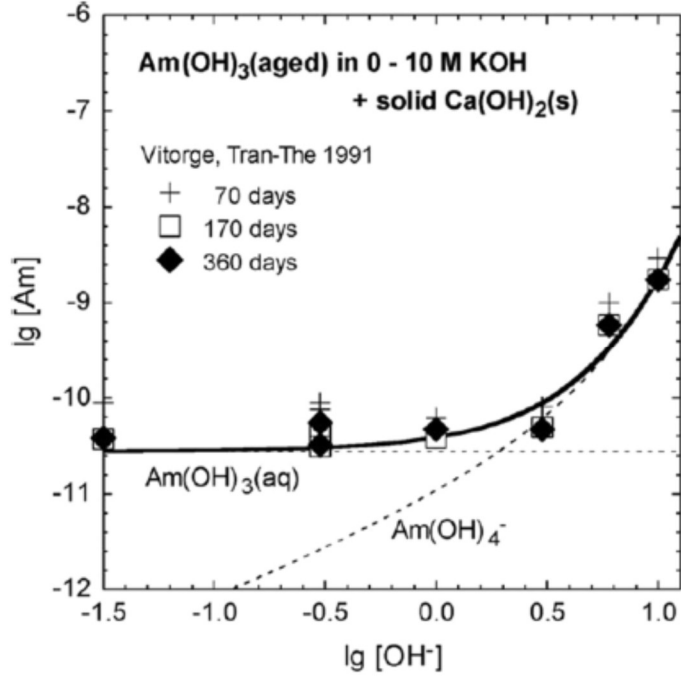


Figure 1.3. Solubility of Aged $\text{Am}(\text{OH})_3(\text{s})$ in increasing alkalinity (0 – 10 M KOH) (Image obtained from Neck et al.^{22,23}).

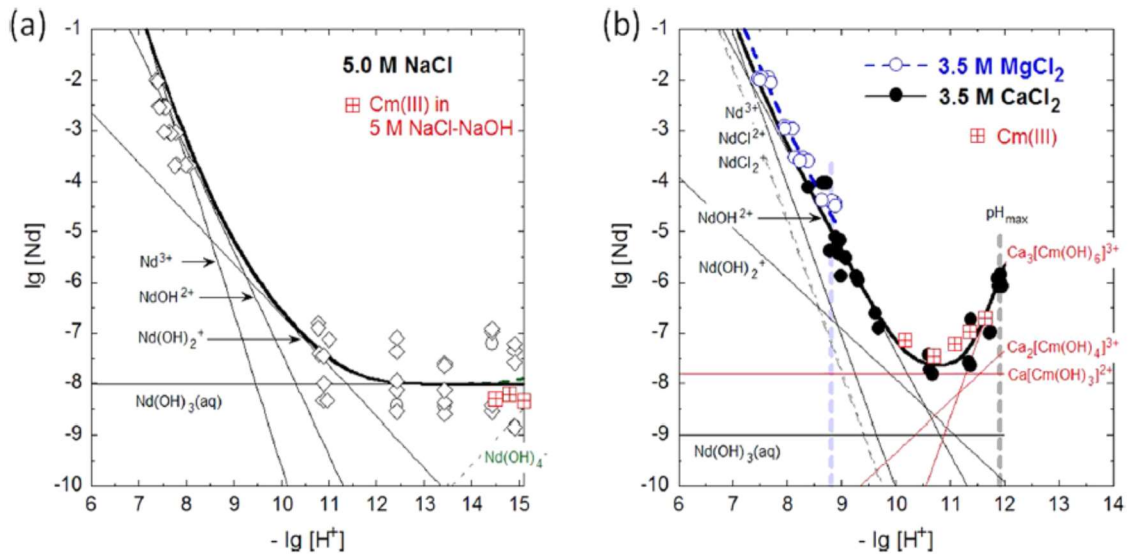


Figure 1.4. Solubility of Nd(III) and Cm(III) under the prevailing alkalinity (a) Solubility of $\text{Nd}(\text{OH})_3$ in 5.0 M NaCl solution. (b) Solubility of $\text{Nd}(\text{OH})_3$ in 3.5 M MgCl_2 and CaCl_2 solution (Image obtained from Neck et al.²²).

1.3 Pretreatment techniques for alkaline HLW

1.3.1 General

Pretreatment techniques are methods used to reduce the overall volume of HLW waste by separating it into HLW and LAW fractions. As in the case of the SRS, LAW is stored onsite in cementitious forms called saltstone or grout, while HLW is incorporated into a borosilicate glass matrix which immobilizes the waste prior to it being stored in geological repositories.⁶ The US DOE has placed strict limits on the amount of radioactivity that should be processed into grout or immobilized for geological repositories using the DOE Order 435.1 and Section 3316, 2005 National Defense Authorization Act.²⁵ For instance, it is mandated that the overall activity of the saltstone grout needs to be below 45.0 nCi/g, and ¹³⁷Cs activity in the grout should never exceed 40.0 μCi/cm³.²⁶ At SRS several methods have been used to process tank waste with special attention to ¹³⁷Cs, ⁹⁰Sr, and the transuranics (TRU), since they generate the bulk of the radioactivity. Figure 1.5 gives an overall schematic of the Integrated Salt Waste Disposal Processing used to separate HLW in the Defense Waste Processing Facility (DWPF) and LAW at the Saltstone Processing Facility (SPF).

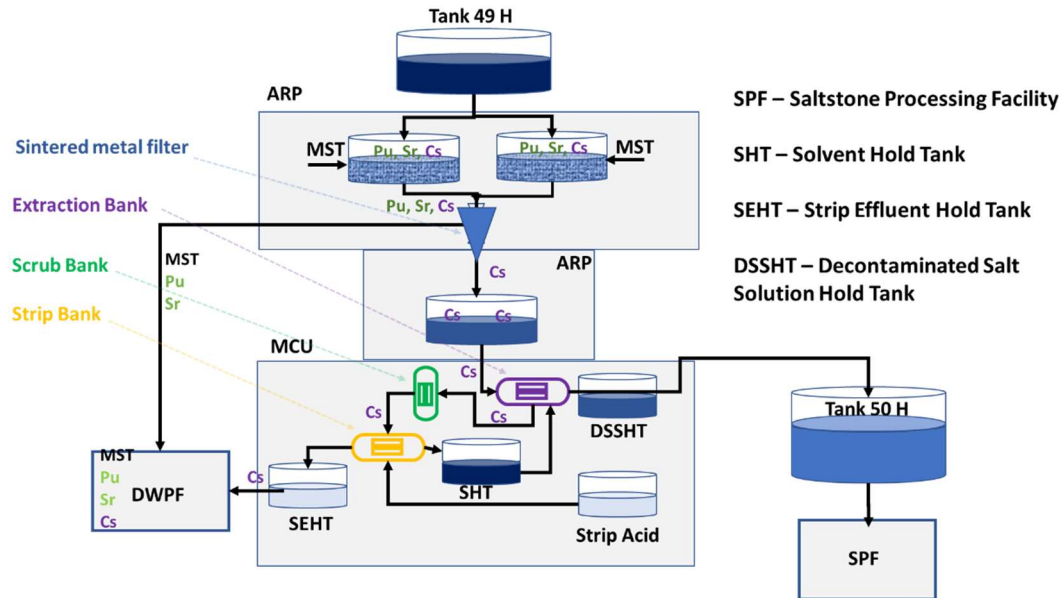


Figure 1.5. Schematic representation of the Integrated Salt Waste Processing Facility at the Savannah River Site.²⁷

1.3.2 Solid-liquid separations

General

Separating solids from solution is one of the preliminary steps required before liquid-liquid solvent extraction: For instance, at SRS, the initial separation of TRU and Sr(II) uses monosodium titanate (MST) during the Actinide Removal Process (ARP) (Figure 1.5), followed by washing of sludge and entrained solids to recover Cr and Al.⁶ Some of the methods which have been proposed and used at SRS to separate solids from liquids are gravity settling and filtration methods (Figure 1.6).

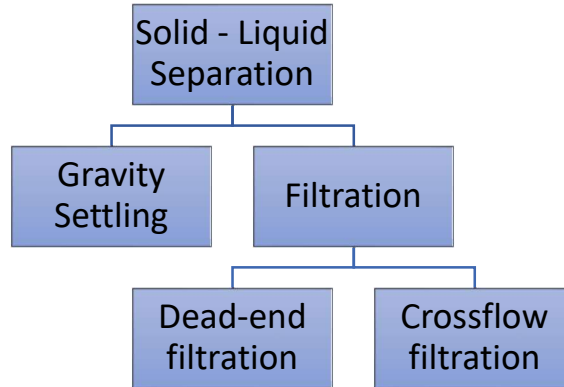


Figure 1.6. Commonly used solid-liquid separation methods at SRS.

Gravity Settling

Gravity settling is used at SRS to separate aqueous soluble metals from insoluble solids in the sludge. It is similar to decantation and involves allowing the solution to settle after washing the solids, in some instances, this is encouraged by adding flocculating agents.^{28,29} The aqueous phase is then collected for onward treatment, while the solids from the sludge (typically of high activity) are sent to DWPF (Figure 1.2).

Filtration

This method involves the separation of insoluble high activity waste from the soluble components in waste tanks, with the two most common methods being the dead-end filtration and the crossflow filtration methods. Dead-end filtration involves the use of a filtration membrane that only allows the liquids to pass through while holding back the solids. In order to improve separation efficiency, several such filters are placed as barriers to the liquid flow. Most dead-end filtration systems are designed in such a way that accumulation of solids on the surface sends a signal that indicates the need for a

change of the membrane or treatment involving chemical washing to regenerate the membrane. The use of dead-end filters however has a major disadvantage: Despite that they typically have a pore size range of just under a micron to several hundreds of microns, most solids in HLW processing are well below 1 micron in size, and as a result, there have been several reported breakthrough events. Such filters are however still useful as a companion treatment method for reducing the amount and size of the solids during processing.^{6,30}

In crossflow filtration, the heterogeneous mixture is forced to pass through a filter tube, where a “filter-tube barrier” collects the solids as solid cakes (Figure 1.7). The solids cakes are then forced to flow as a slurry to one collecting point while the filtrate (or permeate liquid) goes to another.³¹ At SRS, the ARP process employs the use of the crossflow filter to separate the MST, which is loaded with Sr(II) and actinides from the aqueous stream. The permeate is then being fed to the Modular Caustic Side Solvent Extraction Unit (MCU) where Cs(I) is removed.⁶

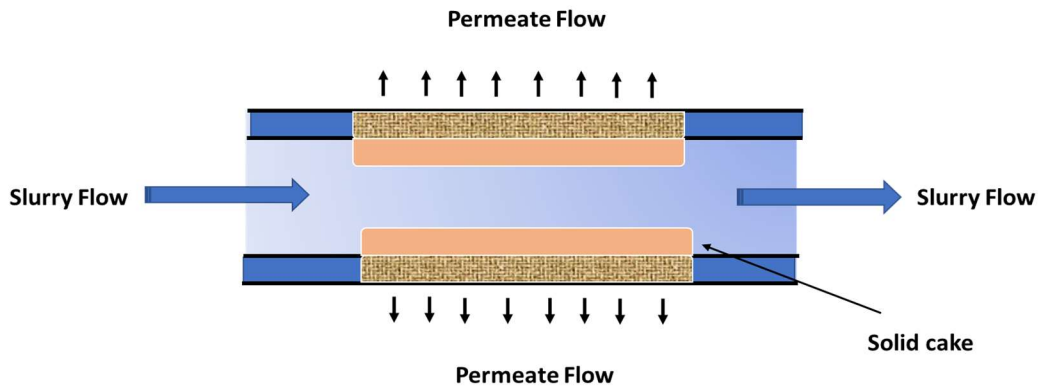


Figure 1.7. A crossflow filter showing the separation of permeate flow from the concentrated slurry. (Wilmarth et al.⁶).

1.3.3 Liquid-liquid separations

While several chelators for f-elements have been reported, particularly regarding the outstanding issue of actinide/lanthanide separation in used nuclear fuel,³²⁻⁴² very few studies exist of f-element complexation in alkaline conditions relevant to HLW separation, which is a unique problem for the US and the former USSR. Many extractants used for metal chelation in acidic media are inadequate in competing with metal hydrolysis in alkaline solutions, and as a result, complexation of f-elements and separation by extraction in very high pHs is a difficult problem. Furthermore, there are interfacial equilibria involved, and the integrity of extractants could be compromised under conditions of high alkalinity, heat, and radioactivity.^{43,44} Organic extractants used for alkaline HLW (such as the calixarenes used for liquid-liquid extraction of Cs) maintain complexation during loading and readily release it under stripping conditions.⁴⁵ A high degree of stability under the prevailing high alkalinity and radioactivity present in HLW has to be ensured after several rigorous stability studies,^{46,47} including on a larger scale.⁴⁸

Based on the complicated nature of alkaline HLW, especially in the presence of several metals with different chemical properties, solvent extraction was found to be particularly efficient for the selective removal of Cs.⁴⁹ Delmau et al. proposed the use of an extraction process comprising of different ligands, each suited to Cs, Sr, and the actinides or the use of serial solvent extractions.⁵⁰ To this end, 4,4'(5')-di(*tert*-butyl)cyclohexane-18-crown-6 (DtBuCH18C6)^{51,52} was synthesized and tested with impressive results for co-extraction and stripping of Cs(I) and Sr(II) under similar

conditions. This was achieved by combining the ligand, 4,4'(5')-di(*tert*-butyl)cyclohexano-18-crown-6 (DtBuCH18C6) (Figure 1.8) and one of several lipophilic carboxylic acids like 2-*n*-dodecyl-2-methylmyristic acid (DMMA), 2-*n*-heptyl-2-methylnonanoic acid (HMNA), 2-*n*-heptylnonanoic acid (HpNA) and 2-*n*-heptyldecanoic acid (HxDA) (Figure 1.8) for Cs(I) and Sr(II) extraction alongside the CSSX solvent system (Table 1.1) in alkaline media.⁵⁰

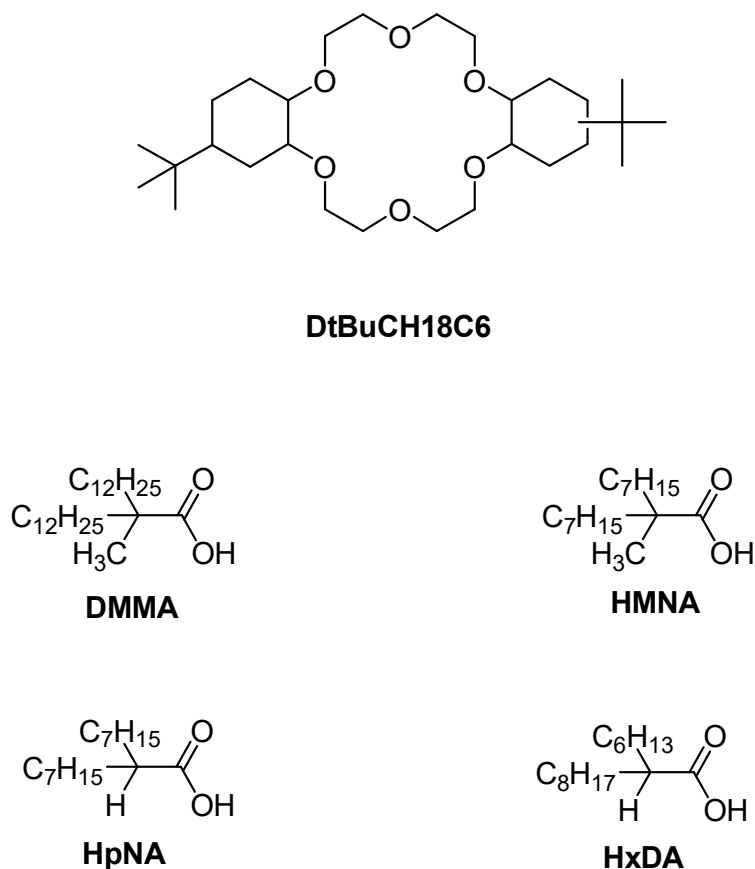


Figure 1.8. Co-ligands used alongside CSSX system for joint Cs(I) and Sr(II) extraction under alkaline conditions.⁵⁰

With regard to f-element chelators, there have been significant contributions by the Raymond group.⁵³⁻⁵⁶ One such extractant was based on 2,3-

dihydroxyterephthalamide (TAM), a catechol derivative, that showed a high binding affinity for Th(IV) with solution thermodynamics giving high binding constants for various TAM derivatives used ($\text{Log } K = 8.28 - 17.47$). TAM analogs are therefore expected to have similar binding properties with Pu(IV).⁵⁵ Similarly other TAM-derived chelators form complexes with Fe(III), Ce(IV), and Pu(IV).⁵³⁻⁵⁶ Using a polyethyleneimine (PEI)/TAM polymer, Gramer et al. prepared a size exclusion ultrafiltration system selective for actinide separation (Figure 1.9) with distribution coefficients $D_{\text{Pu(IV)}} = 1.3 \times 10^3$ at pH 4.5 and $D_{\text{Pu(IV)}} = 4.8 \times 10^6$ at pH 11.5.⁵⁷ Catechol-based ligands can form stable complexes with several metals⁵⁸⁻⁶⁰ including f-elements.^{61,62} Specifically, Kappel et al. demonstrated that catecholamide ligands (CAM) (Figure 1.10) formed complexes with Pu and Am under physiological conditions, with full denticity of the catecholamide more likely for pH > 12.0, suggesting that such catecholamide frameworks are promising for liquid-liquid extraction of f-elements at high pHs,⁵³ such as under HLW conditions.

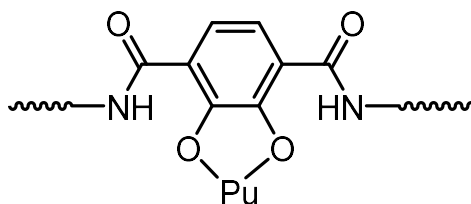
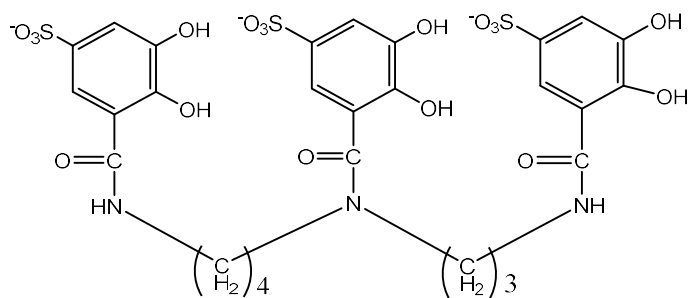
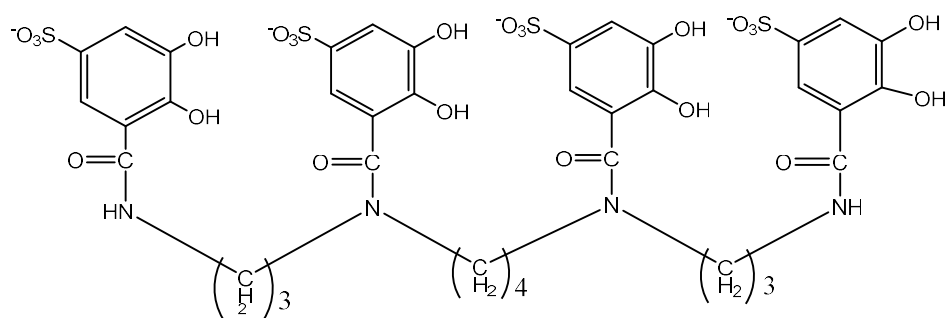


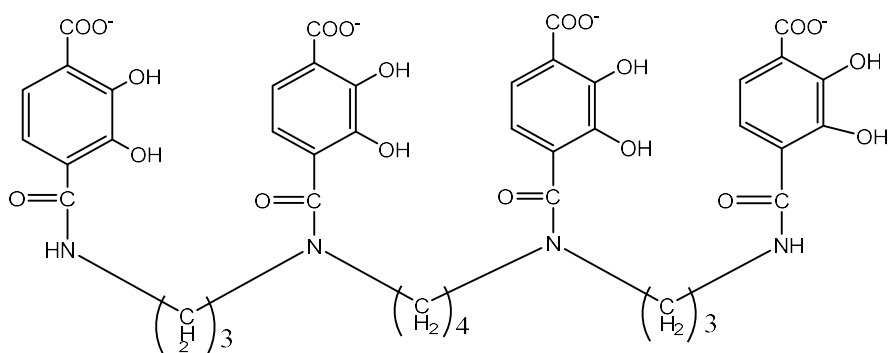
Figure 1.9. TAM derivative upon deprotonation at high alkalinity bound to Pu(IV) via the catecholate oxygens.^{55,57}



(a) 3,4-LICAMS



(b) 3,4,3-LICAMS



(c) 3,4,3-LICAMC

Figure 1.10. Catecholamide ligands studied for actinide removal.⁵³

Complexation and extraction of f-elements under alkaline conditions have also been studied in the former USSR and Russia.⁴¹ Some of the earlier successful extractants for f-elements in alkaline media include aliphatic amine / quaternary ammonium salt systems, such as Aliquat-336,⁶³ chelators with hydroxyl groups, including aminomethyl

derivatives of alkylphenols, such as 2-hydroxy-5-alkylbenzyl-diethanolamine (DEAP),⁶⁴ and alkyl-substituted pyrocatechols, such as 4-(α,α -dioctylethyl) pyrocatechol (DOP)⁶⁵ (Figure 1.11). Other phenolic classes of compounds studied include alkyl-substituted phenol-based oligomers⁶⁶ and a few calix[n]arene analogues.⁶⁷

Aliphatic amine / quaternary ammonium salt systems (QAB), such as Aliquat-336 (an ionic liquid), are typically mixtures of octyl and decyl chain analogs used to extract actinides from carbonate solutions.⁶³ Typically at the pHs of the tank waste, aliphatic amines do not get deprotonated and so anion exchange appears to be the mechanism for actinide extraction.⁶⁷ For this class of extractants, primary amines like decylamine performed better for Am extraction by about a factor of 3 compared to secondary dioctylamine and tertiary trioctylamine.⁶⁷ Aminomethyl derivatives of alkylphenols, such as 2-hydroxy-5-alkylbenzyl-diethanolamine (DEAP) and alkyl-substituted pyrocatechols, such as 4-(α,α -dioctylethyl) pyrocatechol (DOP) have higher extraction efficiency and stability at higher alkalinity than amines or QABs. Studies using these extractants were performed at high alkalinity in the presence of carbonates with up to 3 M DEAP⁶⁴ or 8 M DOP,⁶⁵ and NaOH concentration as high as 6 M in the case of the DOP experiment.⁶⁵ For DOP, the addition of 2 M K_2CO_3 enhanced selective recovery of Bk over Am ($SF_{Bk/Am} \approx 100$)⁶⁸ and also led to group recovery of Am, Cm, and Eu from 2 M KOH.^{68,69} DEAP appeared to be more stable under these conditions than DOP, allowing separation of Am and Cm from other actinides ($SF_{(Am,Cm)/(U,Pu,Ru,Zr,Nb)} > 400$)⁶⁸, and separation of Ce and Eu from other Ln ($SF_{(Ce,Eu)/(Lu,Tm,Tb)} = 10^3$). Pyrocatechols are in general promising extractants for actinides

and rare earth elements (REE), because under the prevailing conditions they are highly soluble in the diluents used and the ligand function is not negatively affected by redox chemistry.⁷⁰ When dilute diethylenetriaminepentamethylphosphonic acid (DTPA) was used as the aqueous phase in the presence of NaOH, increased selectivity for separation of transplutonium elements from REE was observed based on favorable kinetics.⁷⁰ High extraction efficiency (up to 100%) at high pH for Am(III) and Cm(III) was demonstrated by DOP allowing for selective separation from Eu(III) when toluene was used as diluent.⁷⁰ Overall, metal extraction efficiency was mostly poor at lower pH due to less deprotonation of the phenol.⁶⁹ After extraction, metal recovery from the organic phase was easily achieved using inorganic acids.

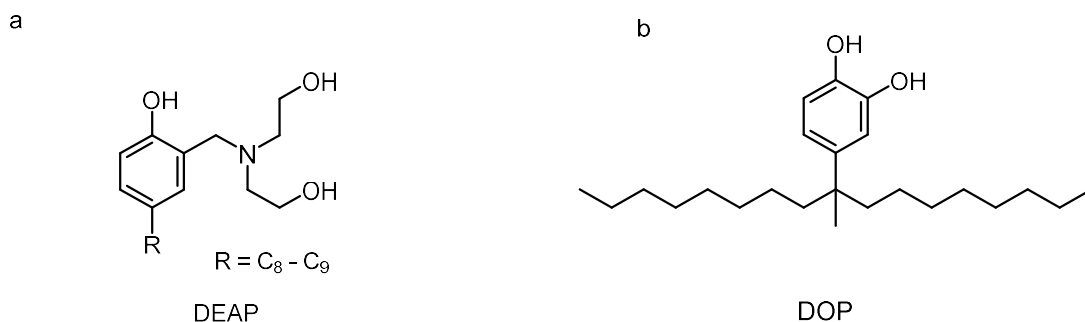


Figure 1.11. (a) 2-hydroxy-5-alkylbenzyl-diethanolamine (DEAP) (b) 4-(α,α -dioctylethyl) pyrocatechol (DOP).^{64,65}

Other examples of f-element extractants are alkylphenol-based oligomers (Figure 1.12). Alkylphenol oligomers studied at pH > 13.0 demonstrated strong extraction for Am.⁶⁶ ($D_{Am} > 100$ with YaRB,⁶⁶ $D_{Am} > 30$ for Oktofor 10S and $D_{Am} > 50$ for Oktofor 101K).^{66,67} Extraction at even higher pH showed similar distribution coefficients, for

Oktofor 101K, but not so for YaRB and Oktofor 10S.⁶⁷ Various derivatized calixarenes have also been studied for the extraction of transplutonium elements.^{68,71-73} In one such study, Smirnov et al.⁶⁸ compared extraction by monomeric *p-tert*-butylphenol vs. by the preorganized *p-tert*-butylcalix[4]arene and revealed that under similar conditions *p-tert*-butylphenol ($D_{Am} < 0.04$) was 10 times less effective than *p-tert*-butylcalix[4]arene ($D_{Am} = 0.38$),⁶⁸ the difference being attributed to cooperativity due to preorganization in *p-tert*-butylcalix[4]arene. In the same study, replacing one or more hydroxyl groups on the lower rim of the *p-tert*-butylcalix[4]arene, with pendant pyridine groups (Figure 1.13), improved separation selectivity for Am over Eu, $SF_{Am/Eu} = 3.0$. Overall, these calixarenes as well as the corresponding monomer showed poor solubility in process solvents.⁷¹

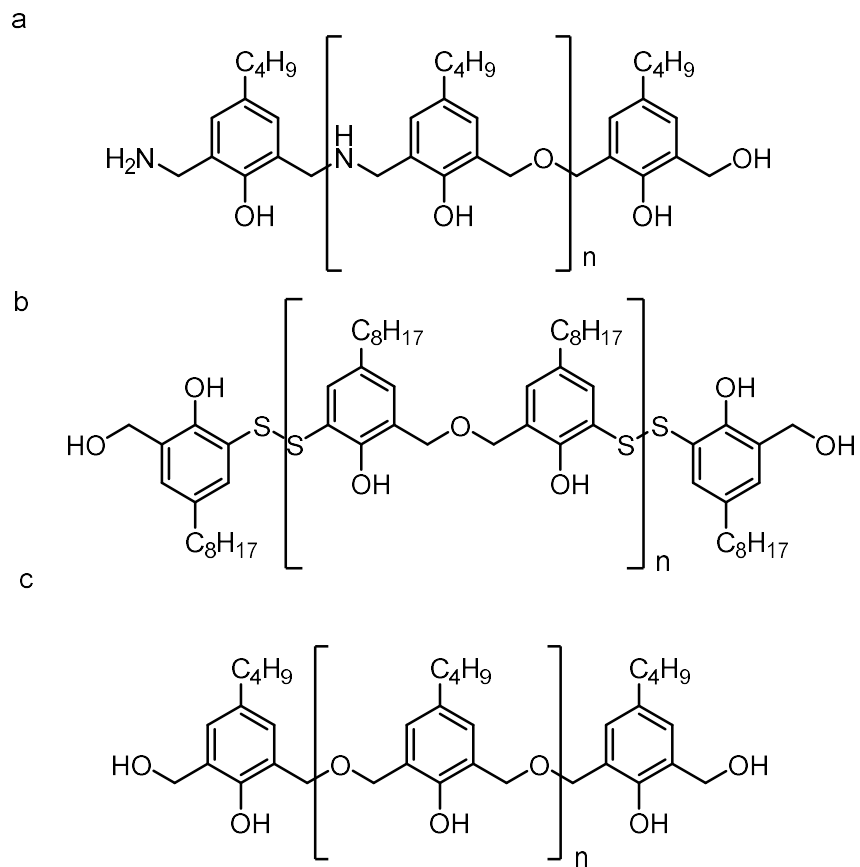


Figure 1.12. Alkylphenol Oligomers: (a) YaRB (b) Oktofor 10S (c) Oktofor 101K⁶⁷

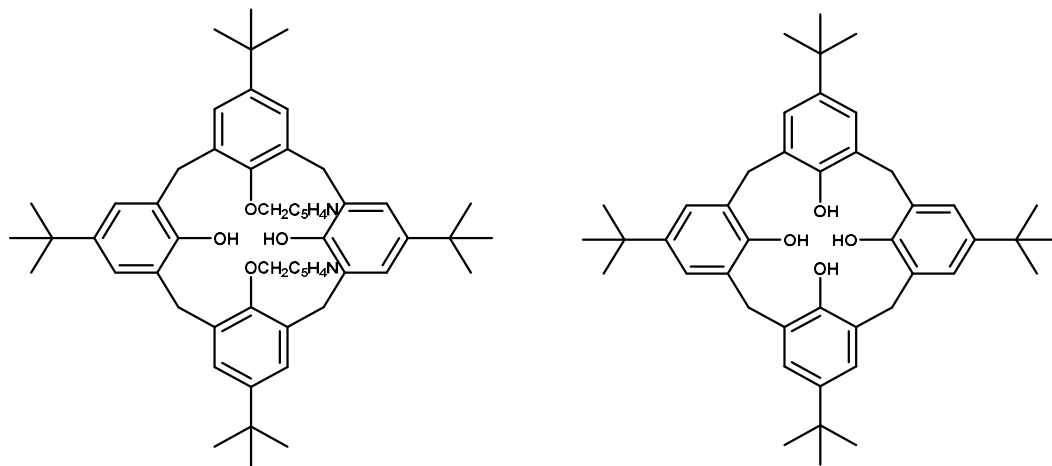
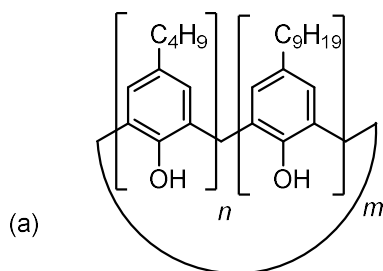


Figure 1.13. (left) *p*-tert-butylcalix[4]arene bearing pendant pyridine groups. (right) *p*-tert-butylcalix[4]arene.⁶⁸

In an attempt to address the issue of poor calixarene solubility, Ivenskaya et al.⁷² synthesized several calix[8]arenes bearing mixed ratios of *tert*-butyl and isononyl groups at the upper rim of the calix[8]arene para to the hydroxyl groups (Figure 1.14). Specifically, for all derivatives maximum extraction efficiency for Cs(I) was observed at pH 13.5 – 14.0 and for Am(III) around pH 13.0 – 13.5. Furthermore, the calix[8]arene with the highest isononyl substitution ratio gave the highest solubility in tetrachloroethylene (TCE), however, this was not translated to higher extraction efficiency. Instead, the calix[8]arene with *tert*-butyl: isononyl ratio of 6:2 gave the highest efficiency for Am(III) with $D_{Am} \approx 3.2$. For Cs(I), modest extraction with $D_{Cs} \approx 4.0$ was observed, which was lower than by the calix[8]arene with *tert*-butyl: isononyl ratio of 8:0 ($D_{Cs} \approx 6.3$). Encouraged by these results, Ivenskaya et al.⁷² proceeded to perform an extraction with real alkaline HLW bearing Cs–137, Pu–239, and Am–241. By measuring the difference in activity after extraction, it was determined that 97% of β -emitting Cs–137 and 71% of γ -emitting TRU radionuclides were extracted after four contacts with fresh organic phase (calix[8]arene with *tert*-butyl: isononyl ratio of 6:2 in tetrachloroethylene).⁷²



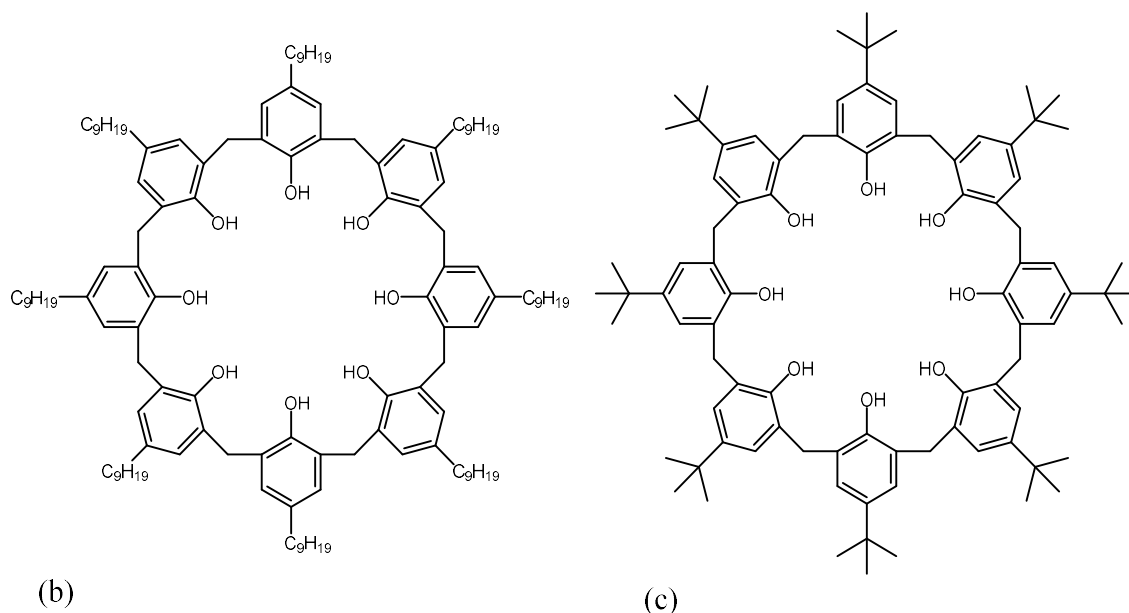


Figure 1.14. (a) *p*-Alkylcalix[8]arenes with a combination of *tert*-butyl and isononyl substituents, n = number of *tert*-butyl groups present, m = number of isononyl groups present. (b) isononylcalix[8]arene (c) *p*-*tert*-butylcalix[8]arene.

1.3.4 HLW processing at the Savannah River Site

General

Although HLW supernatants at SRS contain mainly ^{137}Cs ($t_{1/2} = 30.2$ years), ^{99}Tc ($t_{1/2} = 2.1 \times 10^5$ years), and ^{90}Sr ($t_{1/2} = 29$ years) as well as several non-radioactive cations and anions, there is a significant amount of TRU elements in it, as well.⁶ ^{137}Cs and ^{90}Sr especially, despite their relatively low half-lives, dominate the tank waste and are major factors in waste treatment design, because treatments must ensure considerable selectivity for cesium separation over the overwhelming amount of sodium and potassium in solution. For cesium separation, several methods at SRS have been proposed and adopted with the solvent extraction approach, being the method that was

the most successful and was optimized for scale-up.⁴⁵ Previous methods include (i) In-Tank Precipitation (ITP)⁷⁴ involving the use of sodium tetraphenylborate to precipitate and remove ¹³⁷Cs. This method was discontinued due to the uncontrolled decomposition of sodium tetraphenylborate and the subsequent release of benzene to the tank headspace. (ii) Selective dissolution which involved the removal of soluble Cs and Tc lodged within the interstitial spaces of the saltcake by spraying water at 100 psi and 380 L/min to dislodge any soluble salts of Cs and Tc before further reprocessing.⁸ This approach is however difficult as recovery rates for the metals were dependent on the porosity of the saltcake. (iii) Ion exchange using polymeric organic resins or inorganic materials,^{75,76} including Superlig[®] 644,^{75,77} resorcinol – formaldehyde^{78,79} and crystalline silicotitanate (CST)^{80,81}. Even though high decontamination factors can be achieved with the use of resins, they tend to degrade over a long time due to excessive exposure to chemical and radiolytic attack,⁶ they are often not reusable (as is the case with CST), thus creating a secondary waste problem, and they also have practical handling problems when loaded with Cs, due to very high activity. iv) Solvent extraction using specialized ligands, which was finally adopted as the preferred method for removing Cs at SRS. Specifically, Cs is selectively removed from HLW at SRS by the Caustic Side Solvent Extraction (CSSX) process, while Sr and An are removed by the actinide removal process, which is a solid-liquid crossflow filtration sorption process.

Strontium & Actinide Removal Process (ARP)

The ARP process, as used at SRS, involves the sorbent monosodium titanate (MST) for the removal of ⁹⁰Sr and TRU through sorption. MST was synthesized and used at Sandia National Laboratory; it is an inorganic solid that strongly binds strontium

in alkaline solutions.⁵¹ A scanning electron microscopy image of MST is shown in Figure 1.15.⁶ While MST (added as a finely divided powder) is able to remove most of the Sr in the supernatant stream in the Integrated Salt Waste Processing Facility (ISWPF), multiple loads are required to completely remove the actinides, considerably slowing down the process (Figure 1.19).⁸² This presents a financial and kinetic bottleneck in reaching the DOE deadlines for waste treatment, especially considering that the CSSX process, which removes Cs(I) subsequently, is substantially faster. The slow kinetics of actinide removal by ARP remains a problem, therefore there is an impetus for removing some actinide components by solvent extraction, which is a more rapid method compared to sorption.

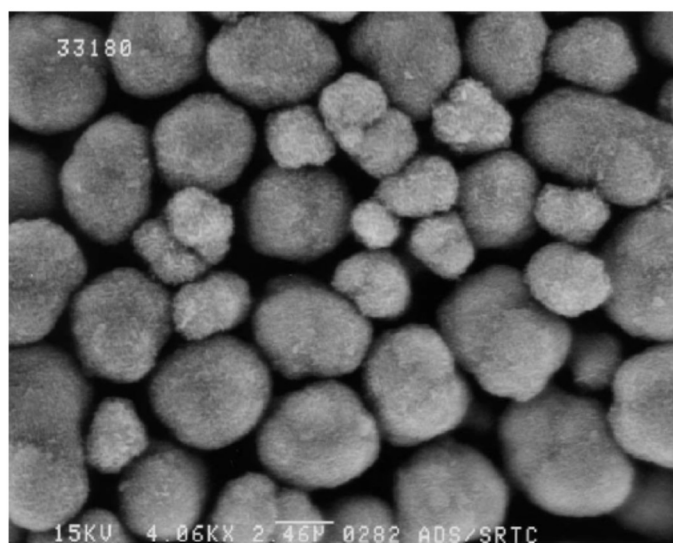


Figure 1.15. Scanning electron microscopy image of monosodium titanate. (Image obtained from Wilmarth et al.⁶).

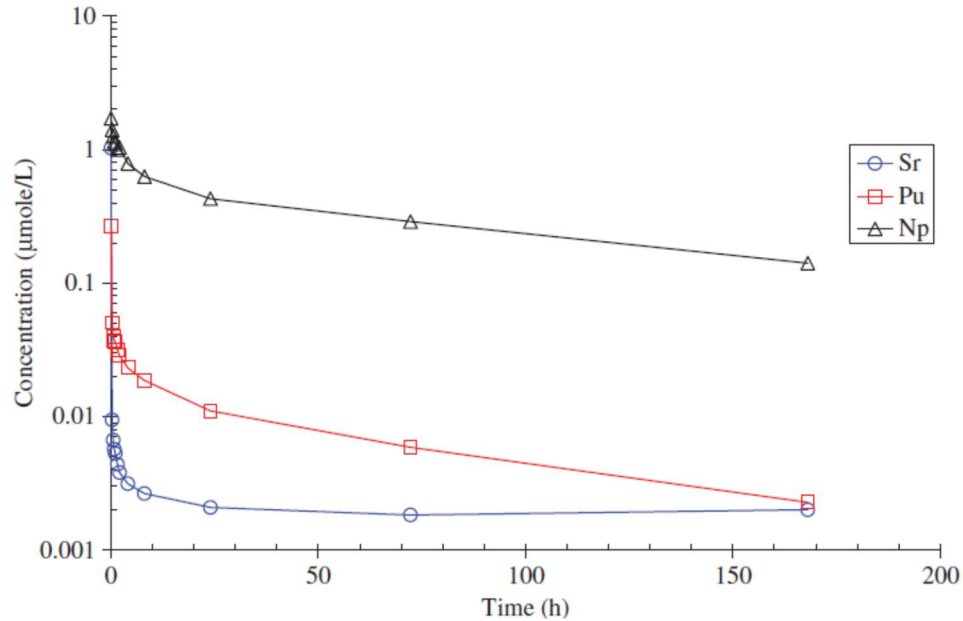


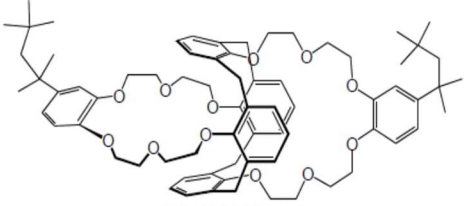
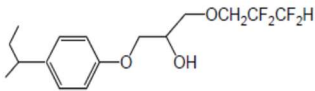
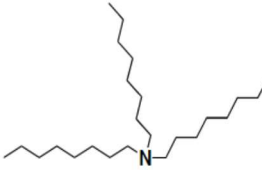
Figure 1.16. Sorption time for strontium, plutonium, and neptunium using 0.4 g/L of MST (Image obtained from Wilmarth et al.⁶).

Cesium removal at the modular Caustic Side Solvent Extraction Unit (MCU)

After the removal of Sr and An, the treated aqueous supernatants are sent to the MCU for Cs removal. ¹³⁷Cs separation from the waste stream is based on solvent extraction using the CSSX solvent, comprised of four components (Table 1.2):^{45,83} (1) The extractant - BOBCalixC6 which is very selective for Cs(I) extraction even in the presence of Na(I) and K(I) (which are predominant in HLW); (2) Cs-7SB, which is a fluorinated alkyl phenoxy-alcohol modifier used to improve the solubility of BOBCalixC6 and inhibit the formation of a third phase; (3) Tris-*n*-(octyl)amine, which is an organic base used to suppress the interference of anionic impurities and to increase stripping efficiency after Cs extraction; and (4) Isopar-L®, which is a commercial hydrocarbon diluent. To carry out liquid-liquid extraction, the organic solvent is pumped through centrifugal contactors while the ARP-treated aqueous stream is pumped in

through the opposite direction creating a counter-current flow.^{6,84} Cs extraction and separation by CSSX is highly effective because of strong complexation resulting in the neutral [(BOBCalixC6)Cs⁺]NO₃⁻ in the organic phase, facilitated through high nitrate concentrations in the aqueous feed.⁴⁵ In order to reduce the interference of the non-radioactive cations Na⁺ and K⁺ which could be partially embedded in the organic solvent system, scrubbing with 0.05 M nitric acid is performed on the organic phase prior to stripping. Back-extraction (or stripping) using dilute nitric acid is then used to release Cs(I) as CsNO₃ from the organic phase into the acidic aqueous phase for onward concentration before vitrification at the DWPF, while the stripped organic phase is reused to contact a fresh Cs-laden stream (Figure 1.17).⁴⁵ Typical decontamination factors (DF), defined as Cs extracted divided by Cs left in raffinate, obtained were over 100000, surpassing the initial target of 40000.^{6,84}

Table 1.2. CSSX components and concentrations for Cs extraction during CSSX (Image obtained from Moyer et al.⁴⁵).

Extractant	Modifier	Suppressor
 <p>BOBCalixC6 Calix[4]arene-bis(<i>tert</i>-octylbenzocrown-6)</p>	 <p>Cs-7SB 1-(2,2,3,3-tetrafluoropropoxy)-3-[4-(<i>sec</i>-butyl)phenoxy]-2-propanol</p>	 <p>TOA Tri-<i>n</i>-octylamine</p>
0.007 M	0.75 M	0.003 M

^aThe components are dissolved in Isopar[®] L diluent, an isoparaffinic hydrocarbon.

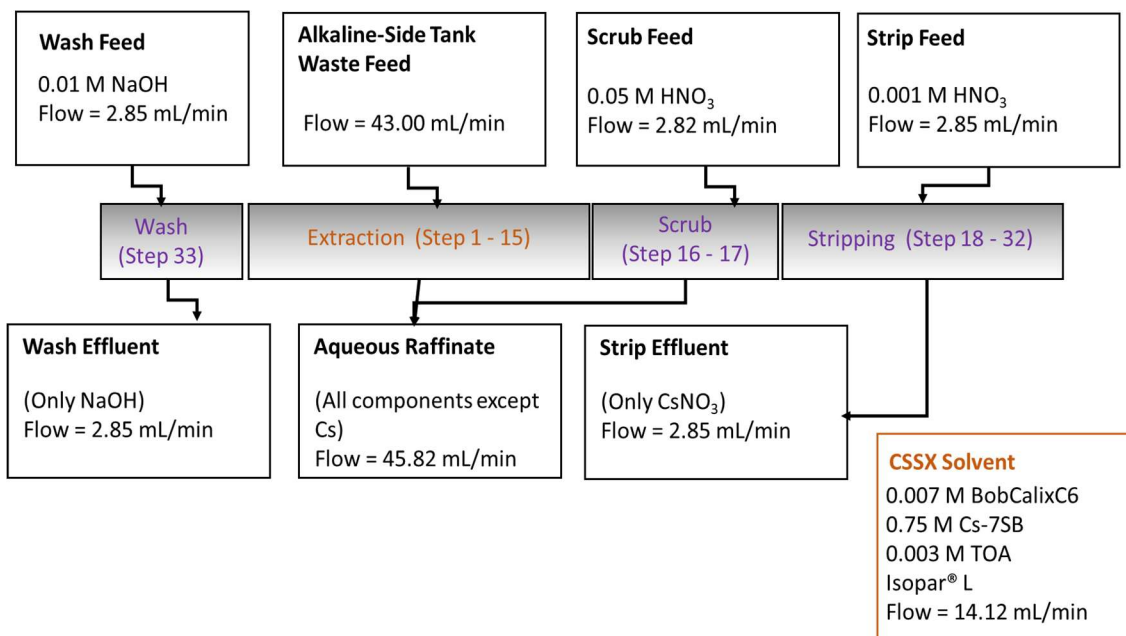
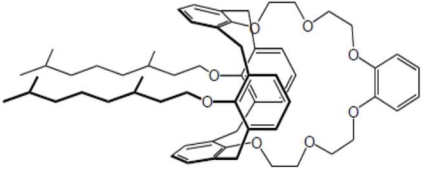
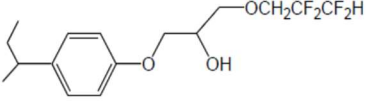
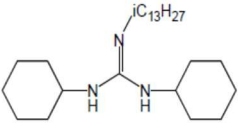


Figure 1.17. Schematic flowsheet for ¹³⁷Cs removal using CSSX at SRS.⁶

Initial testing^{83,85} of CSSX for the ISWPF began when the MCU at SRS came online in April 2008, and within three years it succeeded in processing over 2 million gallons of waste.^{45,48} However, to accelerate the cleanup schedule and improve the CSSX performance, a modification of CSSX was adopted in September 2013, referred to as the Next Generation Caustic Side Solvent Extraction, (NG-CSSX).^{8,86} NG-CSSX with a new solvent system and a more lipophilic extractant, MaxCalix allows higher ligand concentration and therefore higher extraction attained for the same number of contacts between phases. Improved stripping chemistry has also been developed, in which boric acid is used as a stripping agent. The advantage here is that borates formed after stripping are more compatible with the vitrification process. Other modifications include the use of NaOH as scrubbing agent⁴⁵ and a new guanidine suppressor, which is

more compatible with the boric acid stripping.⁸⁷ Table 1.3 gives the components of NG-CSSX.

Table 1.3. NG-CSSX components and concentrations for Cs extraction from HLW (Image obtained from Moyer et al.⁴⁵)

Component	Concentration	Code	Chemical Name	Structure
Extractant	0.050 M	MaxCalix	1,3- <i>alt</i> -25,27-Bis(3,7-dimethyloctyl-1-oxy)calix[4]arene-benzocrown-6	
Modifier	0.50 M	Cs-7SB	1-(2,2,3,3-Tetrafluoropropoxy)-3-(4- <i>sec</i> -butylphenoxy)-2-propanol	
Suppressor	0.003 M	LIX [®] 79	<i>N,N'</i> -Dicyclohexyl- <i>N''</i> -isotridecylguanidine	
Diluent		Isopar L	C ₁₂ -isoparaffinic hydrocarbon	

While BOBCalixC6 and more recently MaxCalix are the extractants of choice for integrated salt waste processing at SRS, these extractants are often expensive and difficult to synthesize, and even NG-CSSX still does not address the issue of residual actinide removal during extraction. An ideal extraction system should be able to remove all highly-radioactive components in a single process. Although CSSX and NG-CSSX are mature and enormously successful processes for Cs removal and have been employed together with ARP for years for integrated treatment, there is plenty of room for improvement: An actinide extractant additive compatible with the CSSX solvent could accelerate overall processing by minimizing the contact time and amount of titanate needed during ARP and thus can greatly improve the overall economics of integrated processing. Therefore, this dissertation aims to study f-element extraction in

alkaline conditions by lipophilic ligands, with the greater long-term goal of improving the CSSX process and overall HLW processing.

1.4 Ligand design criteria

In the design of extractants for actinide separation, especially if solvent extraction is the desired method of separation, several factors must be considered: (i) The ligands should be synthesized in only a few steps from commercially available starting materials, with straightforward synthetic scale-up. (ii) The ligand should typically contain electron-rich “hard Lewis-base” binding sites bearing atoms like O, and N, and in some cases halogens, as these electronegative atoms complement the hard Lewis-acid character of f-elements.⁸⁸ (iii) f-Elements typically have a high coordination number ($CN > 6$) and therefore ligand design must take into account the need to have multiple binding sites. However, the coordination sphere should also be designed to accommodate counterions to give an overall neutral complex, extractable into an organic solvent. Anions, such as nitrates and hydroxides are often bound to the first coordination sphere of the metal to result in neutral complexes. Counteranions in the second sphere are also often involved as well, in case of anionic metal complexes.⁸⁹ (iv) The ligands should exhibit some selectivity for extraction of f-elements. As the Ln(III) component in HLW is minimal, Ln(III) are used in this work as surrogates for An(III), and therefore selectivity for An(III) vs. Ln(III) extraction from alkaline solutions is not necessary. However, selectivity against other metals present in high concentration at HLW, such as Na, K, Sr, Ca, and Cs is critical. Selectivity in the presence of Al and some transition metals present in lower concentrations at some HLW supernates is also highly desirable. (v)

Since most solvent extraction systems are designed to extract metals into organic diluents (like dodecane) from an aqueous phase, a high degree of lipophilicity is expected for ligands to form soluble and stable complexes in the organic phase. Alkyl substituents, including branched alkyls, are especially useful for this purpose. (vi) For ligands to be efficient in the harsh radiolytic and alkaline conditions of HLW, they need to be robust and stable to degradation, hydrolysis, and oxidation under the prevailing conditions. (vii) Metal coordination with the desired ligand should be labile enough to enable fast stripping after extraction, with minimal phase partitioning, thus encouraging the use of the ligand for multiple contacts. (viii) In addition to the above, ligands that are being designed to optimize an existing extraction process, like CSSX or NG-CSSX, need to be compatible with the solvent system already in place so that additional engineering obstacles during process modification are minimized.

1.5 Sulfonamides for metal complexation, extraction, and sensing (including f-elements).

During the early 1930s, sulfonamides or Sulfa drugs as they became popularly called, came to be seen as miracle drugs⁹⁰ because they had vast chemotherapeutic properties for the treatment of bacterial infections like gonorrhea, pneumonia, urinary tract, and intestinal tract infections.⁹¹ Their use was also extended to veterinary and herbicidal purposes.^{92,93} Secondary sulfonamides bear the $R_1-SO_2NH-R_2$ group and apart from being bioactive compounds, they have been very useful as sensors,⁹⁴⁻⁹⁶ and chelators for metals^{94,97-101} for environmental applications due to the presence of electron-rich O- and N- donor sites (when the -NH is deprotonated). Synthesis of sulfonamides vary^{97,102-104} with a common synthetic pathway based on the reaction of a

sulfonyl chloride derivative of choice with nucleophilic amine or aniline derivatives⁹⁷ in the presence of an organic base.

Sulfonamides present an interesting class of compounds for the complexation and extraction of metals, and in our case, f-elements. The direct proximity of the -NH group to the strongly electron-withdrawing sulfonyl group makes them quite acidic¹⁰⁵ (Figure 1.18), with the degree of acidity further tuned by the choice of aryl- or alkyl- substituents at R₁ and R₂,¹⁰⁶ hence in alkaline conditions deprotonation is expected to occur giving rise to ionizable chelates, with deprotonated nitrogen⁹⁷ and sulfonamide- oxygen atoms^{101,107,108} that provide electron-rich N- and S=O binding sites for metals. Therefore, ligands bearing the sulfonamide moiety are versatile Lewis bases for complexation of charge-dense metals (Lewis acids).

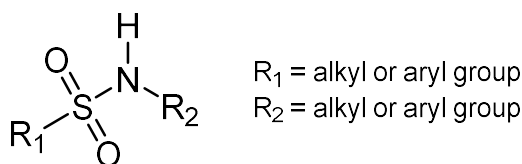


Figure 1.18. Schematic representation of the sulfonamide moiety.

Over the years there has been a steady growing interest in the complexation of metals using sulfonamides. Zhao and coworkers described the synthesis and X-ray characterization of several sulfonamide complexes with aluminum and lithium,¹⁰⁹ Blaschette et al. reported the X-ray structure of an indium-sulfonamide complex bearing two crystallographically independent dimers, with indium atoms linked by two N-S-O bridges,¹¹⁰ Topala and coworkers reported a sulfonamide quinoline derivative bearing a pyridine ring for complexation of Cu(II), Ni(II), Zn(II), and Co(II) along side several

DNA binding studies.¹¹¹ Wenjie et al., on their part reported the synthesis of a bidentate N-heterocyclic carbene-sulfonamide for complexation of palladium.¹¹² In our group, *o*-phenylenediamine-derived sulfonamides were reported to complex,^{97,98} sense,⁹⁴ and extract^{97,98} Pb(II) either with or without a 2,2-bipyridine co-ligand (Figure 1.19).⁹⁷

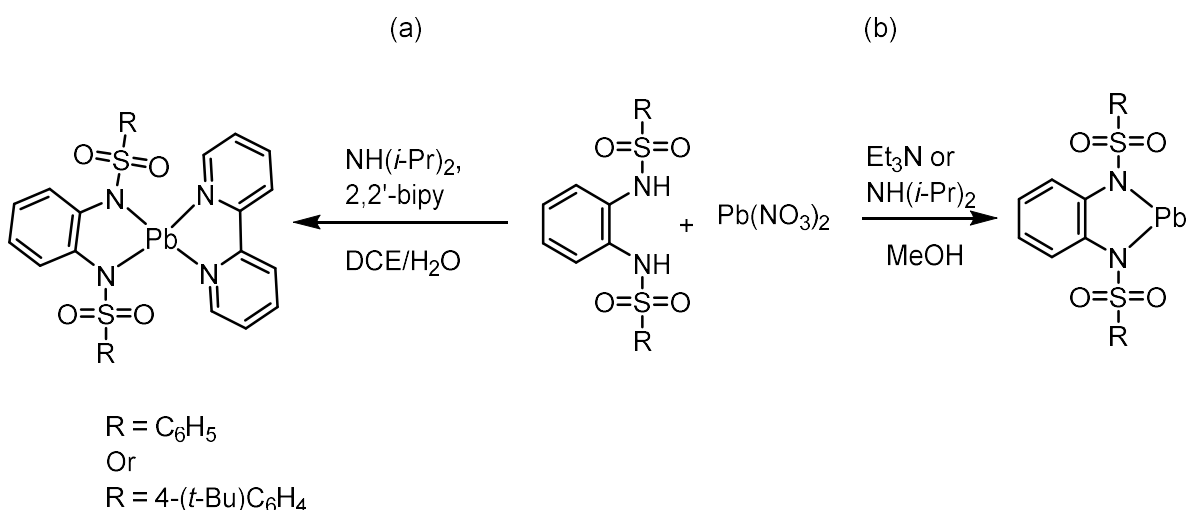


Figure 1.19. Complexation reaction of *o*-phenylenediamine derivatives with $\text{Pb}(\text{NO}_3)_2$ in the presence of organic base diisopropylethylamine and co-ligand bipyridine to give a ternary complex (a) or without the co-ligand giving the binary complex (b).⁹⁷

Sulfonamides have also been studied in our group for f-element complexation and extraction in alkaline conditions. Morozov et al. carried out extraction studies using a preorganized trisulfonamide (4-*i*Pr-tsa) for extraction of Sm(III) (Figure 1.20 (a)), with 52% Sm(III) recovery obtained after a single loading cycle using dichloromethane as organic diluent, followed by stripping with nitric acid.¹⁰⁰ In the same study, DFT calculations revealed a high tendency for hydrolysis of the metal, yet successful complexation and extraction was achieved due to high concentration of nitrate in the aqueous phase, which facilitated peak extraction at pH 10.0. More recently, improved

results for f-element extraction in alkaline conditions were reported by our group, with *o*-phenylenediamine sulfonamide derivatives (dsa) (Figure 1.20 (b)).⁸⁹ These ligands showed up to 81% Sm(III), recovery after a single loading/stripping cycle at pH 13.0. Slope analysis and UV-Vis titration suggested 1:1 ligand stoichiometry, and theoretical DFT calculations revealed the thermodynamically favorable formation of close ion pairs of type $\text{Na}^+[\text{Sm}(\text{dsa}^{2-})(\text{OH})_2 \cdot 2(\text{H}_2\text{O})]^-$ org.

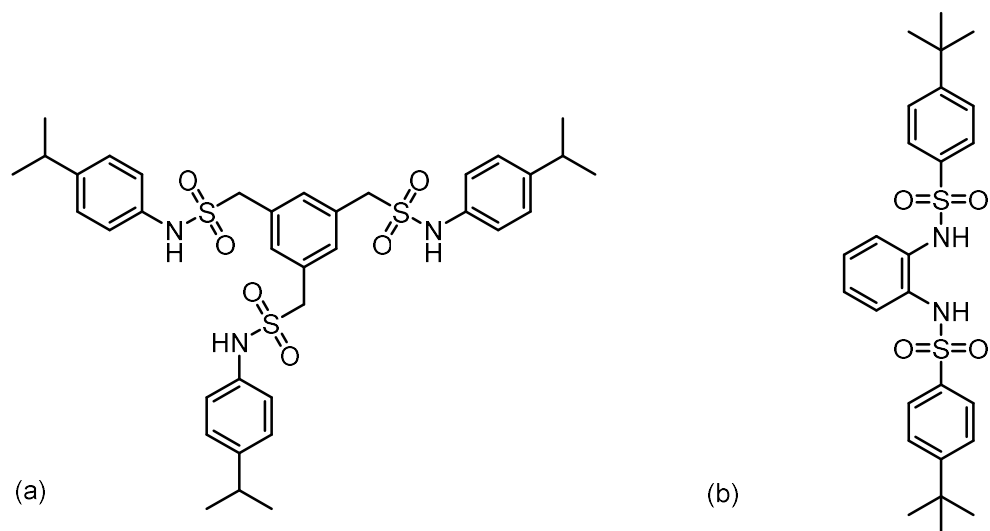


Figure 1.20. Sulfonamide ligands for *f*-element extraction from alkaline medium (a) 4-*ipr*-*tsa*¹⁰⁰ (b) *dsa*⁸⁹

Metal sensing by fluorescence is typically based on photoinduced electron-transfer (PET) or photoinduced charge-transfer (PCT),¹¹³ with PET resulting in an increase in fluorescence intensity, while PCT shows a shift in the excitation and emission bands.¹¹⁴ Fluorescence quenching on the other hand could be as a result of excited-state interactions, molecular rearrangement or collisional quenching due to binding between the fluorescent sample and the quencher.¹¹⁵ The dansyl group is widely used for sensing, as a result of its strong fluorescence. Our group has reported a

dansylamide derivative of *o*-phenylenediamine as a selective Pb(II) sensor vs. Ni(II), Co(II), Cu(II), Zn(II), and Cd(II).⁹⁴ The sensing is based on selective extraction in an organic phase with $D_{\text{Pb(II)}} / D_{\text{M(II)}} = 1410$ (for Zn), 1380 (for Co), 829 (for Cd), 794 (for Ni), 133 (for Cu). Investigation of the organic phase after extraction revealed quenching of the initial ligand fluorescence by 29% as a result of Pb(II) coordination. Other dansylamide ligands have been used for sensing transition metals (Figure 1.21). Wanichacheva and coworkers investigated a fluoroionophore (Figure 1.21 (b)) which gave high sensitivity and selectivity for Hg(II) with turn-on fluorescence even in the presence of other cations in a solution of acetonitrile and water, along with a sub-micromolar detection limit of 2.49×10^{-7} M for Hg(II)¹¹⁶. Tharmaraj and coworkers also developed a fluorescent chemosensor for Hg(II) with selective on-off fluorescence quenching for Hg(II) through twisted intermolecular charge transfer (TICT).¹¹⁷ Likewise, Jiang et al. synthesized a selective fluorescent chemosensor for Zn(II), with initial selectivity for Zn(II) established by UV-Vis titrations and comparison with Na(I), K(I), and Ca(II) titrations that gave no response, while transition metals gave lower responses.¹¹⁴ Fluorescence titrations in a solution of DMSO and water gave fluorescence quenching for Cu, Ni, Mn, Fe, and Co while enhanced fluorescence was observed for Zn (Figure 1.21 (c)).¹¹⁴

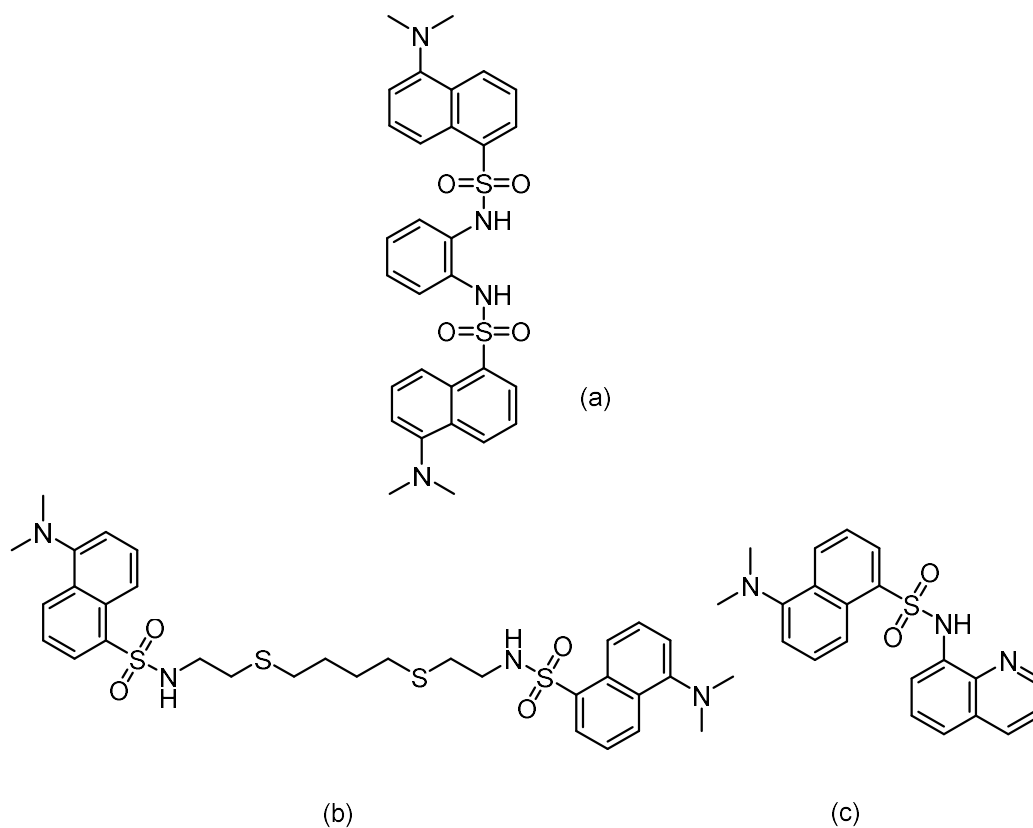


Figure 1.21. (a) Dansylamide derivative of *o*-phenylenediamine for Pb(II) sensing and complexation.⁹⁴ (b) A bis-dansylamide sensor for Hg(II)¹¹⁷ (c) Dansylamide sensor for Zn(II).¹¹⁴

1.6 Methods for quantification of Metal – Ligand interactions

1.6.1 General

There are several forms of covalent and non-covalent interactions between species, of variable strength, and thus many ways to quantify and describe these interactions. With regard to metals, important values of concern are binding (or formation) constants and metal-ligand binding stoichiometry, which is related to coordination number. While techniques used to elucidate metal-ligand interactions

include infrared spectroscopy, NMR, elemental analysis, UV-Vis, fluorescence spectroscopy, and single-crystal X-ray diffraction, spectroscopic titration methods are ideal for quantifying these interactions by determining binding constants.

1.6.2 Binding constant determination by UV-Vis and fluorescence spectroscopy¹¹⁸

For a simple complexation reaction between a metal and a receptor, as given below



the binding constant is obtained from the expression below

$$K_{ab} = \frac{[M_aL_b]}{[M]^a[L]^b} \quad (\text{eq. 1.4})$$

Binding constants can be obtained from a UV-Vis or fluorescence titrations, a typical experiment would involve having a solution of the receptor (Solution A), and with this constant concentration, a solution of the metal (Solution B) is made using Solution A. With metal solution (titrant) having a higher concentration than the constant concentration of the receptor. Solution A is then titrated with Solution B. This gives spectral or fluorescence changes in the absorbance obtained as a result of titrant addition to the receptor. A non-linear fit of the changes in absorbance or fluorescence intensity is then plotted against the total metal concentration and is used to calculate the binding constant. For a 1:1 stoichiometry, equation 1.5 below is used to determine the binding constant. The Hypspec® program is used for more complicated binding stoichiometries, using combinations of 1:1, 1:2, or other binding isotherms.

$$y = \frac{\pm(L+x+K^{-1}-\sqrt{(L+x+K^{-1})^2-4xL}) \times M}{2L} \quad (\text{eq. 1.5})$$

Where y = Cumulative change in absorbance or intensity

$$x = [\text{Ln(III)}]_t$$

L = Ligand concentration

$$M = \Delta \text{Abs}_{\text{max}}$$

K = Binding constant

1.6.3 Solvent extraction studies¹¹⁹

Solvent extraction (or liquid-liquid extraction) is a method used to transfer solutes from one solvent into another. For this study, an organic extractant designed to have binding sites capable of interacting with metals in the aqueous phase and transferring these metals into the organic phase is used. This extractant is dissolved in a solvent called the diluent. Such diluent must be one where the extractant and ideally the formed metal complex after extraction is soluble. It is also expected that the diluent does not interact nor is chemically changed during the extraction. According to Nernst's distribution ratio during extraction, the distribution of the metal between organic and aqueous phases is expressed as below:

$$\text{With regards to concentration, } D_m = \frac{[M^{n+}]_{org.}}{[M^{n+}]_{aq.}} \text{ or } \frac{[M^{n+}]_o - [M^{n+}]_i}{[M^{n+}]_i} \quad (\text{eq. 1.6})$$

$$\text{With regards to activity, } D_m = \frac{A_{org.}}{A_{aq.}} \text{ or } \frac{A_o - A_i}{A_i} \quad (\text{eq. 1.7})$$

This study makes use of ionizable organic extractants in alkaline conditions. Here, extraction by solvation is based on cation exchange, where the ligand is typically neutral (protonated) at low pHs and becomes deprotonated (anionic) when in alkaline environment, presenting electron rich sites for coordination with metals of interest. The complexed metal is then transferred from the aqueous to the organic phase. Recovering the extracted metal from the organic phase involves the process of stripping, in which the chelated metal is stripped off the ligand by using acid on the loaded organic phase. This protonates the ligand in the organic phase and releases the metal into the acidic aqueous phase, a process referred to as back extraction, (or stripping). Quantification of the recovered metal (Ln(III)) concentration in the aqueous phase for this study is typically performed using the Arsenazo-III spectrophotometric method^{120,121} or ICP-MS.

1.7 Dissertation scope and overall summary

This dissertation describes our continued effort in understanding the coordination, complexation, sensing, and extraction of f-elements from alkaline media, with a variety of new sulfonamide-type ligands that contain additional phenolic sites. While aspects of this work have been published in peer-reviewed journals or are in preparation, each separate area of study will be presented here in six chapters, with Chapter 1 dedicated to introducing the significance and review of previous work reported in literature at remediating alkaline HLW. Chapter 2 introduces the synthesis and study of four *o*-sulfonamidophenol ligand derivatives for extraction of Ln(III) (used

as experimental surrogates for An(III)) from alkaline pH, alongside spectrophotometric and theoretical studies performed to further understand the metal-ligand interactions in alkaline solutions. Chapter 3 describes Ln(III) extraction from alkaline solutions using highly lipophilic *o*-sulfonamidophenol ligand derivatives which are compatible with lipophilic industrial process solvents. Chapter 4 describes a dansyl derived *o*-sulfonamidophenol ligand for fluorescence sensing and extraction of Ln(III) from alkaline media. Chapter 5 presents a selective Lu(III) optical sensor from alkaline media based on a nitrophenol-derived *o*-sulfonamide and a remarkable Lu(III) trimer cluster formed with this ligand in the solid-state. Lastly, appendices A, B, and C respectively are dedicated to related studies on *o*-sulfonamidophenol ligand derivatives for Zn(II) complexation, the regioselectivity in the synthesis of sulfonamides vs. sulfonic esters, as well as studies involving some related tripodal sulfonamide designs.

1.8 References

1. National Research Council *Long-term institutional management of US Department of Energy legacy waste sites*; National Academies Press, **2000**.
2. Wiersma, B. J. The Performance of Underground Radioactive Waste Storage Tanks at the Savannah River Site: A 60-Year Historical Perspective. *Journal of the Minerals Metals and Materials* **2014**, *66*, 471-490.
3. Birkett, J. E.; Carrott, M. J.; Fox, O. D.; Jones, C. J.; Maher, C. J.; Roubé, C. V.; Taylor, R. J.; Woodhead, D. A. Recent developments in the Purex process for nuclear fuel reprocessing: Complexant based stripping for uranium / plutonium separation. *CHIMIA International Journal for Chemistry* **2005**, *59*, 898-904.
4. Choppin, G. R.; Morgenstern, A. Radionuclide separations in radioactive waste disposal. *Journal of Radioanalytical and Nuclear Chemistry* **2000**, *243*, 45-51.
5. Kozlov, P. V.; Kazadaev, A. A.; Makarovskii, R. A.; Remizov, M. B.; Verbitskii, K. V.; Logunov, M. V. Development of a process for cesium recovery from the clarified phase of high-level waste storage tanks of the Mayak Production Association with a ferrocyanide sorbent. *Radiochemistry* **2016**, *58*, 295-301.

6. Wilmarth, W. R.; Lumetta, G. J.; Johnson, M. E.; Poirier, M. R.; Thompson, M. C.; Suggs, P. C.; Machara, N. P. Waste-pretreatment technologies for remediation of legacy defense nuclear wastes. *Solvent Extraction and Ion Exchange* **2011**, *29*, 1-48.
7. Gephart, R. E.; Lundgren, R. E.; Gephart, R. E. Hanford tank cleanup: A guide to understanding the technical issues; Battelle Press Columbus, Ohio, **1998**.
8. Chew, D. P.; Hamm, B. A. Liquid Waste System Plan. US Department of Energy Savannah River Remediation, Aiken, SC Report SRR-LWP-2009-00001, Revision 20, **2016**.
9. Ondrejcin, R. S. Composition, and corrosiveness of low-activity waste supernates stored at the Savannah River Plant. DP-1427; Du Pont de Nemours (E.I) and Co., Aiken SC(USA). Savannah River Lab., October **1976**.
10. Fowler, J. R. Composition of F-Area Soluble High-Level Waste DPST-82-390, March 10, **1982**.
11. Stone, J. A.; Kelley, J. A.; McMillan, T. S. Sampling and analyses of SRP high-level waste sludges No. DP-1399. Du Pont de Nemours (EI) and Co., **1976**.
12. Fehner, T. R.; Holl, J. M. Department of Energy 1977-1994: A summary history USDOE Office of Administration and Human Resource Management, Washington, DC (United States). History Div. No. DOE/HR-0098., **1994**.
13. Fredrickson, J. K.; Zachara, J. M.; Balkwill, D. L.; Kennedy, D.; Li, S. W.; Kostandarithes, H. M.; Daly, M. J.; Romine, M. F.; Brockman, F. J. Geomicrobiology of high-level nuclear waste-contaminated vadose sediments at the Hanford Site, Washington State. *Applied and Environmental Microbiology* **2004**, *70*, 4230-4241.
14. Bennett, L. J.; Pedersen, K. S.; Johnston, G. A.; Shoulders, A. Reducing groundwater impacts on the Columbia River from the Hanford Site -. Water Environment Federation, Alexandria, VA (United States), No. CONF-951023, **1996**.
15. Stumm, W.; Morgan, J. J. *Aquatic chemistry: chemical equilibria and rates in natural waters*; John Wiley & Sons: **2012**; Vol. 126.
16. Baes Jr, C. F.; Mesmer, R. E. The Hydrolysis of Cations: Wiley Interscience. *New York* **1976**.
17. Silva, R. J.; Nitsche, H. Actinide environmental chemistry. *Radiochimca Acta* **1995**, *70*, 377-396.

18. Maher, K.; Bargar, J. R.; Brown Jr, G. E. Environmental speciation of actinides. *Inorganic Chemistry* **2013**, *52*, 3510-3532.
19. Choppin, G. R.; Jensen, M. P. Actinides in solution: complexation and kinetics. In *The Chemistry of the Actinide and Transactinide Elements*. Springer: **2008**; pp 2524-2621.
20. Altmaier, M.; Gaona, X.; Fanghänel, T. Recent advances in aqueous actinide chemistry and thermodynamics. *Chemical Reviews* **2013**, *113*, 901-943.
21. Choppin, G. R. Utility of oxidation state analogs in the study of plutonium behavior. *Radiochimica Acta* **1999**, *85*, 89-96.
22. Neck, V.; Altmaier, M.; Rabung, T.; Lützenkirchen, J.; Fanghänel, T. Thermodynamics of trivalent actinides and neodymium in NaCl, MgCl₂, and CaCl₂ solutions: Solubility, hydrolysis, and ternary Ca-M(III)-OH complexes. *Pure and Applied Chemistry* **2009**, *81*, 1555-1568.
23. Vitorge, P. Solubility limits of radionuclides in interstitial water. Americium in cement. Task 3. Characterization of radioactive waste forms. A series of final reports (1985-89). No 34 EUR--13664. Commission of the European Communities **1991**.
24. Rabung, T.; Altmaier, M.; Neck, V.; Fanghänel, T. A TRLFS study of Cm(III) hydroxide complexes in alkaline CaCl₂ solutions. *Radiochimica Acta* **2008**, *96*, 551-560.
25. Bradford, A.; Esh, D.; Ridge, A.; Thaggard, M.; Whited, R.; Treby, S.; Flanders, S.; Camper, L. W. US Nuclear Regulatory Commission Technical Evaluation Report for the US Department of Energy Savannah River Site Draft Section 3116 Waste Determination for Salt Waste Disposal. Technical Report (US Nuclear Regulatory Commission, Washington, DC, 2005), **2005**.
26. Wells, D. Z-Area Saltstone Disposal Facility Groundwater Monitoring Report (1998 Annual Report) No. WSRC-RP-99-00002. Savannah River Site (SRS), Aiken, SC (United States), **1999**.
27. Peters, T. B.; Poirier, M. R.; Fink, S. D. Processing macrobatch 2 at the savannah river site integrated salt disposition process (ISDP). *Separation Science and Technology* **2010**, *45*, 1801-1806.
28. Martino, C. J.; Poirier, M. R.; Fondeur, F. F.; Fink, S. D. Flocculating, Settling, and Decanting for the Removal of Monosodium Titanate and Simulated High-Level Waste Sludge from Simulated Salt Supernate. WSRC-TR-2001-00413, October 16, **2001**

29. Poirier, M. R. Improving the filtration of sludge/monosodium titanate slurries by the addition of flocculants. Savannah River Site (United States), No. WSRC-TR--2001-00175. **2001**.
30. McCabe, D. J. Evaluation and ranking of the tank focus area solid liquid separation needs Westinghouse Savannah River Co., Aiken, SC (United States), No. WSRC-TR-95-0337, **1995**.
31. Porter, M. C. Handbook of industrial membrane technology. **1989**.
32. Peters, C.; Braekers, D.; Kroupa, J.; Kasyan, O.; Miroshnichenko, S.; Rudzevich, V.; Böhmer, V.; Desreux, J. CMPO-calix[4]arenes and the influence of structural modifications on the Eu(III), Am(III), Cm(III) separation. *Radiochimica Acta* **2008**, *96*, 203-210.
33. Dam, H. H.; Reinhoudt, D. N.; Verboom, W. Multicoordinate ligands for actinide/lanthanide separations. *Chemical Society Reviews* **2007**, *36*, 367-377.
34. Kolarik, Z. Complexation and separation of lanthanides (III) and actinides (III) by heterocyclic N-donors in solutions. *Chemical Reviews* **2008**, *108*, 4208-4252.
35. Nash, K. L. A review of the basic chemistry and recent developments in trivalent f-elements separations. *Solvent Extraction and Ion Exchange* **1993**, *11*, 729-768.
36. Hudson, M. J.; Harwood, L. M.; Laventine, D. M.; Lewis, F. W. Use of soft heterocyclic N-donor ligands to separate actinides and lanthanides. *Inorganic Chemistry* **2013**, *52*, 3414-3428.
37. Modolo, G.; Wilden, A.; Geist, A.; Magnusson, D.; Malmbeck, R. A review of the demonstration of innovative solvent extraction processes for the recovery of trivalent minor actinides from PUREX raffinate. *Radiochimica Acta* **2012**, *100*, 715-725.
38. Lehman-Andino, I.; Su, J.; Papathanasiou, K. E.; Eaton, T. M.; Jian, J.; Dan, D.; Albrecht-Schmitt, T. E.; Dares, C. J.; Batista, E. R.; Yang, P. Soft-donor dipicolinamide derivatives for selective actinide (III) / lanthanide (III) separation: the role of S- vs. O-donor sites. *Chemical Communications* **2019**, *55*, 2441-2444.
39. Wang, Y.; Deblonde, G. J.; Abergel, R. J. Hydroxypyridinone Derivatives: A low-pH alternative to polyaminocarboxylates for TALSPEAK-like separation of trivalent actinides from lanthanides. *ACS Omega* **2020**, *5*, 12996-13005.
40. Mei, L.; Ren, P.; Wu, Q.; Ke, Y.; Geng, J.; Liu, K.; Xing, X.; Huang, Z.; Hu, K.; Liu, Y. Actinide separation inspired by self-assembled metal-polyphenolic nanocages. *Journal of the American Chemical Society* **2020**, *142*, 16538-16545.

41. Bessen, N. P.; Jackson, J. A.; Jensen, M. P.; Shafer, J. C. Sulfur donating extractants for the separation of trivalent actinides and lanthanides. *Coordination Chemistry Reviews* **2020**, *421*, 213446.
42. Ionova, G.; Ionov, S.; Rabbe, C.; Hill, C.; Madic, C.; Guillaumont, R.; Krupa, J. C. Mechanism of trivalent actinide/lanthanide separation using bis (2, 4, 4-trimethylpentyl) dithiophosphinic acid (Cyanex 301) and neutral O-bearing co-extractant synergistic mixtures. *Solvent Extraction and Ion Exchange* **2001**, *19*, 391-414.
43. Pathak, S.; Jayabun, S.; Boda, A.; Ali, S. M.; Sengupta, A. Experimental and theoretical insight into the extraction mechanism, kinetics, thermodynamics, complexation, and radiolytic stability of novel calix crown ether in ionic liquid with Sr. *Journal of Molecular Liquids* **2020**, *316*, 113864.
44. Smirnova, A.; Mitrofanov, A.; Matveev, P.; Baygildiev, T.; Petrov, V. A search of a quantitative quantum-chemical approach for radiolytic stability prediction. *Physical Chemistry Chemical Physics* **2020**, *22*, 14992-14997.
45. Moyer, B. A.; Bonnesen, P. V.; Delmau, L. H.; Sloop Jr, F. V.; Williams, N. J.; Birdwell Jr, J. F.; Lee, D. L.; Leonard, R. A.; Fink, S. D.; Peters, T. B. In Development of the Next-Generation Caustic-Side Solvent Extraction (NG-CSSX) Process for Cesium Removal from High-Level Tank Waste–11346; Proceedings Waste Management 2011 Conference, February; **2011**.
46. Bonnesen, P. V.; Delmau, L. H.; Moyer, B. A.; Lumetta, G. J. Development of effective solvent modifiers for the solvent extraction of cesium from alkaline high-level tank waste. *Solvent Extraction and Ion Exchange* **2003**, *21*, 141-170.
47. Lamouroux, C.; Aychet, N.; Lelievre, A.; Jankowski, C. K.; Moulin, C. High-performance liquid chromatography with electrospray ionization mass spectrometry and diode array detection in the identification and quantification of the degradation products of Calix[4]arene crown-6 under radiolysis. *Rapid Communications in Mass Spectrometry* **2004**, *18*, 1493-1503.
48. Pierce, R.; Peters, T.; Caldwell, T.; Crowder, M.; Fink, S. Performance testing of the next-generation CSSX solvent with actual SRS tank waste. *Separation Science and Technology* **2012**, *47*, 2088-2097.
49. Moyer, B. A.; Alexandratos, S. D.; Bonnesen, P. V.; Brown, G. M.; Caton Jr, J. E.; Delmau, L. H.; Duchemin, C. R.; Haverlock, T. J.; Levitskaia, T. G.; Maskarinec, M. P.; Sloop Jr, F. V. Caustic-Side Solvent Extraction Chemical and Physical Properties: Progress in FY 2000 and FY 2001. ORNL/TM-2001/285, Oak Ridge National Laboratory, Oak Ridge, TN **2002**.

50. Delmau, L. H.; Bonnesen, P. V.; Engle, N. L.; Haverlock, T. J.; Sloop Jr, F. V.; Moyer, B. A. Combined extraction of cesium and strontium from alkaline nitrate solutions. *Solvent Extraction and Ion Exchange* **2006**, *24*, 197-217.
51. Gula, M. J.; Bartsch, R. A. Process for the preparation of cis-syn-cis-4, 4'(5')-[di-*t*-butyldicyclohexano]-18-crown-6 U.S. Patent No. 5,478,953. 26. **1995**.
52. Dietz, M.; Bond, A.; Huber, V.; Herlinger, A.; Hay, B. Ligand reorganization energies as a basis for the design of synergistic metal ion extraction systems. *Chemical Communications* **1999**, 1177-1178.
53. Kappel, M. J.; Nitsche, H.; Raymond, K. N. Specific sequestering agents for the actinides. 11. Complexation of plutonium and americium by catecholate ligands. *Inorganic Chemistry* **1985**, *24*, 605-611.
54. Sofen, S. R.; Cooper, S. R.; Raymond, K. N. Crystal and molecular structures of tetrakis (catecholato) hafnate (IV) and-cerate (IV). Further evidence for a ligand field effect in the structure of tetrakis (catecholato) uranate (IV). *Inorganic Chemistry* **1979**, *18*, 1611-1616.
55. Gramer, C. J.; Raymond, K. N. Characterization of 2, 3-Dihydroxyterephthalamides as M (IV) Chelators. *Inorganic Chemistry* **2004**, *43*, 6397-6402.
56. Weitzel, F. L.; Raymond, K. N.; Smith, W. L.; Howard, T. R. Specific sequestering agents for the actinides. 1. N, N', N'', N'''-Tetra (2, 3-dihydroxybenzoyl) tetraazacyclotetra-and-hexadecanes. *Journal of the American Chemical Society* **1978**, *100*, 1170-1172.
57. Gramer, C. J.; Raymond, K. N.; Jarvinen, G. D.; Robison, T. W.; Schroeder, N. C.; Smith, B. F. The Removal of Pu(IV) from Aqueous Solution Using 2, 3-Dihydroxyterephthalamide-Functionalized PEI with Polymer Filtration. *Separation Science and Technology* **2005**, *39*, 321-339.
58. Cooper, S. R.; Koh, Y. B.; Raymond, K. N. Synthetic, structural, and physical studies of bis (triethylammonium) tris (catecholato) vanadate (IV), potassium bis (catecholato) oxovanadate (IV), and potassium tris (catecholato) vanadate (III). *Journal of the American Chemical Society* **1982**, *104*, 5092-5102.
59. Borgias, B. A.; Cooper, S. R.; Koh, Y. B.; Raymond, K. N. Synthetic, structural, and physical studies of titanium complexes of catechol and 3, 5-di-*tert*-butylcatechol. *Inorganic Chemistry* **1984**, *23*, 1009-1016.
60. Harris, W. R.; Carrano, C. J.; Cooper, S. R.; Sofen, S. R.; Avdeef, A. E.; McArdle, J. V.; Raymond, K. N. Coordination chemistry of microbial iron transport compounds. 19. Stability constants and electrochemical behavior of ferric enterobactin and

- model complexes. *Journal of the American Chemical Society* **1979**, *101*, 6097-6104.
61. Zheng, T.; Wan, X.; Zhang, Q.; Jin, B.; Peng, R. Catechol amide derivatized polyhydroxylated fullerene as potential chelating agents of radionuclides: Synthesis, reactive oxygen species scavenging, and cytotoxic studies. *Journal of Inorganic Biochemistry* **2020**, *203*, 110921.
 62. Bergeron, R. J.; Kline, S. J.; Navratil, J. D.; Smith, C. M. Catecholamide "H Shaped" Ligands as Actinide Chelators. *Radiochimica Acta* **1984**, *35*, 47-52.
 63. Nekrasova, V. V.; Karalova, Z. K.; Myasoedov, B. F. Investigation of the behavior of europium and some actinide elements in alkaline tartrate solutions. *Radiokhimiya* **1981**, *23*, 259-263.
 64. Bukina, T. I.; Karalova, Z. K.; Myasoedov, B. F. Separation of Transplutonium Elements from Other Elements in Basic and Carbonate solutions by Extraction with Alkyl-Derivatives of Aminocatechols. *Radiokhimiya* **1990**, *32*, 11-15.
 65. Myasoedov, B. F.; Karalova, Z. K.; Kuznetsova, V. S.; Rodionova, L. M. Americium and europium extraction from alkaline solutions by alkylpyrocatechols. *Radiokhimiya* **1980**, *22*, 347-351.
 66. Karalova, Z.; Lavrinovich, E.; Myasoedov, B. Extraction of transplutonium elements from carbonate solutions by alkyl phenol oligomers. *Radiochemistry* **1990**, *32*, 16-20.
 67. Smirnov, I. V.; Karavan, M. D.; Logunov, M. V.; Tananaev, I. G.; Myasoedov, B. F. Extraction of radionuclides from alkaline and carbonate media. *Radiochemistry* **2018**, *60*, 470-487.
 68. Smirnov, I. V.; Stepanova, E. S.; Drapailo, A. B.; Kalchenko, V. I. Extraction of americium and europium with functionalized calixarenes from alkaline solutions. *Radiochemistry* **2016**, *58*, 42-51.
 69. Karalova, Z. K.; Myasoedov, B. F.; Bukina, T. I.; Lavrinovich, E. A. Extraction, and separation of actinides and lanthanides from alkaline and carbonate solutions. *Solvent Extraction and Ion Exchange* **1988**, *6*, 1109-1135.
 70. Myasoedov, B. F.; Karalova, Z. K.; Nekrasova, V. V.; Rodionova, L. M. Extraction of actinides and lanthanides from alkaline solutions by quaternary ammonium bases and alkylpyrocatechols. *Journal of Inorganic and Nuclear Chemistry* **1980**, *42*, 1495-1499.

71. Smirnov, I. V.; Stepanova, E. S.; Tyupina, M. Y.; Ivenskaya, N. M.; Zaripov, S. R.; Kleshnina, S. R.; Solov'eva, S. E.; Antipin, I. S. Extraction of cesium and americium with *p*-alkylcalix [8] arenes from alkaline solutions. *Radiochemistry* **2016**, *58*, 381-388.
72. Ivenskaya, N. M.; Stepanova, E. S.; Logunov, M. V.; Smirnov, I. V. Extraction of long-lived radionuclides from high-level alkaline waste with *p*-Alkylcalix[8]arene. *Radiochemistry* **2018**, *60*, 378-385.
73. Kuzovkina, E. V.; Lavrinovich, E. A.; Novikov, A. P.; Stepanova, E. S.; Karavan, M. D.; Smirnov, I. V. Kinetics of americium and europium extraction by *tert*-butylthiacalix [4] arene from alkaline media. *Journal of Radioanalytical and Nuclear Chemistry* **2017**, *311*, 1983-1989.
74. Walker, D. D.; Barnes, M. J.; Crawford, C. L.; Peterson, R. A.; Swingle, R. F.; Fink, S. D. In-tank precipitation with tetraphenylborate: recent process and research results. In *Science and Technology for Disposal of Radioactive Tank Wastes*. Springer: **1998**, pp 219-230.
75. Wester, D. W.; Berry, P.; Cook, B. J.; DesChane, J. R.; Rapko, B. M.; Baldwin, D. L.; Carson, K. J.; Darnell, L. P.; Levitskaia, T. G.; Soderquist, C. Z. Ion-exchange Research in Support of Modular Treatment of Savannah River Site Tank Wastes. **2003**.
76. Brown, G. N.; Bray, L. A.; Carlson, C. D. Comparison of organic and inorganic ion exchangers for removal of cesium and strontium from simulated and actual Hanford 241-AW-101 DSSF tank waste No. PNL--10920. Pacific Northwest Lab., **1996**.
77. Kurath, D. E.; Blanchard, D. L.; Bontha, J. R. Small Column Ion Exchange Testing of Superlig 644 for Removal of ¹³⁷Cs from Hanford Tank Waste Envelope A (Tank 241-AW-101). Pacific Northwest National Lab., Richland, WA (US), No. PNWD-3001; BNFL-RPT-014-Rev. **2000**.
78. Fiskum, S. K.; Blanchard, D. L.; Steele, M. J.; Thomas, K. K.; Trang-Le, T.; Thorson, M. R. Spherical Resorcinol-Formaldehyde Resin Testing for Cesium Removal from Hanford Tank Waste Simulant. *Seperation Science and Technology* **2006**, *41*, 2461-2474.
79. Thorson, M. Basis of Recommendation for Use of Spherical Resorcinol Formaldehyde Resin as the Primary Cesium Ion Exchange Resin in the WTP (Vol. 5) 24590-WTP-RPT-RT-07. **2008**.
80. Miller, J. E.; Brown, N. E.; Krumhansl, J. L.; Trudell, D. E.; Anthony, R. G.; Philip, C. V. Development and properties of cesium selective crystalline silicotitanate

- (CST) ion exchangers for radioactive waste applications. In *Science and Technology for Disposal of Radioactive Tank Wastes*. Springer: **1998**, pp 269-286.
81. Bortun, A. I.; Bortun, L. N.; Clearfield, A. Ion exchange properties of a cesium ion-selective titanosilicate. *Solvent Extraction and Ion Exchange* **1996**, *14*, 341-354.
 82. Hobbs, D. T. *Phase IV testing of monosodium titanate adsorption with radioactive waste Savannah River Site (US)*, No. WSRC-TR-99-00286. **1999**.
 83. Norato, M. A.; Beasley, M. H.; Campbell, S. G.; Coleman, A. D.; Geeting, M. W.; Guthrie, J. W.; Kennell, C. W.; Pierce, R. A.; Ryberg, R. C.; Walker, D. D. Demonstration of the caustic-side solvent extraction process for the removal of ^{137}Cs from Savannah River Site high-level waste. *Separation Science and Technology* **2003**, *38*, 2647-2666.
 84. Leonard, R. A.; Aase, S. B.; Arafat, H. A.; Conner, C.; Chamberlain, D. B.; Falkenberg, J. R.; Regalbutto, M. C.; Vandegrift, G. F. Experimental verification of caustic-side solvent extraction for removal of cesium from tank waste. *Solvent Extraction and Ion Exchange* **2003**, *21*, 505-526.
 85. Klatt, L. N.; Birdwell Jr, J. F.; Bonnesen, P. V.; Delmau, L. H.; Foote, L. J.; Lee, D. D.; Leonard, R. A.; Levitskaia, T. G.; Maskarinec, M. P.; Moyer, B. A. Caustic-Side Solvent Extraction Solvent-Composition Recommendation. *ORNL/TM-2001/258, Oak Ridge National Laboratory, Oak Ridge, TN* **2001**.
 86. Roach, B. D.; Williams, N. J.; Moyer, B. A. Thermal degradation of the solvent employed in the next-generation caustic-side solvent extraction process and its effect on the extraction, scrubbing, and stripping of cesium. *Solvent Extraction and Ion Exchange* **2015**, *33*, 576-591.
 87. Delmau, L. H.; Haverlock, T. J.; Bazelaire, E.; Bonnesen, P. V.; Ditto, M. E.; Moyer, B. A. Alternatives to nitric acid stripping in the caustic-side solvent extraction (cssx) process for cesium removal from alkaline high-level waste. *Solvent Extraction and Ion Exchange* **2009**, *27*, 172-198.
 88. Pearson, R. G.; Purcell, R. H.; Saigh, G. S. *J. Am. Chem. Soc. Survey of Progress in Chemistry* **1963**, *85*, 3533.
 89. Govor, E. V.; Morozov, A. N.; Rains, A. A.; Mebel, A. M.; Kavallieratos, K. Spectroscopic and theoretical insights into surprisingly effective Sm(III) extraction from alkaline aqueous media by *o*-Phenylenediamine-derived sulfonamides. *Inorganic Chemistry* **2020**, *59*, 6884-6894.
 90. Lesch, J. E. *The first miracle drugs: how the sulfa drugs transformed medicine*; Oxford University Press, USA, **2007**.

91. Kivelä, A. J.; Kivelä, J.; Saarnio, J.; Parkkila, S. Carbonic anhydrases in normal gastrointestinal tract and gastrointestinal tumours. *World Journal of Gastroenterology* **2005**, *11*, 155.
92. Battaglin, W. A.; Furlong, E. T.; Burkhardt, M. R.; Peter, C. J. Occurrence of sulfonylurea, sulfonamide, imidazolinone, and other herbicides in rivers, reservoirs and groundwater in the Midwestern United States, 1998. *Science of the Total Environment* **2000**, *248*, 123-133.
93. Hirsch, R.; Ternes, T.; Haberer, K.; Kratz, K. Occurrence of antibiotics in the aquatic environment. *Science of the Total Environment* **1999**, *225*, 109-118.
94. Kavallieratos, K.; Rosenberg, J. M.; Chen, W.; Ren, T. Fluorescent sensing and selective Pb (II) extraction by a dansylamide ion-exchanger. *Journal of the American Chemical Society* **2005**, *127*, 6514-6515.
95. Kimura, E.; Aoki, S. Chemistry of zinc (II) fluorophore sensors. *Zinc Biochemistry, Physiology, and Homeostasis*. Springer: **2001**, pp 5-18.
96. Helal, A.; Kim, S. H.; Kim, H. Thiazole sulfonamide based ratiometric fluorescent chemosensor with a large spectral shift for zinc sensing. *Tetrahedron* **2010**, *66*, 9925-9932.
97. Alvarado, R. J.; Rosenberg, J. M.; Andreu, A.; Bryan, J. C.; Chen, W.; Ren, T.; Kavallieratos, K. Structural insights into the coordination and extraction of Pb(II) by disulfonamide ligands derived from o-phenylenediamine. *Inorganic Chemistry* **2005**, *44*, 7951-7959.
98. Kavallieratos, K.; Rosenberg, J. M.; Bryan, J. C. Pb(II) Coordination and synergistic ion-exchange extraction by combinations of sulfonamide chelates and 2, 2'-bipyridine. *Inorganic Chemistry* **2005**, *44*, 2573-2575.
99. Khan, N. U. H.; Zaib, S.; Sultana, K.; Khan, I.; Mougang-Soume, B.; Nadeem, H.; Hassan, M.; Iqbal, J. Metal complexes of tosyl sulfonamides: design, X-ray structure, biological activities, and molecular docking studies. *RSC Advances* **2015**, *5*, 30125-30132.
100. Morozov, A. N.; Govor, E. V.; Anagnostopoulos, V. A.; Kavallieratos, K.; Mebel, A. M. 1, 3, 5-Tris-(4-(iso-propyl)-phenylsulfamoylmethyl) benzene as a potential Am(III) extractant: experimental and theoretical study of Sm(III) complexation and extraction and theoretical correlation with Am(III). *Molecular Physics* **2018**, *116*, 2719-2727.

101. Pritchett, S.; Gantzel, P.; Walsh, P. J. Synthesis and crystal structures of chiral titanium bis (sulfonamido) bis (amide) complexes: Differences in ligand hapticity caused by crystal packing forces. *Organometallics* **1997**, *16*, 5130-5132.
102. Caddick, S.; Wilden, J. D.; Judd, D. B. Direct synthesis of sulfonamides and activated sulfonate esters from sulfonic acids. *Journal of the American Chemical Society* **2004**, *126*, 1024-1025.
103. Pandya, R.; Murashima, T.; Tedeschi, L.; Barrett, A. G. Facile one-pot synthesis of aromatic and heteroaromatic sulfonamides. *Journal of Organic Chemistry* **2003**, *68*, 8274-8276.
104. Wright, S. W.; Hallstrom, K. N. A Convenient preparation of heteroaryl sulfonamides and sulfonyl fluorides from heteroaryl thiols. *Journal of Organic Chemistry* **2006**, *71*, 1080-1084.
105. Cotton, F. A.; Stokely, P. F. Structural basis for the acidity of sulfonamides. Crystal structures of dibenzenesulfonamide and its sodium salt. *Journal of American Chemical Society* **1970**, *92*, 294-302.
106. Dauphin, G.; Kergomard, A. Etude de la dissociation acide de quelques sulfonamides. *Bulletin de la Societe Chimique de France* **1961**, 486-492.
107. Beloso, I.; Castro, J.; García-Vázquez, J. A.; Pérez-Lourido, P.; Romero, J.; Sousa, A. Electrochemical synthesis and structural characterization of silver (I) complexes of N-2-pyridyl sulfonamide ligands with different nuclearity: Influence of the steric hindrance at the pyridine ring and the sulfonamide group on the structure of the complexes. *Inorganic Chemistry* **2005**, *44*, 336-351.
108. Armistead, L. T.; White, P. S.; Gagné, M. R. Synthesis, and Structure of Titanium (IV) Amido Complexes Containing C 2-Symmetric Bis (sulfonamide) Ligands. *Organometallics* **1998**, *17*, 216-220.
109. Zhao, J.; Song, H.; Cui, C. Synthesis and reactions of aluminum sulfonamide alkyls and hydride. *Organometallics* **2007**, *26*, 1947-1954.
110. Blaschette, A.; Michalides, A.; Jones, P. G. Polysulfonylamine: XXVII. Synthese von Dimethylindium-und Bis (trimethylsilylmethyl) indium-dimesylamid sowie Röntgenstrukturanalyse von [(Me₃SiCH₂)₂InN (SO₂Me)₂]₂. *Journal of Organometallic Chemistry* **1991**, *411*, 57-68.
111. Töpala, T.; Pascual-Álvarez, A.; Moldes-Tolosa, M. Á.; Bodoki, A.; Castiñeiras, A.; Torres, J.; Del Pozo, C.; Borrás, J.; Alzuet-Piña, G. New sulfonamide complexes with essential metal ions [Cu(II), Co(II), Ni(II) and Zn(II)]. Effect of the

- geometry and the metal ion on DNA binding and nuclease activity. BSA protein interaction. *Journal of Inorganic Biochemistry* **2020**, *202*, 110823.
112. Tao, W.; Wang, X.; Ito, S.; Nozaki, K. Palladium complexes bearing an N-heterocyclic carbene–sulfonamide ligand for cooligomerization of ethylene and polar monomers. *Journal of Polymer Science Part A: Polymer Chemistry* **2019**, *57*, 474-477.
113. Prodi, L.; Bolletta, F.; Montalti, M.; Zaccheroni, N. Luminescent chemosensors for transition metal ions. *Coordination Chemistry Reviews* **2000**, *205*, 59-83.
114. Jiang, P.; Chen, L.; Lin, J.; Liu, Q.; Ding, J.; Gao, X.; Guo, Z. Novel zinc fluorescent probe bearing dansyl and aminoquinoline groups. *Chemical Communications* **2002**, *13*, 1424-1425.
115. Lakowicz, J. R. Topics in Fluorescence Spectroscopy: Principles; Springer Science & Business Media: Vol. 2, **2006**.
116. Wanichacheva, N.; Watpathomsub, S.; Lee, V. S.; Grudpan, K. Synthesis of a novel fluorescent sensor bearing dansyl fluorophores for the highly selective detection of mercury (II) ions. *Molecules* **2010**, *15*, 1798-1810.
117. Tharmaraj, V and Pitchumani, K. An acyclic dansyl based colorimetric and fluorescent chemosensor for Hg(II) via intramolecular Charge transfer (TICT) *Analytica Chimica Acta* **2012**, *751*, 171-175.
118. Connors, K. A. Binding constants: the measurement of molecular complex stability; Wiley-Interscience: **1987**.
119. Rydberg, J.; Choppin, G. R.; Musikas, C.; Sekine, T. Solvent extraction equilibria. In Solvent Extraction Principles and Practice, Revised and Expanded, CRC Press: **2004**; pp 121-217.
120. Ivanov, V. M.; Ermakova, N. V. Optical and chromaticity characteristics of Arsenazo III complexes of rare-earth elements. *Journal of Analytical Chemistry* **2001**, *56*, 519-523.
121. Savvin, S. B. Analytical use of arsenazo III: determination of thorium, zirconium, uranium and rare earth elements. *Talanta* **1961**, *8*, 673-68

Chapter II: Lanthanide Coordination and Extraction from Alkaline Media by
o-Sulfonamidophenol Derivatives.

Oluwaseun W. Adedoyin, Cristian Gonzalez, Alexander N. Morozov, Indranil
Chakraborty, Evgen V. Govor, Alexander M. Mebel, Raphael G. Raptis, and
Konstantinos Kavallieratos

2.1 Abstract

Four *o*-sulfonamidophenol ligands 4-(*tert*-butyl)-N-(2-hydroxyphenyl)benzenesulfonamide (**L1H₂**), 4-(*tert*-butyl)-N-(5-(*tert*-butyl)-2-hydroxyphenyl)benzenesulfonamide (**L2H₂**), N-(2-hydroxyphenyl)-2,4,6-triisopropylbenzenesulfonamide (**L3H₂**) and, N-(5-(*tert*-butyl)-2-hydroxyphenyl)-2,4,6-triisopropylbenzenesulfonamide (**L4H₂**) were synthesized, characterized, and studied for extraction of lanthanides (La(III), Nd(III), Sm(III) and Eu(III)) from alkaline aqueous phases into organic diluents. The dependence of extraction efficiency on aqueous phase pH, ligand concentration, and polarity of the organic diluent was studied. From the ligands investigated, **L2H₂** gave the highest Ln(III) extraction efficiency in dichloromethane (30.0 mM) with 96.1 (±4.4)% Sm(III) recovery at pH 13.0 and 93.3 (±5.2)% Sm(III) recovery at pH 14.0 after one extraction / stripping cycle. In *n*-dodecane:octanol (80:20, v/v), Sm(III) recoveries of 82.6 (±9.3)% at pH 12.5 and 53.9 (±4.0)% at pH 14.0 were obtained. Maximum extraction was obtained for $[L2H_2]_t/[Sm(III)]_t$ of 2 or higher, suggesting a $[Sm(III)L_2]^-$ 1:2 complexation stoichiometry for the complex formed in the organic phase. UV-Vis titrations and Job

plots in CH₃CN:CH₃OH (96:4, v/v) were also consistent with a 1:2 complexation stoichiometry. UV-Vis titrations in CH₃CN:CH₃OH (96:4, v/v) gave binding constants for the formation of [Sm(III)L₂]⁻ ranging from $\beta_2 = 3.98 (\pm 0.01) \times 10^{10} \text{ M}^{-2}$ to $\beta_2 = 1.26 (\pm 0.04) \times 10^{12} \text{ M}^{-2}$ for the four ligands after non-linear regression analysis of the binding data.

2.2 Introduction

Alkaline high-level waste (HLW) formed during years of reprocessing for nuclear weapons production in the US has been stored in underground tanks at the Hanford Site (Washington) and the Savannah River Site (SRS) in South Carolina.^{1,2} The integrated salt waste processing at SRS, uses two processes applied consecutively, the Actinide Removal Process (ARP) and the Next Generation Caustic-Side Solvent Extraction (NG-CSSX) process.^{1,3} ARP uses monosodium titanate to remove ⁹⁰Sr and actinides by adsorption,^{3,4} while NG-CSSX removes Cs(I) by solvent extraction by a Calixarene extractant.⁵ ARP, being a sorption process, has slower kinetics compared to solvent extraction^{4,6} especially with regards to actinide removal and so it is currently the kinetic bottleneck of overall processing, increasing the facility operation period and lifecycle cost.⁴ The ARP treated stream devoid of Sr and An is fed to the Modular CSSX Unit (MCU) where solvent extraction of the alkaline aqueous stream rich in ¹³⁷Cs occurs with a solvent system comprising of (i) an organic extractant, which is a calixarene derivatized with a crown ether group and is very selective for complexation of Cs(I),⁵ (ii) a fluorinated solvent modifier, and (iii) an amine suppressor⁷ all dissolved in (iv) ISOPAR-L[®], a paraffin-based diluent.^{5,7} As solvent extraction is a fast and efficient

process, extracting actinides, either by modifying NG-CSSX or through a separate process could provide benefits as it would require less contact time with sorbent during ARP and less titanate. Prior attempts in extracting f-elements from alkaline aqueous phases have encouraged ligand designs with electron-rich oxygen and nitrogen chelating sites. Raymond et al. investigated 2,3-dihydroxyterephthalamide (TAM) ligands, for extraction of Fe(III)⁸ and trivalent actinides and lanthanides.⁹⁻¹² A water-soluble TAM-polyethylenimine polymer was studied by Gramer et al. for actinide separation via size-exclusion ultrafiltration.¹³ Other reported ligands include catecholamides for separation of Pu and Am,⁹ aminomethyl derivatives of alkylphenols, such as 2-hydroxy-5-alkylbenzyl-diethanolamine,¹⁴ alkyl-substituted pyrocatechols like 4-(α,α -dioctylethyl)pyrocatechol,¹⁵ alkyl substituted phenol-based oligomers,¹⁶ calixarene and thiacalixarene analogs.¹⁷⁻¹⁹ Sulfonamides have been studied by our group for f-element complexation and extraction from alkaline solutions with very promising results.^{20,21} Specifically, a preorganized trisulfonamide showed Sm(III) recovery of 51.8% from pH 10.0 in CH₂Cl₂.²¹ Calculations using DFT revealed that in the presence of a relatively high concentration of nitrate, complexation of Sm(III) or Am(III) with the ligand is sufficiently strong enough to overcome hydrolysis. More recently, *o*-phenylenediamine-derived disulfonamides gave > 80% Sm(III) recoveries from pH 13.0 aqueous phases into CH₂Cl₂ after a single loading / stripping cycle,²⁰ with DFT calculations suggesting the formation of mixed-ligand anionic M(III)-sulfonamido-hydroxo complexes, with close ion-pair formation in the organic phase. However, no Sm(III) recovery was obtained with any of these ligands from aqueous phases of pH > 13.5, thus limiting their

applicability to HLW. Furthermore, no significant extraction was obtained in highly lipophilic process diluents.

As part of our sustained effort to derive new f-element extraction schemes from alkaline solutions, and eventually improve integrated tank waste processing, we are now reporting efficient Ln(III) recoveries from highly alkaline aqueous phases (1M NaOH) by four *o*-sulfonamidophenol derivatives **L1H₂**, **L2H₂**, **L3H₂** and **L4H₂** (Figure 2.1) into both dichloromethane and the more lipophilic diluent *n*-dodecane:octanol (80:20, v/v). For **L2H₂**, with dichloromethane as a diluent, up to 95% Sm(III) recovery at pH 13.0 and 14.0 was achieved after a single cycle of loading, followed by stripping with dilute nitric acid. When the more lipophilic process solvent *n*-dodecane:octanol (80:20, v/v) was used as the diluent, maximum Sm(III) recoveries of 82.6 (± 9.3)% for **L2H₂** and 58.5 (± 4.0)% for **L4H₂** were obtained at pH 12.5 and 14.0, respectively. The extraction experiments and UV-Vis titrations (CH₃CN:CH₃OH (96:4, v/v)) revealed a 1:2 metal to ligand stoichiometry with binding constants ($\beta_{2(\text{Sm})}$) of $3.16 (\pm 0.20) \times 10^{11} \text{ M}^{-2}$, $3.98 (\pm 0.03) \times 10^{11} \text{ M}^{-2}$, $1.26 (\pm 0.04) \times 10^{12} \text{ M}^{-2}$ and $3.98 (\pm 0.01) \times 10^{10} \text{ M}^{-2}$, for **L1H₂**, **L2H₂**, **L3H₂** and **L4H₂**, respectively. DFT calculations further corroborated the UV-Vis and extraction results. This new sulfonamide family is a vast improvement over our previously reported ligand systems, not only because of its simplicity but also because of increased solubility in process solvents and high extraction efficiency in high alkalinity, pointing to promising application in f-element extraction from alkaline HLW.

2.3 Experimental section

2.3.1 Materials and methods.

All starting materials, reagents, and solvents were purchased from Fisher Scientific or Sigma-Aldrich. ICP-MS standard solutions for samarium, neodymium, europium, and lanthanum (each 1000 $\mu\text{g/L}$) were purchased from Alfa Aesar. Chemicals were standard reagent grade. 4-(*tert*-butyl)-N-(2-hydroxyphenyl) benzenesulfonamide (**L1H₂**) was synthesized according to modification of procedures found in the literature^{22,23} and was found to be spectroscopically identical to the reported compound. Solvents used for titrations were spectroscopic grade and were used without further purification. FT-IR spectra were recorded in the 4000 – 600 cm^{-1} range using a Cary 600 series FT-IR spectrometer. NMR spectra were recorded on a 400 MHz Bruker Avance NMR spectrometer and were referenced using the residual solvent resonances. All chemical shifts, δ , are reported in ppm. Arsenazo-III spectrophotometric studies and other UV-Vis spectra were recorded on a Varian Cary 100 Bio UV-Vis spectrophotometer. ICP-MS experiments were performed on a PerkinElmer NexION® 2000 ICP Mass Spectrometer, and Y(III) (10 ppm) was used as the internal standard. Single Crystal X-ray structures were obtained using a Bruker D8 Quest diffractometer bearing a PHOTON 100 detector and at $T = 298 \text{ K}$.

2.3.2 Synthesis of 4-(*tert*-butyl)-N-(5-(*tert*-butyl)-2-hydroxyphenyl)benzene sulfonamide (L2H₂).

2-amino-4-(*tert*-butyl) phenol (4.00 g, 24.0 mmol) and pyridine (19.33 mL, 240 mmol) were dissolved in 20 mL of CH₂Cl₂. The solution was placed in an ice bath for 10 min. 4-(*tert*-butyl) benzenesulfonyl chloride (6.70 g, 29.0 mmol) previously dissolved in 20 mL of CH₂Cl₂ was added dropwise to the cold stirring solution. After addition the reaction mixture was left stirring under N₂ for 15 h and monitored with TLC (2:1, Hexanes:EtOAc) to ensure completion of the reaction. When the reaction was judged to be complete, ice-cold water (50 mL) was used to wash the organic phase, which was then collected, sequentially washed with 1M HCl, 1M NaHCO₃, and DI water (3 × 25 mL), and dried over anhydrous sodium sulfate. The volatile organic phase was then concentrated under reduced pressure. Purification by column chromatography (8:2, Hexanes:EtOAc), followed by recrystallization from CH₂Cl₂ / petroleum ether gave a white solid, which was dried under vacuum (7.51 g, 86%, yield). ¹H-NMR (400 MHz, CDCl₃): δ 7.62 (d, 2H), 7.46 (d, 2H), 7.12 (dd, 1H), 6.90 (d, 1H), 6.44 (s, 1H), 6.41 (d, 1H), 6.16 (s, 1H), 1.30 (s, 9H), 1.04 (s, 9H). ¹³C-NMR (101 MHz, CDCl₃) δ 157.3, 149.4, 143.8, 134.4, 127.7, 126.1, 125.5, 123.8, 121.9, 116.7, 35.3, 33.4, 31.3, 31.2. FT-IR (cm⁻¹; ATR) 3575 (m), 3488 (w), 3387 (m), 3251 (w), 3035 (w), 2958 (m), 2867 (w), 2904 (w), 1594 (m), 1510 (s), 1437 (m), 1397 (m), 1318 (vs) 1285 (s), 1252 (m), 1225 (s), 1162 (vs), 1111 (s), 1089 (s), 1014 (w), 959 (m), 909 (w), 821 (s), 755 (s), 726 (s). Elemental Analysis (%) for C₂₀H₂₇NO₃S·1H₂O: Calcd. C, 63.30; H, 7.70; N, 3.69. Found C, 63.43; H, 7.73; N, 3.74.

2.3.3 Synthesis of N-(2-hydroxyphenyl)-2,4,6-triisopropylbenzenesulfonamide (L3H₂).

Synthesized using a similar procedure as **L2H₂**, from 2-aminophenol (1.50 g, 13.7 mmol), pyridine (1.88 mL, 23.2 mmol) and 2,4,6-triisopropylbenzenesulfonyl chloride (5.00 g, 16.5 mmol) gave a white solid (2.72 g, 53%, yield). ¹H-NMR (400 MHz, CDCl₃): δ 7.13 (s, 2H), 7.12 (t, 1H), 6.97 (d, 1H), 6.72 (t, 1H), 6.67 (dd, 1H), 6.57 (s, 1H), 6.18 (s, 1H), 3.85 (m, 2H), 2.89 (m, 1H), 1.25 (d, 6H), 1.14 (d, 12). ¹³C-NMR (101 MHz, CDCl₃): δ 153.5, 152.4, 150.5, 131.4, 129.1, 127.2, 124.1, 122.3, 120.4, 117.3, 34.3, 30.4, 24.8, 23.6. FT-IR (cm⁻¹; ATR): 3251 (m, broad; O-H and N-H), 2946 (m), 2862(m), 1600 (m), 1565 (w), 1503 (m), 1468 (w), 1428 (w), 1407 (w), 1384 (w), 1360 (m), 1322 (s), 1279 (m), 1255 (m), 1228 (m), 1144 (s), 1103 (m), 1059 (m), 1035 (m), 996 (w), 943 (m), 916 (m), 880 (m), 832 (m), 760 (s), 727 (w), 664 (s). Elemental Analysis (%) for C₂₁H₂₉NO₃S.: Calcd. C, 67.17; H, 7.78; N, 3.73. Found C, 66.88; H, 7.76; N, 3.74.

2.3.4 Synthesis of N-(5-(*tert*-butyl)-2-hydroxyphenyl)-2,4,6-triisopropylbenzenesulfonamide (L4H₂).

Synthesized using a similar procedure as **L2H₂**, from 2-amino-4-(*tert*-butyl)phenol (5.00 g, 30.3 mmol), pyridine (23.93 mL, 300.2 mmol) and 2,4,6-triisopropylbenzenesulfonyl chloride (10.9 g, 35.9 mmol) gave a white solid (10.09 g, 77 %, yield). ¹H-NMR (400 MHz, CDCl₃): δ 7.13 (s, 2H), 7.11 (dd, 1H), 6.91 (d, 1H), 6.49 (s, 1H), 6.35 (d, 1H), 3.88 (m, 2H), 2.88 (m, 1H), 1.23 (d, 6H), 1.12 (d, 12H), 0.98 (s,

9H). ^{13}C -NMR (101 MHz, CDCl_3): δ 153.6, 150.9, 150.8, 143.6, 131.0, 126.4, 125.1, 124.1, 121.1, 116.7, 34.4, 33.9, 31.3, 30.2, 24.8, 23.7. FT-IR (ATR, cm^{-1}): 3313 (m), 3264 (m), 3047 (w), 2953 (m), 2902 (w), 2864 (m), 1600 (m), 1567 (w), 1512 (m), 1462 (w), 1444 (w), 1426 (w), 1393 (m), 1360 (m), 1323 (s), 1305 (m), 1276 (m), 1258 (m), 1193 (w), 1148 (vs), 1128 (vs), 1092 (w), 1070 (w), 1060 (w), 1036 (w), 952 (m), 902 (w), 880 (m), 844 (w), 818 (s), 754 (w), 735 (m), 677 (vs), 663 (vs), 627 (m). Elemental Analysis (%) for $\text{C}_{25}\text{H}_{37}\text{NO}_3\text{S}$.: Calcd. C, 69.57; H, 8.64; N, 3.25. Found C, 69.61; H, 8.60; N, 3.41.

2.3.5 UV-Vis Titrations

UV-Vis titrations were carried out at constant ligand and NaOH concentrations, with sole variable the concentration of Ln(III), as follows: Stock solutions of **L1H₂**, **L2H₂**, **L3H₂**, or **L4H₂** (1.0 mM) and NaOH (2.2 mM) were prepared in 10.0 mL of methanol. These were then subsequently diluted with acetonitrile (1.00 mL to 25.0 mL) to yield solutions of **L1H₂**, **L2H₂**, **L3H₂**, or **L4H₂** (40.0 μM) and NaOH (88.0 μM) in $\text{CH}_3\text{CN}:\text{CH}_3\text{OH}$ (96:4, v/v) (Solution A). A 4.0×10^{-4} M solution of $\text{Sm}(\text{NO}_3)_3 \cdot 6\text{H}_2\text{O}$ (Solution B) was then prepared by weighing appropriate amount and dissolving this in 10.0 mL of Solution A, resulting in a solution of $\text{Sm}(\text{NO}_3)_3 \cdot 6\text{H}_2\text{O}$ (400.0 μM), ligand (40.0 μM) and NaOH (88.0 μM) in $\text{CH}_3\text{CN}:\text{CH}_3\text{OH}$ (96:4, v/v) (Solution B). Solution A (2.70 mL) was placed in a 1.00 cm cuvette cell and was titrated with solution B in small additions until 0.80 mL total was added. The observed wavelength was from 200 nm to 400 nm as no significant change in absorbance was noticed outside this range. Titration

experiments were done in triplicate independent samples. For reference, a blank solution, comprising a mixed solvent of 0.40 mL methanol and 9.60 mL acetonitrile was used. The stability constants were obtained by the nonlinear least square fitting program HypSpec®,^{24,25} and are reported as average values with standard deviations obtained from triplicate independent experiments.

2.3.6 Continuous variation method (Job Plots)^{26,27}

Stock solutions of ligand / NaOH (0.020 mM / 0.050 mM) in CH₃CN:CH₃OH (96:4, v/v) - Solution A) and Sm(NO₃)₃.6(H₂O) (0.020 mM) in CH₃CN:CH₃OH (96:4, v/v) - Solution B) were prepared, and were mixed in different ratios in 11 vials each with total volume of 5.00 mL, as follows (in mL): 5:0, 4.5:0.5, 4:1, 3.5:1.5, 3:2, 2.5:2.5, 2:3, 1.5:3.5, 1:4, 0.5:4.5, 0:5. UV-Vis spectra were collected and the absorbance at 250 nm was plotted against the molar fraction as ΔA_{250} vs. $[L]_t / ([Sm(III)]_t + [L]_t)$.

2.3.7 pH-dependent extraction and stripping of Sm(III) with CH₂Cl₂ as a diluent and spectrophotometric determination of [Sm(III)]_t.

Aqueous solutions of Sm(III) were prepared (2.0 mM of Sm(NO₃)₃.6(H₂O)), and the pH was adjusted to pH 10.0 – 14.0 by varying the NaOH concentration (1.0 × 10⁻⁴ M – 1.0 M). Ligand stock solutions (30.0 mM) were prepared in CH₂Cl₂. 2.50 mL of each phase were brought into extended contact by rotating sealed vials on a wheel (55 rpm) for 22 h at room temperature (22°C) and then centrifuged for 5 min (3200 rpm) to fully separate the two phases. The organic phases were subsequently collected and filtered in

preparation for stripping. For stripping, 1.00 mL of 0.1M HNO₃ was added to 1.00 mL of the filtered loaded organic phase and both layers were again brought into extensive contact on the rotating wheel for 20 h (55 rpm) at room temperature (22°C), and then centrifuged for 5 min (3200 rpm) to fully separate the two phases. The aqueous phases were collected and Sm(III) was quantified using the Arsenazo-III spectrophotometric method.²⁸ Specifically, solutions were prepared containing 0.10 mL of the aqueous phase after stripping (or the aqueous phase after extraction), 1.00 mL of 1% ascorbic acid, 1.00 mL of 0.2 M formate buffer (pH 3.0) and 2.00 mL of 0.05% Arsenazo-III solution. The pH of this solution was then adjusted to pH 2.6 ± 0.1 using 0.1 M HNO₃ and diluted with water to 25.0 mL. The UV-Vis absorbance of this solution at 652 nm was measured and concentrations were calculated from the slope of a 200 ppm to 500 ppm calibration curve prepared using a 1000 µg/mL Sm(III) standard solution. Reported quantification was expressed in % recovery (eq. 2.1) based on the concentration of Sm(III) quantified after stripping and the initial concentration of Sm(III) before contact with the organic phases.

$$Sm(III)Recovery = \frac{[Sm(III)]_{t(aq.) \text{ after stripping}}}{[Sm(III)]_{t(aq.) \text{ initial}}} \times 100 \% \quad (\text{eq. 2.1})$$

% Sm(III) recoveries were calculated after triplicate independent experiments each with a single loading / stripping cycle and the reported errors were determined from the standard deviation of the triplicate independent experiments.

2.3.8 pH-dependent extraction and stripping of Ln(III) with CH₂Cl₂ as a diluent and ICP-MS determination of [Ln(III)]_t.

Aqueous solutions of La(III), Nd(III), Sm(III), or Eu(III) were prepared (2.0 mM of Sm(NO₃)₃·6(H₂O), Nd(NO₃)₃·6(H₂O), La(NO₃)₃·6(H₂O), or Eu(NO₃)₃·6(H₂O)) and the pH was adjusted to pH 10.0 – 14.0 by varying the NaOH concentration (1.0 × 10⁻⁴ M – 1.0 M). Ligand stock solutions (30.0 mM) were prepared in CH₂Cl₂. 2.50 mL of each phase were brought into extended contact by rotating sealed vials on a wheel (55 rpm) for 22 h at room temperature (22°C) and then centrifuged for 5 min (3200 rpm) to fully separate the two phases. The organic phases were subsequently collected and filtered in preparation for stripping. For stripping, 1.00 mL of 0.1M HNO₃ was added to 1.00 mL of the filtered loaded organic phase and both layers were again brought into extensive contact on the rotating wheel for 20 h (55 rpm) at room temperature (22°C), and then centrifuged for 5 min (3200 rpm) to fully separate the two phases. The aqueous phases were collected and the Ln(III) was quantified using ICP-MS after dilution to 50.0 ppb with 2% HNO₃. For calibration, standard solutions for each Ln(III) were used to prepare Ln(III) solutions with concentrations ranging from 0 ppb to 50.0 ppb in 2% HNO₃. Afterwards, 5.00 μL of 10.0 ppm Y(III) used as internal standard was added to all the samples, and 5.00 mL of the solutions was analysed by ICP-MS and counted for the Ln(III) of interest. Concentrations of recovered Ln(III) were then calculated from the slope obtained from prior calibration. Reported quantification was expressed in % recovery (eq. 2.2) based on the concentration of Ln(III) quantified after stripping and the initial concentration of Ln(III) before contact with the organic phases.

$$\text{Ln(III) Recovery} = \frac{[\text{Ln(III)}]_{t(\text{aq.}) \text{ after stripping}}}{[\text{Ln(III)}]_{t(\text{aq.}) \text{ initial}}} \times 100 \% \quad (\text{eq. 2.2})$$

Percent Ln(III) recoveries were calculated after triplicate independent experiments each with a single loading-stripping cycle. The reported errors were determined from the standard deviation of the triplicate independent experiments.

2.3.9 pH-dependent extraction and stripping of Sm(III) with *n*-dodecane:octanol (80:20, v/v) as a diluent and spectrophotometric determination of [Sm(III)]_t.

These experiments were performed as described in 2.3.7 with the following modifications: *n*-dodecane:octanol (80:20, v/v) was used as diluent.

2.3.10 Extraction and stripping of Sm(III) with CH₂Cl₂ as a diluent with various concentration of L2H₂.

Experiments were performed as described in 2.3.7 except that fourteen test tubes were used with the same aqueous phases (1.0 mM Sm(III) in 0.1 M NaOH - pH = 13.0), and organic phases with varied concentrations of L2H₂ (0 mM – 20.0 mM) in CH₂Cl₂. Contact time of 24 h was used for loading. The aqueous phases were analyzed for Sm(III) by ICP-MS as described in section 2.3.8.

2.3.11 Theoretical Studies of Ln(III) complexation – DFT calculations.

Quantum mechanical calculations by Density Functional Theory (DFT) were used to determine the structures and energetics of Sm(III)-L2 complexation in solution.

Unrestricted DFT calculations were carried out without symmetry restrictions using the B3LYP hybrid density functional (UB3LYP) with the 6-31+G* basis set for H, C, N, O, and Stuttgart Relativistic Small Core 1977 effective core potential for Sm (basis set B0) using Gaussian-09 software. The calculated electronic states were verified by checking the stability of the SCF solutions. Geometry optimizations were carried out in the gas phase. The frequency calculations with basis set B0 were used to confirm that the optimized structures are true minimums on the potential energy surface, obtain zero-point energy (ZPE) corrections, and calculate gas-phase free energies. The Polarizable Continuum Model (PCM) and Solvation Model based on Density (SMD) models were used to take the solvent effect into account.

2.3.12 X-ray crystallography for L1H₂, L2H₂, L3H₂, and L4H₂

White translucent crystals of the ligands were obtained by slow evaporation of dichloromethane ligand solutions (for **L1H₂**, **L3H₂**, and **L4H₂**) or methanol ligand solutions (for **L2H₂**). Crystals suitable for measurement were mounted on a Bruker D8 Quest diffractometer bearing PHOTON II detector and at T = 298 K. Structures were resolved using direct methods and refined by Least Squares using version 2018/3 of ShelXL.²⁹ All non-hydrogen atoms were refined anisotropically while calculations and molecular graphics were performed using SHELXTL 2014 and Olex30 programs. Structural refinement details and associated data are as given in Table 2.3 – 2.14.

2.4 Results and discussion

2.4.1 Synthesis and general characteristics of studied *o*-sulfonamidophenol ligand family

The four *o*-sulfonamidophenol ligands **L1H₂**, **L2H₂**, **L3H₂**, and **L4H₂** (Figure 2.1) were synthesized from the corresponding anilines and sulfonyl chlorides using a modification of reported procedures^{22,23,31} and the latter three, which are newly reported compounds, were characterized by ¹H-NMR, ¹³C-NMR, FT-IR, and elemental analysis. X-ray crystal structures for all four ligands are also newly reported herein. As our prior work with disulfonamides has demonstrated,²⁰ complexing groups located in ortho positions are favorable for f-element complexation, yet no Sm(III) recovery with *o*-phenylenediamine-derived sulfonamides was observed from 1 M NaOH, presumably because of precipitation.²⁰ Furthermore, these earlier ligands are not soluble in practical highly lipophilic diluents, such as *n*-dodecane and *n*-octanol. The *o*-sulfonamidophenol ligands introduced in this work bearing isopropyl and *tert*-butyl groups were chosen in order to provide improved extraction efficiencies, because they are expected to have higher solubility in organic diluents,³² as well as radiolytic stability.^{33,34}

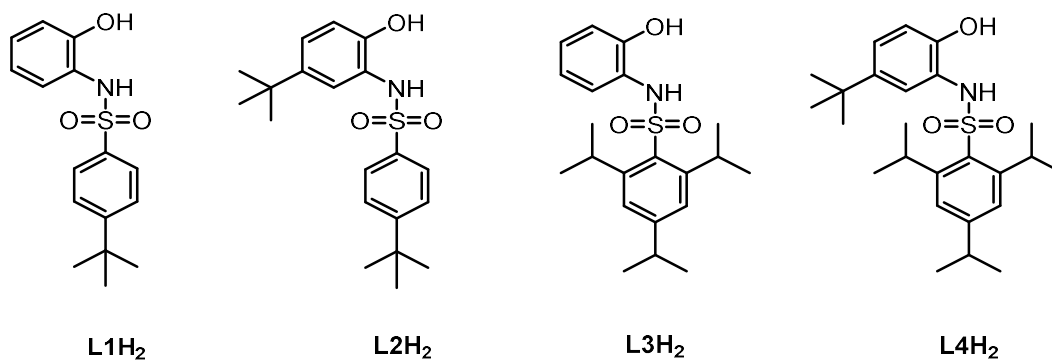


Figure 2.1. *o*-Sulfonamidophenol ligands studied for complexation and extraction of f-elements

2.4.2 UV-Vis titrations

UV-Vis spectrophotometric titrations with Sm(III) under constant ligand and NaOH concentration were carried out in order to elucidate the complexation mode with Sm(III) and the stability of the formed complexes in solution. The solvent of choice was CH₃CN:CH₃OH (96:4, v/v), as it allowed for all components (ligands, Sm(NO₃)₃·6H₂O and NaOH, needed to deprotonate the ligand) to be soluble. Titrations involving all ligands (**L1H₂** - **L4H₂**) (40.0 μM) in the presence of NaOH (88.0 μM) gave hypochromic shifts for the 250 nm absorbance bands (Figure 2.2 a-d) in response to incremental addition of Sm(III) (4.0×10^{-4} M). For **L1H₂** - **L2H₂**, the low energy absorbance at the 300 nm range also gave a hypochromic shift, with an increase at 280 nm (Figure 2.2 a-b). For **L3H₂** - **L4H₂**, the low energy absorbance at the 310 nm area showed a more conspicuous hypochromic shift and a more prominent increase at 280 nm, than for **L1H₂** - **L2H₂**, with two isosbestic points at 275 nm and 287 nm for **L3H₂** and 270 nm and 290 nm for **L4H₂** (Figure 2.2 c-d), confirming the formation of a Sm(III) complex in solution. For all ligands, upon addition of Sm(III) beyond 20 μM, which corresponds to the formation of a 1:2 complex, there were no noticeable observed changes in the spectra, other than a sustained increase at 219 nm attributed to the excess Sm(III) salt. As the saturation at 20 μM of added Sm(III) occurs at half of the original ligand concentration of 40 μM, it suggests the formation of complexes with the formula [Sm(III)L₂], assuming the ligands are bis-deprotonated, and presumably with additional coordination of H₂O or CH₃CN to Sm(III) to satisfy the higher coordination numbers, which are typical for Ln(III). The stability constants obtained for the 1:2 complexes after

non-linear regression analysis of triplicate independent titrations for each ligand to the 1:2 binding isotherm, by the HypSpec® program (Table 2.1) show very high stability for all 1:2 complexes, with the **L3H₂** ligand, containing the triisopropyl substitution in the sulfonyl ring and no substitution on the phenolic ring showing the strongest binding to Sm(III), among the series with a $\beta_2 = 1.26 (\pm 0.04) \times 10^{12} \text{ M}^{-2}$.

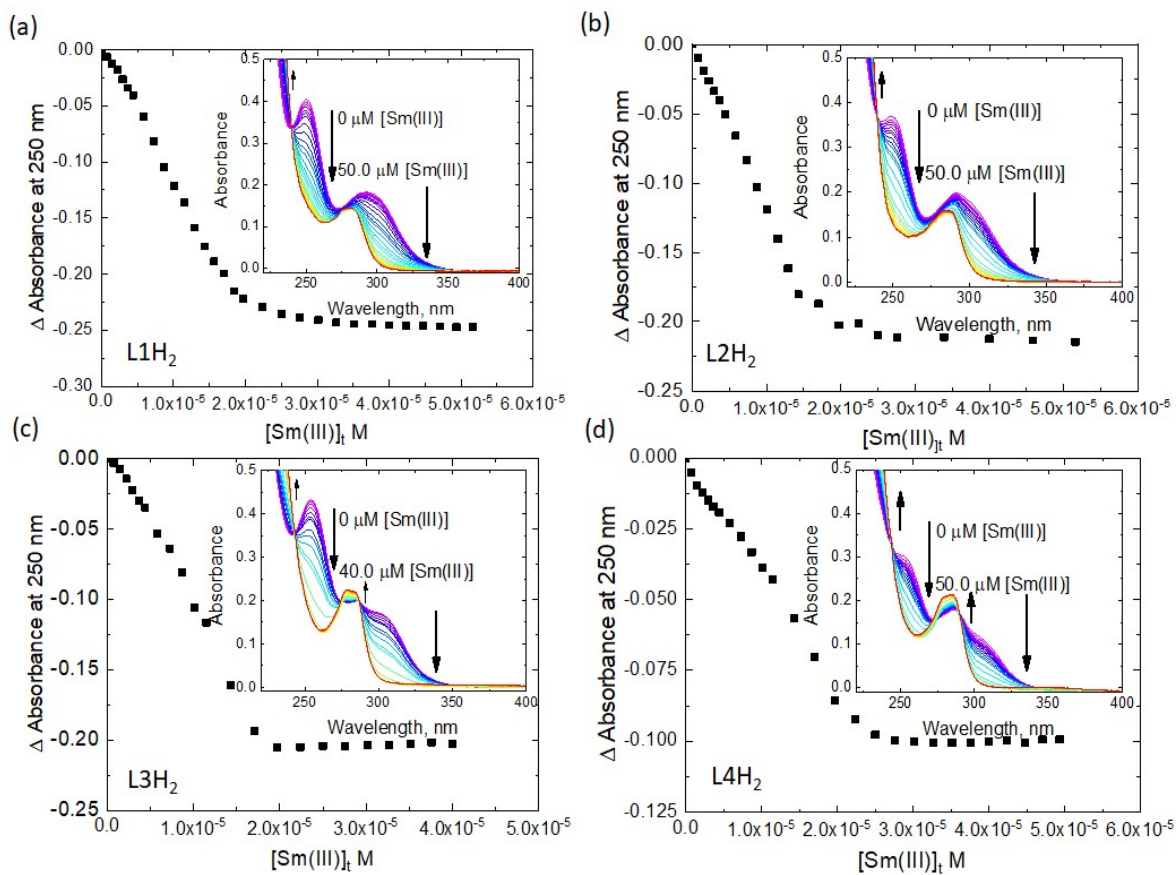


Figure 2.2. UV-Vis titration plots show change in absorbance at 250 nm plotted against concentration of Sm(III). Inset: Changes in UV-Vis spectra of ligands upon titration with $\text{Sm}(\text{NO}_3)_3 \cdot 6\text{H}_2\text{O}$ ($4.0 \times 10^{-4} \text{ M}$) (a) **L1H₂** (b) **L2H₂** (c) **L3H₂**, or (d) **L4H₂** in $\text{CH}_3\text{CN}:\text{CH}_3\text{OH}$ (96:4, v/v) at constant concentrations of **LH₂** ($4.0 \times 10^{-5} \text{ M}$) and NaOH ($8.8 \times 10^{-5} \text{ M}$).

Table 2.1. Stability constants for formation of $[\text{Sm(III)L}_2]^-$ 1:2 complexes from UV-Vis titrations in $\text{CH}_3\text{CN}:\text{CH}_3\text{OH}$ (96:4, v/v).

Ligand	β_2 for $[\text{Sm(III)L}_2]^-$ (M^{-2})
L1H₂	$3.20(\pm 0.20) \times 10^{11}$
L2H₂	$3.98(\pm 0.03) \times 10^{11}$
L3H₂	$1.26(\pm 0.04) \times 10^{12}$
L4H₂	$3.98(\pm 0.01) \times 10^{10}$

2.4.3 Continuous variation method for determination of binding stoichiometry (Job Plots)

Using the method of continuous variation, by mixing solutions of **L2H₂** or **L4H₂** (20.0 μM) and NaOH (50.0 μM) with solutions of $\text{Sm}(\text{NO}_3)_3 \cdot 6\text{H}_2\text{O}$ (20.0 μM) in $\text{CH}_3\text{CN}:\text{CH}_3\text{OH}$ (96:4, v/v) at variable ratios, scatter plots (Job Plots) were obtained with maxima at molar ratios of 0.63 and 0.68 for **L2H₂** and **L4H₂** respectively (Figure 2.3), which are consistent with a 1:2 metal to ligand stoichiometry in solution and in excellent agreement with the titration studies.

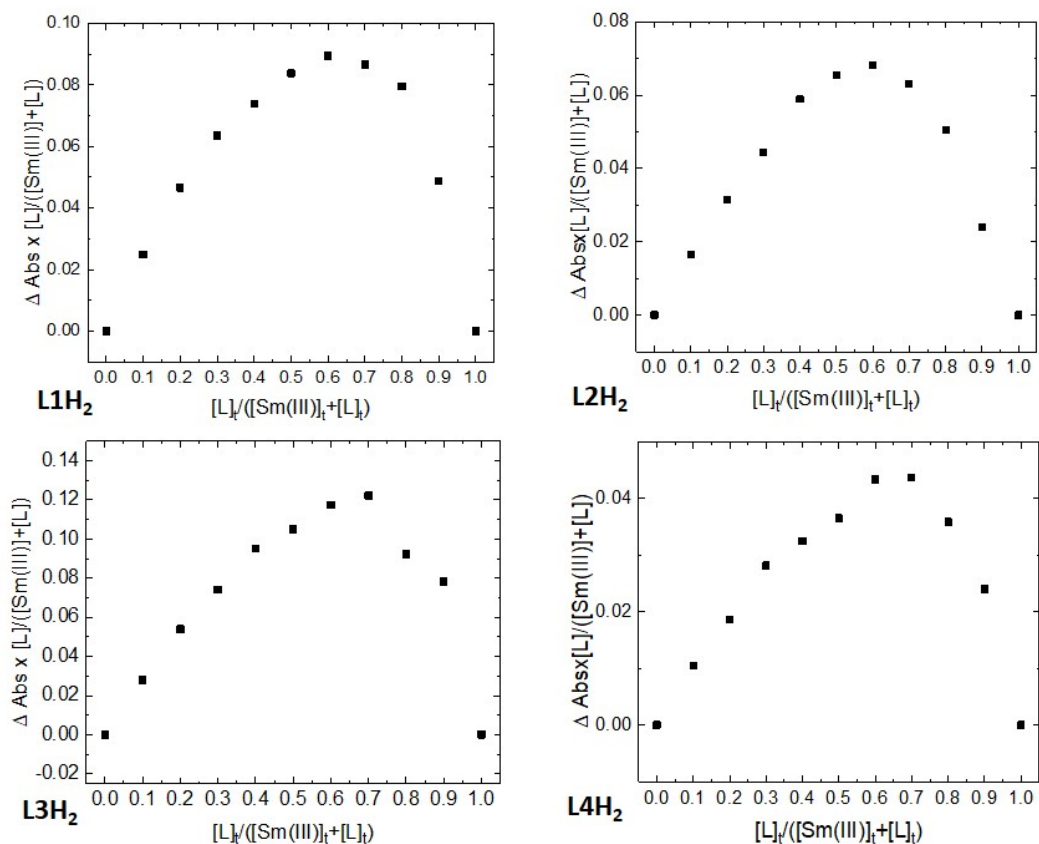


Figure 2.3. Job plots for ligands ($2.0 \times 10^{-5} M$) and NaOH ($5.0 \times 10^{-5} M$), with Sm(III) ($2.0 \times 10^{-5} M$) in $CH_3CN:CH_3OH$ (96:4, v/v). Absorbance taken at 250 nm.

2.4.4 Extraction and recovery of Sm(III) and other Ln(III) with CH_2Cl_2 as a diluent

All four ligands **L1H₂** - **L4H₂** were tested for extraction and recovery of Sm(III) into CH_2Cl_2 from solutions of increasing alkalinity (pH 10.0 - 14.0), using a constant concentration of ligand (30.0 mM) and Sm(III) (2.0 mM). After a single contact of the aqueous phases with the ligand solutions in CH_2Cl_2 , followed by a single stripping contact with 0.1 M HNO_3 the amount of recovered Sm(III) in the aqueous phases after stripping was quantified by the spectrophotometric Arsenazo-III method, with ICP-MS

confirming the results for all ligands (Figure 2.4), peak Sm(III) recoveries were obtained either at pH 12.5 (for **L1H₂**), with 72.8 (± 4.2)%, or at pH 13.0 (for **L2H₂** and **L3H₂**), with 96.1 (± 4.4)% and 57.3 (± 3.6)%, respectively. **L4H₂** on the other hand had a maximum at pH 14.0 with 78.4 (± 16.4)% Sm(III) recovery. These recoveries are significantly higher than prior reported recoveries with disulfonamide ligands reported by our group especially at such high alkalinity,^{20,21} or any other reported ligands for recovery of Ln or An in alkaline conditions. Most notably, and unlike what is the case for our prior disulfonamide work, the effective extraction is maintained even at pH 14.0 for **L2H₂**, **L3H₂**, and **L4H₂**, with corresponding recoveries of 93.3 (± 5.2)%, 41.9 (± 5.3)%, and 78.4 (± 16.4)% respectively, while **L1H₂** shows no extraction at pH 14.0, as it was the case with the prior studied disulfonamides²⁰ and other ligands.^{16,18,35-38} The variations in % Sm(III) recovery with the “dips” observed at pH = 13.5 for **L2H₂** and pH = 13.0 for **L4H₂** are not unexpected, as those variations have been observed in our prior reported work with disulfonamides,²⁰ and also by others for Am(III) recovery by calixarene ligands.^{18,36} However, unlike our prior disulfonamide ligand family, which showed no extraction at pH 14.0, both **L2H₂** and **L4H₂** maintained their impressive Sm(III) extraction ability at highly alkaline conditions. **L2H₂**, which can be considered the best performing ligand in the series, recovers 15.5 (± 11.5)% of Sm(III) at pH 11.5 and shows two maxima at pH 13.0 and 14.0 with 96.1 (± 4.4)% and 93.3 (± 5.2)% respective Sm(III) recoveries (Figure 2.4). In all experiments, for pHs higher than 11.5 precipitation was observed, which was more prominent at higher pHs. It is presumed that the precipitation is due to the formation of less soluble hydroxo adducts of type $[\text{Sm(III)L}_2(\text{OH}^-)_x]^{-(x+1)}$, in which OH⁻ instead of H₂O coordinates to Sm(III), as it was

shown in our prior work with disulfonamides,²⁰ and by others for actinides.³⁹ In all these extraction experiments, complexation is presumed to occur by the ligand in its bis-deprotonated form as the alkaline aqueous phase on contact with the organic phase deprotonates the O- and N- donor sites in the ligand. As deprotonation depends on the acidity of the ligand, ligands with lower acidity would be expected to require higher alkalinity for deprotonation and complex formation. In our case the pK_a of the phenolic moiety is estimated between 9.98 – 10.26⁴⁰⁻⁴² and for the sulfonamide moiety between 9.65 – 11.69,⁴³ The expected order of decreasing acidity, based on the inductive effect of alkyl substituents within the series is $L1H_2 > L2H_2 \geq L3H_2 > L4H_2$, which shows some correlation, with the steep increases observed in Sm(III) recovery for $pH > 11.0$ for $L1H_2$ or $L2H_2$ and $pH > 11.5$ for $L3H_2$ and $L4H_2$ (Figure 2.4). This ligand deprotonation and complexation can only occur for higher pH, and this explains why no extraction was observed at $pH < 11.0$ for any of the ligands. Upon deprotonation, the ligand is presumed to successfully compete with H_2O and OH^- in the Sm(III) coordination sphere, with ion-pair Sm(III) complexes of type $Na[Sm(III)L_2(H_2O)_x]$ and $Na_2[Sm(III)L_2(H_2O)_x(OH)]$ presumably involved in the transfer of Sm(III) to the organic phase. The solubility of such species in organic solvents is very dependent on the nature of the ligand frameworks, and thus ligands like $L2H_2$ and $L4H_2$, which are substituted in both aromatic rings, are more likely to form soluble ion pairs in less polar organic solvents, such as CH_2Cl_2 . Likewise, the extraction variability at higher pH values can be attributed to various degrees of solubility in the organic solvent for ion-paired species of type $Na[Sm(III)L_2(H_2O)_x]$ and $Na_2[Sm(III)L_2(H_2O)_x(OH)]$, especially as more insoluble highly-charged species of the latter type are increasingly formed in

higher pH and may precipitate in varying extents, depending on the ligand frameworks. Therefore the persistent Sm(III) extraction efficiency for **L2H₂** could be attributed to the fact that the two *t*-butyl groups allow soluble ion pair formation, without sterically hindering Sm(III) complexation, even when more highly charged hydroxo species are formed at highly alkaline solutions, while still facilitating deprotonation of ligand and complex formation at pH > 11.0. The more lipophilic **L4H₂**, on the other hand, stabilizes the highly charged ion pairs at alkaline pH, yet its complexation of Sm(III) and satisfaction of its coordination sphere may be sterically hindered by the bulky isopropyl groups. The modest performance of **L1H₂** and its inability to extract any Sm(III) at pH 14.0 is attributed to the insolubility of the formed Sm(III) ion pairs at high pH, while **L3H₂** has a combination of good enough lipophilicity, but also a steric hindrance, and thus performs between **L1H₂** and the most effective ligands (**L4H₂** and **L2H₂**).

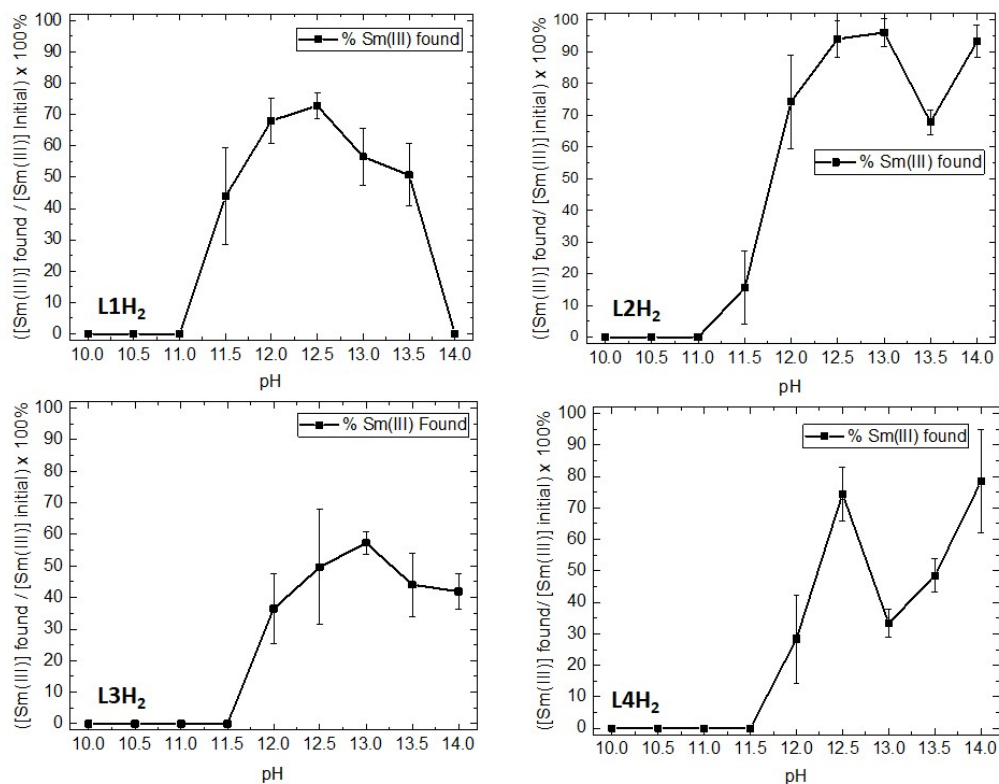


Figure 2.4. Percent Sm(III) recovered after extraction and stripping (0.1 M HNO₃) with **L1H₂**-**L4H₂** (30.0 mM in CH₂Cl₂) for pH 10.0 – 14.0. Initial Sm(III) concentration was 2.0 mM. Sm(III) recovered was quantified using the Arsenazo-III spectrophotometric method (for **L1H₂** and **L2H₂**) and ICP-MS (for **L3H₂** and **L4H₂**).

As **L2H₂** was the best performing ligand, we carried out a detailed investigation into the Sm(III) mass balance by analyzing Sm(III) in the alkaline aqueous phases after extraction (Figure 2.5). Sm(III) quantification was performed using the Arsenazo-III spectrophotometric method.^{20,28} At pH 10.0, 91.8% of the metal remained in the aqueous phase, this being attributed to the ligand not being deprotonated and thus not being available to form a Sm(III) complex. At a pH range of 10.5 - 11.5, there is a decrease in the leftover Sm(III) in the alkaline aqueous phase, but this decrease is not complemented by an increase in Sm(III) recovery after stripping. This is attributed to the loss of Sm(III)

due to precipitation of metal hydroxides, while the ligand cannot effectively compete with OH^- by complexing Sm(III) , as it is still not fully deprotonated. A white visible precipitate was filtered off, before analysis, explaining this Sm(III) loss. Moving on to higher pH (12.5 – 13.0), the mass balance improves, approaching 100%, indicating that complexation competes successfully with hydrolysis, forming soluble and extractable species of type $\text{Na}[\text{Sm(III)L2}_2(\text{H}_2\text{O})_x]$ and $\text{Na}_2[\text{Sm(III)L2}_2(\text{H}_2\text{O})_x(\text{OH})]$. For higher pH (13.5 to 14.0) there is once again loss due to precipitation, which can be attributed to even more highly charged hydroxo species of limited solubility or shifts in equilibria between the more soluble $\text{Na}[\text{Sm(III)L2}_2(\text{H}_2\text{O})_x]$ and the less soluble $\text{Na}_2[\text{Sm(III)L2}_2(\text{H}_2\text{O})_x(\text{OH})]$ favored in more alkaline solutions.

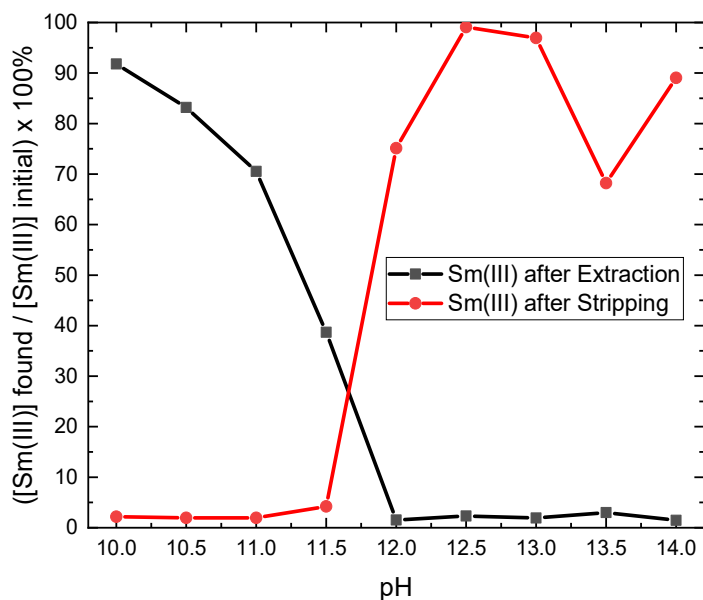


Figure 2.5. Mass balance for Sm(III) recovered after extraction and stripping (0.1 M HNO_3) by L2H_2 (30.0 mM) in CH_2Cl_2 $[\text{Sm(III)}]_i = 2.0 \text{ mM}$. Sm(III) recovered and measured in the acidic aqueous phase after extraction and consecutive stripping is noted by the red circles, while soluble leftover Sm(III) in the aqueous phase is noted by the black squares. Sm(III) recovered was quantified by the Arsenazo-III spectrophotometric method.

To elucidate the metal to ligand binding stoichiometry in the organic phase during extraction, we performed extraction experiments under the same conditions described above at pH 13.0, for which $[\text{Sm(III)}]_t$ was maintained at 1.0 mM and $[\text{L2H}_2]_t$ varied from 0 – 20.0 mM. A steady increase in % Sm(III) recovered was observed by increasing the $\text{L2H}_2/\text{Sm(III)}$ ratio with efficiency spanning from 3% to 84 % (Figure 2.6). Saturation beyond the point in which $[\text{L2H}_2]_t = 2.0$ mM occurred providing additional evidence that 1:2 Sm(III)- L_2 complexes of type $\text{Na}[\text{Sm(III)}\text{L}_2(\text{H}_2\text{O})_x]$ $\text{Na}_2[\text{Sm(III)}\text{L}_2(\text{H}_2\text{O})_x(\text{OH})]$ are formed in CH_2Cl_2 , and in agreement with the observations at the UV-Vis titrations in $\text{CH}_3\text{CN}:\text{CH}_3\text{OH}$ (96:4, v/v).

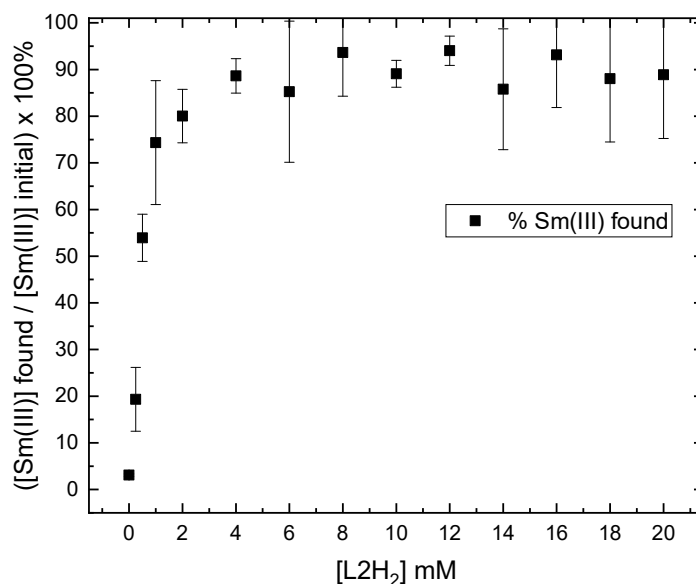


Figure 2.6. Percent Sm(III) recovered after extraction and stripping (0.1 M HNO_3) as a function of increased concentration of L2H_2 at pH 13.0. Aqueous phase: $[\text{Sm(III)}]_t = 1.0$ mM in 0.1 M NaOH. Organic phase: $[\text{L2H}_2]_t = 0 - 20.0$ mM). Sm(III) recovered was quantified using ICP-MS.

As L2H_2 showed strong Sm(III) extraction and recovery at high pH, extraction studies were also performed with other Ln(III). The extraction and recovery by L2H_2

(30.0 mM in CH₂Cl₂) of four lanthanides, La(III), Nd(III), Sm(III), and Eu(III), added as 2.0 mM nitrate hexahydrate salts and added together in the same aqueous phase was determined under the same loading and stripping conditions, as described earlier in this section, followed by ICP-MS analysis. The overall trend for Ln(III) recoveries (Figure 2.7) was similar between different Ln(III), with no Ln(III) extraction for pH < 11.0, and average maxima for extraction of 85% at pH 13.5 and > 70% at pH 14.0. These results further demonstrate the applicability of sulfonamidophenol **L2H₂** for Ln(III) recovery from alkaline conditions and are consistent with the Sm(III) recovery results shown previously (Figure 2.4). The lower percent recovery for each Ln(III) in the combined experiment, compared to the Sm(III)-only experiment is expected as several Ln(III) compete with each other for ligand complexation in the same solution and the overall Ligand/[Ln(III)]_t concentration ratio is lower at 15/4 vs. 15/1 in the Sm(III)-only experiment.

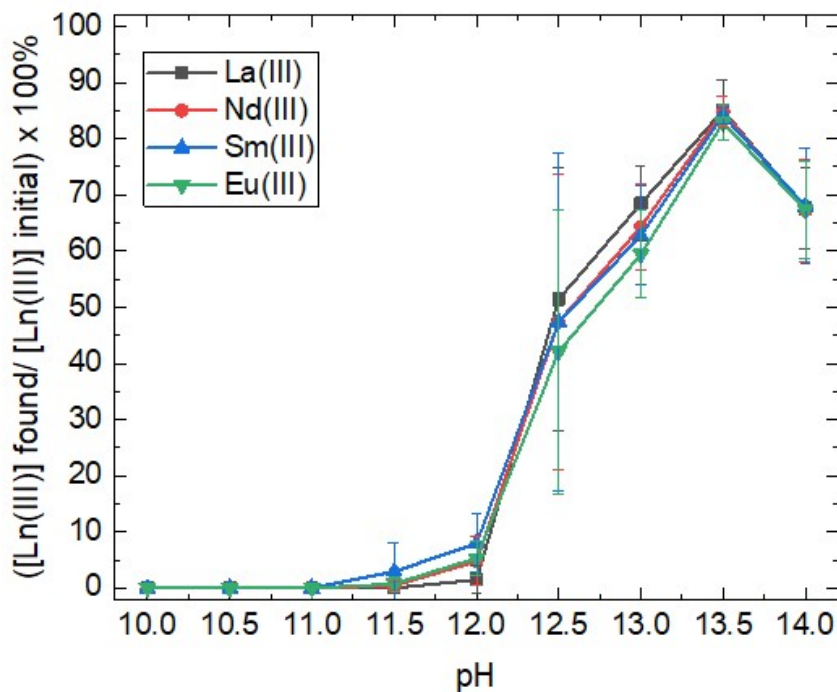


Figure 2.7. Percent La(III), Nd(III), Sm(III), and Eu(III) recovered after extraction and stripping (0.1 M HNO₃) by **L2H₂** (30.0 mM) in CH₂Cl₂ [Ln(III)]_i = 2.0 mM, Ln(III) recovered was quantified using ICP-MS.

2.4.5 Extraction and recovery of Sm(III) with *n*-dodecane:octanol (80:20, v/v) as diluent.

The effect of diluent choice on the extraction efficiency for **L2H₂** and **L4H₂** was also investigated using more lipophilic process solvents, similar to diluents used in industrial separations - these are preferred due to very limited partition and ligand loss after repeated contacts and strips.⁴⁴ For both ligands and after just one extraction / stripping cycle a high percent of Sm(III) was recovered with recovery maxima for **L2H₂** of 82.6 (±9.3)% at pH 12.5 and of 53.9 (±4.0)% at pH 14.0 while **L4H₂** gave a Sm(III)

recovery maximum of 58.5 (± 3.1)% at pH 14.0 (Fig. 2.7). Lower Sm(III) recoveries when the diluent is switched from dichloromethane to *n*-dodecane:octanol (80:20, v/v) are expected^{45,46} and can be attributed to CH₂Cl₂ being more polar (dielectric constant = 9.08 at 20°C)⁴⁷ compared to a mixture of *n*-octanol (dielectric constant = 10.30)⁴⁸ and *n*-dodecane (dielectric constant = 2.01).⁴⁸ Similar trends have been reported elsewhere for extractions involving other metals that suggest ion pair-induced extraction is often favored for diluents with higher dielectric constants.^{45,46,49} And to the best of our knowledge, these recoveries approaching 60% at pH 14.0, and in process solvents are the highest extraction efficiencies for Ln(III) in pH = 14.0 reported in the literature for any ligand system, and provide immediate potential for separation application.

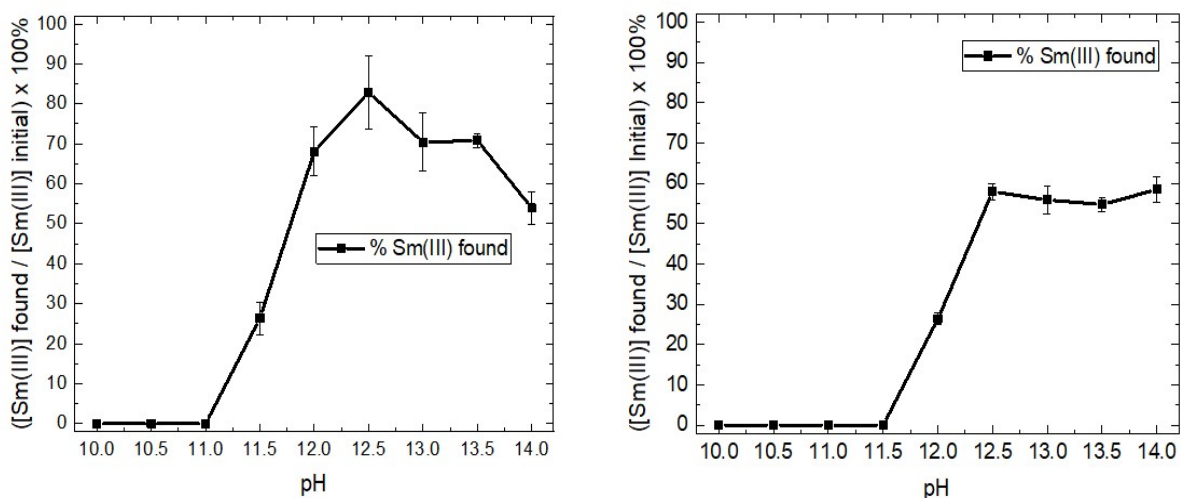


Figure 2.8. Percent Sm(III) recovered after extraction and stripping (0.1 M HNO₃) by **L2H₂** (left) and **L4H₂** (right) (30.0 mM respectively) in *n*-dodecane:octanol (80:20, v/v) [Sm(III)]_t = 2.0 mM. Sm(III) recovered was quantified using the Arsenazo-III spectrophotometric method.

2.4.6 Density Functional Theory (DFT) calculations

DFT quantum mechanical calculations were performed in order to gain insight into the structures, energetics, and coordination mode for the possible 1:2 vs 1:1 Sm(III):L complexes in dichloromethane. For the formation of 1:2 and 1:1 complexes, three likely coordination patterns were obtained for both schemes. For the 1:2 complexation scheme in highly alkaline conditions, Sm(III) exists predominantly in its hydroxide form. Complexes were formed (Figure 2.9 – 2.14) with OH^- , NO_3^- , H_2O , and L^{2-} or L^{2H^-} , satisfying the coordination environment of Sm(III).

Sm(L2)(L2H).2H₂O complex (Coordination Number = 7).

In this complexation scheme, two ligands are bound to one Sm(III), one of the ligands is bis-deprotonated and binds with Sm(III) using the oxygen and nitrogen from the deprotonated -OH and -NH groups, while the second ligand binds in a monodentate fashion, using one oxygen from the now deprotonated -OH (Figure 2.9), the coordination environment is further consolidated by an oxygen from each of the sulfonyl groups on both ligands while two water molecules complete the coordination sphere for the neutral complex and gives this proposed complex a coordination number of 7.

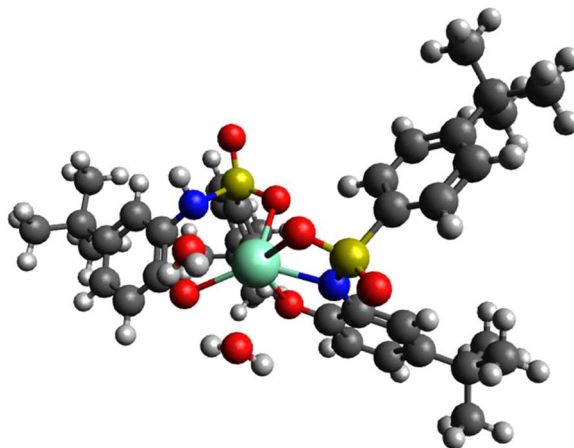
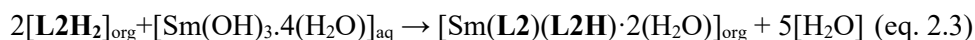


Figure 2.9. Structure of a 1:2 Sm(III) complex with **L2H₂**, **Sm(L2)(L2H).2H₂O**. **L2H** indicates a mono-deprotonated ligand on the phenolic O-atom.

The likely reaction scheme for the formation of this complex is as given in equation 2.3 while important dimensional parameters are given in Table 2.2.



Sm(L2)(L2H)*.2H₂O complex (Coordination Number = 7).

In this complexation scheme, two ligands are bound to one Sm(III), one of the ligands is bis-deprotonated and binds with Sm(III) using the oxygen and nitrogen from the deprotonated -OH and -NH groups while the second ligand binds in a monodentate fashion, using one nitrogen from the now deprotonated -NH (Figure 2.10), the coordination environment is further consolidated by an oxygen from each of the sulfonyl groups on both ligands while two water molecules complete the coordination sphere for the neutral complex and gives this proposed complex a coordination number of 7.

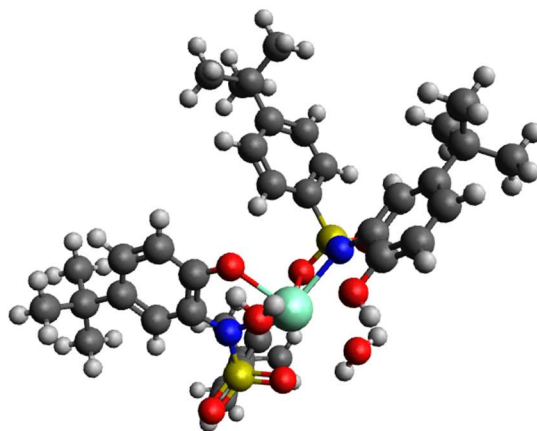


Figure 2.10. Structure of a 1:2 Sm(III) complex with $L2H_2$, $Sm(L2)(L2H)^* \cdot 2H_2O$. ($L2H^*$ indicates a mono-deprotonated ligand on the sulfonamide N-atom).

The likely reaction scheme for the formation of this complex is as given in equation 2.4 while important dimensional parameters are given in Table 2.2.



Na[Sm(L2)₂H₂O] complex (Coordination Number =7).

In this complexation scheme, there is the formation of a close ion pair with a sodium cation and the singly charged anionic complex formed when two bis-deprotonated ligands are bound to the Sm(III) metal center, along with one oxygen from the sulfonyl group on both ligands and a water molecule, bringing the coordination number to 7 (Figure 2.11).

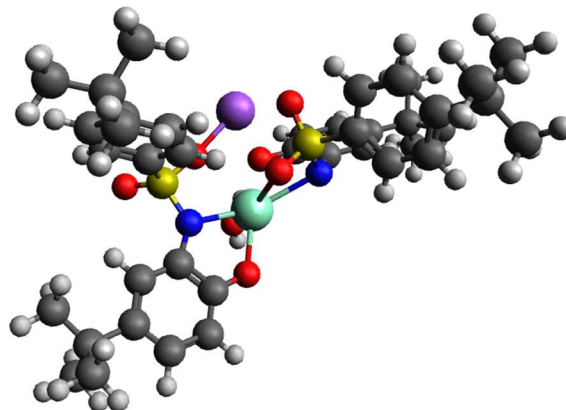


Figure 2.11. Structure of a 1:2 complex of Sm(III) with $L2H_2$, $Na[Sm(L2)_2.H_2O]$ showing close ion-pair formation.

The likely reaction scheme for the formation of this complex is as given in equation 2.5 while important dimensional parameters are given in Table 2.2.

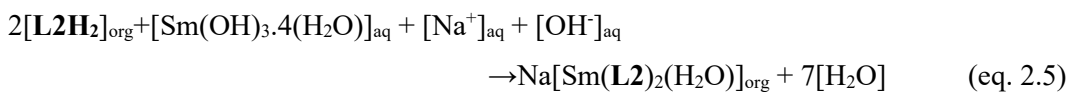


Table 2.2. Selected bond lengths (Å) and coordination number for the calculated $L2/Sm/OH^-/H_2O$ for the 1:2 complexes in dichloromethane. ‘*’ denotes the N-deprotonated $L2H^-$ ligand form.

Complex	Sm–N phenyl	Sm–O phenyl	Sm–O SO ₂	Sm–N phenyl*	Sm–O phenyl*	Sm–O SO ₂ *	Sm–O H ₂ O	Na–O phenyl	Na–O SO ₂	CN
Sm(L2)(L2H).2H ₂ O	2.363	2.276	2.532	2.903	2.392	2.531	2.554 2.546			7
Sm(L2)(L2H)*.2H ₂ O	2.391	2.349	2.625	2.468	2.782	2.499	2.603 2.578			7
Na[Sm(L2) ₂ .H ₂ O]	2.377 2.565	2.218 2.521	2.662 2.559				2.487	2.249	2.292 2.215	7

Sm(L2)(NO₃).(H₂O)₆ complex (Coordination Number =10).

In this 1:1 complexation scheme, a single bis-deprotonated **L2**²⁻ binds with Sm(III) via the phenolic oxygen and the sulfonamide nitrogen and in the process displaces two nitrate anions to give the neutral complex Sm(L2)(NO₃)(H₂O)₆, with six water molecules completing the coordination sphere (Figure 2.12). Overall, the coordination number for this species was 10 and the ΔG obtained was -19 kcal/mol.

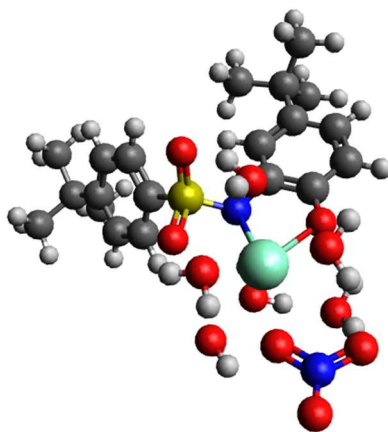
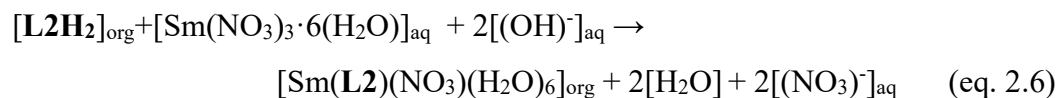


Figure 2.12 Structure of a 1:1 complex of Sm(III) and L2H₂ with structure Sm(L2)(NO₃)(H₂O)₆.

The likely reaction scheme for the formation of this complex is shown in eq 2.6 while the calculated free energy of reaction, and important dimensional parameters are given in Table 2.3.



Sm(L2)(NO₃).(H₂O)₅ complex (Coordination Number = 9).

Similar to the previous complexation scheme, bidentate complexes of L2²⁻ with Sm(III) after displacing two nitrate anions and a molecule of water from the initial Sm(III) nitrate salt, can form in which the sulfonyl oxygen also plays a role in stabilizing the complex. The coordination number of 9 is therefore satisfied by the ligand, with one oxygen from the nitrate anion, five water molecules and an oxygen from the sulfonyl group adjacent to the amide nitrogen (Figure 2.13). Although, the coordination number is lower than in the previously described complex, having fewer water molecules in the coordination sphere appears to offer improved stability for the complex in the organic phase with a ΔG value of -31.5 kcal/mol. The obtained ΔG value indicates more favorable formation during extraction than in the previous model.

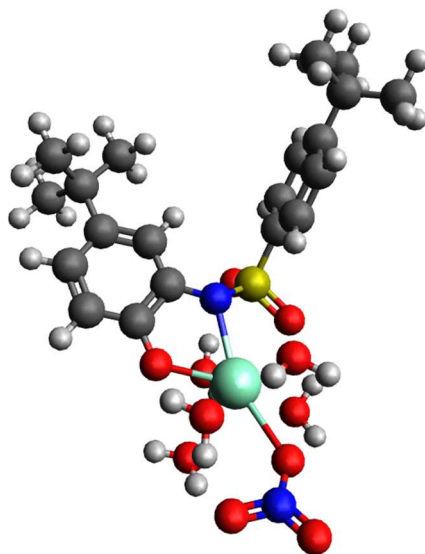
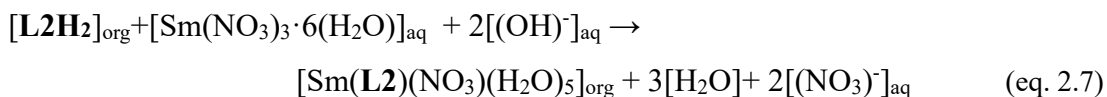


Figure 2.13. Structure of a 1:1 complex of Sm(III) and L2H₂ with structure Sm(L2)(NO₃)(H₂O)₅.

The likely reaction scheme for the formation of this complex is given in eq. 2.7, while calculated free energy of reaction, and important dimensions are given in Table 2.3



Sm(L2)(OH).(H₂O)₅ complex (Coordination Number =9).

The coordination of a bis-deprotonated ligand with Sm(III) where there is a complete displacement of all the nitrate anions from the salt along with a molecule of water was also examined. Here the coordination environment of the complex in the organic phase was consolidated by the sulfonyl oxygen and five water molecules and a hydroxide anion (Figure 2.14). This model brings the coordination number to 9 and the ΔG value to -27.2 kcal/mol.

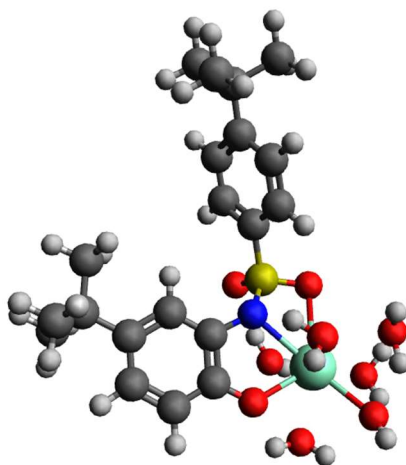


Figure 2.14. Structure of a 1:1 complex of Sm(III) and L2H₂ with structure Sm(L2)(OH)(H₂O)₅.

The likely reaction scheme for this complex is given in equation 2.8 while the calculated free energies of reaction, and important dimensions are given in Table 2.3.

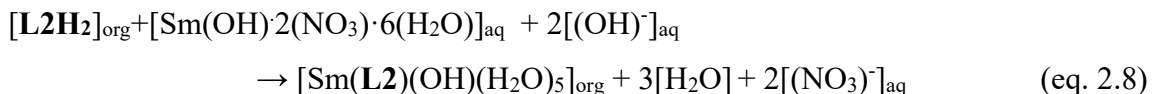


Table 2.3. Selected bond lengths (Å), coordination number (CN) and free energies (kcal/mol) for the calculated **L2**/Sm/OH⁻/NO₃⁻/H₂O 1:1 complexes in dichloromethane.

Complex	Sm – N phenyl (Å)	Sm – O phenyl (Å)	Sm – O SO ₂ (Å)	Sm – O NO ₃ (Å)	Sm – O H ₂ O (Å)	CN	Δ G (kcal/mol)
Sm(L2)(NO ₃)(H ₂ O) ₆	2.570	2.329	2.730	2.711	2.548	10	-19
Sm(L2)(NO ₃)(H ₂ O) ₅	2.441	2.331	2.635	2.575	2.533 – 2.595	9	-31.5
Sm(L2)(OH)(H ₂ O) ₅	2.555	2.274	2.626	2.363	2.525 – 2.664	9	-27.2

According to DFT calculations the formation of close ion pairs of the type Na[Sm(**L2**)₂(H₂O)_x] is likely as an extracted 1:2 complex from the highly alkaline aqueous phase into the organic phase. The sodium counter cation in the outer coordination sphere helps in stabilizing the anionic complex [Sm(**L2**)₂(H₂O)_x]⁻. In addition, the 1:2 complexes are expected to be more favored for the extraction of Sm(III) into an organic solvent (dichloromethane), as it can be inferred by the shorter bond distances between the binding atoms and Sm(III) when comparing Tables 2.2 and 2.3. In both calculated models, it could be inferred that the shorter bond distances between the more electronegative phenolic O- and Sm(III) (ranging from 2.218 – 2.521 Å for the 1:2

complexes and 2.274 – 2.329 Å in the 1:1 complexes) might be due to their stronger coordination compared to the sulfonamide N- and Sm(III) (ranging from 2.363 – 2.565 Å for the 1: 2 and, 2.441 – 2.570 Å for the 1:1 complexes). Likewise, these shorter bond distances might suggest that complexes with **L2** are more stable compared to our previously studied systems where the bidentate disulfonamide, **dsa-3**, gave Sm - N_{dsa} bond distances of 2.414 and 2.448 Å in the neutral complex [Sm(**dsa-3**²⁻)(OH)(H₂O)₃],²⁰ and the trisulfonamide **4-iPr-tsa** gave Sm – N_{tsa} bond distance of 2.620 – 2.747 Å in the complex [Sm(**4-iPr-tsa**³⁻)(H₂O)₃].²¹ Overall, DFT calculations are in good agreement with the experimental study and confirm the likely formation of favored 1:2 complexes as ion paired species of type Na[Sm(**L2**)₂ (H₂O)_x] in the organic phase.

2.4.7 X-ray crystallography.

2.4.7.1 X-ray crystallography for **L1H₂**

White crystals were obtained from slow evaporation of a dichloromethane solution of the ligand. The dihedral angle between both aryl rings was found to be 66.27°, both rings exhibited different degrees of planarity, with the phenolic ring being highly planar with a mean deviation of 0.003 Å and the *tert*-butyl substituted aryl ring being moderately planar with mean deviation of 0.019 Å. No π - π stacking was observed. Intermolecular hydrogen bonding interactions, involving the H of the -OH substituent and an O of the proximal SO₂ moiety was observed with with an O---O distance of 2.87 Å. Figure 2.15 gives the ORTEP representation for X-rays structure while Tables 2.4-2.7 summarize the crystallographic data.

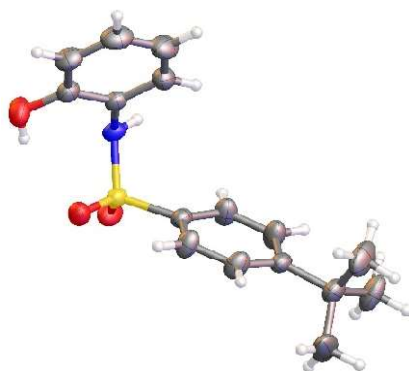


Figure 2.15. ORTEP representation of the crystal structure of **L1H₂** (50% probability ellipsoids).

Table 2.4. Experimental details, crystal data and structural refinement parameters for **L1H₂**

Crystal data	
Chemical formula	C ₁₆ H ₁₉ NO ₃ S
<i>M_r</i>	305.38
Crystal system, space group	Monoclinic, <i>P</i> 2 ₁
Temperature (K)	298
a, b, c (Å)	10.777 (7), 6.4020(4), 11.2246(7)
β (°)	95.148(1)
<i>V</i> (Å ³)	771.37(8)
<i>Z</i>	2
Radiation type	Mo <i>K</i> α
μ (mm ⁻¹)	0.22
Crystal size (mm)	0.20 × 0.17 × 0.10
Data collection	
Diffractometer	Bruker D8 Quest PHOTON II

Absorption correction	Multi-scan
	<i>SADABS</i> 2016/2: Krause, L., Herbst-Irmer, R., Sheldrick G.M. & Stalke D., <i>J. Appl. Cryst.</i> 48 (2015)3-10.
T_{\min} , T_{\max}	0.718, 0.745
No. of measured, independent and observed [$I > 2\sigma(I)$] reflections	8684, 2792, 2758
R_{int}	0.014
$(\sin \vartheta/\lambda)_{\max}$ (\AA^{-1})	0.603
Refinement	
$R[F^2 > 2\sigma(F^2)]$, $wR(F^2)$, S	0.026, 0.071, 1.06
No. of reflections	2792
No. of parameters	225
No. of restraints	37
H-atom treatment	H-atom parameters constrained
$\Delta\rho_{\max}$, $\Delta\rho_{\min}$ ($e \text{\AA}^{-3}$)	0.16, -0.19
Absolute structure	Refined as an inversion twin.
Absolute structure parameter	0.02(8)

Table 2.5. Fractional atomic coordinates and isotropic or equivalent isotropic displacement parameters (\AA^2) for **L1H₂**

	<i>x</i>	<i>y</i>	<i>z</i>	$U_{\text{iso}}^*/U_{\text{eq}}$	Occ. (<1)
S1	-0.39602 (4)	-0.10940 (8)	-0.08556 (4)	0.03876 (15)	
O1	-0.52926 (14)	-0.0956 (4)	-0.09096 (14)	0.0541 (4)	
O004	-0.23334 (18)	-0.3508 (3)	0.16475 (18)	0.0624 (5)	
H004	-0.293751	-0.360617	0.115231	0.094*	
O2	-0.33803 (17)	-0.3099 (3)	-0.08911 (15)	0.0532 (4)	
N1	-0.34674 (16)	-0.0043 (3)	0.04192 (14)	0.0391 (4)	
H1	-0.377652	0.118724	0.048112	0.047*	
C1	-0.34696 (19)	0.0396 (4)	-0.20460 (17)	0.0373 (4)	
C2	-0.3980 (3)	0.2328 (4)	-0.2306 (2)	0.0550 (6)	
H2	-0.452181	0.293134	-0.180460	0.066*	
C3	-0.3679 (3)	0.3358 (4)	-0.3318 (2)	0.0589 (7)	
H3	-0.402040	0.467089	-0.348560	0.071*	
C4	-0.2890 (2)	0.2515 (4)	-0.40910 (19)	0.0443 (5)	
C5	-0.2338 (3)	0.0638 (5)	-0.3764 (2)	0.0567 (7)	
H5	-0.175605	0.007400	-0.423604	0.068*	
C6	-0.2623 (2)	-0.0435 (4)	-0.2755 (2)	0.0532 (6)	
H6	-0.224338	-0.170876	-0.255911	0.064*	
C7	-0.2625 (3)	0.3576 (5)	-0.5264 (2)	0.0561 (6)	
C8	-0.21616 (19)	-0.0051 (3)	0.08104 (18)	0.0375 (4)	
C9	-0.1663 (2)	-0.1777 (4)	0.14249 (19)	0.0436 (5)	
C10	-0.0416 (2)	-0.1747 (5)	0.1871 (2)	0.0578 (7)	
H10	-0.007161	-0.288813	0.229356	0.069*	
C11	0.0305 (2)	-0.0028 (6)	0.1687 (3)	0.0647 (8)	
H11	0.113837	-0.002140	0.198476	0.078*	
C12	-0.0182 (3)	0.1677 (5)	0.1071 (2)	0.0635 (7)	
H12	0.031833	0.282630	0.094796	0.076*	

C13	-0.1430 (2)	0.1673 (4)	0.0633 (2)	0.0505 (5)	
H13	-0.177118	0.282758	0.022122	0.061*	
C0AA	-0.2821 (14)	0.2142 (15)	-0.6287 (8)	0.109 (4)	0.617 (13)
H0AA	-0.226284	0.097675	-0.616895	0.163*	0.617 (13)
H0AB	-0.266229	0.286373	-0.700733	0.163*	0.617 (13)
H0AC	-0.366564	0.164904	-0.635219	0.163*	0.617 (13)
C1AA	-0.3615 (9)	0.5421 (14)	-0.5562 (6)	0.085 (2)	0.617 (13)
H1AA	-0.444085	0.484557	-0.565955	0.128*	0.617 (13)
H1AB	-0.343661	0.610726	-0.628748	0.128*	0.617 (13)
H1AC	-0.356012	0.641098	-0.491731	0.128*	0.617 (13)
C2AA	-0.1379 (6)	0.4556 (15)	-0.5116 (6)	0.094 (3)	0.617 (13)
H2AA	-0.137859	0.566132	-0.453844	0.141*	0.617 (13)
H2AB	-0.117888	0.511585	-0.586932	0.141*	0.617 (13)
H2AC	-0.076936	0.352724	-0.484598	0.141*	0.617 (13)
C0AB	-0.1284 (12)	0.283 (3)	-0.5656 (12)	0.112 (6)	0.383 (13)
H0AD	-0.064890	0.312776	-0.502412	0.168*	0.383 (13)
H0AE	-0.110379	0.355600	-0.636780	0.168*	0.383 (13)
H0AF	-0.130388	0.135054	-0.580911	0.168*	0.383 (13)
C2AB	-0.257 (2)	0.5799 (16)	-0.5189 (12)	0.117 (8)	0.383 (13)
H2AD	-0.339395	0.634429	-0.513481	0.176*	0.383 (13)
H2AE	-0.223859	0.634814	-0.588956	0.176*	0.383 (13)
H2AF	-0.204437	0.620020	-0.449117	0.176*	0.383 (13)
C1AB	-0.354 (2)	0.269 (5)	-0.6209 (15)	0.153 (11)	0.383 (13)
H1AD	-0.339951	0.122103	-0.628706	0.230*	0.383 (13)
H1AE	-0.344932	0.337169	-0.695745	0.230*	0.383 (13)
H1AF	-0.437422	0.291635	-0.598795	0.230*	0.383 (13)

Table 2.6: Atomic displacement parameters (\AA^2)

	U^{11}	U^{22}	U^{33}	U^{12}	U^{13}	U^{23}
S1	0.0404 (3)	0.0421 (3)	0.0333 (2)	-0.0060 (2)	0.00123 (17)	0.0023 (2)
O1	0.0417 (7)	0.0699 (11)	0.0502 (8)	-0.0124 (9)	0.0003 (6)	0.0058 (10)
O004	0.0626 (11)	0.0571 (11)	0.0649 (11)	-0.0059 (9)	-0.0080 (8)	0.0218 (9)
O2	0.0741 (12)	0.0398 (9)	0.0456 (9)	-0.0012 (8)	0.0058 (8)	0.0007 (7)
N1	0.0398 (9)	0.0453 (10)	0.0320 (8)	0.0048 (8)	0.0026 (7)	-0.0017 (7)
C1	0.0382 (10)	0.0434 (11)	0.0296 (9)	-0.0026 (8)	-0.0001 (7)	0.0011 (8)
C2	0.0716 (16)	0.0474 (13)	0.0492 (12)	0.0115 (12)	0.0226 (11)	0.0021 (11)
C3	0.0801 (17)	0.0472 (15)	0.0512 (13)	0.0130 (12)	0.0163 (12)	0.0102 (10)
C4	0.0500 (12)	0.0492 (13)	0.0331 (10)	-0.0059 (10)	0.0003 (9)	0.0030 (9)
C5	0.0589 (15)	0.0675 (16)	0.0461 (13)	0.0162 (13)	0.0186 (11)	0.0091 (12)
C6	0.0546 (13)	0.0573 (15)	0.0489 (13)	0.0180 (11)	0.0109 (10)	0.0126 (10)
C7	0.0702 (15)	0.0618 (17)	0.0366 (11)	-0.0055 (13)	0.0057 (10)	0.0084 (12)
C8	0.0390 (10)	0.0456 (11)	0.0281 (9)	0.0013 (9)	0.0037 (7)	-0.0027 (8)
C9	0.0449 (11)	0.0494 (13)	0.0363 (10)	0.0012 (9)	0.0024 (9)	0.0024 (9)
C10	0.0494 (13)	0.0716 (19)	0.0502 (13)	0.0106 (12)	-0.0078 (11)	0.0029 (11)
C11	0.0413 (13)	0.093 (2)	0.0578 (15)	-0.0049 (14)	-0.0067 (11)	-0.0078 (15)
C12	0.0543 (14)	0.0748 (19)	0.0602 (15)	-0.0230 (14)	-0.0012 (11)	-0.0025 (14)
C13	0.0563 (14)	0.0502 (13)	0.0443 (12)	-0.0077 (11)	-0.0001 (10)	0.0015 (10)
C0AA	0.213 (13)	0.080 (4)	0.037 (3)	-0.039 (6)	0.033 (6)	-0.002 (3)
C1AA	0.098 (5)	0.096 (5)	0.063 (3)	0.026 (4)	0.017 (3)	0.041 (3)
C2AA	0.083 (4)	0.124 (8)	0.075 (4)	-0.029 (4)	0.013 (3)	0.044 (4)
C0AB	0.113 (8)	0.138 (14)	0.096 (9)	0.027 (8)	0.068 (7)	0.051 (10)
C2AB	0.22 (2)	0.058 (5)	0.089 (8)	0.003 (7)	0.087 (12)	0.025 (5)
C1AB	0.162 (14)	0.25 (3)	0.039 (7)	-0.116 (17)	-0.023 (9)	0.040 (10)

Table 2.7: Geometric parameters (Å, °)

S1—O1	1.4346 (15)	C9—C10	1.392 (3)
S1—O2	1.4298 (19)	C10—H10	0.9300
S1—N1	1.6267 (17)	C10—C11	1.373 (4)
S1—C1	1.761 (2)	C11—H11	0.9300
O004—H004	0.8197	C11—C12	1.371 (5)
O004—C9	1.358 (3)	C12—H12	0.9300
N1—H1	0.8603	C12—C13	1.390 (4)
N1—C8	1.436 (3)	C13—H13	0.9300
C1—C2	1.374 (3)	C0AA—H0AA	0.9600
C1—C6	1.371 (3)	C0AA—H0AB	0.9600
C2—H2	0.9300	C0AA—H0AC	0.9600
C2—C3	1.378 (4)	C1AA—H1AA	0.9600
C3—H3	0.9300	C1AA—H1AB	0.9600
C3—C4	1.378 (3)	C1AA—H1AC	0.9600
C4—C5	1.376 (4)	C2AA—H2AA	0.9600
C4—C7	1.531 (3)	C2AA—H2AB	0.9600
C5—H5	0.9300	C2AA—H2AC	0.9600
C5—C6	1.382 (3)	C0AB—H0AD	0.9600
C6—H6	0.9300	C0AB—H0AE	0.9600
C7—C0AA	1.471 (9)	C0AB—H0AF	0.9600
C7—C1AA	1.606 (7)	C2AB—H2AD	0.9600
C7—C2AA	1.479 (7)	C2AB—H2AE	0.9600
C7—C0AB	1.622 (11)	C2AB—H2AF	0.9600
C7—C2AB	1.426 (11)	C1AB—H1AD	0.9600
C7—C1AB	1.496 (16)	C1AB—H1AE	0.9600
C8—C9	1.385 (3)	C1AB—H1AF	0.9600
C8—C13	1.381 (3)		
O1—S1—N1	104.96 (10)	C11—C10—C9	119.9 (2)

O1—S1—C1	107.58 (10)	C11—C10—H10	120.1
O2—S1—O1	119.51 (12)	C10—C11—H11	119.4
O2—S1—N1	106.67 (10)	C12—C11—C10	121.2 (2)
O2—S1—C1	107.65 (10)	C12—C11—H11	119.4
N1—S1—C1	110.30 (10)	C11—C12—H12	120.3
C9—O004—H004	109.9	C11—C12—C13	119.4 (3)
S1—N1—H1	110.6	C13—C12—H12	120.3
C8—N1—S1	120.06 (14)	C8—C13—C12	119.8 (2)
C8—N1—H1	110.8	C8—C13—H13	120.1
C2—C1—S1	120.42 (17)	C12—C13—H13	120.1
C6—C1—S1	119.43 (18)	C7—C0AA—H0AA	109.5
C6—C1—C2	120.0 (2)	C7—C0AA—H0AB	109.5
C1—C2—H2	120.5	C7—C0AA—H0AC	109.5
C1—C2—C3	119.1 (2)	H0AA—C0AA—H0AB	109.5
C3—C2—H2	120.5	H0AA—C0AA—H0AC	109.5
C2—C3—H3	118.8	H0AB—C0AA—H0AC	109.5
C2—C3—C4	122.4 (2)	C7—C1AA—H1AA	109.5
C4—C3—H3	118.8	C7—C1AA—H1AB	109.5
C3—C4—C7	122.7 (2)	C7—C1AA—H1AC	109.5
C5—C4—C3	116.8 (2)	H1AA—C1AA—H1AB	109.5
C5—C4—C7	120.5 (2)	H1AA—C1AA—H1AC	109.5
C4—C5—H5	119.0	H1AB—C1AA—H1AC	109.5
C4—C5—C6	122.0 (2)	C7—C2AA—H2AA	109.5
C6—C5—H5	119.0	C7—C2AA—H2AB	109.5
C1—C6—C5	119.4 (2)	C7—C2AA—H2AC	109.5
C1—C6—H6	120.3	H2AA—C2AA—H2AB	109.5
C5—C6—H6	120.3	H2AA—C2AA—H2AC	109.5
C4—C7—C1AA	109.5 (3)	H2AB—C2AA—H2AC	109.5
C4—C7—C0AB	110.0 (4)	C7—C0AB—H0AD	109.5
C0AA—C7—C4	111.7 (4)	C7—C0AB—H0AE	109.5
C0AA—C7—C1AA	104.5 (6)	C7—C0AB—H0AF	109.5

C0AA—C7—C2AA	114.7 (6)	H0AD—C0AB—H0AE	109.5
C2AA—C7—C4	109.3 (3)	H0AD—C0AB—H0AF	109.5
C2AA—C7—C1AA	106.9 (5)	H0AE—C0AB—H0AF	109.5
C2AB—C7—C4	113.7 (5)	C7—C2AB—H2AD	109.5
C2AB—C7—C0AB	106.2 (9)	C7—C2AB—H2AE	109.5
C2AB—C7—C1AB	116.1 (13)	C7—C2AB—H2AF	109.5
C1AB—C7—C4	106.2 (7)	H2AD—C2AB—H2AE	109.5
C1AB—C7—C0AB	104.2 (12)	H2AD—C2AB—H2AF	109.5
C9—C8—N1	118.75 (19)	H2AE—C2AB—H2AF	109.5
C13—C8—N1	120.6 (2)	C7—C1AB—H1AD	109.5
C13—C8—C9	120.6 (2)	C7—C1AB—H1AE	109.5
O004—C9—C8	123.61 (19)	C7—C1AB—H1AF	109.5
O004—C9—C10	117.2 (2)	H1AD—C1AB—H1AE	109.5
C8—C9—C10	119.1 (2)	H1AD—C1AB—H1AF	109.5
C9—C10—H10	120.1	H1AE—C1AB—H1AF	109.5
S1—N1—C8—C9	-86.1 (2)	C3—C4—C7—C0AA	-128.2 (7)
S1—N1—C8—C13	97.3 (2)	C3—C4—C7—C1AA	-12.9 (5)
S1—C1—C2—C3	-173.0 (2)	C3—C4—C7—C2AA	103.9 (5)
S1—C1—C6—C5	173.1 (2)	C3—C4—C7—C0AB	155.2 (8)
O1—S1—N1—C8	175.50 (17)	C3—C4—C7—C2AB	36.3 (11)
O1—S1—C1—C2	43.4 (2)	C3—C4—C7—C1AB	-92.6 (14)
O1—S1—C1—C6	-133.1 (2)	C4—C5—C6—C1	-0.7 (4)
O004—C9—C10—C11	-179.2 (2)	C5—C4—C7—C0AA	51.7 (7)
O2—S1—N1—C8	47.74 (19)	C5—C4—C7—C1AA	166.9 (5)
O2—S1—C1—C2	173.4 (2)	C5—C4—C7—C2AA	-76.2 (5)
O2—S1—C1—C6	-3.0 (2)	C5—C4—C7—C0AB	-24.9 (9)
N1—S1—C1—C2	-70.6 (2)	C5—C4—C7—C2AB	-143.8 (11)
N1—S1—C1—C6	113.0 (2)	C5—C4—C7—C1AB	87.2 (14)
N1—C8—C9—O004	2.3 (3)	C6—C1—C2—C3	3.4 (4)
N1—C8—C9—C10	-176.1 (2)	C7—C4—C5—C6	-175.4 (3)
N1—C8—C13—C12	176.7 (2)	C8—C9—C10—C11	-0.7 (4)

C1—S1—N1—C8	-68.89 (19)	C9—C8—C13—C12	0.2 (3)
C1—C2—C3—C4	0.6 (4)	C9—C10—C11—C12	0.3 (4)
C2—C1—C6—C5	-3.3 (4)	C10—C11—C12—C13	0.4 (4)
C2—C3—C4—C5	-4.5 (4)	C11—C12—C13—C8	-0.7 (4)
C2—C3—C4—C7	175.4 (3)	C13—C8—C9—O004	178.9 (2)
C3—C4—C5—C6	4.5 (4)	C13—C8—C9—C10	0.5 (3)

2.4.7.2 X-ray crystallography for **L2H₂**

White crystals were obtained from slow evaporation of chloroform from a solution of the ligand in chloroform. The dihedral angle between both aryl rings was found to be 75.16°, the *tert*-butyl substituted aryl ring was fairly planar with mean deviation of 0.01 Å while the phenolic ring was highly planar with mean deviation of 0.009 Å. No π - π stacking was observed, but three types of intermolecular H-bonding was found; (a) O---O involving two proximal SO₂, with an O---O distance of 2.98 Å (b) between O of an SO₂ and the N-H, with an O---N distance of 2.99 Å and (c) between the -OH substituent and the O of methanol, with an O---O distance of 2.73 Å. Figure 2.16 gives the ORTEP representation for the structure while the Tables 2.8-2.11 give the crystallographic data.

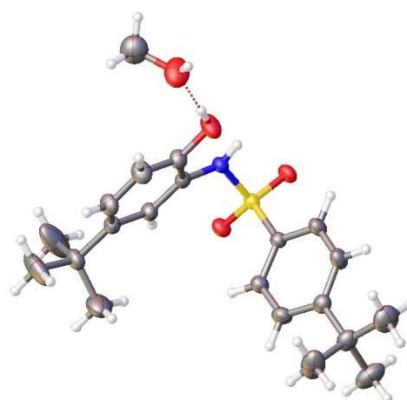


Figure 2.16: ORTEP representation of the crystal structure of **L2H₂** showing intermolecular hydrogen bonding with a molecule of methanol (50% probability ellipsoids)

Table 2.8: Experimental details, crystal data and structural refinement parameters for **L2H₂**

Crystal data	
Chemical formula	C ₂₀ H ₂₇ NO ₃ S·CH ₄ O
<i>M_r</i>	393.53
Crystal system, space group	Triclinic, <i>P</i> -1
Temperature (K)	298
<i>a</i> , <i>b</i> , <i>c</i> (Å)	10.128(1), 10.558(2), 11.091(2)
<i>α</i> , <i>β</i> , <i>γ</i> (°)	71.193(3), 83.279(3), 73.370(3)
<i>V</i> (Å ³)	1075.4(3)
<i>Z</i>	2
Radiation type	Mo <i>Kα</i>
<i>μ</i> (mm ⁻¹)	0.18
Crystal size (mm)	0.20 × 0.18 × 0.07
Data collection	
Diffractionmeter Bruker	<i>APEX</i> -II CCD
Absorption correction	Multi-scan <i>SADABS2016/2</i> (Bruker,2016/2) was used for absorption correction. <i>wR2(int)</i> was 0.0505 before and 0.0377 after correction. The Ratio of minimum to maximum transmission is 0.8833. The <i>λ/2</i> correction factor is Not present.
<i>T_{min}</i> , <i>T_{max}</i>	0.658, 0.745
No. of measured, independent and	6428, 3882, 3307

observed [$I > 2\sigma(I)$]

reflections

R_{int} 0.021

$(\sin \theta/\lambda)_{\text{max}}$ (\AA^{-1}) 0.603

Refinement

$R[F^2 > 2\sigma(F^2)]$, $wR(F^2)$, S 0.049, 0.126, 1.11

No. of reflections 3882

No. of parameters 285

H-atom treatment H atoms treated by a mixture of independent and constrained

refinement

$\Delta\rho_{\text{max}}$, $\Delta\rho_{\text{min}}$ (e \AA^{-3}) 0.26, -0.31

Table 2.9: Fractional atomic coordinates and isotropic or equivalent isotropic displacement parameters (\AA^2)

	x	y	z	$U_{\text{iso}}^*/U_{\text{eq}}$
S1	0.00409 (5)	0.77841 (5)	0.52317 (5)	0.02998 (16)
O1	-0.09338 (15)	0.91142 (15)	0.50585 (16)	0.0381 (4)
O2	-0.04045 (16)	0.65754 (15)	0.59188 (15)	0.0386 (4)
O3	0.37679 (19)	0.83937 (18)	0.5637 (2)	0.0560 (5)
H3	0.450189	0.849483	0.577853	0.084*
N1	0.13168 (19)	0.7814 (2)	0.59808 (18)	0.0330 (4)
O4	0.6193 (2)	0.8725 (3)	0.6168 (2)	0.0792 (7)
H4A	0.675181	0.909603	0.569605	0.119*
C1	0.2536 (2)	0.6691 (2)	0.6263 (2)	0.0319 (5)
C11	0.0682 (2)	0.7625 (2)	0.3728 (2)	0.0315 (5)
C6	0.2505 (2)	0.5316 (2)	0.6774 (2)	0.0358 (5)
C16	0.0989 (2)	0.6341 (2)	0.3525 (2)	0.0388 (5)
C12	0.0859 (3)	0.8770 (2)	0.2749 (2)	0.0429 (6)
C5	0.3697 (2)	0.4235 (2)	0.7080 (2)	0.0378 (5)

C14	0.1586 (2)	0.7375 (2)	0.1309 (2)	0.0392 (5)
C15	0.1430 (3)	0.6237 (3)	0.2322 (2)	0.0436 (6)
C2	0.3799 (2)	0.7017 (2)	0.6086 (2)	0.0403 (5)
C3	0.4989 (3)	0.5953 (3)	0.6379 (3)	0.0503 (7)
C17	0.2002 (3)	0.7223 (3)	-0.0021 (2)	0.0495 (6)
C4	0.4941 (3)	0.4585 (3)	0.6859 (3)	0.0460 (6)
C13	0.1314 (3)	0.8631 (3)	0.1562 (3)	0.0470 (6)
C7	0.3598 (3)	0.2738 (2)	0.7665 (3)	0.0462 (6)
C19	0.0771 (4)	0.7023 (4)	-0.0549 (3)	0.0802 (11)
H19A	0.056161	0.618295	-0.001600	0.120*
H19B	0.099270	0.696533	-0.139863	0.120*
H19C	-0.001458	0.779612	-0.056393	0.120*
C18	0.2352 (4)	0.8523 (4)	-0.0955 (3)	0.0747 (9)
H18A	0.155838	0.930365	-0.104457	0.112*
H18B	0.261778	0.837778	-0.176938	0.112*
H18C	0.309855	0.870101	-0.063321	0.112*
C20	0.3244 (4)	0.6003 (4)	0.0029 (3)	0.0831(11)
H20A	0.398898	0.610760	0.041836	0.125*
H20B	0.352001	0.596677	-0.081957	0.125*
H20C	0.301280	0.515987	0.052184	0.125*
C21	0.6644 (4)	0.8223 (4)	0.7418 (4)	0.0867(11)
H21A	0.743336	0.744025	0.749797	0.130*
H21B	0.591847	0.794417	0.798888	0.130*
H21C	0.688906	0.893898	0.762774	0.130*
C10	0.2932 (4)	0.2335 (4)	0.6737 (4)	0.0906(12)
H10A	0.203430	0.296061	0.653502	0.136*
H10B	0.284735	0.140569	0.711748	0.136*
H10C	0.349329	0.238522	0.597183	0.136*
C8	0.5001 (4)	0.1704 (3)	0.7964 (5)	0.104 (16)
H8A	0.555548	0.175812	0.719471	0.157*
H8B	0.488599	0.078347	0.832426	0.157*
H8C	0.544781	0.191790	0.856251	0.157*
C9	0.2725 (6)	0.2620 (4)	0.8870 (4)	0.1199(19)
H9A	0.316374	0.282223	0.948142	0.180*
H9B	0.261850	0.169463	0.921102	0.180*

H9C	0.183527	0.326782	0.868616	0.180*
H16	0.086 (3)	0.556 (3)	0.422 (3)	0.046 (7)*
H1	0.145 (3)	0.858 (3)	0.573 (2)	0.042 (7)*
H6	0.164 (3)	0.511 (3)	0.693 (2)	0.044 (7)*
H15	0.160 (3)	0.537 (3)	0.218 (3)	0.061 (8)*
H4	0.576 (3)	0.394 (3)	0.700 (2)	0.047 (7)*
H12	0.064 (3)	0.966 (3)	0.290 (3)	0.055 (8)*
H3A	0.584 (3)	0.618 (3)	0.626 (3)	0.066 (9)*
H13	0.139 (3)	0.942 (3)	0.092 (3)	0.069 (9)*

Table 2.10: Atomic displacement parameters (\AA^2)

	U^{11}	U^{22}	U^{33}	U^{12}	U^{13}	U^{23}
S1	0.0294 (3)	0.0246 (3)	0.0348 (3)	-0.0060 (2)	-0.0012 (2)	-0.0083 (2)
O1	0.0322 (8)	0.0276 (8)	0.0517 (10)	-0.0020 (6)	-0.0015 (7)	-0.0134 (7)
O2	0.0388 (9)	0.0308 (8)	0.0454 (9)	-0.0135 (7)	0.0022 (7)	-0.0080 (7)
O3	0.0447 (10)	0.0383 (10)	0.0785 (14)	-0.0173 (8)	-0.0071 (10)	-0.0016 (9)
N1	0.0361 (10)	0.0253 (10)	0.0376 (10)	-0.0076 (8)	-0.0044 (8)	-0.0087 (8)
O4	0.0654 (14)	0.0844 (17)	0.0851 (17)	-0.0426 (13)	-0.0072 (12)	-0.0003 (13)
C1	0.0336 (11)	0.0329 (12)	0.0278 (11)	-0.0070 (9)	-0.0019 (9)	-0.0086 (9)
C11	0.0315 (11)	0.0294 (11)	0.0341 (11)	-0.0068 (9)	-0.0031 (9)	-0.0104 (9)
C6	0.0333 (12)	0.0342 (12)	0.0382 (13)	-0.0079 (10)	-0.0040 (10)	-0.0088 (10)
C16	0.0446 (14)	0.0320 (12)	0.0397 (13)	-0.0114 (11)	0.0010 (11)	-0.0105 (11)
C12	0.0562 (15)	0.0277 (12)	0.0415 (14)	-0.0083 (11)	0.0002 (11)	-0.0089 (11)
C5	0.0387 (12)	0.0344 (12)	0.0379 (12)	-0.0057 (10)	-0.0059 (10)	-0.0093 (10)
C14	0.0351 (12)	0.0417 (13)	0.0380 (13)	-0.0042 (10)	-0.0021 (10)	-0.0131 (11)
C15	0.0476 (14)	0.0369 (13)	0.0492 (15)	-0.0077 (11)	0.0005 (11)	-0.0208 (12)
C2	0.0384 (13)	0.0380 (13)	0.0420 (13)	-0.0122 (10)	-0.0018 (10)	-0.0066 (11)
C3	0.0330 (13)	0.0497 (16)	0.0640 (18)	-0.0144 (12)	-0.0022 (12)	-0.0084 (13)

C17	0.0476 (15)	0.0590 (17)	0.0402 (14)	-0.0069 (13)	0.0023 (11)	-0.0201 (13)
C4	0.0319 (13)	0.0407 (14)	0.0581 (16)	-0.0010 (11)	-0.0069 (11)	-0.0108 (12)
C13	0.0600 (17)	0.0341 (13)	0.0384 (14)	-0.0085 (12)	0.0022 (12)	-0.0044 (11)
C7	0.0419 (14)	0.0321 (13)	0.0572 (16)	-0.0036 (11)	-0.0071 (12)	-0.0071 (12)
C19	0.074 (2)	0.128 (3)	0.0546 (19)	-0.033 (2)	0.0040 (16)	-0.046 (2)
C18	0.084 (2)	0.086 (2)	0.0488 (18)	-0.024 (2)	0.0153 (16)	-0.0191 (17)
C20	0.085 (2)	0.087 (3)	0.0558 (19)	0.017 (2)	0.0063 (17)	-0.0301 (19)
C21	0.082 (3)	0.089 (3)	0.083 (3)	-0.014 (2)	0.006 (2)	-0.029 (2)
C10	0.115 (3)	0.057 (2)	0.110 (3)	-0.038 (2)	-0.036 (2)	-0.014 (2)
C8	0.066 (2)	0.0376 (18)	0.188 (5)	-0.0002 (16)	-0.037 (3)	-0.004 (2)
C9	0.180 (5)	0.052 (2)	0.094 (3)	-0.027 (3)	0.064 (3)	-0.004 (2)

Table 2.11. Geometric parameters (Å, °)

S1—O1	1.4355 (15)	C17—C19	1.531 (4)
S1—O2	1.4264 (15)	C17—C18	1.536 (4)
S1—N1	1.6289 (19)	C17—C20	1.513 (4)
S1—C11	1.759 (2)	C4—H4	0.90 (3)
O3—H3	0.8200	C13—H13	0.92 (3)
O3—C2	1.368 (3)	C7—C10	1.517 (4)
N1—C1	1.429 (3)	C7—C8	1.520 (4)
N1—H1	0.81 (3)	C7—C9	1.505 (4)
O4—H4A	0.8200	C19—H19A	0.9600
O4—C21	1.396 (4)	C19—H19B	0.9600
C1—C6	1.386 (3)	C19—H19C	0.9600
C1—C2	1.394 (3)	C18—H18A	0.9600
C11—C16	1.388 (3)	C18—H18B	0.9600
C11—C12	1.380 (3)	C18—H18C	0.9600
C6—C5	1.391 (3)	C20—H20A	0.9600
C6—H6	0.95 (3)	C20—H20B	0.9600
C16—C15	1.386 (3)	C20—H20C	0.9600
C16—H16	0.96 (3)	C21—H21A	0.9600
C12—C13	1.383 (4)	C21—H21B	0.9600

C12—H12	0.97 (3)	C21—H21C	0.9600
C5—C4	1.385 (3)	C10—H10A	0.9600
C5—C7	1.532 (3)	C10—H10B	0.9600
C14—C15	1.389 (3)	C10—H10C	0.9600
C14—C17	1.533 (3)	C8—H8A	0.9600
C14—C13	1.388 (3)	C8—H8B	0.9600
C15—H15	0.94 (3)	C8—H8C	0.9600
C2—C3	1.379 (4)	C9—H9A	0.9600
C3—C4	1.383 (4)	C9—H9B	0.9600
C3—H3A	0.94 (3)	C9—H9C	0.9600
O1—S1—N1	105.66 (10)	C12—C13—H13	117.7 (19)
O1—S1—C11	108.81 (10)	C14—C13—H13	120.0 (19)
O2—S1—O1	118.21 (10)	C10—C7—C5	109.8 (2)
O2—S1—N1	108.29 (10)	C10—C7—C8	107.1 (3)
O2—S1—C11	107.98 (10)	C8—C7—C5	112.6 (2)
N1—S1—C11	107.43 (10)	C9—C7—C5	109.4 (2)
C2—O3—H3	109.5	C9—C7—C10	108.8 (3)
S1—N1—H1	110.0 (19)	C9—C7—C8	109.1 (3)
C1—N1—S1	122.28 (15)	C17—C19—H19A	109.5
C1—N1—H1	115.0 (19)	C17—C19—H19B	109.5
C21—O4—H4A	109.5	C17—C19—H19C	109.5
C6—C1—N1	122.9 (2)	H19A—C19—H19B	109.5
C6—C1—C2	119.3 (2)	H19A—C19—H19C	109.5
C2—C1—N1	117.7 (2)	H19B—C19—H19C	109.5
C16—C11—S1	119.48 (17)	C17—C18—H18A	109.5
C12—C11—S1	120.49 (17)	C17—C18—H18B	109.5
C12—C11—C16	120.0 (2)	C17—C18—H18C	109.5
C1—C6—C5	122.3 (2)	H18A—C18—H18B	109.5
C1—C6—H6	118.4 (15)	H18A—C18—H18C	109.5

C5—C6—H6	119.3 (15)	H18B—C18—H18C	109.5
C11—C16—H16	118.9 (15)	C17—C20—H20A	109.5
C15—C16—C11	119.2 (2)	C17—C20—H20B	109.5
C15—C16—H16	121.9 (15)	C17—C20—H20C	109.5
C11—C12—C13	119.5 (2)	H20A—C20—H20B	109.5
C11—C12—H12	119.3 (16)	H20A—C20—H20C	109.5
C13—C12—H12	121.2 (16)	H20B—C20—H20C	109.5
C6—C5—C7	120.0 (2)	O4—C21—H21A	109.5
C4—C5—C6	117.2 (2)	O4—C21—H21B	109.5
C4—C5—C7	122.8 (2)	O4—C21—H21C	109.5
C15—C14—C17	120.2 (2)	H21A—C21—H21B	109.5
C13—C14—C15	116.9 (2)	H21A—C21—H21C	109.5
C13—C14—C17	122.9 (2)	H21B—C21—H21C	109.5
C16—C15—C14	122.2 (2)	C7—C10—H10A	109.5
C16—C15—H15	119.0 (18)	C7—C10—H10B	109.5
C14—C15—H15	118.8 (18)	C7—C10—H10C	109.5
O3—C2—C1	117.0 (2)	H10A—C10—H10B	109.5
O3—C2—C3	124.2 (2)	H10A—C10—H10C	109.5
C3—C2—C1	118.8 (2)	H10B—C10—H10C	109.5
C2—C3—C4	121.0 (2)	C7—C8—H8A	109.5
C2—C3—H3A	118.6 (18)	C7—C8—H8B	109.5
C4—C3—H3A	120.3 (18)	C7—C8—H8C	109.5
C14—C17—C18	112.3 (2)	H8A—C8—H8B	109.5
C19—C17—C14	107.9 (2)	H8A—C8—H8C	109.5
C19—C17—C18	107.3 (3)	H8B—C8—H8C	109.5
C20—C17—C14	111.1 (2)	C7—C9—H9A	109.5
C20—C17—C19	110.3 (3)	C7—C9—H9B	109.5
C20—C17—C18	107.9 (3)	C7—C9—H9C	109.5
C5—C4—H4	122.3 (17)	H9A—C9—H9B	109.5
C3—C4—C5	121.3 (2)	H9A—C9—H9C	109.5
C3—C4—H4	116.4 (17)	H9B—C9—H9C	109.5

C12—C13—C14	122.2 (2)		
S1—N1—C1—C6	-46.3 (3)	C6—C1—C2—C3	2.6 (3)
S1—N1—C1—C2	137.93 (19)	C6—C5—C4—C3	1.3 (4)
S1—C11—C16—C15	176.89 (18)	C6—C5—C7—C10	62.2 (3)
S1—C11—C12—C13	-177.5 (2)	C6—C5—C7—C8	-178.6 (3)
O1—S1—N1—C1	-176.31 (17)	C6—C5—C7—C9	-57.2 (4)
O1—S1—C11—C16	-144.85 (18)	C16—C11—C12—C13	

2.4.7.3 X-ray crystallography for **L3H₂**

White crystals were obtained from slow evaporation of dichloromethane from a dichloromethane solution of the ligand. The dihedral angle between both aryl rings was found to be 67.01°, the isopropyl substituted ring was moderately planar with a mean deviation of 0.029 Å, while the phenolic ring was fairly planar with a mean deviation of 0.009 Å. No π - π stacking was observed, but two types of intermolecular H-bonding was found, involving (a) the -OH substituent and one of the O atoms of a proximal SO₂ moiety, with an O...O distance of 2.80 Å and (b) the -OH substituents with the NH group of the proximal molecule with an O...N distance of 2.96 Å. Figure 2.17 gives the ORTEP representation for the structure, while Tables 2.12-2.14 give the crystallographic data.

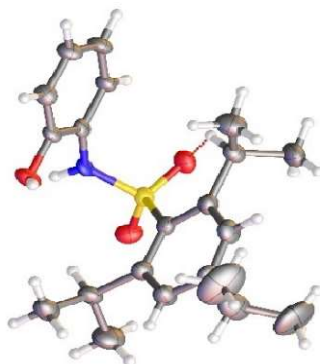


Figure 2.17: ORTEP representation of the crystal structure of **L3H₂** (50% probability ellipsoids).

Table 2.12: Experimental details, crystal data and structural refinement parameters for **L3H₂**.

Crystal data	
Chemical formula	2(C ₂₁ H ₂₉ NO ₃ S)
<i>Mr</i>	751.02
Crystal system, space	Monoclinic, <i>C2/c</i>
Group	
Temperature (K)	298
<i>a</i> , <i>b</i> , <i>c</i> (Å)	35.005(3), 6.3901(6), 22.735(2)
β (°)	123.838(1)
<i>V</i> (Å ³)	4224.0(7)
<i>Z</i>	4
Radiation type	Mo <i>K</i> α
μ (mm ⁻¹)	0.17
Crystal size (mm)	0.15 × 0.15 × 0.10
Data collection	
Diffractometer	Bruker D8 Quest PHOTON II
Absorption correction	Multi-scan
	<i>SADABS</i> 2016/2: Krause, L., Herbst-Irmer, R., Sheldrick G.M. & Stalke D., <i>J. Appl. Cryst.</i> 48 (2015)3-10.
<i>T</i> _{min} , <i>T</i> _{max}	0.574, 0.745
No. of measured, independent and observed [<i>I</i> > 2 σ (<i>I</i>)] reflections	20729, 3856, 3368

R_{int}	0.070
$(\sin \theta/\lambda)_{\text{max}}$ (\AA^{-1})	0.603
Refinement	
$R[F^2 > 2\sigma(F^2)], wR(F^2), S$	0.129, 0.258, 1.31
No. of reflections	3856
No. of parameters	242
No. of restraints	9
H-atom treatment	H-atom parameters constrained
	$w = 1/[\sigma^2(F_o^2) + (0.0603P)^2 + 26.4375P]$
	where $P = (F_o^2 + 2F_c^2)/3$
$\Delta\rho_{\text{max}}, \Delta\rho_{\text{min}}$ (e \AA^{-3})	0.86, -0.35

Table 2.13: Fractional atomic coordinates and isotropic or equivalent isotropic displacement parameters (\AA^2)

	x	y	z	$U_{\text{iso}}^*/U_{\text{eq}}$
S1	0.32675 (5)	-0.0726 (2)	0.47675 (8)	0.0360 (4)
O3	0.27181 (15)	0.4409 (6)	0.4809 (2)	0.0454 (10)
H3	0.285416	0.553324	0.492341	0.068*
O2	0.32521 (14)	-0.1553 (6)	0.4176 (2)	0.0481 (11)
O1	0.33242 (14)	-0.2190 (6)	0.5290 (2)	0.0497 (11)
N1	0.27707 (15)	0.0348 (7)	0.4470 (2)	0.0341 (11)
H1	0.261526	-0.004761	0.463916	0.041*
C16	0.25854 (18)	0.1933 (9)	0.3936 (3)	0.0344 (13)
C21	0.25544 (18)	0.3981 (8)	0.4112 (3)	0.0332 (12)
C6	0.3885 (2)	0.2132 (10)	0.4825 (3)	0.0441 (14)
C1	0.37068 (19)	0.1236 (9)	0.5189 (3)	0.0381 (13)
C18	0.2221 (2)	0.2954 (10)	0.2722 (3)	0.0482 (16)
H18	0.211125	0.262233	0.225560	0.058*
C17	0.24174 (19)	0.1440 (10)	0.3237 (3)	0.0403 (14)
H17	0.243878	0.007428	0.311657	0.048*
C19	0.2186 (2)	0.4974 (10)	0.2903 (3)	0.0486 (16)
H19	0.205437	0.601159	0.255772	0.058*
C2	0.3881 (2)	0.1807 (10)	0.5892 (3)	0.0438 (14)
C20	0.2346 (2)	0.5452 (9)	0.3592 (3)	0.0445 (14)
H20	0.231067	0.680568	0.370575	0.053*
C13	0.3701 (2)	0.1873 (10)	0.4035 (3)	0.0494 (16)
H13	0.340003	0.118658	0.380533	0.059*

C5	0.4269 (2)	0.3416 (11)	0.5217 (4)	0.0585 (18)
H5	0.439496	0.400676	0.498810	0.070*
C10	0.3676 (2)	0.1187 (11)	0.6317 (3)	0.0508 (16)
H10	0.337349	0.056582	0.598337	0.061*
C3	0.4259 (2)	0.3095 (12)	0.6235 (4)	0.0595 (19)
H3A	0.437770	0.347055	0.670173	0.071*
C11	0.3604 (2)	0.3083 (13)	0.6647 (4)	0.066 (2)
H11A	0.389522	0.373101	0.697655	0.099*
H11B	0.346482	0.265019	0.689074	0.099*
H11C	0.340629	0.406551	0.628232	0.099*
C4	0.4469 (2)	0.3854 (13)	0.5913 (4)	0.066 (2)
C15	0.3625 (3)	0.4000 (12)	0.3677 (4)	0.071 (2)
H15A	0.344117	0.486818	0.377183	0.107*
H15B	0.346948	0.380684	0.317548	0.107*
H15C	0.391675	0.466120	0.385997	0.107*
C7	0.4892 (3)	0.5248 (17)	0.6329 (5)	0.093 (3)
H7	0.496851	0.528996	0.681378	0.111*
C14	0.4010 (3)	0.0461 (13)	0.3936 (4)	0.073 (2)
H14A	0.430686	0.110188	0.414847	0.109*
H14B	0.387594	0.025600	0.343955	0.109*
H14C	0.404274	-0.086599	0.415747	0.109*
C12	0.3969 (3)	-0.0461 (15)	0.6865 (4)	0.085 (3)
H12A	0.396707	-0.171658	0.663227	0.127*
H12B	0.384624	-0.075357	0.714376	0.127*
H12C	0.427842	0.004306	0.716813	0.127*
C8	0.5294 (3)	0.436 (2)	0.6380 (7)	0.139 (5)
H8A	0.531695	0.290133	0.649246	0.209*
H8B	0.556567	0.507354	0.674476	0.209*
H8C	0.526255	0.453181	0.593531	0.209*
C9	0.4795 (4)	0.7455 (18)	0.6071 (8)	0.159 (6)
H9A	0.472404	0.750880	0.559827	0.239*
H9B	0.505959	0.830622	0.637697	0.239*
H9C	0.453731	0.796978	0.607194	0.239*

Atomic displacement parameters (\AA^2)

	U_{11}	U_{22}	U_{33}	U_{12}	U_{13}	U_{23}
S1	0.0399 (8)	0.0306 (7)	0.0403 (8)	-0.0066 (6)	0.0241 (6)	-0.0052 (6)
O3	0.065 (3)	0.042 (2)	0.037 (2)	-0.019 (2)	0.033 (2)	-0.0106 (19)
O2	0.058 (3)	0.037 (2)	0.061 (3)	-0.007 (2)	0.040 (2)	-0.013 (2)
O1	0.054 (3)	0.034 (2)	0.050 (3)	-0.0071 (19)	0.022 (2)	0.0022 (19)
N1	0.039 (3)	0.040 (3)	0.036 (2)	-0.011 (2)	0.029 (2)	-0.001 (2)
C16	0.032 (3)	0.040 (3)	0.041 (3)	-0.011 (2)	0.026 (3)	-0.004 (3)
C21	0.038 (3)	0.036 (3)	0.033 (3)	-0.008 (2)	0.024 (2)	-0.001 (2)
C6	0.039 (3)	0.047 (4)	0.049 (4)	-0.007 (3)	0.026 (3)	-0.006 (3)
C1	0.035 (3)	0.037 (3)	0.045 (3)	0.000 (2)	0.024 (3)	-0.003 (3)
C18	0.057 (4)	0.059 (4)	0.028 (3)	-0.009 (3)	0.024 (3)	-0.004 (3)
C17	0.046 (3)	0.045 (3)	0.032 (3)	-0.005 (3)	0.024 (3)	-0.007 (3)
C19	0.059 (4)	0.049 (4)	0.038 (3)	-0.006 (3)	0.027 (3)	0.007 (3)

C2	0.040 (3)	0.049 (4)	0.041 (3)	-0.011 (3)	0.022 (3)	-0.007 (3)
C20	0.055 (4)	0.034 (3)	0.050 (4)	-0.006 (3)	0.033 (3)	-0.002 (3)
C13	0.055 (4)	0.053 (4)	0.050 (4)	-0.011 (3)	0.035 (3)	-0.004 (3)
C5	0.055 (4)	0.067 (4)	0.069 (5)	-0.016 (4)	0.045 (4)	-0.003 (4)
C10	0.052 (4)	0.062 (4)	0.036 (3)	-0.013 (3)	0.023 (3)	-0.008 (3)
C3	0.050 (4)	0.078 (5)	0.052 (4)	-0.016 (4)	0.029 (3)	-0.017 (4)
C11	0.059 (4)	0.089 (6)	0.055 (4)	-0.023 (4)	0.035 (4)	-0.022 (4)
C4	0.047 (4)	0.087 (6)	0.066 (5)	-0.033 (4)	0.032 (4)	-0.025 (4)
C15	0.089 (6)	0.063 (5)	0.061 (5)	-0.005 (4)	0.041 (4)	0.006 (4)
C7	0.078 (5)	0.122 (7)	0.085 (6)	-0.054 (5)	0.049 (5)	-0.026 (5)
C14	0.078 (5)	0.088 (6)	0.070 (5)	0.014 (5)	0.053 (5)	-0.002 (4)
C12	0.090 (6)	0.099 (7)	0.063 (5)	-0.006 (5)	0.041 (5)	0.019 (5)
C8	0.047 (5)	0.163 (11)	0.155 (11)	-0.027 (6)	0.024 (6)	0.002 (9)
C9	0.096 (8)	0.100 (7)	0.220 (15)	-0.053 (6)	0.050 (9)	-0.035 (8)

Table 2.14: Geometric parameters (Å, °)

S1—O2	1.418 (4)	C5—C4	1.356 (10)
S1—O1	1.437 (4)	C10—H10	0.9800
S1—N1	1.626 (5)	C10—C11	1.519 (10)
S1—C1	1.793 (6)	C10—C12	1.513 (10)
O3—H3	0.8200	C3—H3A	0.9300
O3—C21	1.379 (6)	C3—C4	1.383 (9)
N1—H1	0.8600	C11—H11A	0.9600
N1—C16	1.430 (7)	C11—H11B	0.9600
C16—C21	1.391 (8)	C11—H11C	0.9600
C16—C17	1.390 (7)	C4—C7	1.524 (10)
C21—C20	1.361 (8)	C15—H15A	0.9600
C6—C1	1.406 (8)	C15—H15B	0.9600
C6—C13	1.542 (9)	C15—H15C	0.9600
C6—C5	1.393 (9)	C7—H7	0.9800
C1—C2	1.404 (8)	C7—C8	1.458 (14)
C18—H18	0.9300	C7—C9	1.492 (15)
C18—C17	1.371 (8)	C14—H14A	0.9600
C18—C19	1.380 (9)	C14—H14B	0.9600
C17—H17	0.9300	C14—H14C	0.9600
C19—H19	0.9300	C12—H12A	0.9600
C19—C20	1.373 (8)	C12—H12B	0.9600
C2—C10	1.542 (8)	C12—H12C	0.9600
C2—C3	1.372 (9)	C8—H8A	0.9600
C20—H20	0.9300	C8—H8B	0.9600
C13—H13	0.9800	C8—H8C	0.9600
C13—C15	1.530 (9)	C9—H9A	0.9600
C13—C14	1.520 (9)	C9—H9B	0.9600
C5—H5	0.9300	C9—H9C	0.9600
O2—S1—O1	117.2 (3)	C12—C10—H10	107.4
O2—S1—N1	107.2 (2)	C12—C10—C11	111.7 (6)

O2—S1—C1	109.6 (2)	C2—C3—H3A	118.8
O1—S1—N1	104.0 (2)	C2—C3—C4	122.5 (6)
O1—S1—C1	109.3 (3)	C4—C3—H3A	118.8
N1—S1—C1	109.1 (2)	C10—C11—H11A	109.5
C21—O3—H3	109.5	C10—C11—H11B	109.5
S1—N1—H1	119.1	C10—C11—H11C	109.5
C16—N1—S1	121.8 (3)	H11A—C11—H11B	109.5
C16—N1—H1	119.1	H11A—C11—H11C	109.5
C21—C16—N1	119.5 (5)	H11B—C11—H11C	109.5
C17—C16—N1	120.9 (5)	C5—C4—C3	117.6 (6)
C17—C16—C21	119.5 (5)	C5—C4—C7	122.4 (7)
O3—C21—C16	117.9 (5)	C3—C4—C7	119.8 (7)
C20—C21—O3	122.7 (5)	C13—C15—H15A	109.5
C20—C21—C16	119.3 (5)	C13—C15—H15B	109.5
C1—C6—C13	127.4 (5)	C13—C15—H15C	109.5
C5—C6—C1	116.7 (6)	H15A—C15—H15B	109.5
C5—C6—C13	115.9 (5)	H15A—C15—H15C	109.5
C6—C1—S1	120.0 (4)	H15B—C15—H15C	109.5
C2—C1—S1	119.4 (4)	C4—C7—H7	106.0
C2—C1—C6	120.6 (5)	C8—C7—C4	112.6 (9)
C17—C18—H18	120.3	C8—C7—H7	106.0
C17—C18—C19	119.5 (5)	C8—C7—C9	113.4 (10)
C19—C18—H18	120.3	C9—C7—C4	112.2 (9)
C16—C17—H17	119.8	C9—C7—H7	106.0
C18—C17—C16	120.5 (6)	C13—C14—H14A	109.5
C18—C17—H17	119.8	C13—C14—H14B	109.5
C18—C19—H19	120.0	C13—C14—H14C	109.5
C20—C19—C18	120.0 (6)	H14A—C14—H14B	109.5
C20—C19—H19	120.0	H14A—C14—H14C	109.5
C1—C2—C10	125.9 (5)	H14B—C14—H14C	109.5
C3—C2—C1	118.3 (6)	C10—C12—H12A	109.5
C3—C2—C10	115.8 (5)	C10—C12—H12B	109.5
C21—C20—C19	121.2 (6)	C10—C12—H12C	109.5
C21—C20—H20	119.4	H12A—C12—H12B	109.5
C19—C20—H20	119.4	H12A—C12—H12C	109.5
C6—C13—H13	107.3	H12B—C12—H12C	109.5
C15—C13—C6	111.1 (6)	C7—C8—H8A	109.5
C15—C13—H13	107.3	C7—C8—H8B	109.5
C14—C13—C6	111.5 (6)	C7—C8—H8C	109.5
C14—C13—H13	107.3	H8A—C8—H8B	109.5
C14—C13—C15	112.0 (6)	H8A—C8—H8C	109.5
C6—C5—H5	118.1	H8B—C8—H8C	109.5
C4—C5—C6	123.8 (6)	C7—C9—H9A	109.5
C4—C5—H5	118.1	C7—C9—H9B	109.5
C2—C10—H10	107.4	C7—C9—H9C	109.5
C11—C10—C2	111.6 (6)	H9A—C9—H9B	109.5
C11—C10—H10	107.4	H9A—C9—H9C	109.5
C12—C10—C2	111.0 (6)	H9B—C9—H9C	109.5
S1—N1—C16—C21	-110.2 (5)	C1—C6—C5—C4	-1.0 (11)
S1—N1—C16—C17	72.6 (6)	C1—C2—C10—C11	-128.3 (7)
S1—C1—C2—C10	-11.2 (9)	C1—C2—C10—C12	106.4 (8)

S1—C1—C2—C3	171.2 (5)	C1—C2—C3—C4	0.5 (11)
O3—C21—C20—C19	-179.9 (5)	C18—C19—C20—C21	2.4 (9)
O2—S1—N1—C16	-55.7 (5)	C17—C16—C21—O3	179.0 (5)
O2—S1—C1—C6	17.2 (6)	C17—C16—C21—C20	2.3 (8)
O2—S1—C1—C2	-160.6 (5)	C17—C18—C19—C20	-0.4 (10)
O1—S1—N1—C16	179.5 (4)	C19—C18—C17—C16	-0.6 (9)
O1—S1—C1—C6	146.9 (5)	C2—C3—C4—C5	4.9 (12)
O1—S1—C1—C2	-30.8 (5)	C2—C3—C4—C7	-178.9 (8)
N1—S1—C1—C6	-100.0 (5)	C13—C6—C1—S1	9.5 (9)
N1—S1—C1—C2	82.3 (5)	C13—C6—C1—C2	-172.8 (6)
N1—C16—C21—O3	1.8 (7)	C13—C6—C5—C4	178.5 (7)
N1—C16—C21—C20	-175.0 (5)	C5—C6—C1—S1	-171.0 (5)
N1—C16—C17—C18	176.9 (5)	C5—C6—C1—C2	6.7 (9)
C16—C21—C20—C19	-3.3 (9)	C5—C6—C13—C15	-51.6 (8)
C21—C16—C17—C18	-0.3 (8)	C5—C6—C13—C14	74.1 (8)
C6—C1—C2—C10	171.1 (6)	C5—C4—C7—C8	-63.8 (13)
C6—C1—C2—C3	-6.5 (9)	C5—C4—C7—C9	65.7 (13)
C6—C5—C4—C3	-4.7 (12)	C10—C2—C3—C4	-177.3 (7)
C6—C5—C4—C7	179.3 (8)	C3—C2—C10—C11	49.2 (8)
C1—S1—N1—C16	63.0 (5)	C3—C2—C10—C12	-76.1 (8)
C1—C6—C13—C15	127.8 (7)	C3—C4—C7—C8	120.3 (10)
C1—C6—C13—C14	-106.4 (7)	C3—C4—C7—C9	-110.3 (11)

2.4.7.4 X-ray crystallography for **L4H₂**

White crystals were obtained from slow evaporation of a dichloromethane solution of the ligand. The dihedral angle between the two aryl rings was 67.26°, the phenolic ring was fairly planar with mean deviation of 0.013 Å while the isopropyl substituted aryl ring was moderately planar with 0.026 Å. No π - π stacking was observed and only one type of intermolecular H-bonding interaction was found involving O of -OH substituent and an O of the proximal SO₂ moiety, with an O---O distance of 2.87 Å. Figure 2.18 gives the ORTEP representation for the crystal, while Tables 2.15 – 2.18 give the crystallographic data.

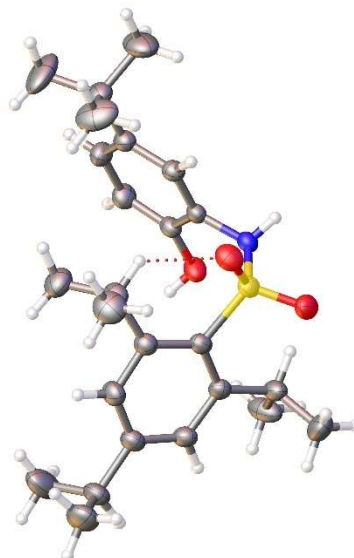


Figure 2.18: ORTEP representation of the crystal structure of **L4H₂** (50% probability ellipsoids), showing intramolecular hydrogen bonding.

Table 2.15: Experimental details, crystal data and structural refinement parameters for **L4H₂**

Crystal data	
Chemical formula	C ₂₅ H ₃₇ NO ₃ S
<i>Mr</i>	431.61
Crystal system, space group	Triclinic, P-1
Temperature (K)	298
a, b, c (Å)	6.3536(8), 13.167(2), 15.915(2)
α, β, γ (°)	104.077(2), 99.698(2), 97.425(2)
V (Å ³)	1252.7 (3)
Z	2
Radiation type	Mo Kα
μ (mm ⁻¹)	0.15
Crystal size (mm)	0.20 × 0.15 × 0.12

Data collection	
Diffractionmeter	Bruker D8 Quest PHOTON II Absorption correction Multi-scan
	SADABS 2016/2: Krause, L., Herbst-Irmer, R., Sheldrick G.M. & Stalke D., J. Appl. Cryst. 48 (2015)3-10.
T_{\min} , T_{\max}	0.603, 0.745
No. of measured, independent and observed [$I > 2\sigma(I)$] reflections	10069, 4533, 3851
R_{int}	0.023
$(\sin \theta/\lambda)_{\text{max}}$ (\AA^{-1})	0.603
Refinement	
$R[F^2 > 2\sigma(F^2)]$, $wR(F^2)$, S	0.052, 0.146, 1.07
No. of reflections	4533
No. of parameters	312
No. of restraints	72
H-atom treatment	H-atom parameters constrained
$\Delta\rho_{\text{max}}$, $\Delta\rho_{\text{min}}$ (e \AA^{-3})	0.63, -0.57

Table 2.16: Fractional atomic coordinates and isotropic or equivalent isotropic displacement parameters (\AA^2)

	x	y	z	$U_{\text{iso}}^*/U_{\text{eq}}$	Occ. (<1)
S1	0.82766 (8)	0.41457 (4)	0.65958 (3)	0.03967 (17)	
O1	0.9614 (2)	0.45804 (13)	0.74557 (11)	0.0533 (4)	
O2	0.9303 (2)	0.36671 (12)	0.59010 (11)	0.0533 (4)	
O3	0.3003 (2)	0.49719 (13)	0.56490 (9)	0.0490 (4)	
H3	0.185455	0.464176	0.568930	0.073*	

N1	0.7336 (3)	0.51166 (12)	0.62682 (10)	0.0380 (4)
H1	0.834849	0.550417	0.613016	0.046*
C00K	0.7118 (4)	0.79956 (18)	0.89484 (15)	0.0532 (6)
C1	0.6023 (3)	0.32174 (15)	0.66616 (13)	0.0379 (4)
C2	0.5468 (4)	0.32402 (16)	0.74859 (13)	0.0424 (5)
C3	0.3933 (4)	0.24036 (18)	0.75160 (14)	0.0499 (5)
H3A	0.358052	0.239661	0.805873	0.060*
C4	0.2904 (4)	0.15827 (16)	0.67829 (15)	0.0460 (5)
C5	0.3375 (4)	0.16320 (16)	0.59785 (14)	0.0450 (5)
H5	0.264843	0.110034	0.547456	0.054*
C6	0.4882 (3)	0.24379 (15)	0.58840 (13)	0.0403 (5)
C7	0.6308 (4)	0.41156 (19)	0.83580 (14)	0.0501 (5)
H7	0.716582	0.471129	0.822860	0.060*
C8	0.4428 (5)	0.4521 (2)	0.87327 (17)	0.0682 (7)
H8A	0.345386	0.469459	0.827960	0.102*
H8B	0.497771	0.514513	0.921918	0.102*
H8C	0.366777	0.397971	0.893556	0.102*
C9	0.7796 (5)	0.3725 (3)	0.90170 (19)	0.0769 (8)
H9A	0.703136	0.310002	0.911500	0.115*
H9B	0.824795	0.427109	0.956693	0.115*
H9C	0.904661	0.355656	0.878508	0.115*
C10	0.1276 (4)	0.06722 (18)	0.68586 (17)	0.0564 (6)
H10	0.083847	0.015896	0.627304	0.068*
C11	-0.0754 (5)	0.1046 (3)	0.7105 (3)	0.0967 (12)
H11A	-0.037759	0.156171	0.767311	0.145*
H11B	-0.176073	0.044984	0.713097	0.145*
H11C	-0.140991	0.136335	0.666769	0.145*
C12	0.2291 (6)	0.0099 (2)	0.7496 (2)	0.0798 (9)
H12A	0.366393	-0.004535	0.736971	0.120*
H12B	0.134699	-0.055856	0.743165	0.120*
H12C	0.250437	0.053792	0.809243	0.120*
C13	0.5128 (4)	0.24102 (17)	0.49418 (14)	0.0508 (6)

H13	0.592548	0.310569	0.495786	0.061*	
C14	0.2921 (5)	0.2234 (2)	0.43183 (16)	0.0728 (9)	
H14A	0.213356	0.154021	0.426404	0.109*	
H14B	0.313194	0.228673	0.374600	0.109*	
H14C	0.211395	0.276466	0.455347	0.109*	
C15	0.6471 (6)	0.1568 (2)	0.4603 (2)	0.0829 (10)	
H15A	0.784519	0.170315	0.500630	0.124*	
H15B	0.670289	0.160101	0.402879	0.124*	
H15C	0.570448	0.087443	0.456210	0.124*	
C16	0.6127 (3)	0.57753 (14)	0.67778 (12)	0.0350 (4)	
C17	0.3927 (3)	0.57087 (15)	0.64452 (13)	0.0383 (4)	
C18	0.2805 (4)	0.64065 (18)	0.68962 (15)	0.0481 (5)	
H18	0.135444	0.639355	0.666239	0.058*	
C19	0.3818 (4)	0.71285 (18)	0.76961 (15)	0.0493 (5)	
H19	0.302235	0.758473	0.799617	0.059*	
C20	0.5995 (3)	0.71907 (16)	0.80639 (13)	0.0416 (5)	
C21	0.7134 (3)	0.65113 (15)	0.75784 (13)	0.0392 (4)	
H21	0.860525	0.655059	0.779474	0.047*	
C22	0.5590 (12)	0.8519 (9)	0.9457 (5)	0.111 (4)	0.564 (10)
H22A	0.468988	0.799448	0.962912	0.166*	0.564 (10)
H22B	0.469431	0.884612	0.909113	0.166*	0.564 (10)
H22C	0.640344	0.905094	0.997549	0.166*	0.564 (10)
C23	0.8643 (14)	0.8836 (5)	0.8738 (4)	0.094 (3)	0.564 (10)
H23A	0.783026	0.917282	0.835441	0.141*	0.564 (10)
H23B	0.969334	0.850978	0.845000	0.141*	0.564 (10)
H23C	0.937445	0.935900	0.927742	0.141*	0.564 (10)
C24	0.8518 (16)	0.7443 (6)	0.9517 (4)	0.094 (3)	0.564 (10)
H24A	0.925566	0.794976	1.006354	0.141*	0.564 (10)
H24B	0.956588	0.715485	0.920283	0.141*	0.564 (10)
H24C	0.760885	0.687851	0.963916	0.141*	0.564 (10)
C25	0.9526 (13)	0.8040 (10)	0.9204 (7)	0.112 (6)	0.436 (10)
H25A	1.022346	0.826537	0.877274	0.167*	0.436 (10)

H25B	0.980793	0.734768	0.922651	0.167*	0.436 (10)
H25C	1.008368	0.853707	0.977481	0.167*	0.436 (10)
C26	0.598 (2)	0.7758 (11)	0.9653 (5)	0.120 (6)	0.436 (10)
H26A	0.650161	0.831745	1.019204	0.180*	0.436 (10)
H26B	0.627016	0.709489	0.975374	0.180*	0.436 (10)
H26C	0.444680	0.771056	0.946326	0.180*	0.436 (10)
C27	0.685 (2)	0.9132 (5)	0.8880 (6)	0.101 (4)	0.436 (10)
H27A	0.533909	0.918102	0.878569	0.152*	0.436 (10)
H27B	0.743663	0.927021	0.839253	0.152*	0.436 (10)
H27C	0.761217	0.964607	0.941910	0.152*	0.436 (10)

Table 2.17: Atomic displacement parameters (\AA^2)

	U^{11}	U^{22}	U^{33}	U^{12}	U^{13}	U^{23}
S1	0.0355 (3)	0.0380 (3)	0.0450 (3)	0.00303 (19)	0.0102 (2)	0.0109 (2)
O1	0.0425 (8)	0.0603 (10)	0.0530 (9)	0.0005 (7)	0.0001 (7)	0.0190 (7)
O2	0.0461 (9)	0.0474 (9)	0.0683 (10)	0.0078 (7)	0.0252 (8)	0.0105 (7)
O3	0.0420 (8)	0.0558 (9)	0.0383 (8)	-0.0101 (7)	0.0081 (6)	0.0024 (6)
N1	0.0389 (9)	0.0356 (8)	0.0382 (9)	-0.0016 (7)	0.0119 (7)	0.0094 (7)
C00K	0.0605 (14)	0.0483 (12)	0.0409 (12)	0.0004 (10)	0.0093 (10)	-0.0008 (9)
C1	0.0389 (10)	0.0336 (10)	0.0421 (11)	0.0040 (8)	0.0096 (8)	0.0123 (8)
C2	0.0468 (12)	0.0400 (11)	0.0392 (11)	0.0038 (9)	0.0078 (9)	0.0115 (9)
C3	0.0603 (14)	0.0505 (12)	0.0404 (11)	0.0006 (10)	0.0161 (10)	0.0158 (10)
C4	0.0526 (13)	0.0373 (11)	0.0497 (12)	0.0027 (9)	0.0129 (10)	0.0158 (9)
C5	0.0547 (13)	0.0336 (10)	0.0433 (11)	0.0005 (9)	0.0102 (10)	0.0081 (8)
C6	0.0491 (12)	0.0311 (9)	0.0420 (11)	0.0065 (8)	0.0128 (9)	0.0105 (8)
C7	0.0552 (13)	0.0521 (13)	0.0368 (11)	-0.0027 (10)	0.0067 (10)	0.0087 (9)
C8	0.0739 (18)	0.0700 (17)	0.0493 (14)	0.0075 (14)	0.0136 (13)	-0.0026 (12)
C9	0.0727 (19)	0.090 (2)	0.0569 (16)	0.0028 (16)	-0.0070 (14)	0.0186 (14)
C10	0.0680 (16)	0.0420 (12)	0.0599 (14)	-0.0052 (11)	0.0206 (12)	0.0179 (10)

C11	0.0676 (19)	0.073 (2)	0.161 (4)	0.0033 (15)	0.046 (2)	0.042 (2)
C12	0.110 (2)	0.0551 (16)	0.085 (2)	0.0069 (16)	0.0318 (18)	0.0345 (15)
C13	0.0716 (15)	0.0361 (11)	0.0407 (11)	-0.0045 (10)	0.0180 (11)	0.0061 (9)
C14	0.101 (2)	0.0582 (15)	0.0439 (13)	-0.0236 (15)	-0.0016 (14)	0.0167 (11)
C15	0.119 (3)	0.0580 (16)	0.0751 (19)	0.0133 (16)	0.0549 (19)	0.0025 (14)
C16	0.0399 (10)	0.0319 (9)	0.0338 (9)	0.0004 (7)	0.0113 (8)	0.0105 (7)
C17	0.0387 (11)	0.0383 (10)	0.0344 (10)	-0.0047 (8)	0.0072 (8)	0.0094 (8)
C18	0.0371 (11)	0.0544 (13)	0.0490 (12)	0.0031 (9)	0.0085 (9)	0.0098 (10)
C19	0.0474 (13)	0.0476 (12)	0.0508 (13)	0.0073 (9)	0.0171 (10)	0.0057 (10)
C20	0.0484 (12)	0.0371 (10)	0.0365 (10)	0.0002 (9)	0.0107 (9)	0.0074 (8)
C21	0.0401 (11)	0.0378 (10)	0.0363 (10)	0.0003 (8)	0.0047 (8)	0.0094 (8)
C22	0.090 (4)	0.130 (8)	0.070 (5)	0.015 (5)	0.017 (3)	-0.048 (5)
C23	0.115 (7)	0.066 (4)	0.071 (4)	-0.034 (4)	0.013 (4)	0.006 (3)
C24	0.127 (7)	0.079 (4)	0.050 (3)	0.009 (4)	-0.025 (4)	0.001 (3)
C25	0.076 (5)	0.118 (10)	0.087 (7)	0.020 (5)	-0.018 (4)	-0.049 (7)
C26	0.165 (11)	0.121 (9)	0.040 (4)	-0.047 (8)	0.036 (5)	-0.012 (5)
C27	0.134 (10)	0.046 (4)	0.091 (6)	0.005 (4)	-0.014 (6)	-0.011 (3)

Table 2.18: Geometric parameters (Å, °)

S1—O1	1.4228 (16)	C3—C4	1.380 (3)
S1—O2	1.4337 (16)	C4—C5	1.377 (3)
S1—N1	1.6371 (17)	C4—C10	1.521 (3)
S1—C1	1.793 (2)	C5—C6	1.389 (3)
O3—C17	1.377 (2)	C6—C13	1.526 (3)
N1—C16	1.429 (2)	C7—C8	1.522 (4)
C00K—C20	1.534 (3)	C7—C9	1.520 (4)
C00K—C22	1.496 (6)	C10—C11	1.517 (4)
C00K—C23	1.512 (6)	C10—C12	1.514 (4)

C00K—C24	1.535 (6)	C13—C14	1.529 (4)
C00K—C25	1.505 (8)	C13—C15	1.535 (4)
C00K—C26	1.504 (7)	C16—C17	1.392 (3)
C00K—C27	1.555 (7)	C16—C21	1.392 (3)
C1—C2	1.409 (3)	C17—C18	1.374 (3)
C1—C6	1.414 (3)	C18—C19	1.384 (3)
C2—C3	1.390 (3)	C19—C20	1.392 (3)
C2—C7	1.534 (3)	C20—C21	1.393 (3)
O1—S1—O2	117.03 (10)	C5—C4—C3	117.42 (19)
O1—S1—N1	108.17 (9)	C5—C4—C10	121.4 (2)
O1—S1—C1	108.89 (9)	C4—C5—C6	123.13 (19)
O2—S1—N1	103.94 (9)	C1—C6—C13	125.79 (18)
O2—S1—C1	110.12 (9)	C5—C6—C1	117.53 (18)
N1—S1—C1	108.30 (9)	C5—C6—C13	116.66 (18)
C16—N1—S1	121.18 (13)	C8—C7—C2	110.68 (19)
C20—C00K—C24	109.3 (3)	C9—C7—C2	110.7 (2)
C20—C00K—C27	108.7 (3)	C9—C7—C8	112.0 (2)
C22—C00K—C20	114.0 (3)	C11—C10—C4	111.7 (2)
C22—C00K—C23	109.2 (5)	C12—C10—C4	111.4 (2)
C22—C00K—C24	110.0 (5)	C12—C10—C11	111.5 (2)
C23—C00K—C20	107.0 (3)	C6—C13—C14	111.5 (2)
C23—C00K—C24	107.1 (5)	C6—C13—C15	110.7 (2)
C25—C00K—C20	115.0 (3)	C14—C13—C15	111.5 (2)
C25—C00K—C27	105.3 (6)	C17—C16—N1	119.12 (17)
C26—C00K—C20	108.0 (4)	C21—C16—N1	121.00 (18)
C26—C00K—C25	111.4 (7)	C21—C16—C17	119.81 (19)
C26—C00K—C27	108.2 (7)	O3—C17—C16	117.75 (18)
C2—C1—S1	120.10 (15)	C18—C17—O3	122.99 (19)
C2—C1—C6	120.79 (18)	C18—C17—C16	119.19 (18)
C6—C1—S1	119.05 (15)	C17—C18—C19	120.4 (2)
C1—C2—C7	127.12 (18)	C18—C19—C20	121.8 (2)
C3—C2—C1	117.25 (19)	C19—C20—C00K	121.7 (2)

C3—C2—C7	115.58 (18)	C19—C20—C21	116.97 (19)
C4—C3—C2	123.4 (2)	C21—C20—C00K	121.27 (19)
C3—C4—C10	121.2 (2)	C16—C21—C20	121.65 (19)

2.5 Conclusions

A family of *o*-sulfonamidophenol derived ligands was studied for complexation and extraction of Ln(III) from highly alkaline aqueous media into organic diluents. **L2H2** showed Sm(III) recoveries as high as 93.3(±5.2)% in dichloromethane and 53.9(±4.0) % in *n*-dodecane:octanol (80:20, v/v) at pH 14.0. Solvent extraction experiments, Job plots, and UV-Vis titrations all confirmed a 1:2 metal–ligand binding stoichiometry. DFT calculations further confirmed that 1-2 complexation can occur, while 1-1 complexes are also possible. Binding constants for complex formation obtained by UV-Vis titrations in the presence of NaOH in CH₃CN:CH₃OH (96:4, v/v) after non-linear regression analysis were determined in the range of $\beta_2 = 3.98 (\pm 0.01) \times 10^{10} \text{ M}^{-2} - 1.26 (\pm 0.04) \times 10^{12} \text{ M}^{-2}$. As these *o*-sulfonamidophenol ligands are easy to synthesize and highly efficient for extraction of Sm(III) into highly lipophilic organic diluents, they have enormous potential for extraction and separation of actinides from alkaline high-level waste.

2.6 Acknowledgement

The author would like to thank Drs. Yong Cai and Guangliang Liu for granting access and providing guidance for the use of the ICP-MS instrument. This work was supported by the U. S. Department of Energy Office of Environmental Management MSIPP program managed by the Savannah River National Laboratory under SRNS contracts BOA 541, TOAs 0000217393, 0000403071 and 0000525181 to FIU. We also

appreciate the support received from the Florida International University Dissertation Year Fellowship for Oluwaseun William Adedoyin (DYF Summer/Fall 2021 Fellow).

2.7 References

1. Wilmarth, W. R.; Lumetta, G. J.; Johnson, M. E.; Poirier, M. R.; Thompson, M. C.; Suggs, P. C.; Machara, N. P. Waste-pretreatment technologies for remediation of legacy defense nuclear wastes. *Solvent Extraction and Ion Exchange* **2011**, *29*, 1-48.
2. Wiersma, B. J. The performance of underground radioactive waste storage tanks at the savannah river site: a 60-year historical perspective. *Journal of Minerals, Metals and Materials* **2014**, *66*, 471-490.
3. Peters, T. B.; Poirier, M. R.; Fink, S. D. Processing macrobatch 2 at the savannah river site integrated salt disposition process (ISDP). *Separation Science and Technology* **2010**, *45*, 1801-1806.
4. Peters, T. B.; Barnes, M. J.; Hobbs, D. T.; Walker, D. D.; Fondeur, F. F.; Norato, M. A.; Fink, S. D.; Pulmano, R. L. Strontium and actinide separations from high level nuclear waste solutions using monosodium titanate. Actual waste testing. *Separation Science and Technology* **2006**, *41*, 2409-2427.
5. Moyer, B. A.; Bonnesen, P. V.; Delmau, L. H.; Sloop Jr, F. V.; Williams, N. J.; Birdwell Jr, J. F.; Lee, D. L.; Leonard, R. A.; Fink, S. D.; Peters, T. B. In *In Development of the Next-Generation Caustic-Side Solvent Extraction (NG-CSSX) Process for Cesium Removal from High-Level Tank Waste-11346*; Proceedings Waste Management 2011 Conference, February; **2011**.
6. Hobbs, D. T.; Peters, T. B.; Taylor-Pashow, K.; Fink, S. D. Development of an improved titanate-based sorbent for strontium and actinide separations under strongly alkaline conditions. *Separation Science and Technology* **2010**, *46*, 119-129.
7. Duncan, N. C.; Roach, B. D.; Williams, N. J.; Bonnesen, P. V.; Rajbanshi, A.; Moyer, B. A. N, N'-dicyclohexyl-N''-isotridecylguanidine as suppressor for the next generation caustic side solvent extraction (NG-CSSX) Process. *Separation Science and Technology* **2012**, *47*, 2074-2087.
8. Raymond, K. N.; Garrett, T. M. Sequestering agents specific for high oxidation state cations. *Pure and Applied Chemistry* **1988**, *60*, 1807-1816.

9. Kappel, M. J.; Nitsche, H.; Raymond, K. N. Specific sequestering agents for the actinides. 11. Complexation of plutonium and americium by catecholate ligands. *Inorganic Chemistry* **1985**, *24*, 605-611.
10. Sofen, S. R.; Cooper, S. R.; Raymond, K. N. Crystal and molecular structures of tetrakis (catecholato) hafnate (IV) and-cerate (IV). Further evidence for a ligand field effect in the structure of tetrakis (catecholato) uranate (IV). *Inorganic Chemistry* **1979**, *18*, 1611-1616.
11. Weitzel, F. L.; Raymond, K. N.; Smith, W. L.; Howard, T. R. Specific sequestering agents for the actinides. N, N', N'', N'''-Tetra (2, 3-dihydroxybenzoyl) tetraazacyclotetra and hexadecanes. *Journal of American Chemical Society* **1978**, *100*, 1170-1172.
12. Gramer, C. J.; Raymond, K. N. Characterization of 2, 3-Dihydroxyterephthalamides as M(IV) Chelators. *Inorganic Chemistry* **2004**, *43*, 6397-6402.
13. Gramer, C. J.; Raymond, K. N.; Jarvinen, G. D.; Robison, T. W.; Schroeder, N. C.; Smith, B. F. The Removal of Pu (IV) from Aqueous Solution Using 2, 3-Dihydroxyterephthalamide Functionalized PEI with Polymer Filtration. *Separation Science and Technology* **2005**, *39*, 321-339.
14. Bukina, T. I.; Karalova, Z. K.; Myasoedov, B. F. Separation of Transplutonium Elements from Other Elements in Basic and Carbonate solutions by Extraction with Alkyl-Derivatives of Aminocatechols. *Radiokhimiya* **1990**, *32*, 11-15.
15. Myasoedov, B. F.; Karalova, Z. K.; Kuznetsova, V. S.; Rodionova, L. M. Americium and europium extraction from alkaline solutions by alkylpyrocatechols. *Radiokhimiya* **1980**, *22*, 347-351.
16. Smirnov, I. V.; Karavan, M. D.; Logunov, M. V.; Tananaev, I. G.; Myasoedov, B. F. Extraction of radionuclides from alkaline and carbonate media. *Radiochemistry* **2018**, *60*, 470-487.
17. Smirnov, I. V.; Stepanova, E. S.; Tyupina, M. Y.; Ivenskaya, N. M.; Zaripov, S. R.; Kleshnina, S. R.; Solov'eva, S. E.; Antipin, I. S. Extraction of cesium and americium with *p*-alkylcalix[8]arenes from alkaline solutions. *Radiochemistry* **2016**, *58*, 381-388.
18. Ivenskaya, N. M.; Stepanova, E. S.; Logunov, M. V.; Smirnov, I. V. Extraction of long-lived radionuclides from high-level alkaline waste with *p*-alkylcalix[8]arene. *Radiochemistry* **2018**, *60*, 378-385.

19. Smirnov, I. V.; Karavan, M. D.; Stepanova, E. S.; Kalchenko, V. I. Extraction of americium and europium with functionalized thiacalix[4]arenes from alkaline solutions. *Radiochemistry* **2016**, *58*, 617-624.
20. Govor, E. V.; Morozov, A. N.; Rains, A. A.; Mebel, A. M.; Kavallieratos, K. Spectroscopic and theoretical insights into surprisingly effective Sm(III) extraction from alkaline aqueous media by *o*-Phenylenediamine-derived sulfonamides. *Inorganic Chemistry* **2020**, *59*, 6884-6894.
21. Morozov, A. N.; Govor, E. V.; Anagnostopoulos, V. A.; Kavallieratos, K.; Mebel, A. M. 1, 3, 5-Tris-(4-(iso-propyl)-phenylsulfamoylmethyl) benzene as a potential Am(III) extractant: experimental and theoretical study of Sm(III) complexation and extraction and theoretical correlation with Am(III). *Molecular Physics* **2018**, *116*, 2719-2727.
22. Wen, K.; Wu, Z.; Huang, B.; Ling, Z.; Gridnev, I. D.; Zhang, W. Solvent-Controlled Pd(II)-Catalyzed Aerobic Chemoselective Intermolecular 1, 2-Aminooxygenation and 1, 2-Oxyamination of Conjugated Dienes for the Synthesis of Functionalized 1, 4-Benzoxazines. *Organic Letters* **2018**, *20*, 1608-1612.
23. KumaraBoominathan, S. S.; ChandruaSenadi, G; KishoreaVandavasi, J. A one-pot hypiodite catalysed oxidative cycloetherification approach to benzoxazoles. *Chemical Communications* **2014**, *51*, 6726 – 6728.
24. Gans, P.; Sabatini, A.; Vacca, A. Investigation of equilibria in solution. Determination of equilibrium constants with the HYPERQUAD suite of programs. *Talanta* **1996**, *43*, 1739-1753.
25. Gans, P.; Sabatini, A.; Vacca, A. Determination of equilibrium constants from spectrophotometric data obtained from solutions of known pH: the program pHab. *Annali di Chimica* **1999**, *89*, 45-49.
26. MacCarthy, P. Simplified experimental route for obtaining Job's curves. *Analytical Chemistry* **1978**, *50*, 2165.
27. Saha, S.; Roy, A.; Roy, K.; Roy, M. N. Study to explore the mechanism to form inclusion complexes of β -cyclodextrin with vitamin molecules. *Scientific Reports* **2016**, *6*, 1-12.
28. Savvin, S. B. Analytical use of arsenazo III: Determination of thorium, zirconium, uranium and rare earth elements. *Talanta* **1961**, *8*, 673-685.
29. Sheldrick, G. M. SHELXS-97, Program for Crystal Structure Determination, University of Göttingen, Germany, **1997**.

30. Dolomanov, O. V.; Bourhis, L. J.; Gildea, R. J.; Howard, J. A.; Puschmann, H. OLEX2: a complete structure solution, refinement and analysis program. *Journal of Applied Crystallography* **2009**, *42*, 339-341.
31. Andersen, K. K.; Gowda, G.; Jewell, L.; McGraw, P.; Phillips, B. T. Substitution at tetracoordinate sulfur (VI). Rearrangement of 2-aminoaryl arenesulfonates to N-(2-hydroxyaryl) arenesulfonamides. *Journal of Organic Chemistry* **1982**, *47*, 1884-1889.
32. Smirnov, I.; Karavan, M. D.; Babain, V. A.; Kvasnitskiy, I.; Stoyanov, E.; Miroschnichenko, S. Effect of alkyl substituents on extraction properties and solubility of calix[4]arene dialkylphosphine oxides. *Radiochimica Acta* **2007**, *95*, 97-102.
33. Alkhuraiji, T. S. Effect of Co-60 irradiation on the degradation and mineralization of sulfonated aromatic compounds in aqueous solutions. *Chemosphere* **2019**, *228*, 769-777.
34. Wilden, A.; Mincher, B. J.; Mezyk, S. P.; Twight, L.; Rosciolo-Johnson, K. M.; Zarzana, C. A.; Case, M. E.; Hupert, M.; Stärk, A.; Modolo, G. Radiolytic and hydrolytic degradation of the hydrophilic diglycolamides. *Solvent Extraction and Ion Exchange* **2018**, *36*, 347-359.
35. Clifford, W. E.; Bullwinkel, E. P.; McClaine, L. A.; Noble Jr, P. The Solvent Extraction of Uranium (VI) from Carbonate Solutions. *Journal of American Chemical Society* **1958**, *80*, 2959-2961.
36. Smirnov, I. V.; Stepanova, E. S.; Drapailo, A. B.; Kalchenko, V. I. Extraction of americium and europium with functionalized calixarenes from alkaline solutions. *Radiochemistry* **2016**, *58*, 42-51.
37. Kuzovkina, E. V.; Lavrinovich, E. A.; Novikov, A. P.; Stepanova, E. S.; Karavan, M. D.; Smirnov, I. V. Kinetics of americium and europium extraction by *tert*-butylthiacalix[4]arene from alkaline media. *Journal of Radioanalytical and Nuclear Chemistry* **2017**, *311*, 1983-1989.
38. Kumar, A.; Sonawane, J.; Rathore, N.; Kapur, H.; Venugopalan, A.; Bajpai, D. Scaling-up experience of actinides partitioning from intermediate level high salted alkaline waste streams of Purex process using Versatic-10 extractant. *Journal of Radioanalytical and Nuclear Chemistry* **2002**, *254*, 469-478.
39. Altmaier, M.; Gaona, X.; Fanghanel, T. Recent advances in aqueous actinide chemistry and thermodynamics. *Chemical Reviews* **2013**, *113*, 901-943.

40. Schultz, T. W. The use of the ionization constant (pKa) in selecting models of toxicity in phenols. *Ecotoxicology and Environmental Safety* **1987**, *14*, 178-183.
41. Gross, K. C.; Seybold, P. G. Substituent effects on the physical properties and pKa of phenol. *International Journal of Quantum Chemistry* **2001**, *85*, 569-579.
42. Liptak, M. D.; Gross, K. C.; Seybold, P. G.; Feldgus, S.; Shields, G. C. Absolute pKa determinations for substituted phenols. *Journal of the American Chemical Society* **2002**, *124*, 6421-6427.
43. Dauphin, G.; Kergomard, A. Etude de la dissociation acide de quelques sulfonamides. *Bulletin de la Societe Chimique de France* **1961**, 486-492.
44. Panja, S.; Mohapatra, P. K.; Tripathi, S. C.; Gandhi, P. M.; Janardan, P. Role of organic diluents on Am (III) extraction and transport behaviour using N, N, N', N'-tetraoctyl-3-oxapentanediamide as the extractant. *Journal of Membrane Science* **2012**, *403*, 71-77.
45. Mohapatra, P. K.; Ansari, S. A.; Sarkar, A.; Bhattacharyya, A.; Manchanda, V. K. Evaluation of calix-crown ionophores for selective separation of radio-caesium from acidic nuclear waste solution. *Analytica Chimica Acta* **2006**, *571*, 308-314.
46. Mohapatra, P. K.; Manchanda, V. K. Ion-pair extraction of tetravalent plutonium from hydrochloric acid medium using crown ethers. *Journal of Inclusion Phenomena and Molecular Recognition in Chemistry* **1996**, *25*, 257-265.
47. Fennell, C. J.; Li, L.; Dill, K. A. Simple liquid models with corrected dielectric constants. *The Journal of Physical Chemistry B* **2012**, *116*, 6936-6944.
48. Haynes, W. M. Handbook of chemistry and physics; CRC press: **2014**.
49. Patra, K.; Sadhu, B.; Sengupta, A.; Patil, C. B.; Mishra, R. K.; Kaushik, C. P. Achieving highly efficient and selective cesium extraction using 1, 3-di-octyloxy-calix[4]arene-crown-6 in n-octanol based solvent system: experimental and DFT investigation. *RSC Advances* **2021**, *11*, 21323-21331.

Chapter III: Highly-Lipophilic Alkylated Sulfonamides for Ln(III) Extraction
from Alkaline Solutions into Organic Diluents.

Oluwaseun W. Adedoyin, Xinrui Zhang, Cristian Gonzalez, and Konstantinos
Kavallieratos

3.1 Abstract

Two new ligands; i) the sulfonamidophenol - N-(5-(*tert*-butyl)-2-hydroxyphenyl)-4-(dodecan-3-yl)benzenesulfonamide (**msa**) and ii) the disulfonamide - N,N'-(1,2-phenylene)bis(4-(dodecan-3-yl)benzenesulfonamide) (**dsa**) bearing the 4-dodecan-3-yl lipophilic alkyl chain were synthesized with the purpose of complexing and extracting Ln(III) from alkaline solutions into the lipophilic organic diluent *n*-dodecane. Ln(III) were used as experimental surrogates for An(III), with the goal of developing practical separation processes for HLW in process solvents commonly used in practical extraction processes. When **msa** (20.0 mM) or **dsa** (20.0 mM) dissolved in *n*-dodecane and in the presence of trioctylamine were contacted with Sm(III) solutions, at pH 12.5 or 13.5, respectively, followed by stripping with 0.1M HNO₃. 40.9 (±7.7)% and 50.7 (±1.2)% of Sm(III) was recovered respectively after just one extraction / stripping cycle. Slope analysis for Sm(III) extracted by **dsa** in *n*-dodecane at pH 12.0 indicates the formation of a 1:1 Sm(III)-**dsa** complex during extraction. UV-Vis Job plots in CH₃CN:CH₃OH (96:4, v/v) also showed 1:1 stoichiometry. UV-Vis titrations followed by non-linear regression analysis of the 1-1 binding isotherms gave binding constants of 1.60 (±0.70) × 10⁶ M⁻¹ for the Sm(III)-**msa** complex and 7.90 (±0.40) × 10⁷ M⁻¹ for the Sm(III)-**dsa** complex in

CH₃CN:CH₃OH (96:4, v/v) in agreement with the Job plots and slope analysis results from the extraction experiments.

3.2 Introduction

The problem of f-element separation by extraction with regard to Ln / An separations for facilitating transmutation and minor actinide recycling has been widely studied in acidic conditions, especially as there is a large volume of untreated acidic used nuclear fuel.¹⁻¹⁰ In contrast, the problem of actinide separation from highly alkaline High-level waste (HLW), stored at the Hanford and the SRS - a result of years of nuclear weapons production, has received much less attention, despite the fact that this presents an acute environmental problem, due to constant deterioration of carbon steel tanks that have been used for years for its storage.¹¹ The chemistry and speciation of actinides in acidic HLW is a topic of intense research and debate^{12,13} however the chemistry and separation of actinides in caustic HLW is not well understood, as it has a very complicated composition due to high pH, high ionic strength, and the presence of precipitated salts of both radioactive and nonradioactive elements. The radiotoxicity in alkaline HLW is due mainly to the contributions of ¹²⁷Cs, ⁹⁰Sr and the transuranic (TRU) actinides.^{14,15}

Alkaline HLW reprocessing, has focused for years in separating the radioactive fission products ¹³⁷Cs and ⁹⁰Sr, with less emphasis on the TRU elements, as these were believed to be mainly concentrated in the insoluble sludge and could be directly vitrified and separated from the larger volume of low activity waste (LAW).¹⁶ However, due to the high ionic strength and alkalinity of HLW, there is a substantial amount of TRU activity

in the tank supernates,¹² and their effective separation does present a problem.^{13,17} For Cs(I) separation, the Caustic-Side Solvent Extraction (CSSX) process has been developed at Oak Ridge National Laboratory using a calix[4]arene-crown-6 extractant, alongside an alkylphenoxyl alcohol solvent modifier to allow higher loading of the calixarene in the non-polar diluent Isopar-L[®], and a trioctylamine suppressor, used to facilitate stripping.^{15,18} The CSSX process exhibits fast and selective extraction for Cs(I) over Na(I) and K(I), which are much more prevalent in alkaline HLW, with decontamination factors over 40000,^{19,20} ⁹⁰Sr and actinides in the supernate are currently removed by sorption on monosodium titanate through the Actinide Removal Process (ARP).²¹ Although the ARP process is very effective for removal of Sr and An, being a sorption process, it remains the kinetics bottleneck of the integrated salt waste processing at SRS currently, and often requires multiple contacts (“strikes”) with titanate, in order to bring α -activity of the TRU elements present to low enough levels suitable for LAW storage. Thus, there is a strong research impetus to derive solvent extraction and separation methods for actinides from alkaline solutions, with the goal to create an integrated HLW processing, either by modifying the CSSX process or by deriving a new pre- or post-CSSX actinide extraction step, with the goal to minimize the time and amount of titanate needed during ARP. In such experiments lanthanides could be used as effective actinide surrogates,²² as the amount of Ln component in HLW is relatively low, the need to selectively separate An from high backgrounds of alkali and alkali earth metals is the main challenge.^{23,24}

In order to achieve the goal of extracting An from alkaline solutions, several organic ligands, have been developed, including alkylpyrocatechols,²⁵

alkyl(aminomethyl)phenols,²⁶ oligomers of alkyl phenols with -N, -O and S₂-bridging groups,^{27,28} in addition, thiacalix-crowns^{29,30} and calix[4]arenes^{31,32} have also been studied. For example, 4-(α,α -dioctylethyl)pyrocatechol (DOP) of the alkylpyrocatechol family is considered one of the more efficient actinide extractants from alkaline solutions.^{25,33} Aminomethyl derivatives of alkylphenols, 2-hydroxy-5-alkylbenzyl diethanolamine (DEAP) and its dimeric analog bis(2-hydroxy-5-alkylbenzyl)amine (CAAP) allow combined recovery of Am(III) and Cm(III) over REE and other fission products with a separation factor over 400 in pH 12.8-13.7.²⁷ Calix[8]arenes derivatives have also exhibited good extraction for Cs, Am, and Pu from alkaline solutions.³⁴ Despite the promise of these extractants for f-element extraction and separation, from alkaline conditions, they suffer several shortcomings, such as poor stability, synthetic difficulty, poor kinetics, or impractical stripping conditions. In the area of nuclear waste management, developing more efficient, industrially applicable extractants that can perform well in hydrocarbonic solvents, and allow no or minimal partition to the aqueous phase, therefore offering full solvent recycling is a major challenge.³⁵ Exploring the chemistry and coordination behavior of such ligands with trivalent actinides and lanthanides under highly alkaline conditions, is also a problem that has not attracted the attention it deserves.³⁶ In previous studies from our group,³⁷⁻³⁹ several relatively simple and easily available sulfonamide ligands have demonstrated reasonable extraction of f-elements from alkaline solutions, both experimentally and by DFT calculations.^{39,40} Govor et al. recently reported a family of *o*-phenylenediamine-derived disulfonamides, which exhibited excellent extraction efficiency from alkaline aqueous media, after just one loading / stripping cycle, with up to 81% Sm(III) recovery

at pH 13.0-13.5.³⁹ However, these ligands did not extract Sm(III) at pH 14.0 and dichloromethane was used as the organic diluent, which is not ideal for industrial applications. More recently, we developed simpler monosulfonamidophenol extractants ligands with impressive Sm(III) recoveries of over 90% which persist even at pH 14.0.^{41,42} However, even these improved ligands demonstrated limiting capacity in non-polar organic diluents, and cannot be used in the preferred diluent *n*-dodecane due to solubility problems in this very non-polar solvent.

As part of our continuing efforts to bring this work closer to the application stage, we have now developed the highly-lipophilic monosulfonamidophenol ligand N-(5-(*tert*-butyl)-2-hydroxyphenyl)-4-(dodecan-3-yl)benzenesulfonamide (**msa**) and the disulfonamide analog N,N'-(1,2-phenylene)bis(4-(dodecan-3-yl)benzenesulfonamide) (**dsa**) (Figure 3.1), for improved solubility in industrial process solvents. Using *n*-dodecane as diluent, and trioctylamine (which is used to both facilitate deprotonation and simulate the CSSX solvent conditions that are used at SRS), 40.9 (± 7.7)% and 50.7 (± 1.2)% of Sm(III) was recovered from pH 12.5 and 13.5 by **msa** and **dsa** respectively. Job plots, extraction slope analysis and UV-Vis titrations, all suggest a 1:1 Sm(III) complexation in solution for both the **dsa** and **msa** ligands. This study brings closer the possibility of actual industrial application of sulfonamide ligands as extractants for An(III) from highly alkaline HLW.

3.3 Experimental section

3.3.1 Materials and methods

All starting materials, reagents and solvents were purchased from Fisher Scientific or Sigma-Aldrich. The two sulfonamide ligands are new compounds that were synthesized by modifications of methods reported in the literature.^{43,44} 4-(dodecane-3-yl)benzenesulfonyl chloride which is a starting material for both sulfonamides was synthesized based on a modification of previously reported method for a different analog,⁴⁵ and it is fully characterized herein. Chemicals were standard reagent grade; solvents were spectroscopic grade and were used without further purification. FT-IR spectra were recorded on the 4000 – 600 cm^{-1} range using a Cary 600 series FT-IR spectrometer. NMR spectra were recorded on a 400 MHz Bruker Avance NMR spectrometer and were referenced using the residual solvent resonances, all chemical shifts, δ , were reported in ppm. UV-Vis spectra were recorded on a Varian Cary 100 Bio UV-Vis spectrophotometer. ICP-MS experiments were performed on a PerkinElmer NexION® 2000 ICP Mass Spectrometer, and Y(III) (10 ppm) was used as the internal standard.

3.3.2 Synthesis of 4-(dodecane-3-yl)benzenesulfonyl chloride (1).

Following the procedure of Blotny and coworkers,⁴⁵ 4-(dodecan-3-yl)benzenesulfonic acid (5.00 g; 15.3 mmol) and 2.13 mL of triethylamine (15.3 mmol) was left to stir in 40 mL of dried acetone under a stream of N_2 . To this stirring solution, cyanuric chloride (2.82 g; 15.3 mmol) was added and the reaction mixture was brought to

reflux for 20 h. After letting to cool to room temperature, the yellow suspension was filtered off through a celite pad. The collected filtrate was then concentrated and purified using column chromatography (Hexanes:EtOAc; 9:1) to give the product as a clear liquid (2.96 g, 56% yield). ¹H-NMR (400 MHz, CDCl₃): δ 7.96 (d, 2H), 7.38 (d, 2H), 2.63 (m, 1H), 1.66 (m, 2H), 1.56 (m, 2H), 1.22 (m, 14H), 0.85 (m, 6H). ¹³C-NMR (101 MHz, CDCl₃) δ 155.6, 142.2, 129.3, 127.5, 46.5, 46.3, 39.9, 36.7, 36.4, 31.9, 29.9, 27.6, 27.3, 22.9, 20.7, 14.3. FT-IR (cm⁻¹; ATR): 2955 (m), 2925 (s), 2854 (s), 1591 (m), 1489 (w), 1463 (m), 1412 (m), 1377 (s), 1306 (w), 1281 (w), 1177 (s), 1112 (w), 1082 (m), 1014 (w), 834 (m), 761 (m), 724 (m), 667 (m), 640 (s). Elemental Analysis for C₁₈H₂₉ClO₂S: Calcd. C, 62.68; H, 8.47. Found C, 62.94; H, 8.71.

3.3.3 Synthesis of N-(5-(*tert*-butyl)-2-hydroxyphenyl)-4-(dodecan-3-yl)benzenesulfonamide (msa).

To a solution of 2-amino-4-(*tert*-butyl)phenol (1.50 g, 9.09 mmol) and pyridine (10.98 mL, 136 mmol) in 20 mL of 1,2-dichloroethane, stirring in an ice bath, a solution of **1** (3.45 g, 10.1 mmol) dissolved in 20 mL of 1,2-dichloroethane was added dropwise. After addition, the ice bath was removed, and the reaction was left for 5 h to stir at room temperature under N₂. The reaction was then quenched by adding ice-cold water and the organic layer was collected, sequentially washed with 1.0 M HCl, 1.0 M NaHCO₃ and 1.0 M brine (3 × 35 mL each), and dried with MgSO₄. Excess solvent was removed using a rotary evaporator, and the product was purified by column chromatography (Hexanes:EtOAc; 9:1), (2.58 g, 60% yield). ¹H-NMR (400 MHz, CDCl₃): δ 7.63 (d, 2H), 7.22 (d, 2H), 7.13 (dd, 1H), 6.90 (d, 1H), 6.55 (s, 1H), 6.49 (s, 1H), 6.35 (s, 1H), 2.53 (m,

1H), 1.61 (m, 2H), 1.49 (m, 2H), 1.19 (s, 14H), 1.07 (s, 9H), 0.81 (m, 6H). ¹³C-NMR (101 MHz, CDCl₃): δ 153.0, 149.4, 143.8, 134.8, 128.3, 127.8, 125.6, 123.6, 121.8, 116.8, 46.2, 45.9, 38.9, 36.7, 36.4, 31.2, 29.8, 27.5, 27.2, 22.6, 20.6, 14.4. FT-IR (cm⁻¹; ATR): 3425 (m), 3249 (m), 2955 (s), 2924 (s), 2854 (m), 1596 (m), 1514 (m), 1459 (m), 1387 (m), 1363 (m), 1319 (s), 1290 (m), 1252 (w), 1224 (m), 1156 (vs), 1123 (m), 1089 (m), 1016 (w), 952 (m), 898 (m), 872 (w), 821 (m), 790 (w), 728 (m), 702 (w), 678 (m). Elemental Analysis for C₂₈H₄₃NO₃S: Calcd. C, 70.99; H, 9.15; N, 2.96. Found C, 71.22; H, 9.34; N, 3.06.

3.3.4 Synthesis of N,N'-(1,2-phenylene)bis(4-(dodecan-3-yl)benzenesulfonamide) (dsa).

A solution of 1,2-phenylenediamine (540 mg, 4.99 mmol) and pyridine (4.95 mL, 61.5 mmol) in 25 mL of 1,2-dichloroethane was added dropwise to **I** (4.13 g, 12.0 mmol) in 75 mL of 1,2-dichloroethane at 0°C. The reaction mixture was then refluxed for 5 h under N₂. The organic layer was sequentially washed with 1.0 M HCl, 0.2 M NaHCO₃, and H₂O (3 x 35 mL each), and dried with Na₂SO₄. The volatiles were removed by rotary evaporation, and the product was purified by column chromatography (Hexanes:EtOAc; 9:1), (1.03 g, 38% yield). ¹H-NMR (400 MHz, CDCl₃): δ 7.38 (d, 4H), 7.19 (d, 4H), 6.97 (d, 2H), 6.91 (s, 2H), 6.82 (s, 2H), 2.52 (m, 2H), 1.61 (m, 4H), 1.49 (m, 4H), 1.18 (s, 28H), 0.81 (m, 12H). ¹³C-NMR (101 MHz, CDCl₃) δ 153.2, 135.9, 128.7, 128.7, 128.0, 127.9, 127.6, 77.7, 77.4, 77.1, 48.3, 46.5, 46.3, 40.4, 39.2, 38.5, 37.1, 36.7, 32.4, 29.9, 27.9, 27.5, 23.2, 22.3, 20.9, 14.6, 12.4. FT-IR (cm⁻¹; ATR): 3246 (m), 2955 (m), 2923 (s), 2853 (s), 1597 (m), 1498 (m), 1464 (m), 1410 (m), 1330 (s), 1275 (m), 1244 (w), 1188

(w), 1160 (vs), 1090 (m), 1046 (w), 1016 (w), 919 (m), 833 (m), 753 (m), 724 (m), 675 (s), 651 (m). Elemental Analysis for $C_{42}H_{64}N_2O_4S_2$: Calcd. C, 69.57; H, 8.90; N, 3.86. Found C, 69.66; H, 9.03; N, 3.96.

3.3.5 UV-Vis titrations

msa was titrated with Sm(III) at constant concentration of **msa** and NaOH as follows: A solution of **msa** (1.0 mM) and NaOH (2.2 mM) was prepared in 10.0 mL of methanol. 1.00 mL of this solution was diluted to 25.0 mL with acetonitrile to give a solution of **msa** (40 μ M) and NaOH (88 μ M) in $CH_3CN:CH_3OH$ 96:4 (v/v) (Solution A). A solution of $Sm(NO_3)_3 \cdot 6H_2O$ (4.0×10^{-4} M) was prepared by diluting weighed quantity of $Sm(NO_3)_3 \cdot 6H_2O$ to 10.0 mL with solution A. A volume of 2.70 mL of solution A was placed in the cuvette cell, and titrated with Solution B in small additions until 0.80 mL total was added. Titration experiments were performed in triplicate independent samples. For reference, a blank solution, (mixed solvent containing 0.40 mL methanol and 9.60 mL acetonitrile) was used. The stability constants were obtained by non-linear regression analysis to the 1:1 binding isotherm and were reported as average values of the binding data from triplicate independent experiments with errors derived from standard deviations of the triplicate experiments.

dsa was titrated with Sm(III) at constant concentration of **dsa** and NaOH with a similar protocol as above and the following modifications: Solution B (8.0×10^{-4} M of $Sm(NO_3)_3 \cdot 6H_2O$) was prepared as previously described and added to the separate samples bearing Solution A in increasing volumes 10.0 μ L – 1000.0 μ and the resulting solutions

were analyzed by UV-Vis spectroscopy after 2 h to ensure that thermodynamic equilibrium was reached.

3.3.6 Determination of complex stoichiometry by the continuous variation method (Job plot)

Two stock solutions of ligand (Solution A) and Sm(III) (Solution B) were prepared, with each bearing equal molarity. Solution A of ligand (20.0 μM) and NaOH (50.0 μM) was prepared in $\text{CH}_3\text{CN}:\text{CH}_3\text{OH}$ (96:4, v/v) as in 3.3.5. Solution B of Sm(III) (20.0 μM) was prepared by dissolving a weighed amount of $\text{Sm}(\text{NO}_3)_3 \cdot 6\text{H}_2\text{O}$ in $\text{CH}_3\text{CN}:\text{CH}_3\text{OH}$ (96:4, v/v). Mixed solutions of A and B were prepared in 11 vials each with total volume of 5.00 mL. The volumes added from both solutions were in the following ratios (in mL) 5:0, 4.5:0.5, 4:1, 3.5:1.5, 3:2, 2.5:2.5, 2:3, 1.5:3.5, 1:4, 0.5:4.5, 0:5. UV-Vis spectra were recorded for each one of these solutions, and a Job plot was constructed by plotting $\Delta A_{250\text{nm}}$ against the mol fraction $[\text{L}]_t / ([\text{Sm}(\text{III})]_t + [\text{L}]_t)$ for **msa** or $\Delta A_{260\text{nm}}$ against the mol fraction $[\text{L}]_t / ([\text{Sm}(\text{III})]_t + [\text{L}]_t)$ for **dsa**.

3.3.7 pH-dependent experiments for extraction & recovery of Sm(III) into *n*-dodecane by dsa or msa in the presence or absence of trioctylamine with spectrophotometric quantification of Sm(III).

Nine vials containing solutions of Sm(III) (2.0 mM) in various pH ($1.0 \times 10^{-4} \text{M}$ – 1.0 M of NaOH), were prepared. Solutions of ligand (20.0 mM) in *n*-dodecane and trioctylamine (40.0 mM) were also prepared. 2.50 mL of the aqueous and organic phases (either with or without trioctylamine) were then brought into extended contact by rotating the sealed vials extensively on a wheel for 20 h (55 rpm) at room temperature (22 °C).

The tubes were then centrifuged for 5 min (3200 rpm) and the organic phases were collected and filtered. Stripping of Sm(III) was performed by adding 1.00 mL of 0.1 M HNO₃ to 1.00 mL of the loaded organic phases and the two phases were again brought into contact on the rotating wheel for 20 h (55 rpm) at room temperature (22 °C), centrifuged for 5 min (3200 rpm) and the aqueous phase was collected and quantified for Sm(III) using the Arsenazo-III spectrophotometric method.⁴⁶ Sm(III) recovered after stripping was quantified by making a solution comprised of 0.10 mL of the aqueous stripped phase (or the aqueous phase after extraction for mass balance studies), 1.00 mL of 1% ascorbic acid, 1.00 mL of 0.2 M formate buffer (pH 3.0) and 2.00 mL of 0.05% Arsenazo-III solution. The pH of this solution was then adjusted to pH 2.6 ± 0.1 using 0.1 M HNO₃ and was brought to 25.0 mL with DI water. The absorbance of this solution was then measured at 652 nm using UV-Vis, and concentrations were calculated based on prior calibrations. using Sm(III) solutions of known concentration ranging from 200.0 ppm to 500.0 ppm. Reported quantification was expressed in percentages (eq. 3.1) based on the concentration of Sm(III) recovered after stripping to the starting concentration of Sm(III) used for the extraction.

$$\% \text{ Recovered} = \frac{[Sm(III)]_t \text{ in aqueous phase after stripping}}{[Sm(III)]_t \text{ in aqueous phase before extraction}} \times 100 \quad (\text{eq. 3.1})$$

All experiments were performed with independent triplicate samples in order to derive standard deviations that are reflected in the reported Sm% recovery errors.

3.3.8 pH-dependent experiments for extraction & recovery of Ln(III) into *n*-dodecane with quantification of Ln(III) by ICP-MS.

This experiment was performed for **msa**, in a similar procedure as the one described in 3.3.7 except that each individual vial contained a combined solution of several lanthanides - La(III), Nd(III), Sm(III), and Eu(III) each of 2.0 mM concentration respectively in the same aqueous phase and in various pHs (1.0×10^{-4} M – 1.0 M of NaOH). Trioctylamine was not added in this experiment. The amounts of Ln(III) recovered after stripping were quantified by diluting the stripped aqueous phase 1/10000 in 2% HNO₃. For calibration, standard solutions of La(III), Nd(III), Sm(III), and Eu(III) were used to prepare solutions with concentrations ranging from 0 ppb to 50.0 ppb in 2% HNO₃. Afterwards, 5.00 μL of 10.0 ppm Y(III) as internal standard was added to all the samples, and 5.00 mL of the solution was then submitted for analysis using ICP-MS. Concentrations of recovered Ln(III) were then calculated based from the slope obtained from the calibration. Reported quantification was expressed in percentages (eq. 3.2) based on the concentration of Ln(III) recovered after stripping to the starting concentration of Ln(III) used for the extraction.

$$\% \text{ Recovered} = \frac{[\text{Ln(III)}]_{t \text{ in aqueous phase after stripping}}}{[\text{Ln(III)}]_{t \text{ in aqueous phase before extraction}}} \times 100 \quad (\text{eq. 3.2})$$

All experiments were performed with independent triplicate samples in order to derive standard deviations that are reflected in the reported Ln(III) % recovery errors.

3.3.9 Determination of complex stoichiometry in extraction by slope analysis⁴⁷

For slope analysis experiments, a solution of Sm(III) (2.0×10^{-4} M) and NaOH (10^{-2} M) was contacted with solutions of varying concentrations of **dsa** (2.0×10^{-2} M to 4.0×10^{-2} M) and Oct₃N (4.0×10^{-2} M to 8.0×10^{-2} M). The extraction and stripping experiments were performed as described in section 3.3.7. The concentration of Sm(III) in the aqueous phase was determined by the Arsenazo-III spectrophotometric method. The distribution coefficient, D was obtained after determining the quantity of recovered Sm(III), and the slope from the plot of Log D_{Sm} vs Log [**dsa**] was used to determine the stoichiometry of the formed Sm-dsa complex in the organic phase.

3.4 Results and discussion

3.4.1 Synthesis

The **msa** and **dsa** sulfonamide ligands (Figure 3.1) are newly reported compounds synthesized using modification of reported procedures,^{43,44} and were characterized by ¹H-NMR, ¹³C-NMR and elemental analysis. Lipophilic alkyl substituents were incorporated into the ligand design to improve solubility and investigate the efficiency of Ln(III) complexation and extraction in less polar industrial process solvents.

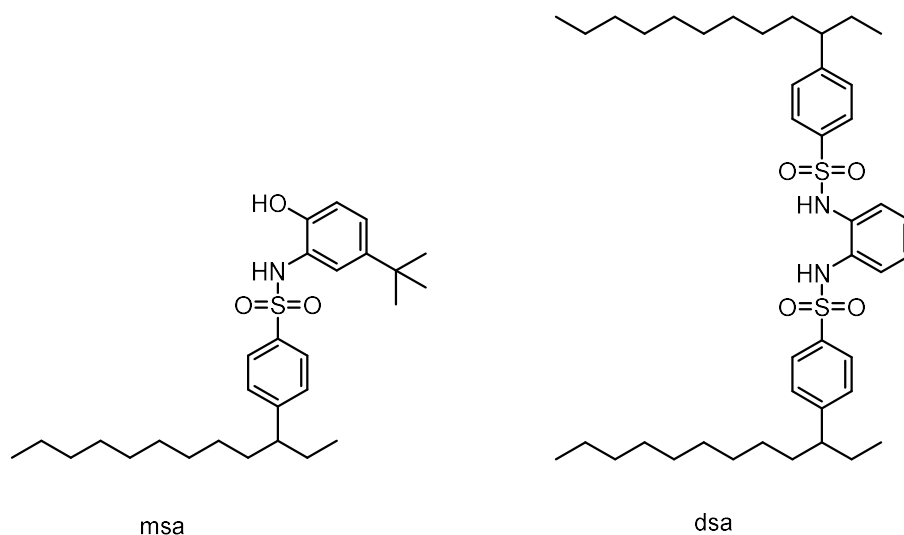


Figure 3.1. Schematic drawing of sulfonamide extractants *msa* and *dsa*.

3.4.2 UV-Vis spectroscopic study of Ln(III) complexation

The complexation behaviour of **msa** and **dsa** for Sm(III) was investigated using UV-Vis titrations of ligand and NaOH with Sm(III) in CH₃CN:CH₃OH (96:4, v/v) at constant ligand and NaOH concentration. With either ligand, control experiments indicated no change in spectra in the absence of NaOH, which suggests that complexation only occurs in alkaline environment for these ligands. For **msa** (4.0×10^{-5} M), decreases in the absorption bands at 250 nm and 295 nm were observed when titrated with Sm(III) (4.0×10^{-4} M), with the 295 nm band also shifting to 286 nm, and an absorbance increase in the 275-280 nm area, along with two apparent isosbestic points at 241 nm and 271 nm indicative of Sm(III) complexation (Figure 3.2 - left). The increase in absorbance at 206 nm is due to excess Sm(NO₃)₃. Non-linear regression analysis of the absorbance decrease at 250 nm fitted to the 1:1 binding isotherm gave a binding constant of $K_{11} = 1.60 (\pm 0.70)$

$\times 10^6 \text{ M}^{-1}$. The observed satisfactory fit to the 1:1 binding model (Figure 3.2 - right), and saturation of the curve at $4.0 \times 10^{-5} \text{ M}$ of Sm(III), which corresponds to 1 eq. of added Sm(III) is strongly indicative of 1:1 complexation.

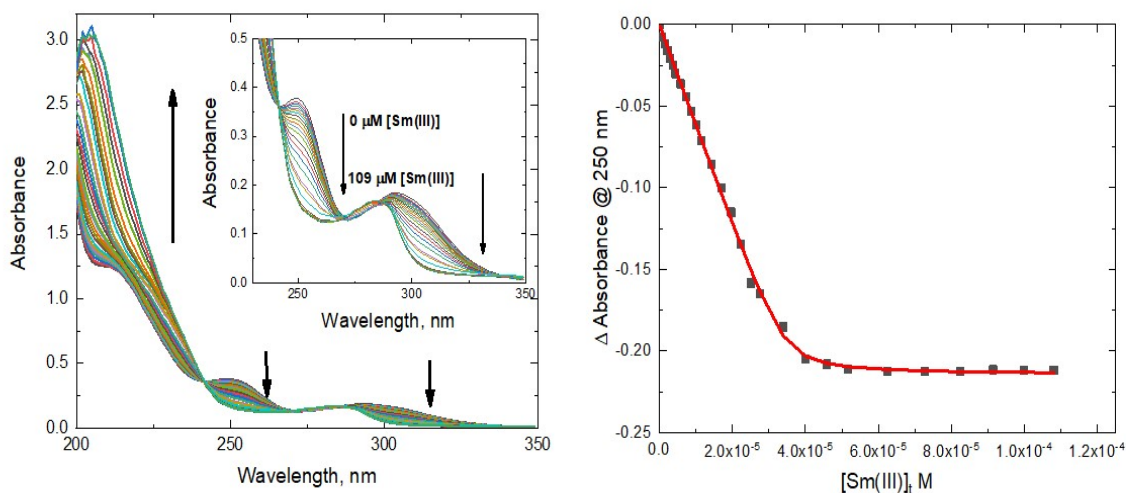


Figure 3.2. (left) UV-Vis spectra for titration of *msa* ($4.0 \times 10^{-5} \text{ M}$) and NaOH ($8.8 \times 10^{-5} \text{ M}$) with Sm(III) ($4.0 \times 10^{-4} \text{ M}$) in $\text{CH}_3\text{CN}:\text{CH}_3\text{OH}$ (96:4, v/v). Inset: Expanded spectra for 0.0 – 0.5 absorbance range, and 220 – 350 nm wavelength range. (right): Titration plot showing the absorbance change at 250 nm plotted against concentration of Sm(III). The solid line shows the actual nonlinear regression fitting to the 1:1 binding isotherm.

For **dsa**, the titrations with Sm(III) in $\text{CH}_3\text{CN}:\text{CH}_3\text{OH}$ (96:4, v/v), performed under similar conditions, and at constant **dsa** and NaOH concentrations (Figure 3.3) showed an absorbance increase at 243 nm, a decrease of the ligand bands at 260 nm and 308 nm and an isosbestic point at 250 nm, suggesting complex formation. Non-linear regression analysis of the decrease in absorbance at 260 nm fitted to the 1:1 binding isotherm gave a binding constant of $K_{11} = 7.90 (\pm 0.40) \times 10^7 \text{ M}^{-1}$.

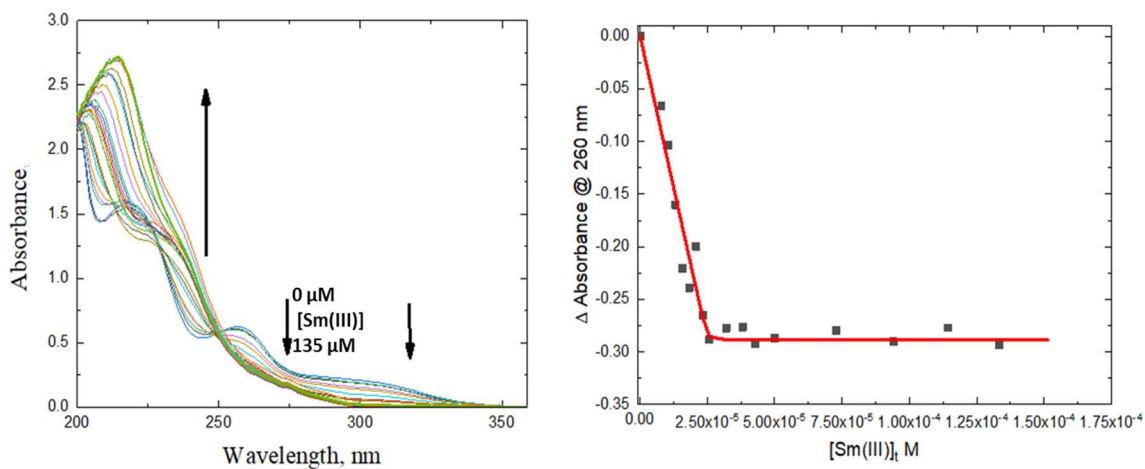


Figure 3.3. (left) UV-Vis spectra for titration of *dsa* ($4.0 \times 10^{-5} M$) and NaOH ($8.0 \times 10^{-5} M$) with Sm(III) ($8.0 \times 10^{-4} M$) in $CH_3CN:CH_3OH$ (96:4, v/v). (right): Titration plot showing the absorbance change at 260 nm plotted against concentration of Sm(III). The solid line shows the actual nonlinear regression fitting to the 1:1 binding isotherm.

Using the continuous variation method in which equimolar solutions of ligand and Sm(III) are mixed in variable ratios, a Job plot (Figure 3.4) was obtained with a maximum at 0.5 molar ratio for both *msa* and *dsa* which confirms the 1:1 metal to ligand stoichiometry in solution.

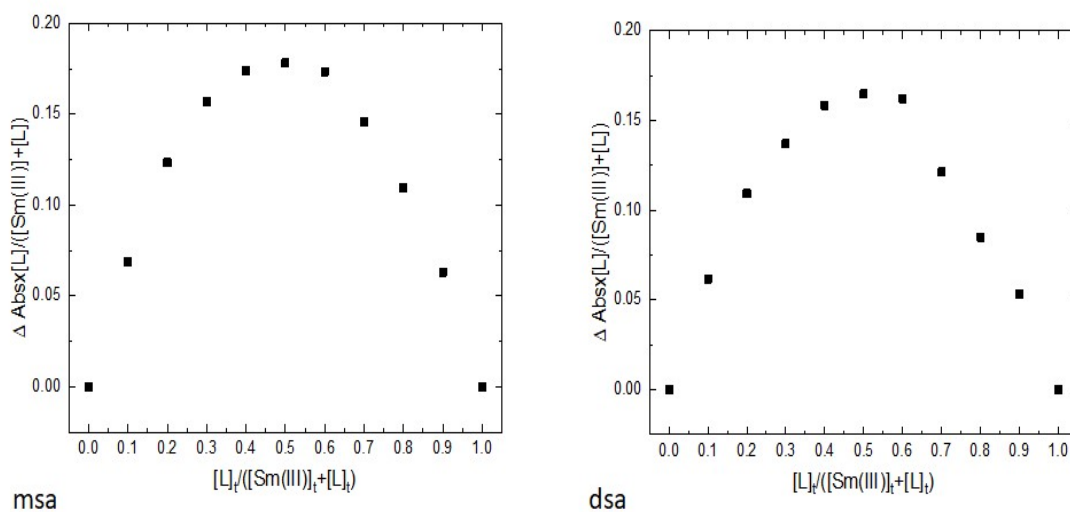


Figure 3.4. Job plots ($A_{250\text{ nm}}$) for **msa** (left) and ($A_{260\text{ nm}}$) for **dsa** (right). Solution A: $[L]_t = 2.0 \times 10^{-5}\text{ M}$, $[\text{NaOH}] = 5.0 \times 10^{-5}\text{ M}$ in $\text{CH}_3\text{CN}:\text{CH}_3\text{OH}$ (96:4, v/v). Solution B: $[\text{Sm(III)}]_t = 2.0 \times 10^{-5}\text{ M}$ in $\text{CH}_3\text{CN}:\text{CH}_3\text{OH}$ (96:4, v/v).

3.4.3 Extraction studies

3.4.3.1 pH-dependent experiments for extraction and recovery of Sm(III) into *n*-dodecane by **dsa** or **msa** in the presence or absence of trioctylamine with spectrophotometric quantification of Sm(III).

The two ligands **msa** and **dsa** were tested either with or without trioctylamine (2 eq.) for extraction and recovery of Sm(III) into dodecane from solutions of increasing alkalinity, using constant concentration of ligand (20.0 mM) and Sm(III) (2.0 mM). After a single contact of the source aqueous phases with the ligand solutions in *n*-dodecane, followed by a single stripping contact with 0.1 M HNO_3 the amount of recovered Sm(III) in the aqueous phases was quantified by the Arsenazo-III spectrophotometric method.⁴⁶ For Sm(III) extraction experiments using **msa**, maximum extraction was obtained at pH

12.5 with 40.9 (± 7.7)% Sm(III) recovered in the presence of trioctylamine (Figure 3.5 - left). At the all-important pH 14.0 (high pH being relevant due to alkalinity of waste tanks at SRS), however, the maximum recovery obtained was only 11.9 (± 8.9)% when trioctylamine was present, but higher at 27.6 (± 6.8)% without trioctylamine, a result fairly consistent with our prior studies.⁴¹ In general, however, the % Sm(III) recoveries with or without the presence of trioctylamine were fairly similar, within experimental error, and with no clearly apparent trends, other than the aforementioned difference at pH 14.0. Incidentally, at pH 13.5 in the absence of trioctylamine for **msa** there was a trough in extraction which is very similar at the same pH for **L2H₂** in Chapter 2 of this dissertation. For pH 10.0 – 11.0, no Sm(III) was recovered, an expected finding, as the conditions were not alkaline enough to deprotonate the ligand. In the case of **dsa**, the extraction pattern showed general similarities with the results for extraction by the less lipophilic disulfonamides in CH₂Cl₂³⁹ with impressive Sm(III) recovery maxima at 56.8 (± 14.9)% at pH 12.0 and 50.7 (± 1.2)% at pH 13.5 in the presence of trioctylamine, which compare very favorably with the prior recoveries obtained in dichloromethane. As for the prior disulfonamide analogs, no Sm(III) was recovered at pH 14.0. Unlike for **msa**, for which the overall trend for Sm(III) recoveries was similar with or without trioctylamine, the extraction efficiency of Sm(III) for **dsa** was consistently higher when trioctylamine was present. (Figure 3.5 - right). At pH 11.5, **dsa** (with trioctylamine) showed an extraction efficiency of 37.8 (± 8.2)% for Sm(III) extracted into the organic phase while no Sm(III) was recovered in the absence of the organic base. “Troughs” in Sm(III) recoveries were observed at pH 13.0, which are also consistent, with our prior work.⁴¹ In summary these extraction results and in comparison with prior work with less lipophilic analogs for **msa**

(Chapter 2), and **dsa**³⁹ demonstrate that the impressive capability of these ligands to extract Sm(III) is maintained to a great extent with the lipophilic analogs when the non-polar *n*-dodecane is used as diluent. While **dsa** demonstrates overall higher recoveries than **msa** in dodecane (especially in the presence of trioctylamine), at almost the entirety of the pH range, up to pH = 13.5, **msa** is clearly superior at the all-important pH 14.0, which indicates great promise for applicability. To our knowledge, these are the first ligands reported that can extract f-elements from alkaline solutions into *n*-dodecane, with **msa** specifically, being the only ligand that can do so at pH 14.0, with a reasonable recovery. The recoveries obtained are clearly superior to any other ligands reported in the literature that can function in non-polar organic solvents, such as *n*-dodecane.

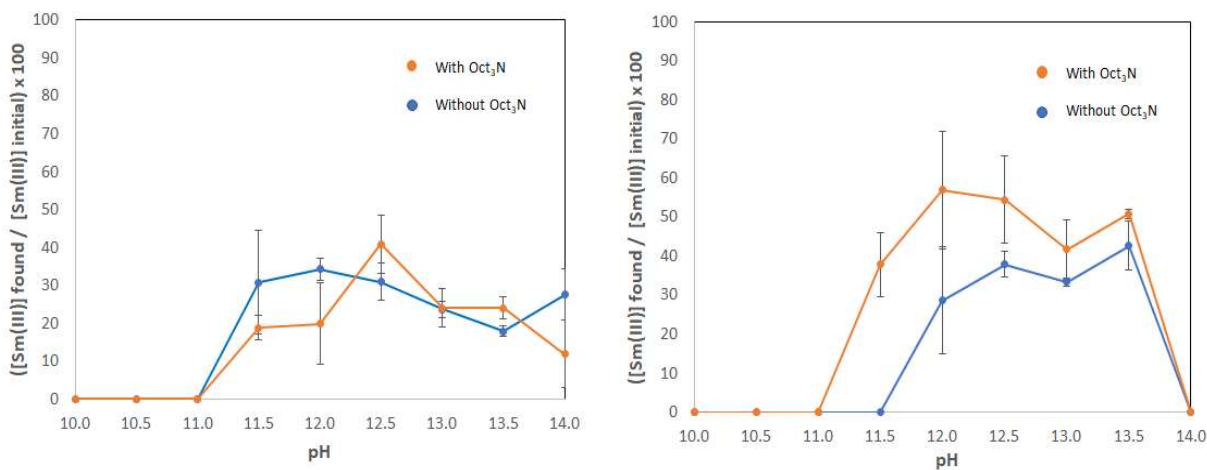


Figure 3.5. Percent Sm(III) recovered after extraction and subsequent stripping (0.1M HNO₃) using **msa** (20.0 mM) (left) or **dsa** (20.0 mM) (right) with or without the presence of trioctylamine (40.0 mM). $[Sm(III)]_i = 2.0$ mM.

Slope analysis for **dsa** at pH 12.0

In order to gain insight into the Sm(III) complex formation in solution during extraction by **dsa**, slope analysis experiments were conducted by measuring Sm(III) recovery as a function of increasing concentration of **dsa** (20.0 mM – 40.0 mM) in *n*-dodecane at constant [Sm(III)]_t (0.2 mM) at pH 12.0, and under identical extraction and stripping conditions with the ones previously described. Based on the extraction two-phase complex formation equilibrium, the slope of the log-log plot of distribution ratio *D* vs. [dsa]_t corresponds to the number of extractant molecules coordinated to Sm(III) in the organic phase.⁴⁷ The log-log plot (Figure 3.6), shows a straight line with a slope of 0.95 ($R^2 = 0.986$) confirming 1:1 Sm(III)/**dsa** complexation. This finding is consistent with the UV-Vis titration experiment and also with our prior work on CH₂Cl₂ extraction by less lipophilic **dsa** analogs.³⁹

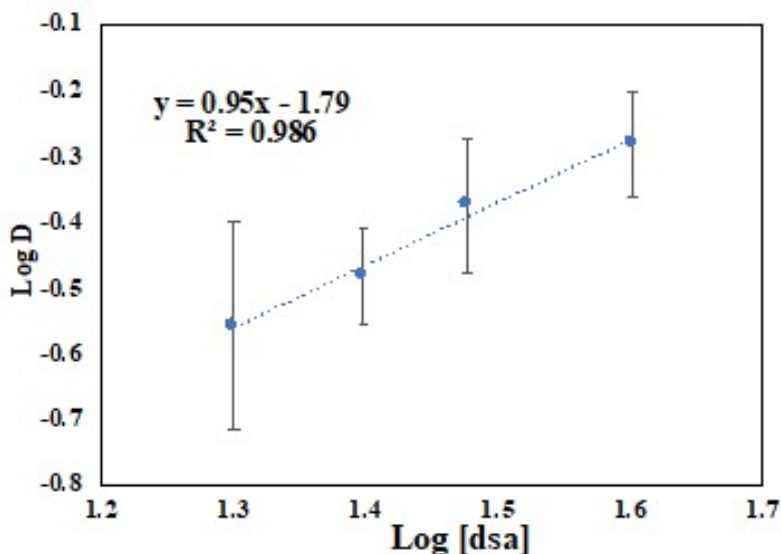


Figure 3.6. Log-log Plot of D_{Sm} vs. $[dsa]_t$ (20.0 mM – 40.0 mM) in *n*-dodecane at pH 12.0. $[Sm(III)]_t = 2.0 \times 10^{-4}$ M).

3.4.3.2 pH-dependent experiments for extraction and recovery of Ln(III) into *n*-dodecane by **msa** with quantification of Ln(III) by ICP-MS.

Since the results for Sm(III) extraction and recovery showed promise, we decided to test the efficiency of **msa** (20.0 mM) to extract Ln(III) into *n*-dodecane from a solution bearing a combined solution of four Ln(III) - La(III), Nd(III), Sm(III) and Eu(III) each at 2.0 mM concentration respectively in the same aqueous phase and in various pHs (1.0×10^{-4} M – 1.0 M of NaOH) under similar experimental conditions as described in section 3.4.3.1, but without trioctylamine. For quantification of the metals in the aqueous phase after stripping, ICP-MS was used, with appropriate standard solutions and separate calibration curves for all Ln(III). The results (Figure 3.7), show similar trends as for the Sm(III)-only experiments (Figure 3.5 - left), with the overall trend for the lanthanide recovered after stripping showing similarity with recoveries as high as 38.6 (± 15.1)% for Sm(III) and 35.9 (± 11.2)% for Eu(III) at pH 12.0, 20% at pH 14.0 for all Ln(III), and negligible extraction at pH 10.0 – 11.0. The slightly lower recoveries for each Ln(III) than for the Sm(III)-only experiment are expected, as the concentration ratio of ligand to total Ln(III) in this experiment is 4 times lower (10/4 vs. 10/1). Interestingly, significant separation between Ln(III) was observed at pH 12.0 with Sm(III) and Eu(III) recoveries of 40% while Nd(III) is recovered at 21.7 (± 5.9)%, and La(III) only at 5.3 (± 0.6)%. Thus, **msa** offers potential for selective separation of early from later lanthanides within the series, a current challenge of enormous environmental significance, as some Ln(III) are strategic materials of limited supply that are hard to separate from other rare earths.

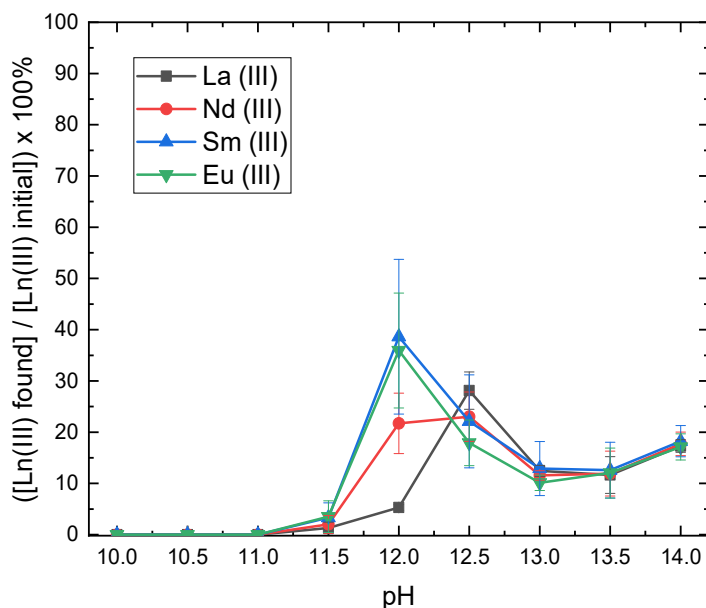


Figure 3.7. Percent recovered for La(III), Nd(III), Sm(III), and Eu(III) after extraction and subsequent stripping (0.1M HNO₃) using *msa* (20.0 mM) in *n*-dodecane in absence of trioctylamine. [Ln(III)]_i = 2.0 mM for each Ln.

3.5 Conclusion

A detailed study of Ln(III) extraction was conducted using the lipophilic monosubstituted sulfonamidophenol N-(5-(*tert*-butyl)-2-hydroxyphenyl)-4-(dodecan-3-yl)benzenesulfonamide (**msa**) and the disulfonamide N,N'-(1,2-phenylene)bis(4-(dodecan-3-yl)benzenesulfonamide) (**dsa**). Both ligands were designed for potential application in actinide recovery from strongly alkaline solutions. Maximum Sm(III) extraction efficiencies of 40.9 (±7.7)% and 56.8 (±14.9)% were achieved at pH 12.5 for **msa** and at pH 12.0 for **dsa**, respectively after only one loading / stripping cycle. Sm(III) recovery at pH 14.0 was observed both with and without an organic base for **msa**. Job plot for **msa** in CH₃CN:CH₃OH (96:4, v/v) is suggestive of 1:1 stoichiometry for Sm(III)

complexation. Slope analysis in *n*-dodecane at pH 12.0 indicated 1:1 Sm(III)-**dsa** stoichiometry. UV-Vis titration results for both **msa** and **dsa** gave binding constants of $K_{11} = 1.60 (\pm 0.70) \times 10^6 \text{ M}^{-1}$ and $K_{11} = 7.90 (\pm 0.40) \times 10^7 \text{ M}^{-1}$, respectively, for Sm(III) complex formation, with complexation stoichiometry from these titrations in agreement with Job plots and the slope analysis experiments. Overall, these results are expected to encourage further studies where sulfonamides with improved designs and more lipophilic substituents could be used in process solvents for extraction of actinides from highly alkaline nuclear waste.

3.6 Acknowledgement

The author would like to thank Drs. Yong Cai and Guangliang Liu for access to the ICP-MS instrument and advice for its use. This work was supported by the U.S. Department of Energy Office of Environmental Management MSIPP program managed by the Savannah River National Laboratory under SRNS contracts BOA 541, TOAs 0000217393, 0000403071 and 0000525181 to FIU. We also appreciate the support received from the Florida International University Dissertation Year Fellowship for Oluwaseun William Adedoyin (DYF Summer/Fall 2021 Fellow).

3.7 References

1. Wang, Y.; Deblonde, G. J.; Abergel, R. J. Hydroxypyridinone Derivatives: A low-pH alternative to polyaminocarboxylates for TALSPEAK-like separation of trivalent actinides from lanthanides. *ACS Omega* **2020**, *5*, 12996-13005.
2. Mei, L.; Ren, P.; Wu, Q.; Ke, Y.; Geng, J.; Liu, K.; Xing, X.; Huang, Z.; Hu, K.; Liu, Y. Actinide separation inspired by self-assembled metal–polyphenolic nanocages. *Journal of the American Chemical Society* **2020**, *142*, 16538-16545.
3. Bessen, N. P.; Jackson, J. A.; Jensen, M. P.; Shafer, J. C. Sulfur donating extractants for the separation of trivalent actinides and lanthanides. *Coordination Chemistry Reviews* **2020**, *421*, 213446.
4. Ionova, G.; Ionov, S.; Rabbe, C.; Hill, C.; Madic, C.; Guillaumont, R.; Krupa, J. C. Mechanism of trivalent actinide/lanthanide separation using bis (2, 4, 4-trimethylpentyl) dithiophosphinic acid (Cyanex 301) and neutral O-bearing co-extractant synergistic mixtures. *Solvent Extraction and Ion Exchange* **2001**, *19*, 391-414.
5. Kolarik, Z. Complexation and separation of lanthanides (III) and actinides (III) by heterocyclic N-donors in solutions. *Chemical Reviews* **2008**, *108*, 4208-4252.
6. Nash, K. L. A review of the basic chemistry and recent developments in trivalent f-elements separations. *Solvent Extraction and Ion Exchange* **1993**, *11*, 729-768.
7. Lewis, F. W.; Hudson, M. J.; Harwood, L. M. Development of highly selective ligands for separations of actinides from lanthanides in the nuclear fuel cycle. *Synlett* **2011**, *18*, 2609-2632.
8. Lehman-Andino, I.; Su, J.; Papathanasiou, K. E.; Eaton, T. M.; Jian, J.; Dan, D.; Albrecht-Schmitt, T. E.; Dares, C. J.; Batista, E. R.; Yang, P. Soft-donor dipicolinamide derivatives for selective actinide (III) / lanthanide (III) separation: the role of S- vs. O-donor sites. *Chemical Communications* **2019**, *55*, 2441-2444.
9. Hudson, M. J.; Harwood, L. M.; Laventine, D. M.; Lewis, F. W. Use of soft heterocyclic N-donor ligands to separate actinides and lanthanides. *Inorganic Chemistry* **2013**, *52*, 3414-3428.
10. Modolo, G.; Wilden, A.; Geist, A.; Magnusson, D.; Malmbeck, R. A review of the demonstration of innovative solvent extraction processes for the recovery of trivalent minor actinides from PUREX raffinate. *Radiochimica Acta* **2012**, *100*, 715-725.
11. Spencer, B. B.; Collins, J. L.; Hunt, R. D. Caustic Leaching of SRS Tank 12H Sludge With and Without Chelating Agents; United States. Department of Energy: **2003**.

12. Altmaier, M.; Gaona, X.; Fanghänel, T. Recent advances in aqueous actinide chemistry and thermodynamics. *Chemical Reviews* **2013**, *113*, 901-943.
13. Rabung, T.; Altmaier, M.; Neck, V.; Fanghänel, T. A TRLFS study of Cm(III) hydroxide complexes in alkaline CaCl₂ solutions. *Radiochimica Acta* **2008**, *96*, 551-560.
14. Wilmarth, W. R.; Lumetta, G. J.; Johnson, M. E.; Poirier, M. R.; Thompson, M. C.; Suggs, P. C.; Machara, N. P. Waste-pretreatment technologies for remediation of legacy defense nuclear wastes. *Solvent Extraction and Ion Exchange* **2011**, *29*, 1-48.
15. Peters, T. B.; Poirier, M. R.; Fink, S. D. Processing macrobatch 2 at the savannah river site integrated salt disposition process (ISDP). *Separation Science and Technology* **2010**, *45*, 1801-1806.
16. Lambert, D. P.; Miller, D. H.; Peeler, D. K.; Smith, M. E.; Stone, M. E. Impact of Alkali Source on Vitrification of SRS High Level Waste. *TIC (calc)* **2005**, *1324*, 901.
17. Neck, V.; Altmaier, M.; Rabung, T.; Lützenkirchen, J.; Fanghänel, T. Thermodynamics of trivalent actinides and neodymium in NaCl, MgCl₂, and CaCl₂ solutions: Solubility, hydrolysis, and ternary Ca-M(III)-OH complexes. *Pure and Applied Chemistry* **2009**, *81*, 1555-1568.
18. Roach, B. D.; Williams, N. J.; Duncan, N. C.; Delmau, L. H.; Lee, D. L.; Birdwell Jr, J. F.; Moyer, B. A. Radiolytic treatment of the next-generation caustic-side solvent extraction (NGS) solvent and its effect on the NGS process. *Solvent Extraction and Ion Exchange* **2015**, *33*, 134-151.
19. Norato, M. A.; Beasley, M. H.; Campbell, S. G.; Coleman, A. D.; Geeting, M. W.; Guthrie, J. W.; Kennell, C. W.; Pierce, R. A.; Ryberg, R. C.; Walker, D. D. Demonstration of the caustic-side solvent extraction process for the removal of ¹³⁷Cs from Savannah River Site high level waste. *Separation Science and Technology* **2003**, *38*, 2647-2666.
20. Delmau, L. H.; Haverlock, T. J.; Bazelaire, E.; Bonnesen, P. V.; Ditto, M. E.; Moyer, B. A. Alternatives to Nitric Acid Stripping in the Caustic-Side Solvent Extraction (CSSX) Process for Cesium Removal from Alkaline High-Level Waste. *Solvent Extraction and Ion Exchange* **2009**, *27*, 172-198.
21. Hobbs, D. T.; Peters, T. B.; Taylor-Pashow, K.; Fink, S. D. Development of an improved titanate-based sorbent for strontium and actinide separations under strongly alkaline conditions. *Separation Science and Technology* **2010**, *46*, 119-129.
22. Krauskopf, K. B. Thorium and rare-earth metals as analogs for actinide elements. *Chemical Geology* **1986**, *55*, 323-335.

23. Peters, T. B.; Barnes, M. J.; Hobbs, D. T.; Walker, D. D.; Fondeur, F. F.; Norato, M. A.; Fink, S. D.; Pulmano, R. L. Strontium and actinide separations from high level nuclear waste solutions using monosodium titanate (II). Actual waste testing. *Separation Science and Technology* **2006**, *41*, 2409-2427.
24. Hobbs, D. T.; Barnes, M. J.; Pulmano, R. L.; Marshall, K. M.; Edwards, T. B.; Bronikowski, M. G.; Fink, S. D. Strontium and actinide separations from high level nuclear waste solutions using monosodium titanate (I). Simulant testing. *Separation Science and Technology* **2005**, *40*, 3093-3111.
25. Karalova, Z. K.; Myasoedov, B. F.; Bukina, T. I.; Lavrinovich, E. A. Extraction and separation of actinides and lanthanides from alkaline and carbonate solutions. *Solvent Extraction and Ion Exchange* **1988**, *6*, 1109-1135.
26. Karalova, Z. K.; Bukina, T. I.; Devirts, E. A.; Agaev, B. F.; Myasoedov, B. F. Solvent extraction of americium and europium from alkaline and carbonate solutions by 2-hydroxy-5-alkylbenzyl dilthanolamine. *Radiokhimiya* **1987**, *29*, 767-772.
27. Karalova, Z.; Lavrinovich, E.; Myasoedov, B. Extraction of transplutonium elements from carbonate solutions by alkyl phenol oligomers. *Radiochemistry* **1990**, *32*, 16-20.
28. Lavrinovich, E. A.; Karalova, Z. K.; Myasoedov, B. F. Use of *p*-tert-butylformaldehyde oligomer for actinides isolation from complexing substances solutions with high pH value. *Radiokhimiya* **1993**, *35*, 99-103.
29. Kuzovkina, E. V.; Lavrinovich, E. A.; Novikov, A. P.; Stepanova, E. S.; Karavan, M. D.; Smirnov, I. V. Kinetics of americium and europium extraction by *tert*-butylthiacalix[4]arene from alkaline media. *Journal of Radioanalytical and Nuclear Chemistry* **2017**, *311*, 1983-1989.
30. Smirnov, I. V.; Karavan, M. D.; Stepanova, E. S.; Kal'chenko, V. I. Extraction of americium and europium with functionalized thiacalix[4]arenes from alkaline solutions. *Radiochemistry* **2016**, *58*, 617-624.
31. Smirnov, I. V.; Stepanova, E. S.; Drapailo, A. B.; Kalchenko, V. I. Extraction of americium and europium with functionalized calixarenes from alkaline solutions. *Radiochemistry* **2016**, *58*, 42-51.
32. Smirnov, I. V.; Stepanova, E. S. Extraction of americium with substituted calix[4]arenes from alkaline solutions. *Procedia Chemistry* **2016**, *21*, 203-210.
33. Karalova, Z. K.; Myasoedov, B. F.; Rodionova, L. M.; Kuznetsova, V. S. Extraction of transplutonium elements from carbonate solutions by alkylpyrocatechol. *Radiokhimiya* **1983**, *25*, 187-191.

34. Smirnov, I. V.; Stepanova, E. S.; Tyupina, M. Y.; Ivenskaya, N. M.; Zaripov, S. R.; Kleshnina, S. R.; Solov'eva, S. E.; Antipin, I. S. Extraction of cesium and americium with *p*-alkylcalix[8]arenes from alkaline solutions. *Radiochemistry* **2016**, *58*, 381-388.
35. Panja, S.; Mohapatra, P. K.; Tripathi, S. C.; Gandhi, P. M.; Janardan, P. Role of organic diluents on Am(III) extraction and transport behaviour using N, N, N', N'-tetraoctyl-3-oxapentanediamide as the extractant. *Journal of Membrane Science* **2012**, *403*, 71-77.
36. National Research Council Alternatives for high-level waste salt processing at the Savannah River Site; National Academies Press: **2000**.
37. Govor, E.; Anagnostopoulos, V.; Morozov, A.; Mebel, A.; Raptis, R.; Kavallieratos, K. Trivalent f-metal coordination and extraction by tripodal sulfonamide ligands and analogs; *Abstracts of papers of the American Chemical Society*; ACS USA: **2017**.
38. Zhang, X.; Adedoyin, O. W.; Bertoli, M. L. M.; Govor, E. V.; Kavallieratos, K. Sulfonamide ligand frameworks for Sm(III) Extraction from alkaline high-level waste. *RAD Conference Proceedings* **2020**, *4*, 173-178.
39. Govor, E. V.; Morozov, A. N.; Rains, A. A.; Mebel, A. M.; Kavallieratos, K. Spectroscopic and theoretical insights into surprisingly effective Sm(III) extraction from alkaline aqueous media by *o*-Phenylenediamine-derived sulfonamides. *Inorganic Chemistry* **2020**, *59*, 6884-6894.
40. Morozov, A. N.; Govor, E. V.; Anagnostopoulos, V. A.; Kavallieratos, K.; Mebel, A. M. 1, 3, 5-Tris-(4-(iso-propyl)-phenylsulfamoylmethyl) benzene as a potential Am(III) extractant: experimental and theoretical study of Sm(III) complexation and extraction and theoretical correlation with Am(III). *Molecular Physics* **2018**, *116*, 2719-2727.
41. Adedoyin, W. O. *o*-Sulfonamidophenol ligands and derivatives for f-element sensing, complexation and extraction from alkaline high-level waste. Chapter II. Doctoral Thesis, Florida International University, Miami, USA. February **2022**.
42. Adedoyin, W. O.; Morozov, N. A.; Chakraborty, I.; Gabriela Ortega.; Christopher J. Dares.; Raptis, G. R.; Mebel, A. M.; Kavallieratos, K.; A *p*-nitrophenol-sulfonamide Lu(III) optical sensor forms a unique Lu(III)- μ -hydroxo trimer in the solid state. **2022** (manuscript in preparation).
43. KumaraBoominathan, S. S.; ChandruaSenadi, G; KishoreaVandavasi, J. A one-pot hypiodite catalysed oxidative cycloetherification approach to benzoxazoles. *Chemical Communications* **2014**, *51*, 6726 – 6728.

44. Andersen, K. K.; Gowda, G.; Jewell, L.; McGraw, P.; Phillips, B. T. Substitution at tetracoordinate sulfur (VI). Rearrangement of 2-aminoaryl arenesulfonates to N-(2-hydroxyaryl) arenesulfonamides. *Journal of Organic Chemistry* **1982**, *47*, 1884-1889.
45. Blotny, G. A new, mild preparation of sulfonyl chlorides. *Tetrahedron Letters* **2003**, *44*, 1499-1501.
46. Savvin, S. B. Analytical use of Arsenazo III: Determination of thorium, zirconium, uranium and rare earth elements. *Talanta* **1961**, *8*, 673-685.
47. Sasaki, Y.; Sugo, Y.; Suzuki, S.; Tachimori, S. The novel extractants, diglycolamides, for the extraction of lanthanides and actinides in HNO₃ *n*-dodecane system. *Solvent Extraction and Ion Exchange* **2001**, *19*, 91-103.

Chapter IV: Fluorescence Sensing and Extraction of Ln(III) from Alkaline Solutions
with a Dansyl *o*-Sulfonamidophenol Ligand.

Oluwaseun W. Adedoyin, Cristian Gonzalez, Indranil Chakraborty, Raphael G. Raptis,
and Konstantinos Kavallieratos

4.1 Abstract

To address the threat of radioactive contamination at US DOE sites, our group has introduced several sulfonamide ligands for the extraction of Sm(III), which is used as a surrogate for radioactive trivalent actinides. In this work, a new dansyl-derived *o*-sulfonamidophenol fluorescent sensor - N-(5-(*tert*-butyl)-2-hydroxyphenyl)-5-(dimethylamino)naphthalene-1-sulfonamide (**1**) has been synthesized for efficient extraction and *in situ* sensing of Sm(III). Fluorescence sensing experiments using **1** was able to detect trace amounts of Sm(III) in the presence of NaOH in CH₃CN:CH₃OH (96:4, v/v) solution, with limit of detection (LOD) for Sm(III) as low as 0.094 μM obtained for a linear range of 0 – 1.12 μM. Fluorescence titration of **1** with Sm(III) gave threefold enhancement based on chelation enhanced fluorescence (CHEF), with a binding constant for the formed 1:2 Sm(III)-sulfonamide complex of $\beta_{2(\text{Sm})} = 2.00 (\pm 0.02) \times 10^{11} \text{ M}^{-2}$ in a solution of CH₃CN:CH₃OH (96:4, v/v) and in the presence of NaOH. Analysis of the UV-Vis titration was consistent for an initial 1:2 metal–ligand complex formation followed by 1:1 complex as additional Sm(III) was added, with binding constants of $\beta_{2(\text{Sm})} = 7.40 (\pm 0.10) \times 10^{11} \text{ M}^{-2}$ and $\beta_{1(\text{Sm})} = 6.10 (\pm 0.08) \times 10^6 \text{ M}^{-1}$, respectively. Spectroscopic titrations with Yb(III) gave only 1:2 complexation with $\beta_{2(\text{Yb})} = 6.61 (\pm 0.02) \times 10^{13} \text{ M}^{-2}$ determined by UV-Vis titrations and $\beta_{2(\text{Yb})} = 4.36 (\pm 0.11) \times$

10^{13} M^{-2} , determined by fluorescence titrations. Remarkable Sm(III) extraction efficiency from aqueous phases at pH 13.0 into dichloromethane was also achieved, with 92.2 (± 13.5)% Sm(III) recovered after only a single loading-stripping cycle.

4.2 Introduction

Research interest into chemosensors for cationic and anionic species has grown considerably since they were discovered over a century ago due to growing application in the various fields of biology, chemistry, environmental sciences and engineering.¹ Optical sensors, in particular, have the advantage of ease of use as well as *in situ* detection of analytes of interest using less expensive equipment.¹ Several sensors have been developed which are based on changes in either UV-Vis, fluorescence, or both.^{1,2} Such sensors are often compounds bearing a binding site or receptor, where upon interaction with an analyte changes occur in a signaling unit. This signaling unit is called a chromophore in the case of optical sensing and a fluorophore in fluorescence sensing. Fluorescence sensing is of particular interest because of its low limits of detection.³ Some of the more common fluorophores include dansyl,^{4,5} quinolone,⁶ rhodamine,⁷ anthracene,⁸ and naphthalene.⁹ In fluorescence sensing, several mechanisms leading to fluorescent changes have been described in the literature. These include but are not limited to; photoinduced electron transfer (PET),¹⁰ ligand to metal charge transfer (LMCT),¹¹ metal to ligand charge transfer (MLTC),¹² Förster resonance energy transfer (FRET),¹³ aggregation induced emission (AIE),¹⁴ and twisted intermolecular charge transfer (TICT).¹⁵ These changes could give rise to either a chelation enhanced fluorescence (CHEF)^{6,16} also called turn-on fluorescence or a chelation enhanced

quenching (CHEQ)¹⁷ also called turn-off fluorescence. The dansyl moiety is one of the preferred fluorescence signaling units due to its ease of incorporation into molecular frameworks and large Stokes shift. Since their discovery by Weber in 1951,¹⁸ nonfluorescent dansyl chlorides have been used to react with amines to form fluorescent dansylamides with environmentally sensitive fluorescent quantum yields and emission maxima. In 2002, Jiang et al., using a fluorescent probe bearing a dansyl and aminoquinoline groups demonstrated good selective recognition for Zn(II) *in vitro*,¹⁹ while in our group, fluorescence quenching was observed when a bisdansylated sulfonamide was titrated with Pb(II). Extraction studies using the same ligand showed selective recovery of Pb(II) from aqueous media by a factor 133 – 1410 times higher than for other studied metals.⁴ With regard to f-elements, Ganjali et al. reported a fluorescence sensor which gave enhanced fluorescence selectivity for Pr(III) in CH₃CN:H₂O (9:1, v/v).²⁰ Likewise, Faridbod et al. demonstrated sensing using a turn-on fluorescent chemosensor for Lu(III) in EtOH:H₂O (1:9, v/v) solution.²¹ Xia et al. used a 18-crown-6 based luminescence sensor to demonstrate fluorescence quenching for early Ln(III) while later Ln(III) gave no response.²² Interestingly, Das et al. reported a sensor bearing a diazo group with selectivity for Nd(III) over other Ln(III) where a LM₂ complex was formed after the formation of a LM intermediate.²³

With regard to alkaline high-level waste accumulated during nuclear weapons manufacturing, separation of transuranic f-elements is a challenge, as there is a need to reduce the overall waste volume and mobility. To this end, our group has studied lanthanide extraction and sensing due to the chemical similarities of trivalent lanthanides and their radioactive actinide counterparts, by using ligands bearing N- and O- donating

groups. Due to the nature of this waste, having an extractant which is stable under alkaline and radiolytic conditions is therefore vital, and when such sequestering agents combine good extraction efficiency with fluorescence sensing, they could greatly improve the ability of nuclear engineers to efficiently separate transuranic elements while monitoring extraction progress *in situ*. Herein, we report a fluorescent *o*-sulfonamidophenol derivative – N-(5-(*tert*-butyl)-2-hydroxyphenyl)-5-(dimethylamino)naphthalene-1-sulfonamide (**1**) with electron-rich O- and N- chelating sites bearing a dansyl moiety as a fluorescent signaling unit for sensing and extraction of Ln(III) in alkaline conditions. Addition of Sm(III) or Yb(III) in CH₃CN:CH₃OH (96:4, v/v) to **1** (in alkaline solutions) gave a threefold turn-on fluorescence with LOD for Sm(III) as low as 0.094 μM, while no significant changes were observed for addition of Na(I), K(I), Cs(I) and Sr(II). Job plots and UV-Vis titrations suggested both 1:2 and 1:1 metal to ligand complexation stoichiometry for Sm(III), with spectroscopic titrations giving binding constants of $\beta_{2(\text{Sm})} = 7.40 (\pm 0.10) \times 10^{11} \text{ M}^{-2}$, $\beta_{1(\text{Sm})} = 6.10 (\pm 0.08) \times 10^6 \text{ M}^{-1}$ (UV-Vis titration) and $\beta_{2(\text{Sm})} = 2.00 (\pm 0.02) \times 10^{11} \text{ M}^{-2}$ (fluorescence titration) in CH₃CN:CH₃OH (96:4, v/v). Under similar conditions, Yb(III) gave only 1:2 complexation stoichiometry with $\beta_{2(\text{Yb})} = 6.61 (\pm 0.02) \times 10^{13} \text{ M}^{-2}$ (UV-Vis titration) and $\beta_{2(\text{Yb})} = 4.36 (\pm 0.11) \times 10^{13} \text{ M}^{-2}$ (fluorescence titration). Extraction studies gave recoveries as high as 92.2 (±13.5)% for Sm(III) after only a single contact of aqueous phase (pH 13.0) with dichloromethane (DCM) solutions of **1**, and subsequent stripping with 0.1 HNO₃.

4.3 Experimental section

4.3.1 Materials and methods

All starting materials, reagents and solvents were purchased from Fisher Scientific or Sigma-Aldrich. Chemicals were standard reagent grade; solvents were spectroscopic grade and were used without further purification. Metals used were either chlorides or nitrate salts with their respective waters of crystallization. FT-IR spectra were recorded on the 4000 – 600 cm^{-1} range using a Cary 600 series FT-IR spectrometer. NMR spectra were recorded on a 400 MHz Bruker Avance NMR spectrometer and were referenced using the residual solvent resonances, all chemical shifts, δ , were reported in ppm. UV-Vis spectra were recorded on a Varian Cary 100 Bio UV-Vis spectrophotometer. Fluorescence spectra were measured on a Cary Eclipse fluorescence spectrophotometer set at $\lambda_{\text{exc}} = 360$ nm and slit width set at 10 nm for emission and excitation. ICP-MS experiments were performed on a PerkinElmer NexION® 2000 ICP Mass Spectrometer, and Y(III) (10 ppm) was used as the internal standard. Single Crystal X-ray structures were obtained using a Bruker D8 Quest diffractometer bearing PHOTON II detector and at $T = 298$ K.

4.3.2 Synthesis of N-(5-(*tert*-butyl)-2-hydroxyphenyl)-5-(dimethylamino)naphthalene-1-sulfonamide (1)

2-amino-4-(*tert*-butyl) phenol (2.00 g, 12.1 mmol) and pyridine (9.75 mL, 121 mmol) were left to stir in a round bottom flask containing 15 mL of CH_2Cl_2 and placed in an ice bath for 10 min. A solution of dansyl chloride (3.27 g, 12.1 mmol) in 10 mL of CH_2Cl_2 was added dropwise to the cold stirring solution. The reaction was allowed to

proceed under N₂ for 15 h. The reaction was monitored with TLC (Hexanes:EtOAc ; 2:1) and when it was judged to be complete, ice-cold water was used to wash the organic phase, which was then separated by solvent extraction. This organic phase was sequentially washed with 1M HCl, 1M NaHCO₃, and brine (3 × 25 mL for each), after which it was dried over anhydrous magnesium sulfate. The filtrate was collected, and the volatiles were concentrated under reduced pressure. The crude product was subsequently recrystallized from CH₂Cl₂ using petroleum ether and dried under vacuum, giving a lime green solid (2.86 g, 59.2% yield). ¹H-NMR (400 MHz, CDCl₃): δ 8.52 (d, 1H), 8.34 (d, 1H), 8.07 (d, 1H), 7.62 (t, 1H), 7.39 (t, 1H), 7.23 (d, 1H), 6.98 (dd, 1H), 6.80 (d, 1H), 6.46 (s, 1H), 6.43 (s, 1H), 6.10 (s, 1H), 2.88 (s, 6H), 0.80 (s, 9H) ¹³C-NMR (101 MHz, CDCl₃) δ 152.1, 149.3, 143.5, 132.4, 131.2, 131.1, 129.8, 129.7, 128.9, 125.5, 123.3, 123.2, 121.4, 116.5, 110.5, 115.4, 45.4, 33.5, 30.9 FT-IR (cm⁻¹; ATR) 3432 (m), 3278 (m), 2948 (m), 2863 (w), 2829 (w), 2788 (w), 2109 (w), 1611 (w), 1594 (m), 1510 (s), 1437 (m), 1397 (m), 1318 (vs), 1285 (s), 1252 (m), 1225 (s), 1162 (vs), 1567 (m), 1508 (m), 1455 (m), 1428 (m), 1391 (w), 1352 (s), 1303 (s), 1229 (s), 1200 (m), 1158 (s), 1143 (s), 1059 (m), 951 (m), 897 (m), 822 (s), 785 (s), 740 (m), 693 (m), 676 (m), 654 (w). Elemental Analysis for C₂₂H₂₆N₂O₃: Calcd. C, 66.31; H, 6.58; N, 7.03. Found C, 66.33; H, 6.58; N, 6.98.

4.3.3 Selectivity studies

Pre-weighed amounts of $\text{Sm}(\text{NO}_3)_3$, $\text{Sr}(\text{NO}_3)_3$, $\text{Na}(\text{NO}_3)_3$, $\text{K}(\text{NO}_3)_3$ and $\text{Cs}(\text{NO}_3)_3$ with their respective waters of crystallization were dissolved in solutions containing 4.0 μM of **1** and 8.8 μM NaOH in $\text{CH}_3\text{CN}:\text{CH}_3\text{OH}$ (96:4, v/v), such that metal concentration was 4.0 μM (equimolar to concentration of **1**). In a similar fashion, pre-weighed amounts of $\text{Yb}(\text{NO}_3)_3$, $\text{Sm}(\text{NO}_3)_3$, $\text{Sr}(\text{NO}_3)_3$, $\text{Na}(\text{NO}_3)_3$, $\text{K}(\text{NO}_3)_3$, $\text{Cs}(\text{NO}_3)_3$, $\text{Pb}(\text{NO}_3)_3$, SnCl_2 , BaCl_2 , $\text{Co}(\text{NO}_3)_3$, PdCl_2 , HgCl_2 , RuCl_3 , $\text{Ag}(\text{NO}_3)_3$, and CrCl_3 with their respective waters of crystallization were dissolved in a solution containing 4.0 μM of **1** and 16 μM NaOH in $\text{CH}_3\text{CN}:\text{H}_2\text{O}$ (99:1, v/v), such that the metal concentration was 4.0 μM (equimolar to concentration of **1**). Fluorescence spectra of these solutions were then obtained in a quartz cuvette of 1 cm path length at 25 °C.

4.3.4 Fluorescence titrations

Fluorescence titrations were carried out at constant ligand and NaOH concentrations, with sole variable the concentration of the Ln(III), as follows: Stock solutions of **1** (1.0 mM) and NaOH (2.2 mM) in $\text{CH}_3\text{CN}:\text{CH}_3\text{OH}$ (96:4, v/v) was diluted to yield solutions of **1** (4.0 or 5.0 μM) and NaOH (8.8 or 11.0 μM) in $\text{CH}_3\text{CN}:\text{CH}_3\text{OH}$ (96:4, v/v) (Solution A). A 40.0 μM solution of $\text{Sm}(\text{NO}_3)_3 \cdot 6\text{H}_2\text{O}$ or a 50.0 μM solution of $\text{Yb}(\text{NO}_3)_3 \cdot 6\text{H}_2\text{O}$ (Solution B) was then prepared using Solution A, resulting in a solution of $\text{Sm}(\text{NO}_3)_3 \cdot 6\text{H}_2\text{O}$ (40.0 μM) or $\text{Yb}(\text{NO}_3)_3 \cdot 6\text{H}_2\text{O}$ (50.0 μM) respectively prepared in Solution A (4.0 or 5.0 μM) and NaOH (8.8 or 11.0 μM) in $\text{CH}_3\text{CN}:\text{CH}_3\text{OH}$ (96:4, v/v) (Solution B). Solution A (2.70 mL) placed in a 1.00 cm cuvette cell was titrated with Solution B in increasing additions (0 – 0.88 mL). The binding constants

were obtained using non-linear regression analysis for the 1:1 and / or 1:2 binding isotherms using the HypSpec®,^{24,25} program. All spectroscopic measurements were performed in triplicate, and the binding constants were determined by obtaining the average from three independent experiments with the error defined as the standard deviation from the triplicate independent experiments.

4.3.5 Job plots

Two stock solutions of **1** (Solution A) and Ln(III) (Solution B) were prepared, with each bearing equal molarity. Solution A of **1** and NaOH of concentrations 20 μM and 50 μM , respectively, was prepared in $\text{CH}_3\text{CN}:\text{CH}_3\text{OH}$ (96:4, v/v). Solution B of Sm(III) or Yb(III) (20 μM) was prepared by dissolving $\text{Sm}(\text{NO}_3)_3 \cdot 6\text{H}_2\text{O}$ or $\text{Yb}(\text{NO}_3)_3 \cdot 6\text{H}_2\text{O}$ in a $\text{CH}_3\text{CN}:\text{CH}_3\text{OH}$ (96:4, v/v). The metal and ligand solutions were prepared in 11 vials with total volume of 5.00 mL. A combined volume added from both solutions was in a ratio (in mL) as follows; 5:0, 4.5:0.5, 4:1, 3.5:1.5, 3:2, 2.5:2.5, 2:3, 1.5:3.5, 1:4, 0.5:4.5, 0:5. The UV-Vis spectra were recorded and the absorbance at 250 nm was plotted vs. the mol. fraction ratio $[\text{L}]_t/([\text{Ln}(\text{III})]_t+[\text{L}]_t)$.

4.3.6 UV-Vis titrations

UV-Vis titrations were carried out at constant ligand and NaOH concentrations, with sole variable the concentration of the Ln(III), as follows: **Solution A**: A Solution of **1** (1.0 mM) and NaOH (2.2 mM) was prepared in 10.0 mL of methanol. This was then diluted by taking 1.00 mL of the methanol solution and diluting to 25.0 mL with acetonitrile to give final concentrations of 4.0×10^{-5} M for **1** and 8.8×10^{-5} M for NaOH.

Solution B: A solution of Sm(III) or Yb(III) (4.0×10^{-4} M) was prepared by weighing appropriate amounts of hexahydrate Ln(III) nitrate salts and diluting to 10.0 mL with Solution A. With a starting volume of 2.70 mL of Solution A in the cuvette cell, Solution B was then gradually added to solution A until 0.80 mL total was added. The observed wavelength was from 200 nm to 450 nm as no significant changes in absorbance were noticed outside this range. For reference blank, a solution comprising of 0.40 mL methanol and 9.60 mL acetonitrile was used. The stability constants were determined from the binding data by non-linear regression analysis using the HypSpec® program, and average values with standard deviations were obtained from triplicate independent experiments.

4.3.7 pH-dependent extraction and stripping of Sm(III) with CH₂Cl₂ as diluent and spectrophotometric determination of [Sm(III)]_t.

Aqueous solutions of Sm(III) were prepared (2.0 mM of Sm(NO₃)₃·6(H₂O)), and the pH was adjusted to pH 10.0 – 14.0 by varying the NaOH concentration (1.0×10^{-4} M – 1.0 M). Stock solutions of ligand **1** (20.0 mM) were prepared in CH₂Cl₂. 2.50 mL of each phase were brought into extended contact by rotating sealed vials on a wheel (55 rpm) for 22 h at room temperature (22 °C) and then centrifuged for 5 min (3200 rpm) to fully separate the two phases. The organic phases were subsequently collected and filtered in preparation for stripping. For stripping, 1.00 mL of 0.1 M HNO₃ was added to 1.00 mL of the filtered loaded organic phase and both layers were again brought into extensive contact on the rotating wheel for 20 h (55 rpm) at room temperature (22 °C), and then centrifuged for 5 min (3200 rpm) to fully separate the two phases. The aqueous

phases were collected and the Sm(III) was quantified using the Arsenazo-III spectrophotometric method.²⁸ Specifically, solutions were prepared containing 0.10 mL of the aqueous phase after stripping (or the aqueous phase after extraction), 1.00 mL of 1% ascorbic acid, 1.00 mL of 0.2 M formate buffer (pH 3.0) and 2.00 mL of 0.05% Arsenazo-III solution. The pH of this solution was then adjusted to pH 2.6 ± 0.1 using 0.1 M HNO₃ and diluted with DI water to 25.0 mL. The UV-Vis absorbance of this solution at 652 nm was measured and concentrations were calculated from the slope of a 200 ppm to 500 ppm calibration curve prepared using 1000 µg/mL Sm(III) standard solution. Reported quantification was expressed in % recovery (eq. 4.1) based on the concentration of Sm(III) quantified after stripping and the initial concentration of Sm(III) before contact with the organic phases.

$$Sm(III) Recovery = \frac{[Sm(III)]_{t(aq.) \text{ after stripping}}}{[Sm(III)]_{t(aq.) \text{ initial}}} \times 100\% \quad (\text{eq. 4.1})$$

Percent Sm(III) recoveries were calculated after triplicate independent experiments each with a single loading / stripping cycle. The reported errors were determined from the standard deviation of triplicate independent experiments. Alternatively, Sm(III) recovered after stripping was quantified using ICP-MS by diluting the stripped aqueous phase 10000 times in 2% HNO₃. For calibration, standard solutions of Sm(III) were used to prepare Sm(III) solutions with concentrations ranging from 0 ppb to 50.0 ppb in 2% HNO₃. Afterwards, 5.00 µL of 10.0 ppm Y(III) as internal standard was added to all the samples, and 5.00 mL of the solution was analysed by ICP-MS. Concentrations of recovered Sm(III) were then calculated from the slope obtained from the prior

calibration. Reported quantification was expressed in percentages (eq. 4.2), based on the concentration of Sm(III) quantified after stripping to the starting concentration of Sm(III) used for the extraction.

$$\% \text{ Sm Recovered} = \frac{[\text{Sm (III)}]_{t \text{ in aqueous phase after stripping}}}{[\text{Sm (III)}]_{t \text{ in aqueous phase before extraction}}} \times 100 \quad (\text{eq. 4.2})$$

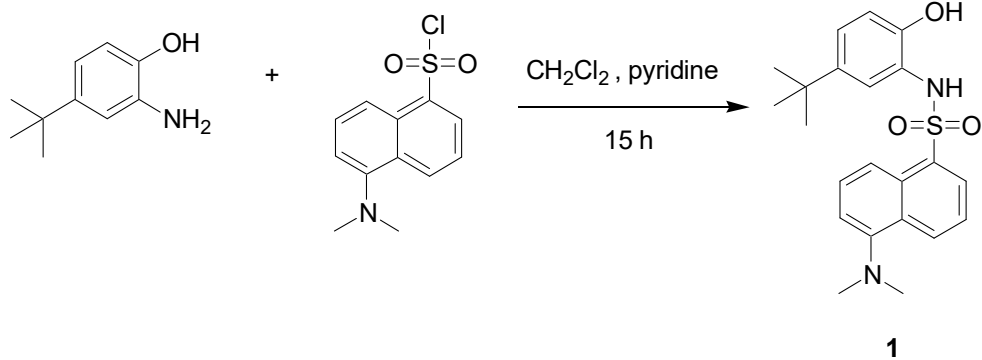
4.3.8 X-ray crystallography studies

Yellowish green crystals of **1** were obtained by slow evaporation of chloroform from a solution of **1** in chloroform. Structural refinement details and associated data are as given in Tables 4.2 – 4.4. A crystal suitable for measurement was mounted on a Bruker D8 Quest diffractometer bearing a PHOTON II detector and at T = 298 K. Structures were resolved using direct methods and refined by Least Squares using version 2018/3 of ShelXL.²⁶ All non-hydrogen atoms were refined anisotropically while calculations and molecular graphics were performed using SHELXTL 2014 and Olex²⁷ programs.

4.4 Results and discussion

4.4.1 Synthesis

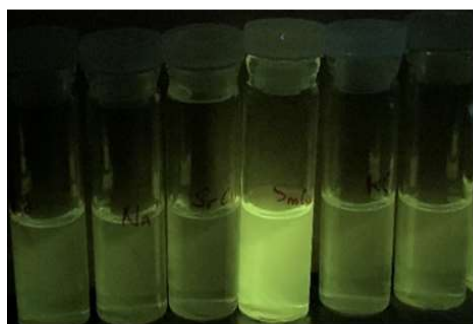
Dansylamide ligand **1**, which is a newly reported compound, was synthesized by a modification of previously reported procedure²⁸ for analogous compounds and was characterized by ¹H-NMR, ¹³C-NMR, FT-IR, and elemental analysis.



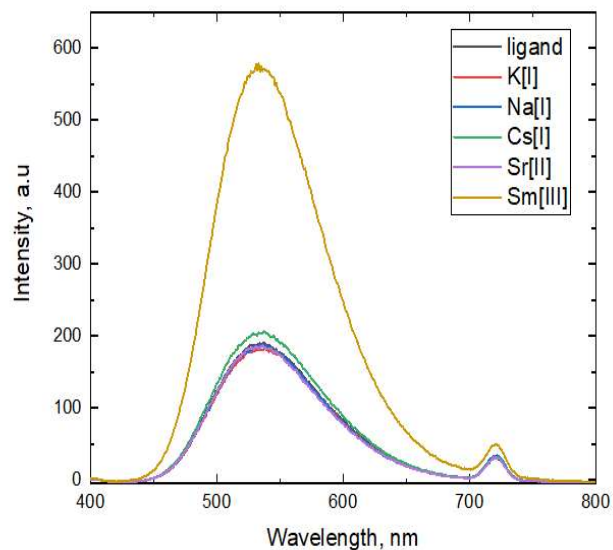
Scheme 4.1. Synthesis of dansylamide ligand **1**.

4.4.2 Selectivity studies

The dansylamide ligand **1** exhibited considerable selectivity for sensing Sm(III) *vs.* several other metals. When equimolar concentrations of the ligand and the metals were examined, notable changes in the fluorescence intensity at 540 nm ($\lambda_{\text{exc}} = 360$ nm) in CH₃CN:CH₃OH (96:4, v/v) was observed only for Sm(III) (Figure 4.1). Specifically, Sm(III) (4.0×10^{-6} M) increased the fluorescence intensity of **1** (4.0×10^{-6} M) in the presence of 2.2 equivalents of NaOH by about threefold while Sr(II), Na(I), K(I), and Cs(I) caused little to no changes when added at the same concentration, This suggests that **1** can be used as a turn-on sensor for f-elements *vs.* other metals which are prevalent in alkaline HLW.



(a)



(b)

Figure 4.1. (a) Visual fluorescence changes of **1** (4.0×10^{-6} M) and 2.2 equivalents of NaOH in the presence of equimolar concentrations of several metals. Fluorescence changes from left: **1**, Na(I), Sr(II), Sm(III) K(I) and Cs(I) in $\text{CH}_3\text{CN}:\text{CH}_3\text{OH}$ (96:4, v/v) ($\lambda_{\text{exc}}=360$ nm). (b) Fluorescence spectra of **1** (4.0×10^{-6} M) and 2.2 equivalents of NaOH in the presence of equimolar concentrations of Na(I), K(I), Cs(I), Sr(II) and Sm(III) in $\text{CH}_3\text{CN}:\text{CH}_3\text{OH}$ (96:4, v/v) ($\lambda_{\text{exc}}=360$ nm).

Likewise, similar experiments were carried out using **1** (4.0×10^{-6} M) and 4 equivalents of NaOH in the presence of equimolar concentration of Na(I), K(I), Cs(I), Ag(I), Ba(II), Hg(II), Sr(II), Pb(II), Co(II), Ru(III), Cr(III), Yb(III), or Sm(III) in $\text{CH}_3\text{CN}:\text{H}_2\text{O}$ (99:1, v/v) ($\lambda_{\text{exc}}=360$ nm). This experiment revealed fluorescence response of **1** to several of the tested metals in varying degrees (Figure 4.2). Overall, the fluorescence enhancement due to Ln(III) was higher in comparison to other tested metals with the exception of Cr(III).

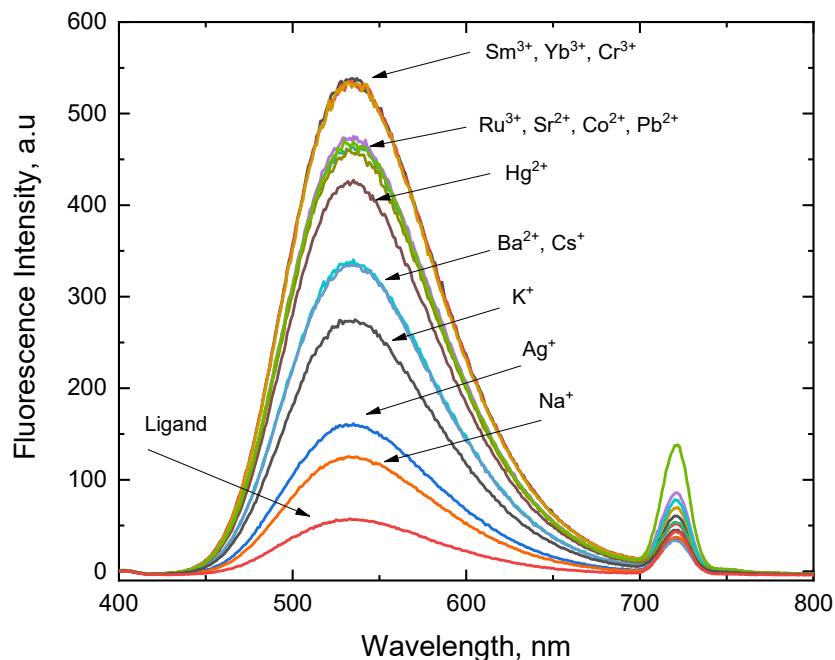


Figure 4.2. Fluorescence emission spectra showing response of **1** (4.0×10^{-6} M) and 4 equivalents of NaOH in the presence of equimolar concentration of Na(I), K(I), Cs(I), Ag(I), Ba(II), Hg(II), Sr(II), Pb(II), Co(II), Ru(III), Cr(III), Yb(III) and Sm(III) in CH₃CN:H₂O (99:1 v/v) ($\lambda_{exc}=360$ nm).

4.4.3 Fluorescence titrations

A solution of **1** (4.0×10^{-6} M) with 2.2 equivalents of NaOH in CH₃CN:CH₃OH (96:4, v/v) gave an emission at 540 nm ($\lambda_{exc}=360$ nm). Fluorescence of **1**, exhibited about threefold increase when titrated with Sm(III) (4.0×10^{-5} M) (Figure 4.3a). This fluorescence turn-on behavior might be attributed to chelation enhanced fluorescence (CHEF) as the ligand exhibited the observed fluorescence enhancement only for Sm(III) in the presence of NaOH. Having an alkaline environment for such ligands is also paramount for effective complexation with f-elements and NaOH plays the role of deprotonating the ligand's hydroxyl -OH and sulfonamide -NH. Upon deprotonation, the O- and N- atoms then chelate to Sm(III) leading to ligand to metal charge transfer in the

complex. No fluorescence change in **1** (5.0×10^{-6} M) for the addition of Sm(III) (5.0×10^{-3} M) was observed in control experiments where NaOH was absent (Figure 4.4b). Likewise, control experiments performed for the addition of only NaOH (5.0×10^{-2} M) and no Sm(III) to **1** (5.0×10^{-6} M) (Figure 4.4a) showed only some fluorescence quenching but no enhancement, which underscores the premise that fluorescence enhancement is due to the formation of a complex in solution. Gradual addition of Sm(III) to constant concentration of **1** led to a steady increase in fluorescence intensity and the plot of the fluorescence intensity at 540 nm vs. $[\text{Sm(III)}]_t$ led to an eventual saturation of the emission beginning at about 2.0×10^{-6} M, which is indicative of 1:2 binding stoichiometry (Figure 4.3b). The binding constant for the 1:2 complex $\beta_{2(\text{Sm})} = 2.0 (\pm 0.02) \times 10^{11} \text{ M}^{-2}$ was obtained after non-linear regression analysis of the changes in fluorescence intensity at $\lambda = 540$ nm. Fluorescence titration experiments did not give useful binding information for the 1:1 complex formation, even after substantial excess Sm(III) addition, presumably because the two complexes may have very similar fluorescence properties, and therefore formation of the 1:1 complex from the 1:2 complex, as more Sm(III) was added did not substantially change the fluorescence. The limit of detection was determined to be $0.094 \mu\text{M}$ when linearity was taken from $0 - 1.12 \mu\text{M}$, with limit of quantification of $0.283 \mu\text{M}$, which is similar to previously-reported values for other Ln(III) sensors.^{20,21} Such low limit of detection would imply that **1** could serve as a suitable sensor for Ln(III) even at trace levels under alkaline conditions which are typical for HLW.

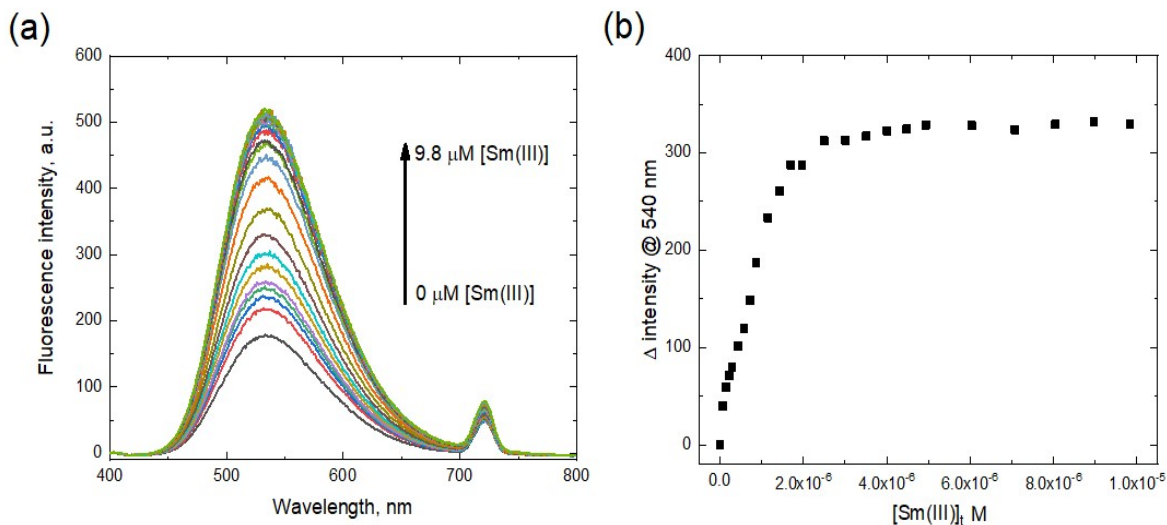


Figure 4.3. (a) Changes in fluorescence emission spectra of **1** due to titration of **1** (4.0×10^{-6} M) and 2.2 equivalents of NaOH with Sm(III) (4.0×10^{-5} M, 0 – 0.88 mL) in $\text{CH}_3\text{CN}:\text{CH}_3\text{OH}$ (96:4, v/v) ($\lambda_{\text{exc}}=360$ nm). (b) Changes in intensity of **1** with increasing concentration of Sm(III).

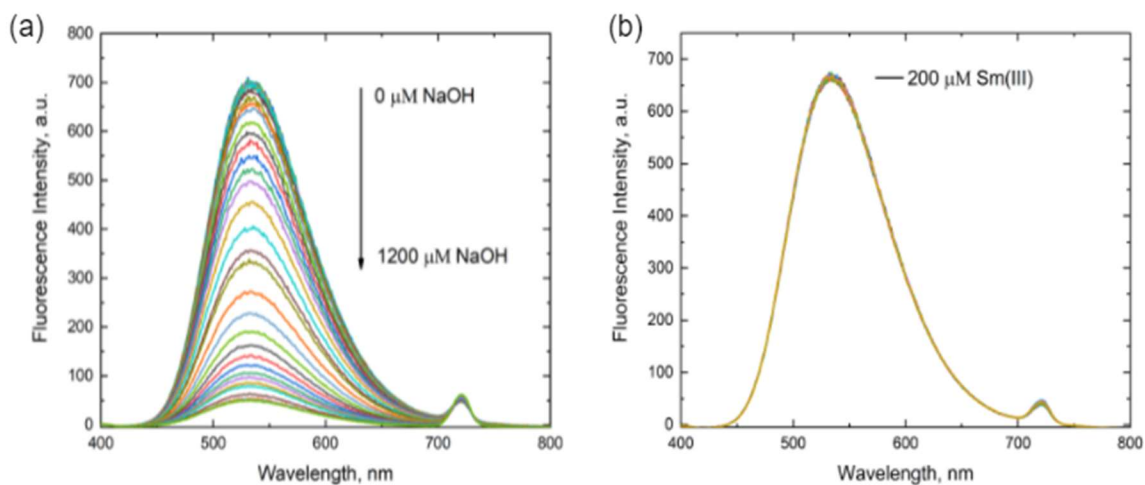


Figure 4.4. (a): Fluorescence titration spectra of **1** (5.0×10^{-6} M) after addition of NaOH (5.0×10^{-2} M) (no metal present) in $\text{CH}_3\text{CN}:\text{CH}_3\text{OH}$ (96:4 v/v). $\lambda_{\text{exc}} = 360$ nm. (b) Fluorescence titration spectra of **1** (5.0×10^{-6} M) after titration with Sm(III) (5.0×10^{-3} M) (no base present) in $\text{CH}_3\text{CN}:\text{CH}_3\text{OH}$ 96:4 v/v. $\lambda_{\text{exc}} = 360$ nm.

For Yb(III) titrations, the fluorescence emission spectral changes of **1** (5.0×10^{-6} M) and NaOH (2.2 eq.) in $\text{CH}_3\text{CN}:\text{CH}_3\text{OH}$ (96:4, v/v) at increasing concentrations of

added Yb(III) (5.0×10^{-5} M) show similarities with the Sm(III) titration experiments, indicating fluorescence enhancement (Figure 4.5) with emission at 534 nm ($\lambda_{\text{exc}} = 360$ nm). The plot of the fluorescence intensity at 534 nm vs. $[\text{Yb(III)}]_t$ shows saturation at 2.5×10^{-6} M of added Yb(III) for $[\mathbf{1}]_t = 5.0 \times 10^{-6}$ M, which is strongly indicative of a 1:2 Yb(III): $\mathbf{1}$ binding stoichiometry. Non-linear regression fitting to the 1:2 binding isotherm using the Hypspec® program gave a binding constant for 1:2 for the Yb(III): $\mathbf{1}$ complex formation of $\beta_{2(\text{Yb})} = 4.36 (\pm 0.11) \times 10^{13} \text{ M}^{-2}$.

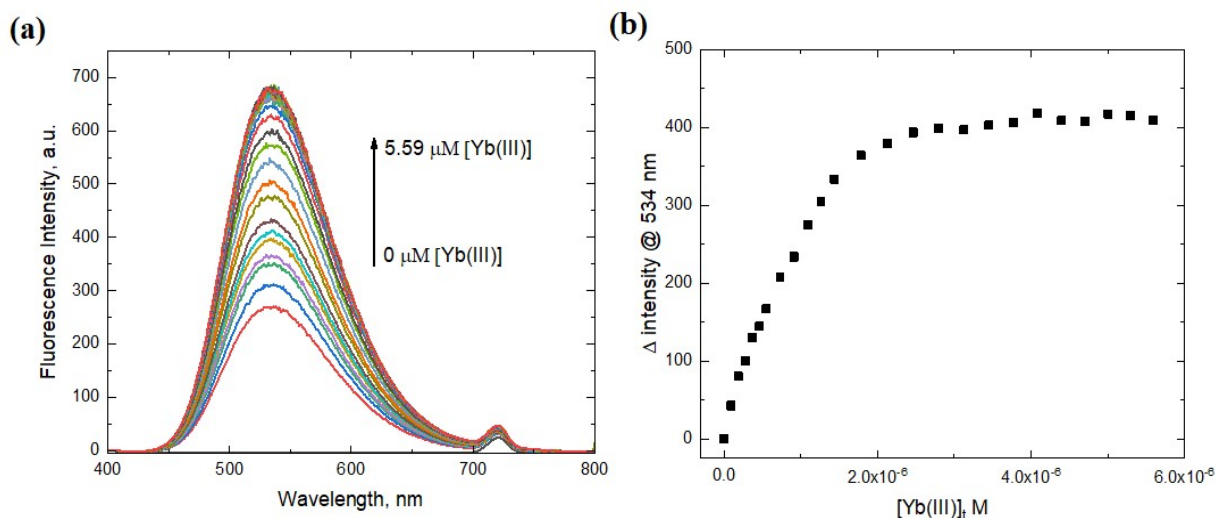


Figure 4.5. (a) Changes in fluorescence emission spectra of $\mathbf{1}$ due to titration of $\mathbf{1}$ (5.0×10^{-6} M) and 2.2 equivalents of NaOH with Yb(III) (5.0×10^{-5} M, 0 – 0.88 mL) in $\text{CH}_3\text{CN}:\text{CH}_3\text{OH}$ (96:4, v/v) ($\lambda_{\text{exc}}=360$ nm). (b) Changes in intensity of $\mathbf{1}$ with increasing concentration of Yb(III).

4.4.4 Job plots

To further elucidate the binding stoichiometry for the formation of complexes of $\mathbf{1}$ with Sm(III) and Yb(III), we used the continuous variation method (Job plot). Solutions of ligand (2.0×10^{-5} M) with 2.5 equivalents of NaOH and Ln(III) (2.0×10^{-5}

M) were prepared in $\text{CH}_3\text{CN}:\text{CH}_3\text{OH}$ (96:4, v/v) in several molar ratios to obtain bell shaped curves for Sm(III) (Figure 4.6) and Yb(III) (Figure 4.7). For Sm(III), (Figure 4.6) the inflection point was observed at 0.59, which is between 0.5 (theoretical value for the 1:1 complex) and 0.67 (theoretical value for the 1:2 complex). Therefore, and in agreement with the titration data, both 1:1 and 1:2 complexes are formed for Sm(III). For Yb(III) (Figure 4.6), however, the inflection point was further shifted to the right at 0.62 suggesting that the 1:2 complex formation is dominant for Yb(III).

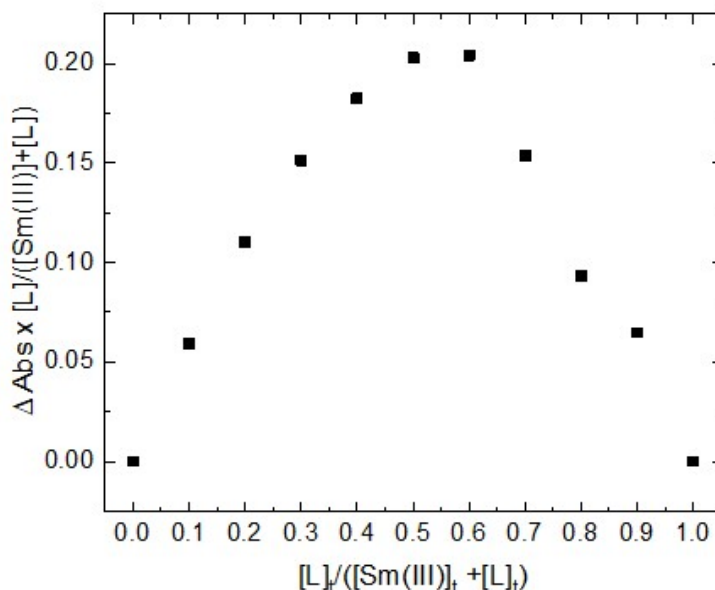


Figure 4.6. Job plot of **1** ($2.0 \times 10^{-5} \text{ M}$) with 2.2 equivalents of NaOH and Sm(III) ($2.0 \times 10^{-5} \text{ M}$) using changes in absorbance on UV-Vis spectra in $\text{CH}_3\text{CN}:\text{CH}_3\text{OH}$ (96:4, v/v). Absorbance was taken at 250 nm.

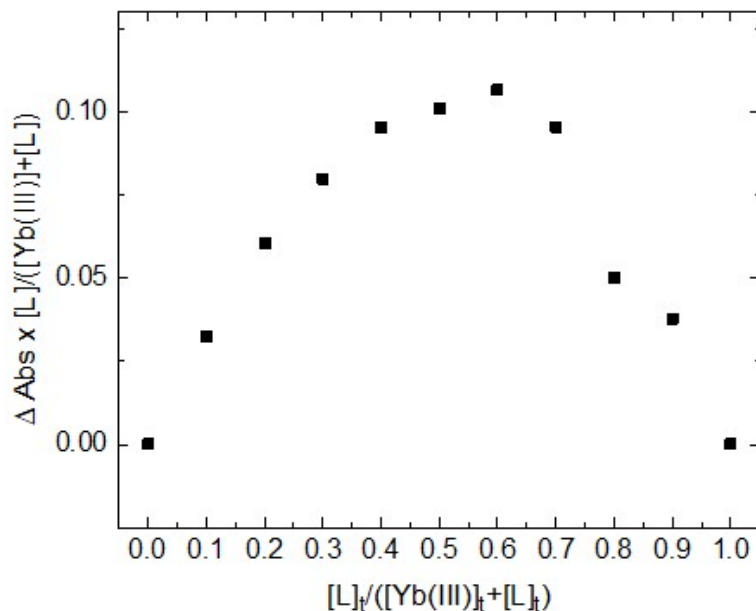


Figure 4.7. Job plot of **1** (2.0×10^{-5} M) with 2.2 equivalents of NaOH and Yb(III) (2.0×10^{-5} M) using changes in absorbance on UV-Vis spectra in $\text{CH}_3\text{CN}:\text{CH}_3\text{OH}$ (96:4, v/v). Absorbance was taken at 250 nm.

4.4.5 UV-Vis titrations

In the presence of 2.2 equivalents of NaOH, **1** showed two prominent absorption bands at 250 nm (due π to π^* transition) and 303 nm. With incremental addition of Sm(III) (4.0×10^{-4} M) to constant concentration of **1** (4.0×10^{-5} M), a hypochromic shift was observed for the absorbances at 250 nm and 303 nm accompanied by slight red shifts to 257 nm and 355 nm respectively. These changes, in addition to isosbestic points at 234 nm, 261 nm, 288 nm and 343 nm confirmed the formation of a complex between **1** and Sm(III) (Figure 4.8a). A closer examination of the titration curves obtained at $\lambda = 303$ nm shows a sigmoidal profile, with two knee points at 2.0×10^{-5} M and 4.0×10^{-5} M due to the Sm(III) added (Figure 4.8b). Gradual changes at A_{303} were observed until the 1:2 Sm(III)/**1** point was reached, followed by more abrupt changes upon further addition

of Sm(III), and then a saturation after the 1:1 Sm(III)/**1** point. This might suggest the initial formation of a 1:2 Sm(III)-ligand complex followed by a 1:1 complex only after addition of more metal. This observation is in good agreement with the Job plot experiments. The stability constants for both complexes were determined from the changes in absorption at $\lambda = 303$ nm after non-linear regression analysis. Binding constants of $\beta_{1(\text{Sm})} = 6.10 (\pm 0.08) \times 10^6 \text{ M}^{-1}$ and $\beta_{2(\text{Sm})} = 7.40 (\pm 0.10) \times 10^{11} \text{ M}^{-2}$ for the 1:1 and 1:2 complexes, respectively, were obtained from three independent titrations. The 1-2 formation constants obtained were similar for both the UV-Vis and the fluorescence titrations. This agreement confirms the formation of the same 1:2 complex in the initial phase of the titration, while the UV-Vis experiment is more sensitive than fluorescence to the latter formation of a 1:1 complex after excess Sm(III) addition.

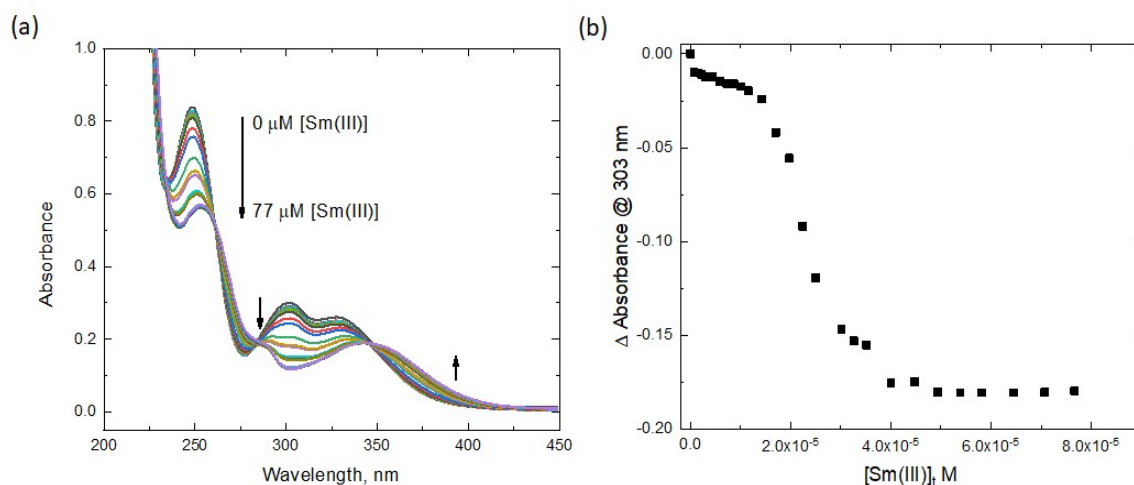


Figure 4.8. (a) Spectral changes of **1** due to titration of **1** ($4.0 \times 10^{-5} \text{ M}$) and 2.2 equivalents of NaOH with Sm(III) ($4.0 \times 10^{-4} \text{ M}$, 0 – 0.88 mL) in $\text{CH}_3\text{CN}:\text{CH}_3\text{OH}$ (96:4, v/v). (b) Titration curve showing change in absorbance of **1** as a result of added Sm(III) at 303 nm.

Analogous experiments for Yb(III) gave similar results, but with some notable differences (Figure 4.9). The UV-Vis spectra for the titration of **1** (4.0×10^{-5} M) and NaOH (8.8×10^{-5} M) with Yb(III) (4.0×10^{-4} M) in CH₃CN:CH₃OH (96:4, v/v) (Figure 4.9a) show a decrease in the ligand maximum absorbance at 250 nm, a decrease of the absorbance at 303 nm, and an increase in absorbance with broadening at 375 nm after titration with Yb(III), resembling the titration with Sm(III). However, unlike for Sm(III), the initial responses to the addition of Yb(III) were more abrupt until the 1:2, Yb(III)/**1** point and showed saturation with further addition of Yb(III) indicating that the formation of 1:2 complex is dominant if not exclusive, with very little to no 1:1 complex formation. Non-linear regression analysis of the plot of change in A₃₀₃ vs. [Yb(III)]_t (Figure 4.9b) and non-linear regression fitting into the 1:2 binding isotherm for the formation of the Yb(III)/**1** 1:2 complex gave a binding constant of $\beta_2 = 6.61 (\pm 0.02) \times 10^{13} \text{ M}^{-2}$.

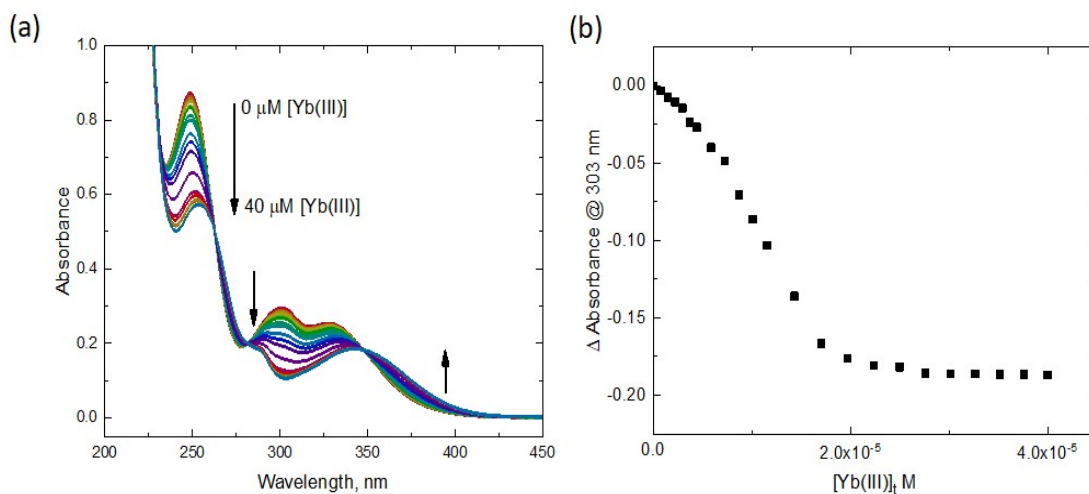


Figure 4.9. (a) Spectral changes of **1** due to titration of **1** (4.0×10^{-5} M) and 2.2 equivalents of NaOH with Yb(III) (4.0×10^{-4} M, 0 – 0.88 mL) in CH₃CN:CH₃OH (96:4, v/v). (b) Titration curve showing change in absorbance of **1** as a result of added Yb(III) at 303 nm.

4.4.6 Extraction and recovery of Sm(III) with CH₂Cl₂ as diluent

Extraction studies were performed from pH 10.0 – 14.0, followed by stripping of the loaded organic phase using 0.1 M nitric acid. The amount of Sm(III) recovered after stripping was determined using ICP-MS. Maximum extraction was obtained at pH 13.0 with 92.2 (\pm 13.5)% while 73.4 (\pm 16.5)% extraction was obtained at pH 14.0 (Figure 4.10). The extraction efficiencies for Sm(III) recorded at pH = 13.0 and pH = 14.0 are remarkably high for just a single extraction / stripping cycle when compared to previous studies.^{29,30} For the pH range of 10.0 – 11.5 there was negligible extraction of Sm(III) into the organic phase (Figure 4.10). Poor extraction efficiency at lower alkalinity compared to higher alkalinity clearly underscores the need for deprotonation of **1** for effective extraction. Only at higher alkalinities does **1** become deprotonated, revealing its O- and N- binding sites. Overall, such behavior suggests that deprotonation of **1** is favored at high pH, and only in such alkalinity would optimum extraction of f-elements can be achieved. Therefore, **1** in addition to being an effective sensor, is also a promising candidate for extraction of f-elements from alkaline HLW.

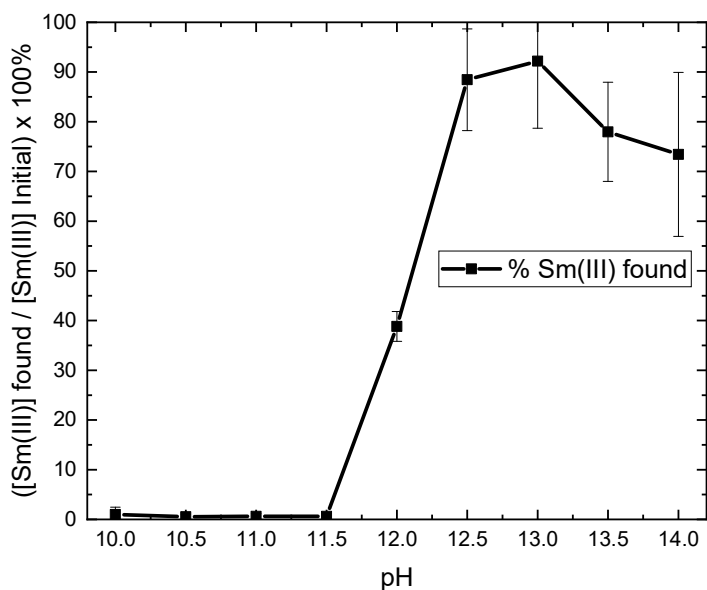


Figure 4.10. Percent Sm(III) recovered after extraction and consecutive stripping using **I** for pH 10.0 – 14.0. Initial Sm(III) concentration in the aqueous phase was 2.0 mM and $[I]_i$ in the organic phase (dichloromethane) was 20.0 mM. Quantification of Sm(III) was performed by ICP-MS.

In order to account for unextracted Sm(III), the aforementioned Sm(III) extraction experiments were also carried out by measuring the Sm(III) concentration in the aqueous phase after loading, and comparing with the amount of Sm(III) recovered after stripping (Figure 4.11) to determine the mass balance. At lower alkalinity (pH 10.0 – 11.5), it was observed that a significant amount of the Sm(III) remained unextracted in the aqueous phase. This may be attributed to the ligand not being completely deprotonated and thus not being able to effectively coordinate with the metal. It should also be noted that at such low alkalinity Sm(III) is soluble and available to be quantified with ease. For higher pHs (10.5 to 11.5) the unextracted Sm(III) in the aqueous phase decreased substantially, but this decrease is not complemented by an increase in Sm(III)

found after stripping in these region (Figure 4.11), this could be due to partial precipitation as a result of the formation of insoluble hydroxide salts. And as is part of the quantification process to avoid interference, such precipitates are filtered off before metal quantification, and therefore are not detected in the recovery experiments for Sm(III). The fact that the overall mass balance worsens at even higher pHs is consistent with the hypothesis of increasing loss of Sm(III) due to precipitation at higher pHs (>12.5).

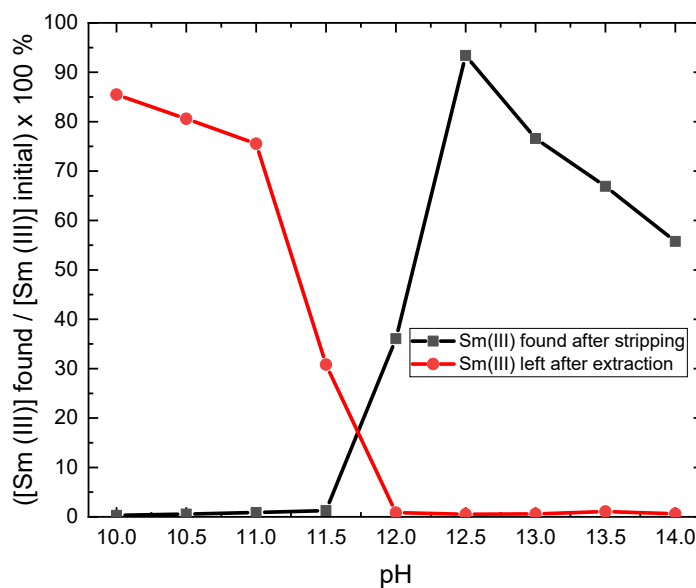


Figure 4.11. Mass balance for extraction experiment, showing Sm(III) recovered and measured in the acidic aqueous phase after extraction with the ligand solution (20.0 mM) and consecutive stripping (0.1 M HNO₃) (black squares) and unextracted Sm(III) in the alkaline aqueous phase after contact with ligand solution (20.0 mM) (red circles) for pH 10.0 – 14.0. Initial Sm(III) concentration in the alkaline aqueous phase was 2.0 mM. Quantification of Sm(III) was done using the Arsenazo-III spectrophotometric method.

4.4.7 Quantification of Sm(III) using the Arsenazo III spectrophotometric method vs. ICP-MS

Comparison between the Arsenazo-III spectrophotometric method and the ICP-MS method for quantification of Sm(III) was performed for pH 10.0 – 14.0. Results obtained gave values that were within reasonable agreement. This experiment shows that both methods can be used with a fairly good degree of accuracy for quantification of Sm(III) recovered after stripping (Figure 4.12).

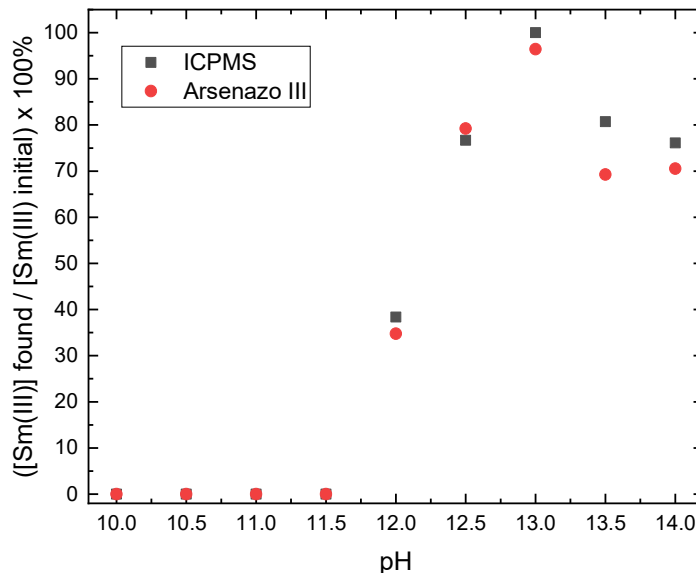


Figure 4.12. Comparison of ICP-MS and the Arsenazo-III method for quantification of Sm(III) recovered for pH 10.0 – 14.0 after stripping of the loaded organic phase with 0.1 M nitric acid.

4.4.8 X-ray crystallography studies

Neon green crystals were obtained from slow evaporation of a solution of **1** in chloroform. The X-ray structure of ligand **1** was solved in a triclinic P-1 space group with a full molecule within the asymmetric unit. The dihedral angle between the

quinoline ring and the aryl ring was 56.4° . While the aryl ring is highly planar with deviation from planarity of 0.005 \AA , the quinoline moiety is significantly deviated from planarity with 0.047 \AA . Although no intermolecular π - π stacking interactions have been noted noticeable intermolecular and intramolecular hydrogen bonding interactions are clearly visible. The intermolecular interaction involves one of the O atoms of the $-\text{SO}_2$ fragment of a molecule and the N-H group of a proximal molecule (O---H-N with an O---N distance of 2.97 \AA). The intramolecular interaction involves the H atom of the OH substituent on the aryl group and one of the O atoms of the $-\text{SO}_2$ moiety of the same molecule (O---H-O, with an O---O distance of 2.84 \AA) (Figure 4.13). The crystallographic data are provided in Tables 4.1-4.4.

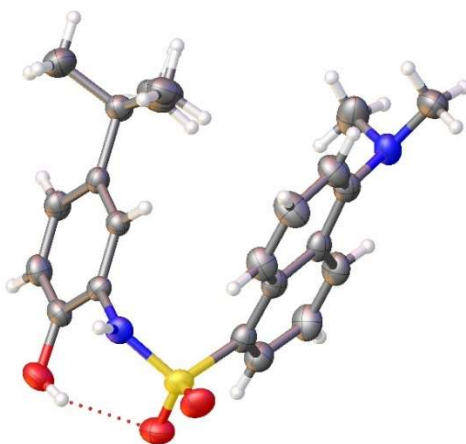


Figure 4.13. ORTEP representation of the crystal structure of **1** showing intramolecular hydrogen bonding (50% probability ellipsoids).

Table 4.1: Experimental details for **1**

Crystal data

Chemical formula $\text{C}_{22}\text{H}_{26}\text{N}_2\text{O}_3\text{S}$

Mr 398.51

Crystal system, space group Triclinic, P -1

Temperature (K)	298
a, b, c (Å)	8.385(3), 8.757(3), 14.066(5)
α, β, γ (°)	100.723(4), 91.132(5), 91.636(5)
V (Å ³)	1014.1 (6)
Z	2
Radiation type	Mo K α
μ (mm ⁻¹)	0.19
Crystal size (mm)	0.18 × 0.15 × 0.07
Data collection	
Diffractometer	Bruker D8 Quest PHOTON II
Absorption correction	Multi-scan <i>SADABS</i> 2016/2: Krause, L., Herbst-Irmer, R., Sheldrick G.M. & Stalke D., <i>J. Appl. Cryst.</i> 48 (2015)3-10.
T_{\min}, T_{\max}	0.617, 0.745
No. of measured, independent and observed [$I > 2\sigma(I)$] reflections	6231, 3268, 2610
R_{int}	0.026
$(\sin \theta/\lambda)_{\text{max}}$ (Å ⁻¹)	0.587
Refinement	
R[F2 > 2 σ (F2)], wR(F2), S	0.059, 0.143, 1.09
No. of reflections	3268
No. of parameters	259
H-atom treatment	H-atom parameters constrained
$\Delta\rho_{\text{max}}, \Delta\rho_{\text{min}}$ (e Å ⁻³)	0.38, -0.33

Table 4.2: Fractional atomic coordinates and isotropic or equivalent isotropic displacement parameters (\AA^2) for **1**

	<i>x</i>	<i>y</i>	<i>z</i>	$U_{\text{iso}}^*/U_{\text{eq}}$
S1	0.31709 (10)	0.83887 (9)	0.39829 (5)	0.0429 (3)
O1	0.1590 (3)	0.8526 (3)	0.36187 (17)	0.0584 (7)
O2	0.3489 (3)	0.8915 (3)	0.49912 (15)	0.0550 (6)
O3	0.2091 (3)	0.9966 (3)	0.19943 (17)	0.0538 (6)
H3	0.190418	0.992473	0.255905	0.081*
N1	0.7509 (4)	0.2320 (3)	0.29815 (19)	0.0506 (7)
N2	0.4361 (3)	0.9412 (3)	0.34294 (17)	0.0408 (6)
H2	0.484201	1.023604	0.374713	0.049*
C1	0.3685 (4)	0.6422 (3)	0.3616 (2)	0.0415 (8)
C2	0.2564 (4)	0.5470 (4)	0.3076 (2)	0.0497 (8)
H2A	0.157387	0.584871	0.294611	0.060*
C3	0.2905 (5)	0.3917 (4)	0.2717 (3)	0.0569 (10)
H3A	0.212053	0.324789	0.237789	0.068*
C4	0.4371 (4)	0.3387 (4)	0.2861 (2)	0.0510 (9)
H4	0.458446	0.235435	0.261291	0.061*
C5	0.5588 (4)	0.4365 (4)	0.3380 (2)	0.0421 (8)
C6	0.7158 (4)	0.3822 (4)	0.3481 (2)	0.0446 (8)
C7	0.8245 (5)	0.4764 (4)	0.4065 (3)	0.0565 (9)
H7	0.925877	0.440571	0.415824	0.068*
C8	0.7860 (5)	0.6258 (4)	0.4524 (3)	0.0621 (10)
H8	0.862301	0.687164	0.492139	0.074*
C9	0.6398 (4)	0.6839 (4)	0.4404 (2)	0.0514 (9)
H9	0.617235	0.784262	0.470899	0.062*
C10	0.5224 (4)	0.5906 (4)	0.3814 (2)	0.0411 (7)
C11	0.7564 (6)	0.2186 (5)	0.1933 (3)	0.0737 (12)
H11A	0.671493	0.276024	0.171556	0.111*
H11B	0.744097	0.111141	0.162856	0.111*
H11C	0.857039	0.259784	0.176392	0.111*
C12	0.8877 (5)	0.1600 (4)	0.3348 (3)	0.0619 (10)
H12A	0.984175	0.211878	0.320434	0.093*
H12B	0.888661	0.052269	0.304567	0.093*
H12C	0.880496	0.168246	0.403592	0.093*
C13	0.4609 (4)	0.8943 (3)	0.2413 (2)	0.0350 (7)
C14	0.3482 (4)	0.9244 (3)	0.1741 (2)	0.0400 (7)
C15	0.3801 (4)	0.8823 (4)	0.0772 (2)	0.0466 (8)
H15	0.305879	0.900973	0.031025	0.056*
C16	0.5200 (4)	0.8133 (4)	0.0481 (2)	0.0442 (8)
H16	0.539564	0.788071	-0.017771	0.053*
C17	0.6334 (4)	0.7799 (3)	0.1136 (2)	0.0362 (7)
C18	0.5999 (4)	0.8221 (3)	0.2103 (2)	0.0355 (7)
H18	0.673313	0.801164	0.256213	0.043*
C19	0.7855 (4)	0.6971 (4)	0.0777 (2)	0.0441 (8)
C20	0.8825 (5)	0.7946 (5)	0.0190 (3)	0.0726 (12)
H20A	0.817995	0.815143	-0.034033	0.109*
H20B	0.974558	0.738974	-0.005548	0.109*
H20C	0.916189	0.891192	0.059662	0.109*
C21	0.7379 (5)	0.5406 (5)	0.0151 (3)	0.0735 (12)

H21A	0.669036	0.483436	0.050576	0.110*
H21B	0.831901	0.482741	-0.050576	0.110*
H21C	0.682931	0.556987	-0.042490	0.110*
C22	0.8903 (5)	0.6670 (5)	0.1617 (3)	0.0666 (11)
H22A	0.919469	0.764107	0.203211	0.100*
H22B	0.984920	0.616327	0.136891	0.100*
H22C	0.832500	0.601723	0.197760	0.100*

Table 4.3: Atomic displacement parameters (\AA^2) for **1**

	U^{11}	U^{22}	U^{33}	U^{12}	U^{13}	U^{23}
S1	0.0467 (5)	0.0441 (5)	0.0355 (4)	0.0036 (3)	0.0096 (3)	0.0001 (3)
O1	0.0440 (15)	0.0634 (16)	0.0661 (16)	0.0056 (12)	0.0077 (12)	0.0061 (12)
O2	0.0658 (16)	0.0583 (15)	0.0361 (12)	-0.0007 (12)	0.0145 (11)	-0.0048 (10)
O3	0.0504 (15)	0.0553 (15)	0.0562 (14)	0.0182 (11)	0.0008 (11)	0.0091 (12)
N1	0.067 (2)	0.0415 (16)	0.0429 (15)	0.0084 (14)	0.0061 (13)	0.0064 (12)
N2	0.0500 (17)	0.0334 (13)	0.0349 (13)	0.0020 (12)	0.0045 (11)	-0.0046 (10)
C1	0.053 (2)	0.0386 (17)	0.0322 (16)	-0.0021 (15)	0.0025 (14)	0.0053 (13)
C2	0.049 (2)	0.052 (2)	0.0489 (19)	-0.0033 (16)	-0.0023 (16)	0.0108 (16)
C3	0.065 (3)	0.046 (2)	0.056 (2)	-0.0120 (18)	-0.0123 (18)	0.0044 (16)
C4	0.066 (3)	0.0369 (18)	0.0476 (19)	-0.0047 (16)	-0.0012 (17)	0.0018 (14)
C5	0.059 (2)	0.0388 (17)	0.0283 (15)	-0.0013 (15)	0.0002 (14)	0.0068 (12)
C6	0.055 (2)	0.0448 (19)	0.0340 (16)	0.0017 (16)	0.0030 (14)	0.0079 (14)
C7	0.056 (2)	0.056 (2)	0.056 (2)	0.0102 (18)	-0.0101 (18)	0.0055 (17)
C8	0.062 (3)	0.060 (2)	0.058 (2)	0.0021 (19)	-0.0211 (19)	-0.0041 (18)
C9	0.063 (2)	0.0446 (19)	0.0416 (18)	0.0015 (16)	-0.0109 (16)	-0.0036 (14)
C10	0.049 (2)	0.0438 (18)	0.0306 (15)	-0.0004 (14)	-0.0012 (13)	0.0080 (13)
C11	0.119 (4)	0.053 (2)	0.047 (2)	0.005 (2)	0.016 (2)	0.0017 (17)
C12	0.061 (3)	0.054 (2)	0.073 (3)	0.0145 (19)	0.016 (2)	0.0128 (19)
C13	0.0399 (18)	0.0304 (15)	0.0331 (15)	-0.0019 (13)	0.0044 (13)	0.0016 (12)
C14	0.0429 (19)	0.0329 (16)	0.0439 (18)	0.0056 (13)	0.0001 (14)	0.0063 (13)
C15	0.055 (2)	0.0456 (19)	0.0407 (18)	0.0045 (16)	-0.0083 (15)	0.0123 (14)
C16	0.059 (2)	0.0419 (18)	0.0316 (16)	0.0049 (16)	0.0032 (15)	0.0051 (13)
C17	0.0454 (19)	0.0323 (15)	0.0314 (15)	0.0011 (13)	0.0027 (13)	0.0067 (12)
C18	0.0381 (18)	0.0325 (15)	0.0359 (16)	0.0018 (13)	0.0014 (13)	0.0063 (12)
C19	0.047 (2)	0.0457 (18)	0.0395 (17)	0.0085 (15)	0.0067 (14)	0.0068 (14)
C20	0.070 (3)	0.078 (3)	0.075 (3)	0.016 (2)	0.029 (2)	0.026 (2)
C21	0.076 (3)	0.053 (2)	0.083 (3)	0.018 (2)	0.008 (2)	-0.012 (2)
C22	0.060 (3)	0.085 (3)	0.057 (2)	0.030 (2)	0.0117 (19)	0.015 (2)

Table 4.4: Geometric parameters (\AA , $^\circ$) for **1**

S1—O1	1.428 (3)	C11—H11A	0.9600
S1—O2	1.425 (2)	C11—H11B	0.9600
S1—N2	1.626 (3)	C11—H11C	0.9600

S1—C1	1.771 (3)	C12—H12A	0.9600
O3—H3	0.8200	C12—H12B	0.9600
O3—C14	1.365 (4)	C12—H12C	0.9600
N1—C6	1.414 (4)	C13—C14	1.388 (4)
N1—C11	1.460 (4)	C13—C18	1.381 (4)
N1—C12	1.455 (5)	C14—C15	1.378 (4)
N2—H2	0.8600	C15—H15	0.9300
N2—C13	1.434 (4)	C15—C16	1.370 (5)
C2—H2A	0.9300	C17—C18	1.378 (4)
C2—C3	1.400 (5)	C17—C19	1.533 (4)
C3—H3A	0.9300	C18—H18	0.9300
C3—C4	1.351 (5)	C19—C20	1.524 (5)
C4—H4	0.9300	C19—C21	1.523 (5)
C4—C5	1.413 (4)	C19—C22	1.524 (5)
C5—C6	1.426 (5)	C20—H20A	0.9600
C5—C10	1.418 (4)	C20—H20B	0.9600
C6—C7	1.363 (5)	C20—H20C	0.9600
C7—H7	0.9300	C21—H21A	0.9600
C7—C8	1.397 (5)	C21—H21B	0.9600
C8—H8	0.9300	C21—H21C	0.9600
C8—C9	1.360 (5)	C22—H22A	0.9600
C9—H9	0.9300	C22—H22B	0.9600
C9—C10	1.412 (4)	C22—H22C	0.9600
O1—S1—N2	107.37 (15)	N1—C12—H12A	109.5
O1—S1—C1	107.06 (15)	N1—C12—H12B	109.5
O2—S1—O1	118.02 (15)	N1—C12—H12C	109.5
O2—S1—N2	106.00 (14)	H12A—C12—H12B	109.5
O2—S1—C1	111.23 (15)	H12A—C12—H12C	109.5
N2—S1—C1	106.55 (14)	H12B—C12—H12C	109.5
C14—O3—H3	109.5	C14—C13—N2	120.5 (3)
C6—N1—C11	114.0 (3)	C18—C13—N2	119.6 (3)
C6—N1—C12	116.3 (3)	C18—C13—C14	120.0 (3)
C12—N1—C11	110.9 (3)	O3—C14—C13	123.2 (3)
S1—N2—H2	119.9	O3—C14—C15	118.5 (3)
C13—N2—S1	120.1 (2)	C15—C14—C13	118.3 (3)
C13—N2—H2	119.9	C14—C15—H15	119.6
C2—C1—S1	116.1 (3)	C16—C15—C14	120.7 (3)
C2—C1—C10	122.1 (3)	C16—C15—H15	119.6
C10—C1—S1	121.6 (2)	C15—C16—H16	119.0
C1—C2—H2A	120.1	C15—C16—C17	122.1 (3)
C1—C2—C3	119.7 (3)	C17—C16—H16	119.0
C3—C2—H2A	120.1	C16—C17—C19	120.3 (3)
C2—C3—H3A	119.9	C18—C17—C16	116.7 (3)
C4—C3—C2	120.2 (3)	C18—C17—C19	123.0 (3)
C4—C3—H3A	119.9	C13—C18—H18	118.9
C3—C4—H4	119.3	C17—C18—C13	122.2 (3)
C3—C4—C5	121.5 (3)	C17—C18—H18	118.9
C5—C4—H4	119.3	C20—C19—C17	110.5 (3)
C4—C5—C6	121.1 (3)	C20—C19—C22	108.4 (3)
C4—C5—C10	119.0 (3)	C21—C19—C17	108.6 (3)
C10—C5—C6	119.9 (3)	C21—C19—C20	109.9 (3)
N1—C6—C5	118.3 (3)	C21—C19—C22	108.0 (3)

C7—C6—N1	123.0 (3)	C22—C19—C17	111.5 (3)
C7—C6—C5	118.7 (3)	C19—C20—H20A	109.5
C6—C7—H7	119.5	C19—C20—H20B	109.5
C6—C7—C8	121.1 (3)	C19—C20—H20C	109.5
C8—C7—H7	119.5	H20A—C20—H20B	109.5
C7—C8—H8	119.2	H20A—C20—H20C	109.5
C9—C8—C7	119.2	C19—C21—H21A	109.5
C9—C8—H8	121.6 (3)	H20B—C20—H20C	109.5
C8—C9—H9	120.2	C19—C21—H21B	109.5
C8—C9—C10	119.6 (3)	C19—C21—H21C	109.5
C10—C9—H9	120.2	H21A—C21—H21B	109.5
C5—C10—C1	117.2 (3)	H21A—C21—H21C	109.5
C9—C10—C1	123.8 (3)	H21B—C21—H21C	109.5
C9—C10—C5	118.9 (3)	C19—C22—H22A	109.5
N1—C11—H11A	109.5	C19—C22—H22B	109.5
N1—C11—H11B	109.5	C19—C22—H22C	109.5
N1—C11—H11C	109.5	H22A—C22—H22B	109.5
H11A—C11—H11B	109.5	H22A—C22—H22C	109.5
H11A—C11—H11C	109.5	H22B—C22—H22C	109.5
H11B—C11—H11C	109.5		
S1—N2—C13—C14	78.7 (3)	C5—C6—C7—C8	-2.7 (5)
S1—N2—C13—C18	-102.8 (3)	C6—C5—C10—C1	174.6 (3)
S1—C1—C2—C3	176.8 (3)	C6—C5—C10—C9	-4.8 (4)
S1—C1—C10—C5	-171.7 (2)	C6—C7—C8—C9	-0.5 (6)
S1—C1—C10—C9	7.7 (4)	C7—C8—C9—C10	1.0 (6)
O1—S1—N2—C13	-67.2 (3)	C8—C9—C10—C1	-177.7 (3)
O1—S1—C1—C2	1.0 (3)	C8—C9—C10—C5	1.7 (5)
O1—S1—C1—C10	176.4 (2)	C10—C1—C2—C3	1.5 (5)
O2—S1—N2—C13	165.8 (2)	C10—C5—C6—N1	-175.6 (3)
O2—S1—C1—C2	131.3 (3)	C10—C5—C6—C7	5.3 (5)
O2—S1—C1—C10	-53.4 (3)	C11—N1—C6—C5	69.7 (4)
O3—C14—C15—C16	178.2 (3)	C11—N1—C6—C7	-111.3 (4)
N1—C6—C7—C8	178.2 (3)	C12—N1—C6—C5	-159.3 (3)
N2—S1—C1—C2	-113.6 (3)	C12—N1—C6—C7	19.7 (5)
N2—S1—C1—C10	61.7 (3)	C13—C14—C15—C16	-0.4 (5)
N2—C13—C14—O3	-0.9 (5)	C14—C13—C18—C17	1.1 (4)
N2—C13—C14—C15	177.6 (3)	C14—C15—C16—C17	1.3 (5)
N2—C13—C18—C17	-177.4 (3)	C15—C16—C17—C18	-1.1 (5)
C1—S1—N2—C13	47.2 (3)	C15—C16—C17—C19	177.7 (3)
C1—C2—C3—C4	-3.6 (5)	C16—C17—C18—C13	-0.1 (4)
C2—C1—C10—C5	3.4 (5)	C16—C17—C19—C20	61.4 (4)
C2—C1—C10—C9	-177.3 (3)	C16—C17—C19—C21	-59.2 (4)
C2—C3—C4—C5	0.6 (5)	C16—C17—C19—C22	-178.0 (3)
C3—C4—C5—C6	-176.4 (3)	C18—C13—C14—O3	-179.3 (3)
C3—C4—C5—C10	4.4 (5)	C18—C13—C14—C15	-0.8 (4)
C4—C5—C6—N1	5.2 (4)	C18—C17—C19—C20	-119.9 (3)
C4—C5—C6—C7	-173.9 (3)	C18—C17—C19—C21	119.5 (3)
C4—C5—C10—C1	-6.2 (4)	C18—C17—C19—C22	0.7 (4)
C4—C5—C10—C9	174.4 (3)	C19—C17—C18—C13	-178.9 (3)

4.5 Conclusions

A chemosensor based on the *o*-sulfonamidophenol framework, and bearing the dansyl fluorophore shows reasonable sensing selectivity in presence of 2.2 equivalents of NaOH in CH₃CN:CH₃OH (96:4, v/v) for f-elements Sm(III) and Yb(III). Detection limits for Sm(III) as low as 0.094 μM was obtained for a linear range of 0 – 1.12 μM, with Sm(III) and Yb(III) demonstrating a threefold enhancement of fluorescence based on CHEF, while showing negligible responses to K(I), Na(I), Cs(I), and Sr(II). UV-Vis and fluorescence studies were consistent with 1:2 metal to ligand complex formation for Sm(III), with a binding constant of $\beta_{2(\text{Sm})} = 7.40(\pm 0.10) \times 10^{11} \text{ M}^{-2}$ (UV-Vis) and $\beta_{2(\text{Sm})} = 2.00 (\pm 0.02) \times 10^{11} \text{ M}^{-2}$ (fluorescence), and for Yb(III) with $\beta_{2(\text{Yb})} = 6.61 (\pm 0.02) \times 10^{13} \text{ M}^{-2}$ (UV-Vis) and $\beta_{2(\text{Yb})} = 4.36 (\pm 0.11) \times 10^{13} \text{ M}^{-2}$ (fluorescence). f-Element extraction from alkaline aqueous phases into organic phase (CH₂Cl₂), was observed with efficiency of 92.2 (±13.5)% at pH 13.0 for recovered Sm(III) after only one extraction / stripping cycle. Therefore, this sensor shows great prospects not only for sensing but also for extraction. These results can be expanded into actinide extraction and *in situ* sensing of actinides in HLW.

4.6 Acknowledgement

The author would like to thank Drs. Yong Cai and Guangliang Liu for granting access and providing advice for the use of the ICP-MS instrument. This work was supported by the U.S. Department of Energy Office of Environmental Management MSIPP program managed by the Savannah River National Laboratory under SRNS

contracts BOA 541, TOAs 0000217393, 0000403071 and 0000525181 to FIU. We also appreciate the support received from the Florida International University Dissertation Year Fellowship for Oluwaseun William Adedoyin (DYF Summer/Fall 2021 Fellow).

4.7 References

1. Wu, D.; Sedgwick, A. C.; Gunnlaugsson, T.; Akkaya, E. U.; Yoon, J.; James, T. D. Fluorescent chemosensors: the past, present and future. *Chemical Society Reviews* **2017**, *46*, 7105-7123.
2. Kaur, B.; Kaur, N.; Kumar, S. Colorimetric metal ion sensors—a comprehensive review of the years 2011–2016. *Coordination Chemistry Reviews* **2018**, *358*, 13-69.
3. Yeung, M. C.; Yam, V. W. Luminescent cation sensors: from host–guest chemistry, supramolecular chemistry to reaction-based mechanisms. *Chemical Society Reviews* **2015**, *44*, 4192-4202.
4. Kavallieratos, K.; Rosenberg, J. M.; Chen, W.; Ren, T. Fluorescent sensing and selective Pb(II) extraction by a dansylamide ion-exchanger. *Journal of the American Chemistry Society* **2005**, *127*, 6514-6515.
5. Wanichacheva, N.; Watpathomsub, S.; Lee, V. S.; Grudpan, K. Synthesis of a novel fluorescent sensor bearing dansyl fluorophores for the highly selective detection of mercury (II) ions. *Molecules* **2010**, *15*, 1798-1810.
6. Ahmed, B. N.; Ghosh, P. A chelation enhanced selective fluorescence sensing of Hg(II) by a simple quinoline substituted tripodal amide receptor. *Dalton Transactions* **2011**, *40*, 12540-12547.
7. Kim, S. K.; Swamy, K.; Chung, S.; Kim, H. N.; Kim, M. J.; Jeong, Y.; Yoon, J. New fluorescent and colorimetric chemosensors based on the rhodamine and boronic acid groups for the detection of Hg(II). *Tetrahedron Letters* **2010**, *51*, 3286-3289.
8. Sung, K.; Fu, H.; Hong, S. A Fe(III) / Hg(II) selective anthracene-based fluorescent PET sensor with tridentate ionophore of amide / β -amino alcohol. *Journal of Fluorescence* **2007**, *17*, 383-389.
9. Sahana, A.; Banerjee, A.; Das, S.; Lohar, S.; Karak, D.; Sarkar, B.; Mukhopadhyay, S. K.; Mukherjee, A. K.; Das, D. A naphthalene-based Al(III) selective fluorescent sensor for living cell imaging. *Organic & Biomolecular Chemistry* **2011**, *9*, 5523-5529.

10. Daly, B.; Ling, J.; De Silva, A. P. Current developments in fluorescent PET (photoinduced electron transfer) sensors and switches. *Chemical Society Reviews* **2015**, *44*, 4203-4211.
11. Jiang, H.; Tatsu, Y.; Lu, Z.; Xu, Q. Non-, micro-, and mesoporous metal-organic framework isomers: reversible transformation, fluorescence sensing, and large molecule separation. *Journal of the American Chemical Society* **2010**, *132*, 5586-5587.
12. Cannizzo, A.; van Mourik, F.; Gawelda, W.; Zgrablic, G.; Bressler, C.; Chergui, M. Broadband femtosecond fluorescence spectroscopy of [Ru(bpy)₃]₂. *Angewandte Chemie International Edition English* **2006**, *118*, 3246-3248.
13. Dos Remedios, C. G.; Moens, P. D. Fluorescence resonance energy transfer spectroscopy is a reliable "ruler" for measuring structural changes in proteins: dispelling the problem of the unknown orientation factor. *Journal of Structural Biology* **1995**, *115*, 175-185.
14. Kwok, R. T.; Leung, C. W.; Lam, J. W.; Tang, B. Z. Biosensing by luminogens with aggregation-induced emission characteristics. *Chemical Society Reviews* **2015**, *44*, 4228-4238.
15. Sasaki, S.; Drummen, G. P.; Konishi, G. Recent advances in twisted intramolecular charge transfer (TICT) fluorescence and related phenomena in materials chemistry. *Journal of Materials Chemistry C* **2016**, *4*, 2731-2743.
16. Antina, E. V.; Bumagina, N. A.; Vyugin, A. I.; Solomonov, A. V. Fluorescent indicators of metal ions based on dipyrromethene platform. *Dyes and Pigments* **2017**, *136*, 368-381.
17. Liu, K.; Zhao, X.; Liu, Q.; Huo, J.; Li, Z.; Wang, X. A novel multifunctional BODIPY-derived probe for the sequential recognition of Hg(II) and I⁻, and the fluorometric detection of Cr(III). *Sensors Actuators B: Chem.* **2017**, *239*, 883-889.
18. Weber, G. Polarization of the fluorescence of macromolecules. 2. Fluorescent conjugates of ovalbumin and bovine serum albumin. *Biochemical Journal* **1952**, *51*, 155.
19. Jiang, P.; Chen, L.; Lin, J.; Liu, Q.; Ding, J.; Gao, X.; Guo, Z. Novel zinc fluorescent probe bearing dansyl and aminoquinoline groups. *Chemical Communications* **2002**, 1424-1425.
20. Ganjali, M. R.; Hosseini, M.; Ghafarloo, A.; Khoobi, M.; Faridbod, F.; Shafiee, A.; Norouzi, P. Selective recognition of Pr³ based on fluorescence enhancement sensor. *Materials Science and Engineering: C* **2013**, *33*, 4140-4143.

21. Faridbod, F.; Sedaghat, M.; Hosseini, M. E.; Ganjali, M. R.; Khoobi, M.; Shafiee, A.; Norouzi, P. Turn-on fluorescent chemosensor for determination of lutetium ion. *Spectrochimica Acta Part A: Molecular and Biomolecular Spectroscopy* **2015**, *137*, 1231-1234.
22. Xia, W.; Schmehl, R. H.; Li, C. A Fluorescent 18-Crown-6 Based Luminescence Sensor for Lanthanide Ions. *Tetrahedron* **2000**, *56*, 7045-7049.
23. Das, P.; Ghosh, A.; Das, A. Unusual specificity of a receptor for Nd(III) among other lanthanide ions for selective colorimetric recognition. *Inorganic Chemistry* **2010**, *49*, 6909-6916.
24. Gans, P.; Sabatini, A.; Vacca, A. Determination of equilibrium constants from spectrophotometric data obtained from solutions of known pH: the program pHab. *Annali di Chimica* **1999**, *89*, 45-49.
25. Gans, P.; Sabatini, A.; Vacca, A. Investigation of equilibria in solution. Determination of equilibrium constants with the HYPERQUAD suite of programs. *Talanta* **1996**, *43*, 1739-1753.
26. Sheldrick, G. M. SHELXS-97, Program for Crystal Structure Determination, University of Göttingen, Germany, **1997**.
27. Dolomanov, O. V.; Bourhis, L. J.; Gildea, R. J.; Howard, J. A.; Puschmann, H. OLEX2: a complete structure solution, refinement and analysis program. *Journal of Applied Crystallography* **2009**, *42*, 339-341.
28. KumaraBoominathan, S. S.; ChandruaSenadi, G; KishoreaVandavasi, J. A one-pot hypoiodite catalysed oxidative cycloetherification approach to benzoxazoles. *Chemical Communications* **2014**, *51*, 6726 – 6728.
29. Govor, E. V.; Morozov, A. N.; Rains, A. A.; Mebel, A. M.; Kavallieratos, K. Spectroscopic and Theoretical Insights into Surprisingly Effective Sm(III) Extraction from Alkaline Aqueous Media by o-Phenylenediamine-Derived Sulfonamides. *Inorganic Chemistry* **2020**, *59*, 6884-6894.
30. Morozov, A. N.; Govor, E. V.; Anagnostopoulos, V. A.; Kavallieratos, K.; Mebel, A. M. 1, 3, 5-Tris-(4-(iso-propyl)-phenylsulfamoylmethyl) benzene as a potential Am(III) extractant: experimental and theoretical study of Sm(III) complexation and extraction and theoretical correlation with Am(III). *Molecular Physics* **2018**, *116*, 2719-2727.

Chapter V: A *p*-Nitrophenol-sulfonamide Lu(III) Optical Sensor Forms a Unique
Lu(III)- μ -hydroxo Trimer in the Solid State.

Oluwaseun W. Adedoyin, Alexander N. Morozov, Indranil Chakraborty, Gabriela Ortega, Raphael G. Raptis, Christopher J. Dares, Alexander M. Mebel, and Konstantinos Kavallieratos

5.1 Abstract

Optical sensing of Lu(III) was demonstrated in alkaline conditions by a *p*-nitrophenol-sulfonamide ligand (**LH**₂) in its bis-deprotonated form (**L**²⁻). Color change from bright yellow to colorless occurred in acetonitrile in the presence of Lu(III), and to a lesser extent in the presence of other Ln(III), but not with Na(I), K(I), Cs(I), Sr(II), Pb(II), Ag(I), and Co(II). The blue shift in the UV-Vis low energy band was unique for Ln(III) and was accurately corroborated by TD-DFT calculations for the formation of a 1:1 complex with formula Lu-L(NO₃)(H₂O)₅. Non-linear regression analysis of the UV-Vis binding data gave a binding constant of $K_{11(\text{Lu})} = 5.8 (\pm 0.4) \times 10^6 \text{ M}^{-1}$, $K_{11(\text{La})} = 2.8 (\pm 0.8) \times 10^6 \text{ M}^{-1}$ and $K_{11(\text{Sm})} = 3.0 (\pm 0.4) \times 10^6 \text{ M}^{-1}$, and confirmed a 1:1 complexation in the studied lanthanides, with Lu(III) exhibiting stronger binding over other Ln(III). Electrochemical studies revealed two ligand-based oxidation events at 0.65 V and 0.85 V vs Fc⁺/Fc and a single reduction event at 0.14 V indicating complexation. Two distinctive complexes were characterized using X-ray crystallography. One structure showed the unique Lu(III) trimer (Et₃NH)₅[Lu₃(μ ₃-OH)₂(**LH**)₆(μ -**L**)₃] while the other

gave an octahedral complex $(\text{Et}_3\text{NH})_3[\text{Lu}(\text{LH})_6]$ with notable distortions from octahedral symmetry.

5.2 Introduction

There has been a steady growth in commercial¹ and biomedical²⁻⁵ applications of lanthanides (Ln), which underscores the need for selective ligands for their separation and sensing. As Ln(III) are surrogates for minor actinides, such as Am(III) and Cm(III), understanding their coordination chemistry with new ligand families could lead to applications in nuclear technology, and significant research effort has been dedicated to the separation of trivalent actinides from lanthanides.⁶⁻¹⁴ Lanthanides are present as fission products in spent nuclear fuel,^{10,11,15} they typically have large neutron absorption cross sections that makes them compete for neutrons needed for transmutation of minor actinides, and thus complicate nuclear waste management.¹⁴⁻¹⁷ Aside from nuclear technology, lanthanides, such as ¹⁷⁷Lu have drawn the attention of the radiopharmaceutical industry for applications in nuclear medicine and therapy,^{18,19} while Eu(III), Pr(III), and Yb(III) have found application as NMR shift reagents.^{20,21} In electronics manufacturing Eu and Nd provide electroluminescent materials for LED screens.^{1,22,23}

Colorimetric and fluorescent sensing is often based on spectroscopic changes upon metal binding within the π -electron system induced by Ligand to Metal Charge Transfer (LMCT) or Metal to Ligand Charge Transfer (MLCT) in a photoactive unit (chromophore or fluorophore).²⁴⁻²⁶ An optical sensor capable of detecting f-elements in alkaline conditions would be of importance in understanding the role of f-elements in

complicated alkaline high-level waste (HLW) tank mixtures at the Savannah River and Hanford US DOE sites – a legacy from the cold-war era.²⁵ Therefore, detecting f-elements in the presence of competing species, which are present in high concentrations in HLW such as Na(I), K(I), Cs(I), and Sr(II), is a critical feature of such a sensor.²⁶ The design of optical sensors for Ln(III) has to take into consideration their tendency to have a stable 3+ oxidation state,^{27,28} high coordination number (CN > 7)^{27,29,30} and preference for binding in mainly an electrostatic fashion, which is more pronounced than for An(III).^{8,27,28,31-34} Previously reported colorimetric sensors for Ln(III) include a chromogenic Schiff-base derived calixarene for sensing Dy(III) and Er(III),³³ a spirobenzopyran calixarene,³⁵ an azo-calixarene³⁶ and a malonamide-functionalized gold nanoparticle sensor for Eu(III).³⁷ Fluorescent Ln(III) sensors include examples with crown ether,³⁸ diazo,³⁹ and bis-pyrene moieties.⁴⁰ The examples reported by Hosseini et al.,⁴¹ Kumar et al.,⁴² and Faridbod et al.⁴³ have shown selectivity for Lu(III) over Zn(II), Hg(II), Cd(II), Al(III) and other Ln(III). Sulfonamide ligands and derivatives have shown great promise for separation and sensing of toxic metals⁴⁴ and lanthanides.^{31,41,45} Including recent work in our group with trisulfonamide and disulfonamide ligands as Sm(III) extractants in alkaline conditions.^{31,45} Prompted by these prior examples, as well as from the elegant work of Myasoedov et al.,⁴⁶ and Smirnov et al.,⁴⁷ with pyrocatechol analogs for f-element separation, we decided to explore the Ln(III) binding and sensing properties of the simpler and easier to synthesize N-(2-hydroxy-5-nitrophenyl)-4-methylbenzene sulfonamide (**LH₂**), which is based on the *o*-sulfonamidophenol framework. The phenolic group, placed ortho to the sulfonamide allows formation of a favorable 5-member ring upon complexation, *p*-nitrophenol also has high acidity,

facilitating Ln(III) binding under alkaline conditions, and giving the sensor the characteristic yellow nitrophenolate color in its deprotonated form.⁴⁸ Herein we report a *p*-nitrophenolsulfonamide (**LH₂**) as a μM level optical sensor for Lu(III) in alkaline conditions, forming a 1:1 complex in acetonitrile solution in its bis-deprotonated form (**L²⁻**). The sensor was highly effective even in the presence of a high-background matrix of other metals present in HLW. TD-DFT corroborated the spectral changes and perfectly matched the experimental absorption maximum for the formed Lu(III) complex. The X-ray crystal structure showed the formation of a unique Lu(III) trimeric cluster in the solid state.

5.3 Experimental section

5.3.1 Materials and methods

All chemicals and materials were purchased from Fisher Scientific or Sigma-Aldrich. Chemicals and solvents were standard reagent grade and were used without further purification, except that spectroscopic grade CH₃CN was used for all titration experiments. All metals used in this study were nitrate salts and lanthanide nitrate salts used were in their hexahydrate form. UV–Vis spectra were recorded on a Varian Cary 100 Bio UV–Vis spectrophotometer. FT-IR spectra were recorded on a Cary 600 series FT-IR spectrometer. X-ray diffraction studies were carried out on a Bruker D8 Quest with PHOTON 100 detector. N-(2-hydroxy-5-nitrophenyl)-4-methylbenzenesulfonamide (**LH₂**) was synthesized as previously reported^{49,50} and was found spectroscopically identical to the reported compound. Its X-ray structure is newly reported herein.

5.3.2 UV-visible spectroscopic studies

5.3.2.1 Sensor response for addition of Lu(III) vs. other metals

A solution of **LH₂** (50.0 μM) and 2.5 equivalents of diisopropylethylamine (DIPEA) (125.0 μM) in acetonitrile was prepared, 5.00 mL of this solution was added to separate vials containing nitrate salts of La(III), Sm(III), Lu(III), Co(II), Pb(II), Sr(II), Ag(I), Na(I), K(I), Cs(I), and Ca(II), in preweighed amounts such that 50.0 μM concentration of each metal will be obtained (1:1 ratio of **M** to **L**). These solutions were then allowed to stand for an hour before the UV-Vis spectra were collected to ensure thermodynamic equilibrium.

5.3.2.2 UV-Vis titrations with Ln(III) salts and determination of binding constants

UV-Vis titrations were carried out at constant ligand and DIPEA concentration (2.5 eq.) as follows: In a typical experiment a solution of **LH₂** (10.0 μM) and DIPEA (25.0 μM) in acetonitrile (spectroscopic grade) was prepared (Solution A). A 100.0 μM Ln(III) solution (Solution B) was prepared by dissolving appropriate quantity of $\text{Ln}(\text{NO}_3)_3 \cdot 6\text{H}_2\text{O}$ in solution A, thus maintaining a constant concentration of **LH₂** and DIPEA upon titration of solution A with solution B. 2.70 mL of solution A was placed in a 1 cm quartz UV-Vis cuvette and solution B was added in increments of 5.00 – 200.00 μL single additions until up to 970.00 μL total of solution B was added. The binding constants were calculated by non-linear regression analysis and fitting to the 1-1 binding isotherm (eq. 5.1).⁵¹ Binding constants were obtained from triplicate independent measurements.

$$y = \frac{\pm(L+x+K^{-1}-\sqrt{(L+x+K^{-1})^2-4xL}) X M}{2L} \quad (\text{eq. 5.1})$$

Where y = Cumulative change in absorbance or intensity

$x = [\text{Ln(III)}]_t$

L = Ligand concentration

$M = \Delta\text{Abs}_{\text{max}}$

K = binding constant

5.3.2.3 UV-Vis sensing response for Lu(III) vs. competing metals in HLW

UV-Vis titrations with Lu(III) vs. other metals present in HLW were carried out as previously described, except that NaNO_3 , KNO_3 , $\text{Sr}(\text{NO}_3)_2$, or CsNO_3 were added instead of $\text{Lu}(\text{NO}_3)_6 \cdot 6\text{H}_2\text{O}$ in solution B in separate experiments.

5.3.2.4 UV-Vis sensing response for Lu(III) in the presence of competing metals

UV-Vis titrations with Lu(III) vs. other metals present in HLW were carried out as previously described, except that NaNO_3 (5.0×10^{-3} M), KNO_3 (1.0×10^{-3} M), and $\text{Sr}(\text{NO}_3)_2$ (2.0×10^{-4} M), were all included together in solution A before it would be titrated with the $\text{Lu}(\text{NO}_3)_6 \cdot 6\text{H}_2\text{O}$ solution (solution B), thus ensuring a constant concentration of LH_2 (10.0 μM), DIPEA (25.0 μM), NaNO_3 (5.0×10^{-3} M), KNO_3 (1.0×10^{-3} M), and $\text{Sr}(\text{NO}_3)_2$ (2.0×10^{-4} M) during the entire titration with Lu(III). The limit of detection (LOD) of the sensor was calculated by the standard deviation σ , of the response observed after titration, and the slope S , of the regression line for the competitive titration curve at the initial linear response range (0 – 4.93 μM) of added Lu(III) was used to obtain the LOD⁵² as:

$$LOD = \frac{3.3\sigma}{S} \quad (\text{eq. 5.2})$$

σ = Residual standard deviation of the linear regression line obtained after titration

S = Slope of the titration curve

5.3.3 DFT calculations

The B3LYP hybrid functional,^{53,54} was employed for Density Functional Theory (DFT) calculations. The 6-31+G* basis set for H, C, N, O⁵⁵ and S⁵⁶ atoms was combined with Stuttgart Small Core RECP and (14s13p10d8f6g)/[6s6p5d4f3g] valence basis for Lu.⁵⁷ The initial guess of wave function for structures of interest was obtained using Hartree-Fock (HF) calculations followed by the stability check. The HF and following DFT calculations were carried out using the ground states spin multiplicities 1 corresponding to the electronic configurations [Xe]4f¹⁴ of Lu(III). The stability of the optimized structures was checked by running frequency calculations to ensure the absence of imaginary frequencies. The gas phase free energy, including zero-point energy (ZPE), was calculated at T = 298.15 K and P = 1 atm. Solvent contributions to the gas-phase free energies were estimated as single-point hydration energy for a gas-phase optimized molecular structure within the self-consistent reaction field (SCRF) using PCM⁵⁸ model with Gaussian-09 default parameters for acetonitrile. Calculations of the oscillator strength for S0 → S1 excitations were carried out using TD-DFT⁵⁹/B3LYP. In

TD-DFT calculations, the solvent effect of acetonitrile was taken into account using PCM model.

5.3.4 Electrochemistry

Electrochemical data were acquired using a CH Instruments 630E potentiostat. Cyclic voltammetry (CV) experiments were performed using a single compartment cell with a glassy carbon disc working electrode, a silver/silver chloride (Ag/AgCl) pseudo-reference electrode, and a carbon rod counter electrode. Electrochemistry solutions were deoxygenated by bubbling argon for 20 min prior to any experiments, and during experiments, a positive argon pressure was maintained in the headspace above the solution. A small amount of ferrocene was added to the electrochemistry solutions to calibrate the reference electrode.

5.3.5 X-ray crystallography

Yellow crystals of **LH₂** suitable for X-ray crystallography were obtained by slow evaporation of the solvent from a solution of **LH₂** (5.0 mg) in dichloromethane (5 mL) at ambient temperature. To obtain crystals of $(\text{Et}_3\text{NH})_5[\text{Lu}_3(\mu_3\text{-OH})_2(\text{LH})_6(\mu\text{-L})_3]$, a solution of $\text{Lu}(\text{NO}_3)_3 \cdot 6\text{H}_2\text{O}$ (25.0 mg, 0.054 mmol) in methanol (5 mL) was layered carefully on a solution of **LH₂** (50.0 mg, 0.163 mmol) and 4.2 equivalents of Et_3N (95.00 μL , 0.341 mmol) in dichloromethane (5 mL). After several weeks, fragile, amber platelike crystals of $(\text{Et}_3\text{NH})_5[\text{Lu}_3(\mu_3\text{-OH})_2(\text{LH})_6(\mu\text{-L})_3]$ were obtained. To obtain crystals of $(\text{Et}_3\text{NH})_3[\text{Lu}(\text{LH})_6]$, a solution of $\text{Lu}(\text{NO}_3)_3 \cdot 6\text{H}_2\text{O}$ (152.0 mg, 0.325 mmol) in

methanol (5 mL) was added to a solution of **LH₂** (100.0 mg, 0.325 mmol) and 2.1 equivalents of Et₃N (95.00 μL, 0.683 mmol) in dichloromethane (5 mL). After stirring for an hour, 3 mL of the formed solution was collected and layered carefully with diethyl ether (3 mL). This solution was allowed to slowly evaporate, and gave yellow crystals of (Et₃NH)₃[Lu(**LH**)₆] after several weeks. Suitable crystals of **LH₂**, (Et₃NH)₅Lu₃(μ₃-OH)₂(**LH**)₆(μ-L)₃] and (Et₃NH)₃[Lu(**LH**)₆] were submitted for X-ray crystallographic analysis.

5.4 Results and discussion

5.4.1 UV-Visible spectroscopic studies

5.4.1.1 General

Data from the spectroscopic changes of **LH₂** were used to gain insight into complexation stoichiometry and the strength of complexation between the ligand and the tested metals.

5.4.1.2 Sensor response for addition of Lu(III) vs. other metals

Optical response to Lu(III) for the deprotonated ligand was observable with the naked eye at 50.0 μM concentration for the 1:1 ratio of both metal and ligand in a solution of acetonitrile, and was confirmed by UV-Vis spectroscopic titrations (Figure 5.1). When diisopropylethylamine (DIPEA-2.5 eq.) was added to a solution of **LH₂** (50.0 μM) in acetonitrile the solution turned bright yellow, a color typical of the *p*-nitrophenolate anion. To this yellow solution, addition of Lu(NO₃)₃·6H₂O at 1:1 ratio to the ligand gave complete instant decoloration, while adding Co(II), Pb(II), Sr(II), Ag(I),

Na(I), K(I) Cs(I) and Ca(II), as nitrate salts under identical conditions, showed no visible changes, La(III) and Sm(III), however showed only a slight decoloration (Figure 5.1). UV-Vis spectra of these solutions which were independently taken (Figure 5.2) suggested that Lu(III) gave the most prominent blue shift from 432 nm to 398 nm, while lesser blue shifts were observed for La(III) and Sm(III). Other metals like Sr(II), K(I), Na(I) and Cs(I) did not cause any noticeable change in the spectrum of the receptor, Ca(II), Co(II), Pb(II) and Ag(I) caused a hypochromic shifts in absorbance, but without any blue or red shift in the absorbance of the receptor, hence the color stayed the same. The color changes with Ln(III) were instantaneous and measurement of the UV-Vis spectrum immediately and after 1 h did not give any noticeable differences, which suggests that thermodynamic equilibrium is achieved in a short time.

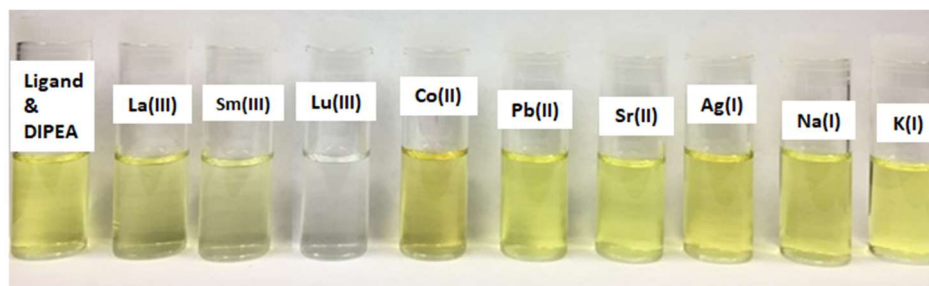


Figure 5.1. Visible color changes of LH_2 ($50.0 \mu\text{M}$) and DIPEA ($125.0 \mu\text{M}$) in CH_3CN before and after the addition of various metals ($50.0 \mu\text{M}$) - $\text{La}(\text{NO}_3)_3 \cdot 6\text{H}_2\text{O}$, $\text{Sm}(\text{NO}_3)_3 \cdot 6\text{H}_2\text{O}$, $\text{Lu}(\text{NO}_3)_3 \cdot 6\text{H}_2\text{O}$, $\text{Co}(\text{NO}_3)_2 \cdot 6\text{H}_2\text{O}$, $\text{Pb}(\text{NO}_3)_2$, $\text{Sr}(\text{NO}_3)_2$, $\text{Ag}(\text{NO}_3)$, NaNO_3 , KNO_3 in CH_3CN .

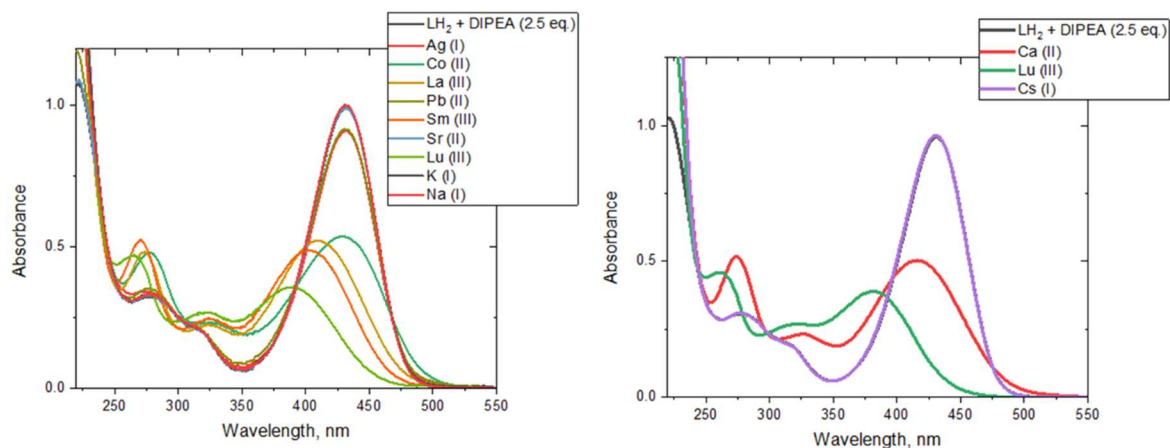


Figure 5.2. UV-Vis spectra for LH_2 ($50.0 \mu\text{M}$) and DIPEA ($125.0 \mu\text{M}$) in CH_3CN before and after addition of various metals ($50.0 \mu\text{M}$). Left: Spectra before and after addition of $\text{Ag}(\text{NO}_3)$, $\text{Co}(\text{NO}_3)_2 \cdot 6\text{H}_2\text{O}$, $\text{La}(\text{NO}_3)_3 \cdot 6\text{H}_2\text{O}$, $\text{Pb}(\text{NO}_3)_2$, $\text{Sm}(\text{NO}_3)_3 \cdot 6\text{H}_2\text{O}$, $\text{Sr}(\text{NO}_3)_2$, $\text{Lu}(\text{NO}_3)_3 \cdot 6\text{H}_2\text{O}$, KNO_3 , and NaNO_3 . Right: Spectra before and after addition of $\text{Ca}(\text{NO}_3)_2 \cdot 4\text{H}_2\text{O}$, $\text{Lu}(\text{NO}_3)_3 \cdot 6\text{H}_2\text{O}$, and CsNO_3 .

5.4.1.3 UV-Vis titrations with Ln(III) salts and determination of binding constants

UV-Vis titration was used to monitor the changes in the spectra of the sensor after Lu(III) additions under constant sensor concentration. Incremental Lu(III) addition ($0 - 17.0 \mu\text{M}$) to LH_2 ($10.0 \mu\text{M}$) / DIPEA ($25.0 \mu\text{M}$) in acetonitrile gave a blue shift of the low energy (LE) absorption at $\lambda_{\text{max}} = 432 \text{ nm}$ ($\epsilon = 29,000 \text{ M}^{-1} \text{ cm}^{-1}$) to $\lambda_{\text{max}} = 398 \text{ nm}$ with three clear isosbestic points at 403 nm , 313 nm and 289 nm , along with a notable decrease of the absorption intensity at 432 nm (Figure 5.3). A new high-energy (HE) band was observed for the complex at 270 nm and saturation was obtained after addition of 1 equivalent of Lu(III), strongly suggesting 1:1 complexation. Plotting the $A_{432 \text{ nm}}$ vs. $[\text{Ln}(\text{III})]_t$ upon titration with several Ln(III) salts at constant ligand / DIPEA concentration and non-linear regression analysis of the binding curve fitted to the 1-1

binding isotherm gave binding constants of $K_{11(\text{Lu})} = 5.8 (\pm 0.4) \times 10^6 \text{ M}^{-1}$ for the formation of the Lu(III) complex (Figure 5.3), which is in similar range with other reported Lu(III) receptors.⁴¹⁻⁴³ For La(III) and Sm(III) lower binding constants of $K_{11(\text{La})} = 2.8 (\pm 0.8) \times 10^6 \text{ M}^{-1}$ and $K_{11(\text{Sm})} = 3.0 (\pm 0.4) \times 10^6 \text{ M}^{-1}$, respectively, were obtained. The stronger coordination of the sulfonamidophenol with Lu(III) vs. earlier Ln(III) is consistent with the size contraction across the Ln series⁴² and prior examples with other O- and N- donor ligands.⁶⁰ Control titration experiments performed with addition of Lu(III) i) to DIPEA (without **LH**₂) and ii) to **LH**₂ (without DIPEA) demonstrated that the ligand can only complex Lu(III) in its deprotonated form as a result of the alkalinity of the medium, and that the spectral changes in both the LE and HE bands are due to Ln(III) complexation and not due to interaction with DIPEA (Figure 5.4). **LH**₂ is expected to be in a bis-deprotonated form in alkaline conditions as the *p*-nitrophenolic OH has a pK_a in the range of 7.15 - 7.91,^{61,62,63} while the sulfonamide NH has an estimated pK_a of 7 - 8.⁶⁴

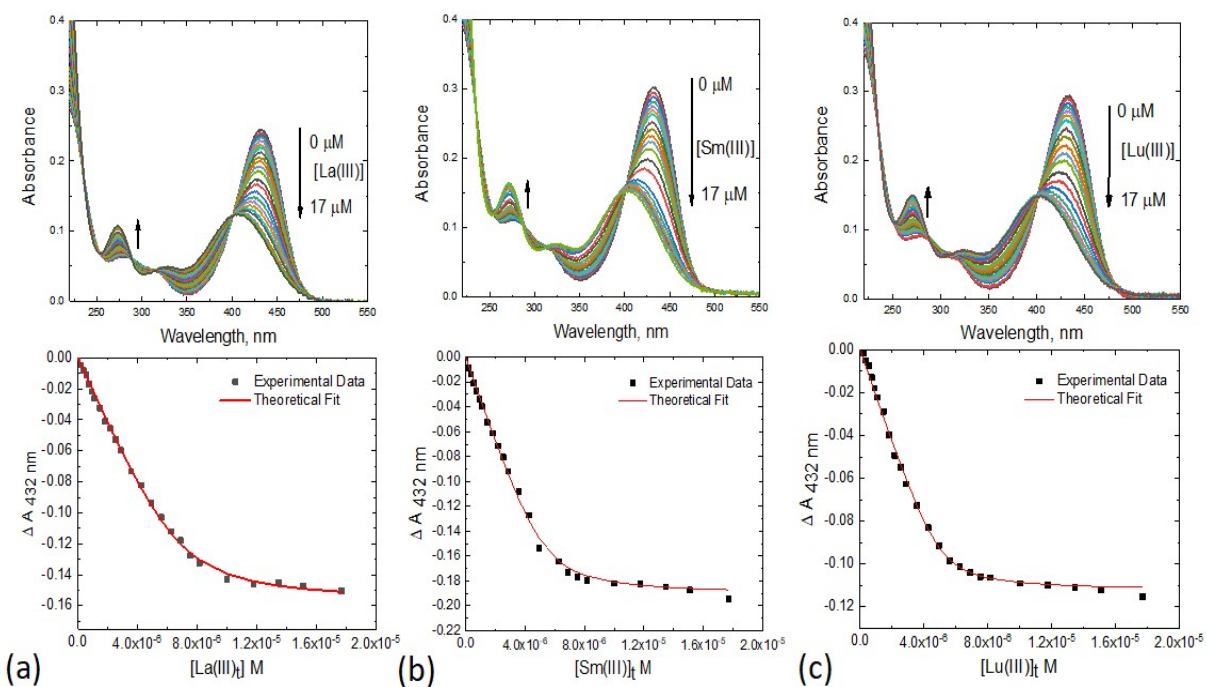


Figure 5.3. UV-Vis titration spectra for LH_2 ($1.0 \times 10^{-5} \text{ M}$) / DIPEA ($2.5 \times 10^{-5} \text{ M}$) with $\text{Ln}(\text{NO}_3)_3 \cdot 6\text{H}_2\text{O}$ ($1.0 \times 10^{-4} \text{ M}$) in CH_3CN (top), and fitted titration plots of $\Delta A_{432 \text{ nm}}$ vs. $[\text{M}]_t$ (bottom) for (a) La(III) (b) Sm(III) (c) Lu(III).

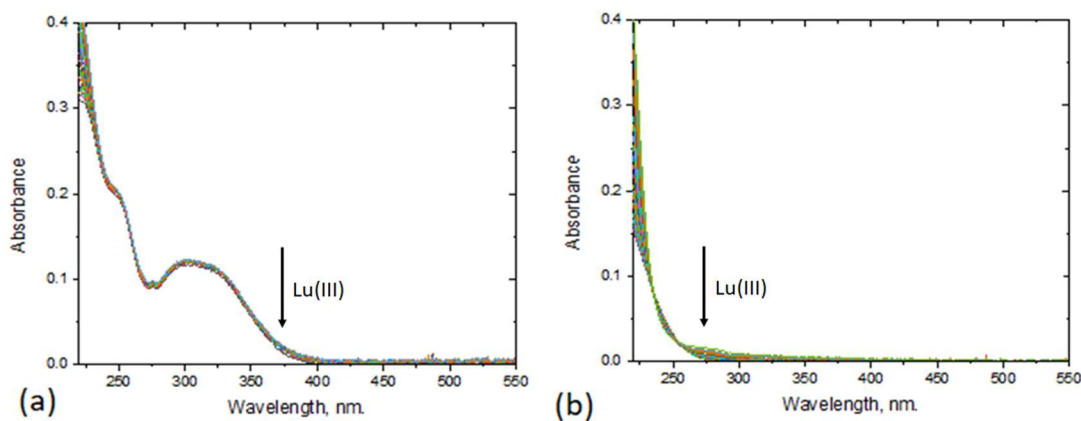


Figure 5.4. Control titrations of (a) LH_2 ($1.0 \times 10^{-5} \text{ M}$) without DIPEA in CH_3CN with $\text{Lu}(\text{NO}_3)_3 \cdot 6\text{H}_2\text{O}$ ($0 - 1.7 \times 10^{-5} \text{ M}$ added) (b) DIPEA ($2.5 \times 10^{-5} \text{ M}$) without LH_2 in CH_3CN with $\text{Lu}(\text{NO}_3)_3 \cdot 6\text{H}_2\text{O}$ ($0 - 1.7 \times 10^{-5} \text{ M}$ added).

5.4.1.4 UV-Vis sensing response for Lu(III): Comparison in the presence of competing metals

Titration of LH_2 (1.0×10^{-5} M) and DIPEA (2.5×10^{-5} M) with Na(I), K(I), Cs(I) or Sr(II) (each at 1.0×10^{-4} M respectively) showed no changes in the UV-Vis spectra compared to changes in absorbance exhibited when Lu(III) (1.0×10^{-4} M) was used for the titration (Figure 5.5). Competitive experiments were also performed to compare the sensing response at high background concentrations of potentially competing metals (Na/Lu and K/Lu ratios as high as 5000 and 1000 respectively), which simulate alkaline HLW conditions (Figure 5.6). Monitoring the changes in the LE absorbance ($\lambda_{\text{max}} = 432$ nm) at gradually increasing concentration of Lu(III) (0 – 12.0 μM) and in the presence of constant excess concentration of Na(I) (5.0×10^{-3} M), K(I) (1.0×10^{-3} M) and Sr(II) (2.0×10^{-4} M) revealed only minimal changes with a practically identical response in the presence *vs.* absence of the Na/K/Sr matrix (Figure 5.6). Thus the sensor is not only highly selective for Lu(III) in the presence of these metals in alkaline conditions, but also shows a linear response range of 0 – 4.93 μM for Lu(III) detection with a limit of detection as low as 0.207 μM , in the presence of these metals.

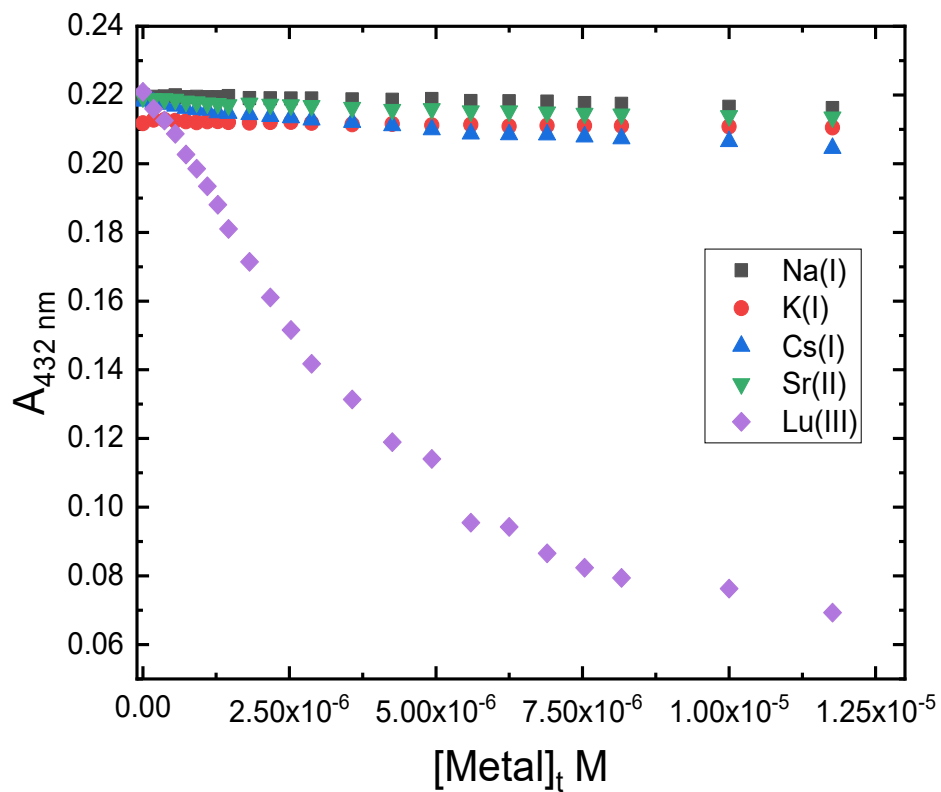


Figure 5.5. (a) Plots of A_{432nm} vs $[M]_t$ for titrations of LH_2 ($1.0 \times 10^{-5} M$) and DIPEA ($2.5 \times 10^{-5} M$) with Na(I), K(I), Sr(II) or Lu(III) (each $1.0 \times 10^{-4} M$) when titrated independently in CH_3CN .

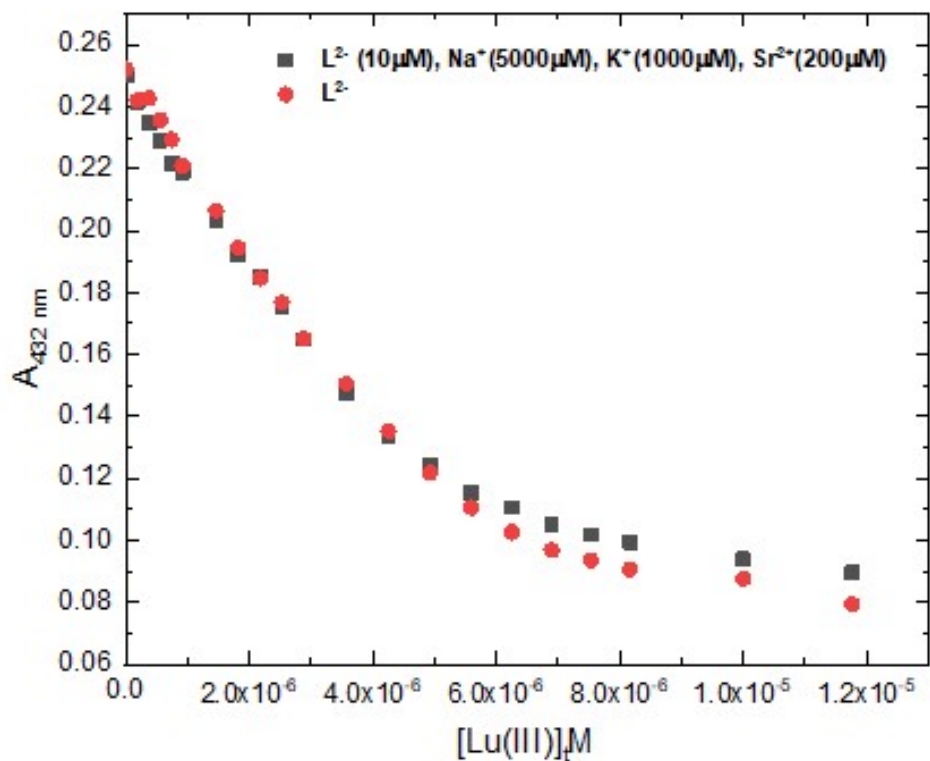


Figure 5.6. Competitive titration of LH_2 ($1.0 \times 10^{-5} \text{ M}$) with Lu(III) ($0 - 1.2 \times 10^{-5} \text{ M}$ added) in excess constant concentration of other metals ($\text{Na(I)} = 5.0 \times 10^{-3} \text{ M}$, $\text{K(I)} = 1.0 \times 10^{-3} \text{ M}$, $\text{Sr(II)} = 2.0 \times 10^{-4} \text{ M}$) in CH_3CN (black). Titration of LH_2 with Lu(III) in absence of other metals (red).

5.4.2 DFT calculations

To gain insight into the structure of the complex in solution and changes in the electronic environment of the ligand upon Lu(III) complexation, DFT calculations were performed, which also included a study for the HOMO to LUMO transition in the ligand LH_2 , bis-deprotonated ligand L^{2-} , and the formed complex in CH_3CN , for which the structure $\text{Lu(III)L(NO}_3\text{)(H}_2\text{O)}_5$ showed an energy minimum (Figure 5.7). In this complex, L binds in a bidentate fashion through the phenolate O- and sulfonamide N-, with five H_2O and one monodentate NO_3 completing an 8-coordinate environment. The

calculated bond lengths (Å) were found to be Lu – O = 2.138; Lu – N = 2.656; Lu – O (NO₃⁻) = 2.459; Lu – O (H₂O) = 2.293 – 2.463. The changes in electron density and energies of the HOMO and LUMO provide explanation for the changes in the experimental spectra (Figure 5.7 and 5.8). The HOMO and LUMO for L²⁻ (Figure 5.8 - left) as compared to LH₂ (Figure 5.9), predictably shows electron density shifts from the tolyl ring to the *o*-nitrophenyl ring. Upon complexation (Figure 5.8 - right) some of this electron density is transferred to the metal, and as a result of complexation, the energy gap between the HOMO and LUMO increases from to 2.54 eV in L²⁻, to 3.11 eV for Lu(III)L(NO₃)(H₂O)₅. The TD-DFT calculation corresponded to λ_{max} of 489 nm and 398 nm, with oscillator strengths of 0.1875 and 0.1934, respectively. These computed λ_{max} values show reasonable agreement with the experimentally observed λ_{max} of 432 nm and 398 nm for L²⁻ and the Lu(III) complex (Figure. 5.10).

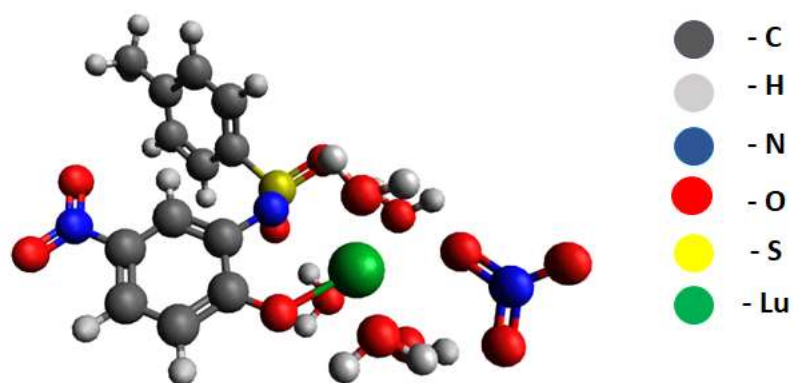


Figure 5.7. DFT optimization of the Lu(III) complex in CH₃CN, minimized as Lu(III)L(NO₃)(H₂O)₅.

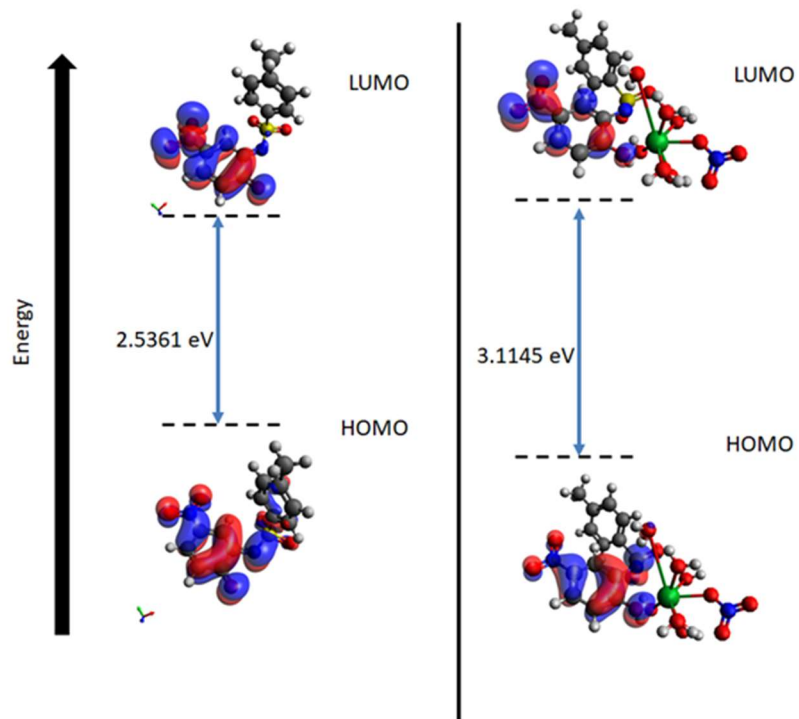


Figure 5.8. HOMO – LUMO energy transitions for L^{2-} (left) and $Lu(III)L(NO_3)(H_2O)_5$ (right).

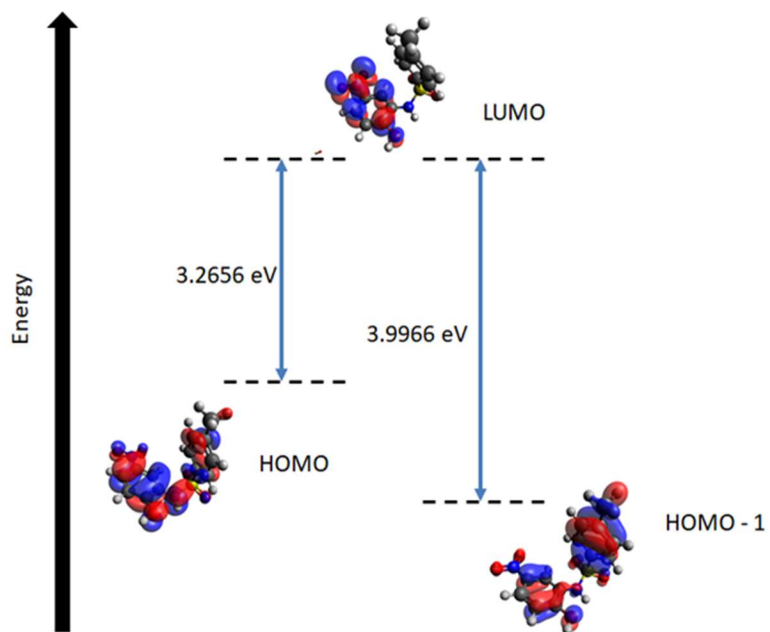


Figure 5.9. HOMO – LUMO (left) and HOMO-1 – LUMO (right) transitions in the ligand LH_2 .

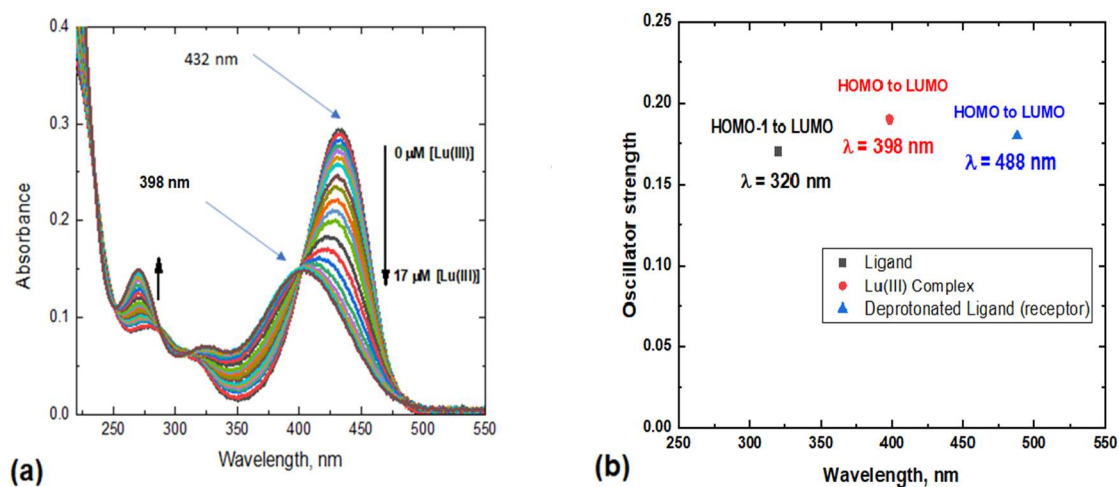


Figure 5.10. (a) Experimental UV-Vis Spectra of LH_2 ($1.0 \times 10^{-5} \text{ M}$) and DIPEA ($2.5 \times 10^{-5} \text{ M}$) upon titration with Lu(III) ($1.0 \times 10^{-4} \text{ M}$) showing wavelength maxima for L^{2-} at 432 nm and the Lu(III)-L complex at 398 nm. (b) Absorption spectra from TD-DFT calculations showing calculated wavelengths and oscillator strengths for LH_2 , L^{2-} and the Lu(III)-L complex $\text{Lu(III)L(NO}_3)(\text{H}_2\text{O})_5$.

5.4.3 Electrochemistry

Acetonitrile solutions containing 0.1 M tetrabutylammonium hexafluorophosphate (TBAPF₆) were used for all electrochemical experiments. CVs of 1.0 mM ligand LH_2 with 2.5 equivalents of DIPEA featured a single irreversible oxidation event at 0.39 V vs. Fc^+/Fc (Figure 5.11). Scan rate-dependent studies between 10 mV/s and 400 mV/s indicated that this feature was a diffusion-limited solution-based oxidation event. As expected, CVs of 1.0 mM Lu(III) nitrate do not feature any redox events within the solvent window of interest (Figure 5.12). CVs of a solution containing 0.1 M TBAPF₆ and a mixture of 1.0 mM Lu(III) and 1.0 mM LH_2 (with 2.5 equivalents of DIPEA) were acquired after mixing for 30 min. The formation of a complex was consistent with the CVs, which were different from those of the individual components

(Figure 5.13). Two ligand-based irreversible oxidation events at 0.65 V vs. Fc^+/Fc and 0.85 V vs. Fc^+/Fc , and a reduction at 0.14 V vs. Fc^+/Fc was observed. At slow scan rates, there was a shoulder corresponding to the re-reduction of the product formed after the second oxidation at 0.73 V vs. Fc^+/Fc . The difference in redox potential between the oxidation and reduction events for this couple was 120 mV, and is indicative of an electrochemically irreversible event ($\Delta E = 120$ mV). Varying the scan limits indicates that the reduction at 0.14 V is present even if only the first oxidation event occurs (Figure 5.14). Scan-rate dependent studies from 200 mV/s to 20 mV/s show that all three observed redox events are diffusion limited (Figure 5.15). The slopes of lines representing the peak current vs. the square-root of the scan rate for both oxidation events were equal, indicating that they have similar diffusion coefficients. The reduction event was less pronounced at slower scan rates, indicating that there are both chemical, and electrochemical steps involved in the oxidation events, such that at slow scan rates, significant chemical transformation had occurred near the electrode surface, resulting in negligible concentration of the species responsible for the reduction at 0.14 V. Titrating **LH₂** into a solution containing Lu(III) without the addition of DIPEA resulted in no net complexation (Figure 5.16).

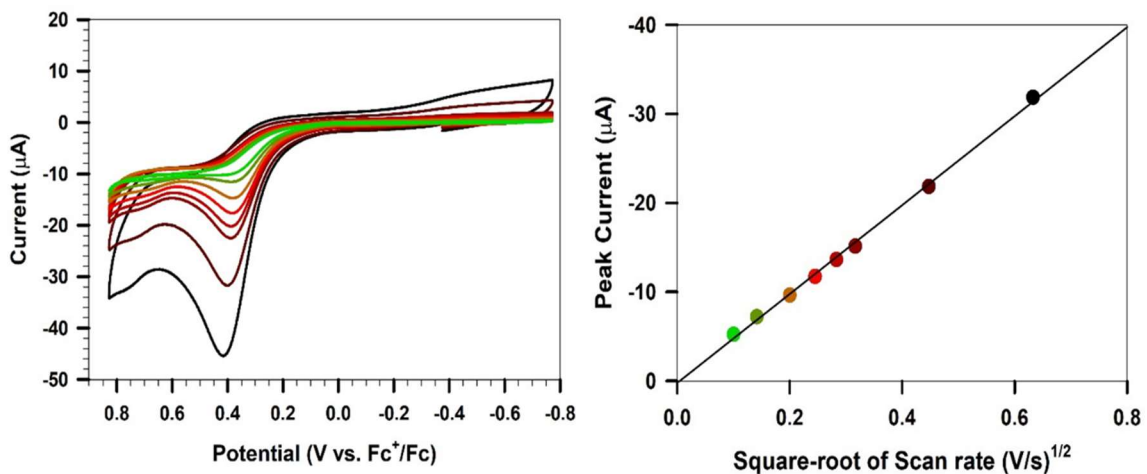


Figure 5.11. Left: CVs of 1.0 mM of free ligand LH_2 with 2.5 equivalents of DIPEA with scan rates varying from 400 mV/s (black), to 10 mV/s (green); Right: associated peak currents at each acquired scan rate.

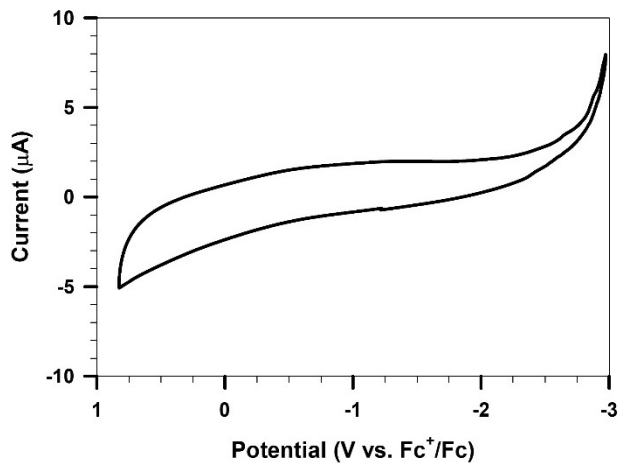


Figure 5.12. CV of a 1.0 mM Lu(III) solution acquired at 100 mV/s, showing no redox events.

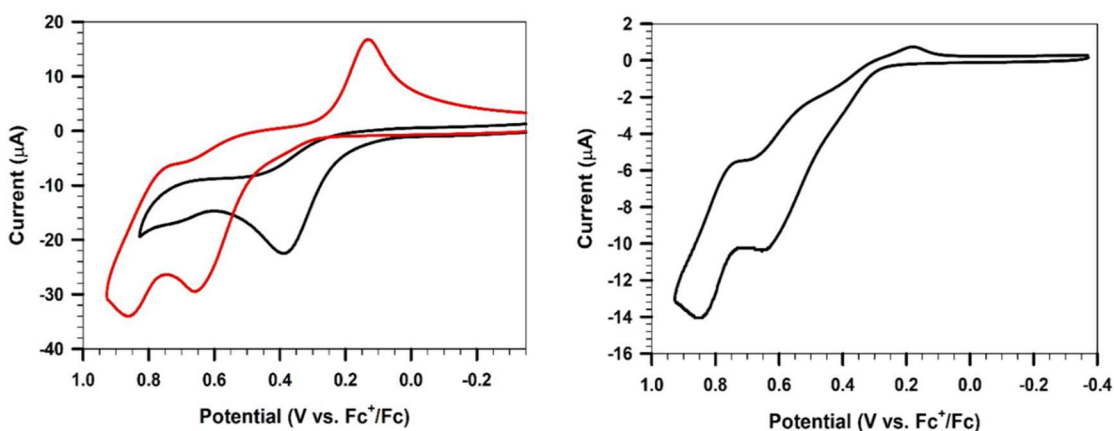


Figure 5.13. Left: Comparisons of CVs at 100 mV/s containing solutions of 1.0 mM LH_2 and 2.5 equivalents of DIPEA without Lu(III) (black), and with 1.0 mM Lu(III) (red). Right: CV at 20 mV/s of a solution containing 1.0 mM $\text{Lu}(\text{NO}_3)_3 \cdot \text{H}_2\text{O}$ and 1.0 mM LH_2 (with 2.5 equivalents of DIPEA) after mixing for 30 min.

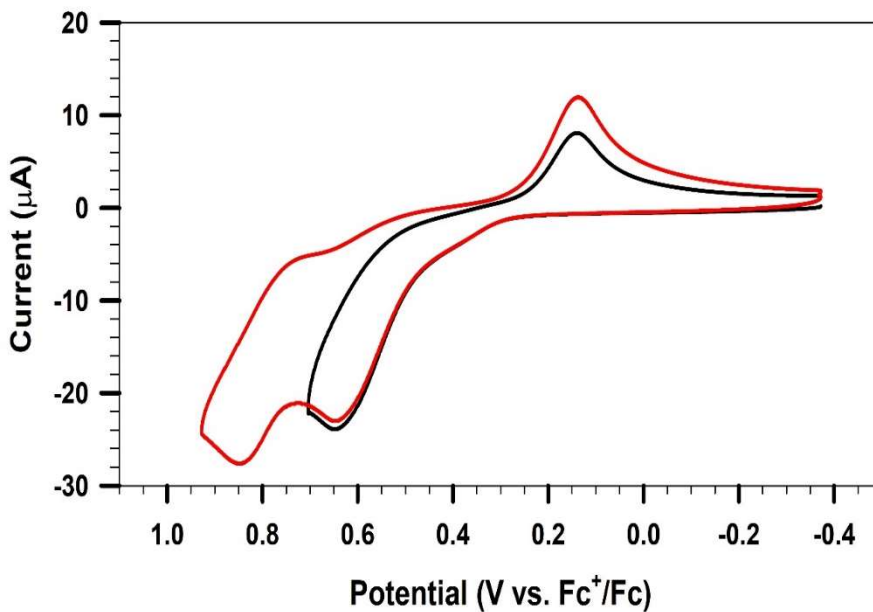


Figure 5.14. CV cycles of a solution containing 1.0 mM Lu(III) and 1.0 mM LH_2 (with 2.5 added equivalents of DIPEA). The first scan (black) reverses direction after the first oxidation event (+0.7 V), while the second scan (red) features both ligand-based oxidation events.

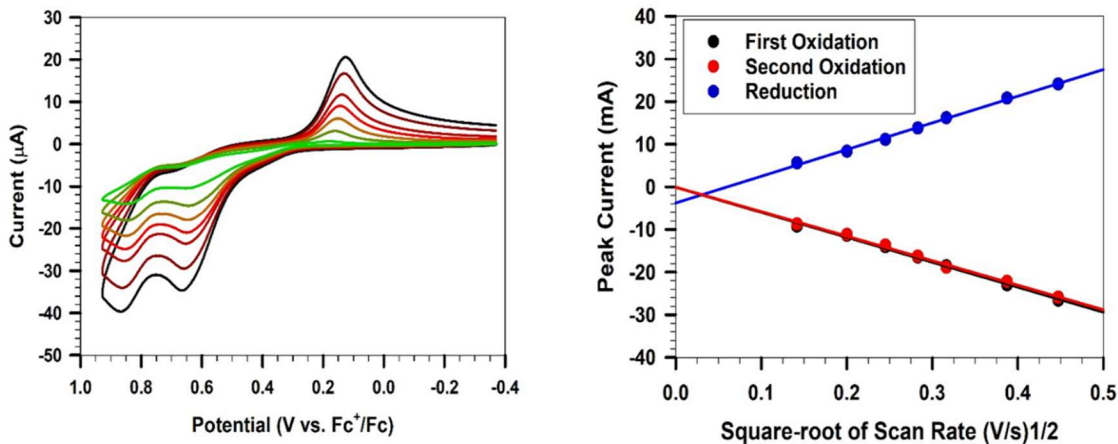


Figure 5.15. Left: CVs of a solution containing 1.0 mM of Lu(III), 1.0 mM LH₂, and 2.5 equivalents of DIPEA with scan rates varying from 200 mV/s (black) to 20 mV/s (green); Right: associated peak currents at each acquired scan rate for the first oxidation event at 0.65 V (black), the second oxidation event at 0.85 V (red), and the reduction event at 0.14 V (blue).

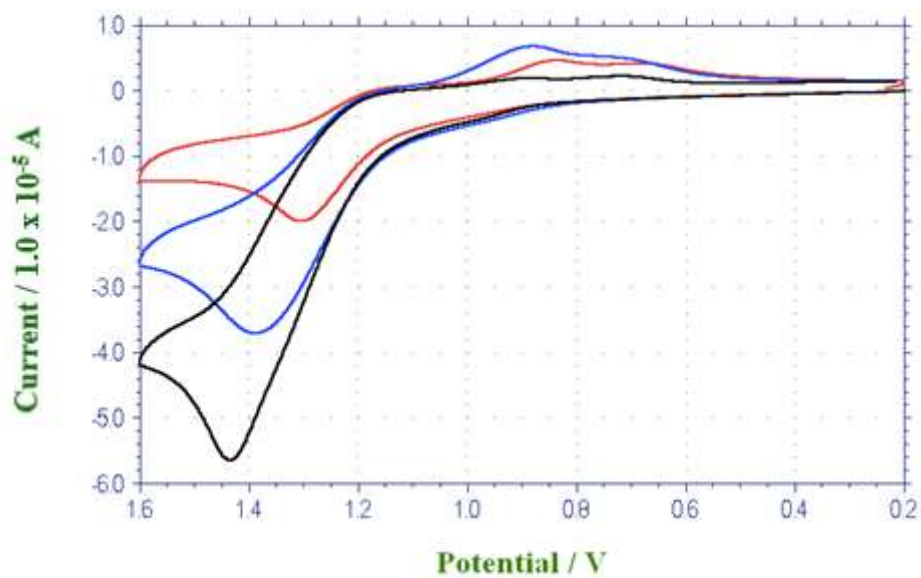


Figure 5.16. CVs of a solution containing 1.0 mM of Lu(III) and 1.0 mM LH₂ (red), 2.0 mM LH₂ (blue), 3.0 mM LH₂ (black), without any DIPEA. The scan rate in all cases is 100 mV/s, and the potential is referenced to Ag/AgCl.

5.4.4 X-ray crystallography for LH_2 , $(\text{Et}_3\text{NH})_5[\text{Lu}_3(\mu_3\text{-OH})_2(\text{LH})_6(\mu\text{-L})_3]$ and $(\text{Et}_3\text{NH})_3[\text{Lu}(\text{LH})_6]$

5.4.4.1 X-ray crystallography for LH_2

Yellow crystals of LH_2 suitable for X-ray crystallography were obtained by slow evaporation of dichloromethane from a solution of the ligand in dichloromethane at ambient temperature. LH_2 crystallized in the monoclinic system and space group $P2_1/c$. Both the aryl rings of the ligand are highly planar (with mean deviation, 0.006 Å). All bond lengths are within the expected ranges for LH_2 . Table 5.1 gives the summary of the single X-ray crystallographic data of LH_2 while its structure is as shown in Figure 5.17.

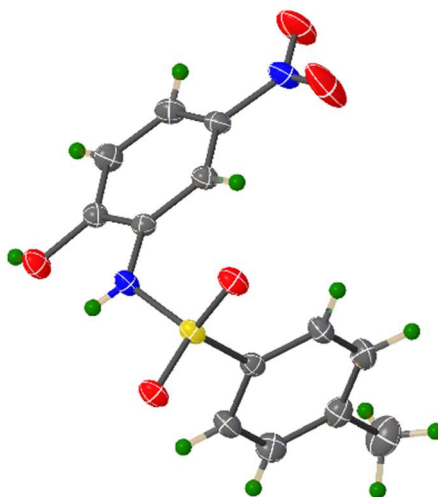


Figure 5.17. X-ray crystal structure of LH_2 (ORTEP plot - 50% probability ellipsoids).

Table 5.1: Crystal data and structure refinement for LH_2

Crystal data

Chemical formula $\text{C}_{13}\text{H}_{12}\text{N}_2\text{O}_5\text{S}$

Mr 1233.22

Crystal system, space group	Monoclinic, $P2_1/c$
Temperature (K)	298
a, b, c (Å)	9.698(2), 13.667(2), 10.472(2)
β (°)	95.075 (7)
V (Å ³)	1382.5 (4)
Z	4
Radiation type	Mo $K\alpha$
μ (mm ⁻¹)	0.26
Crystal size (mm)	0.25 × 0.21 × 0.17
Data collection	
Diffractometer	Bruker D8 Quest PHOTON 100
Absorption correction	Multi-scan <i>SADABS</i> 2016/2: Krause, L., Herbst-Irmer, R., Sheldrick G.M. & Stalke D., <i>J. Appl. Cryst.</i> 48 (2015)3-10.
T_{\min}, T_{\max}	0.708, 0.745
No. of measured, independent and observed [$I > 2\sigma(I)$] reflections	13808, 2331, 2203
R_{int}	0.014
$(\sin \theta/\lambda)_{\text{max}}$ (Å ⁻¹)	0.588
Refinement	
$R[F^2 > 2\sigma(F^2)], wR(F^2), S$	0.031, 0.083, 1.05
No. of reflections	2331
No. of parameters	238

H-atom treatment All H-atom parameters refined
 $\Delta\rho_{\max}, \Delta\rho_{\min}$ (e Å⁻³) 0.26, -0.29

Table 5.2: Fractional atomic coordinates and isotropic or equivalent isotropic displacement parameters (Å²) for **LH₂**

	<i>x</i>	<i>y</i>	<i>z</i>	<i>U</i> _{iso} */ <i>U</i> _{eq}
S1	0.17223 (4)	0.54670 (3)	0.87427 (3)	0.03302 (15)
O5	0.11787 (12)	0.57068 (8)	0.99341 (10)	0.0427 (3)
O4	0.21603 (12)	0.62610 (8)	0.79670 (11)	0.0425 (3)
O1	-0.09478 (13)	0.32188 (10)	0.73927 (12)	0.0476 (3)
N2	0.04647 (14)	0.48819 (10)	0.79046 (13)	0.0358 (3)
C1	0.06723 (15)	0.43606 (11)	0.67606 (14)	0.0314 (3)
O3	0.3383 (2)	0.51828 (15)	0.41850 (18)	0.1029 (7)
C6	-0.00896 (16)	0.34972 (11)	0.64998 (15)	0.0356 (3)
C11	0.3942 (2)	0.31722 (14)	1.00777 (19)	0.0499 (4)
C5	0.00467 (19)	0.29811 (13)	0.53743 (16)	0.0438 (4)
O2	0.28764 (19)	0.39533 (14)	0.29823 (14)	0.0841 (5)
C7	0.30789 (16)	0.46181 (11)	0.90036 (14)	0.0335 (3)
N1	0.27233 (17)	0.44456 (12)	0.39293 (14)	0.0520 (4)
C2	0.15751 (17)	0.46804 (12)	0.58989 (15)	0.0356 (3)
C8	0.42068 (18)	0.46359 (14)	0.82805 (17)	0.0437 (4)
C4	0.09670 (19)	0.32866 (13)	0.45217 (16)	0.0438 (4)
C12	0.29454 (19)	0.38927 (13)	0.99167 (16)	0.0433 (4)
C10	0.50579 (18)	0.31525 (13)	0.93354 (18)	0.0467 (4)
C13	0.6102 (3)	0.2331 (2)	0.9482 (3)	0.0737 (7)
C3	0.17218 (16)	0.41241 (12)	0.48060 (14)	0.0371 (4)
C9	0.51837 (19)	0.38987 (15)	0.84538 (18)	0.0513 (5)
H2	-0.003 (2)	0.4633 (14)	0.8344 (19)	0.043 (5)*
H12	0.221 (2)	0.3895 (14)	1.0401 (19)	0.053 (5)*

H5	-0.045 (2)	0.2433 (16)	0.5201 (19)	0.055 (5)*
H2A	0.207 (2)	0.5258 (15)	0.6043 (18)	0.048 (5)*
H8	0.428 (2)	0.5169 (15)	0.768 (2)	0.056 (5)*
H9	0.600 (2)	0.3913 (16)	0.797 (2)	0.066 (6)*
H4	0.108 (2)	0.2933 (15)	0.375 (2)	0.059 (6)*
H11	0.384 (2)	0.2685 (17)	1.070 (2)	0.065 (6)*
H1	-0.127 (2)	0.2727 (17)	0.721 (2)	0.059 (7)*
H13A	0.579 (4)	0.180 (3)	0.896 (4)	0.138 (13)*
H13B	0.700 (4)	0.253 (3)	0.934 (4)	0.138 (13)*
H13C	0.622 (4)	0.207 (3)	1.036 (4)	0.149 (15)*

Atomic displacement parameters (\AA^2) for **LH₂**

	U_{11}	U_{22}	U_{33}	U_{12}
S1	0.0433 (2)	0.0267 (2)	0.0306 (2)	-0.00174 (14)
O5	0.0562 (7)	0.0380 (6)	0.0364 (6)	-0.0024 (5)
O4	0.0583 (7)	0.0291 (6)	0.0422 (6)	-0.0036 (5)
O1	0.0544 (7)	0.0429 (7)	0.0474 (7)	-0.0141 (6)
N2	0.0396 (7)	0.0359 (7)	0.0333 (7)	-0.0030 (6)
C1	0.0355 (8)	0.0303 (7)	0.0284 (7)	0.0041 (6)
O3	0.1369 (17)	0.0970 (13)	0.0851 (12)	-0.0635 (13)
C6	0.0374 (8)	0.0337 (8)	0.0357 (8)	0.0007 (6)
C11	0.0567 (11)	0.0404 (10)	0.0525 (10)	-0.0006 (8)
C5	0.0509 (10)	0.0357 (9)	0.0445 (9)	-0.0073 (8)
O2	0.1081 (13)	0.0999 (13)	0.0502 (9)	-0.0173 (11)
C7	0.0394 (8)	0.0315 (8)	0.0302 (7)	-0.0037 (6)
N1	0.0626 (10)	0.0586 (10)	0.0369 (8)	-0.0026 (8)
C2	0.0415 (8)	0.0335 (8)	0.0319 (8)	-0.0022 (7)
C8	0.0435 (9)	0.0482 (10)	0.0408 (9)	-0.0033 (7)
C4	0.0546 (10)	0.0426 (9)	0.0343 (8)	0.0025 (8)
C12	0.0477 (9)	0.0423 (9)	0.0420 (9)	-0.0003 (7)

C10	0.0436 (9)	0.0428 (10)	0.0527 (10)	0.0022 (7)
C13	0.0612 (14)	0.0611 (15)	0.097 (2)	0.0196 (12)
C3	0.0425 (8)	0.0405 (9)	0.0286 (7)	0.0032 (7)
C9	0.0417 (9)	0.0619 (12)	0.0521 (11)	0.0037 (8)

Geometric parameters (Å, °)

S1—O5	1.4347 (11)	C11—C10	1.387 (3)
S1—O4	1.4418 (11)	C5—C4	1.382 (3)
S1—N2	1.6455 (14)	O2—N1	1.218 (2)
S1—C7	1.7573 (16)	C7—C8	1.385 (2)
O1—C6	1.3600 (19)	C7—C12	1.391 (2)
N2—C1	1.4234 (19)	N1—C3	1.462 (2)
C1—C6	1.406 (2)	C2—C3	1.392 (2)
C1—C2	1.383 (2)	C8—C9	1.384 (3)
O3—N1	1.210 (2)	C4—C3	1.377 (2)
C6—C5	1.390 (2)	C10—C13	1.511 (3)
C11—C12	1.380 (3)	C10—C9	1.388 (3)
O5—S1—O4	117.86 (7)	C8—C7—C12	120.96 (15)
O5—S1—N2	105.24 (7)	C12—C7—S1	117.60 (12)
O5—S1—C7	110.07 (7)	O3—N1—O2	122.66 (17)
O4—S1—N2	107.85 (7)	O3—N1—C3	118.59 (15)
O4—S1—C7	109.31 (7)	O2—N1—C3	118.74 (16)
N2—S1—C7	105.75 (7)	C1—C2—C3	118.73 (15)
C1—N2—S1	122.60 (11)	C9—C8—C7	118.70 (17)
C6—C1—N2	118.20 (13)	C3—C4—C5	118.22 (15)
C2—C1—N2	122.41 (14)	C11—C12—C7	119.06 (16)
C2—C1—C6	119.39 (14)	C11—C10—C13	120.4 (2)
O1—C6—C1	116.38 (14)	C11—C10—C9	118.50 (17)
O1—C6—C5	123.43 (15)	C9—C10—C13	121.1 (2)
C5—C6—C1	120.19 (14)	C2—C3—N1	118.30 (15)

C12—C11—C10	121.21 (17)	C4—C3—N1	118.95 (14)
C4—C5—C6	120.66 (16)	C4—C3—C2	122.74 (15)
C8—C7—S1	121.35 (13)	C8—C9—C10	121.51 (17)

5.4.4.2 X-ray crystallography for $(\text{Et}_3\text{NH})_5[\text{Lu}_3(\mu_3\text{-OH})_2(\text{LH})_6(\mu\text{-L})_3]$

The formation of a trimeric Lu(III) cluster was confirmed by X-ray diffraction studies, with crystal data, data collection, and structural refinement details summarized in Table 5.3 below. The trimeric Lu(III) complex was solved and refined in a Hexagonal, $P6_3/m$ space group. Single crystal X-ray diffraction of fragile amber needle-like crystals obtained from slow evaporation of solutions of LH_2 , Et_3N , and $\text{Lu}(\text{NO}_3)_3(\text{H}_2\text{O})_6$ revealed the structure of a Lu(III) complex with anionic formula $[\text{Lu}_3(\mu_3\text{-OH})_2(\text{LH})_6(\text{L})_3]^{5-}$ (Figure 5.18 and 5.19) along with 5 triethylammonium counteranions. Despite some shortcomings due to severe disorder, which prevented complete convergence during refinement, the connectivity and the geometry was revealed unambiguously, showing a unique bis(μ -hydroxo) trinuclear Lu(III) cluster formed by three bis-deprotonated ligands (L^{2-}) binding equatorially. Each Lu(III) is also coordinated at axial positions to two mono deprotonated ligands (LH^-) through the phenolato oxygen. Each bidentate ligand forms a Lu-O-Lu bridge via the phenolato oxygen, while two additional $\mu_3\text{-OH}$ cap the three Lu(III) above and below the $\text{Lu}_3(\text{III})$ plane. Polynuclear hydroxo-bridged Ln(III) complexes are hard to isolate due to difficulty in controlling their coordination spheres, as Ln(III) are hard acids.^{65,66} Several clusters with hydroxo – bridged d- and f-

elements have been reported, but this is to the best of our knowledge the first cluster with a unique hydroxo-bridged trinuclear core motif for Lu(III).⁶⁵⁻⁶⁹

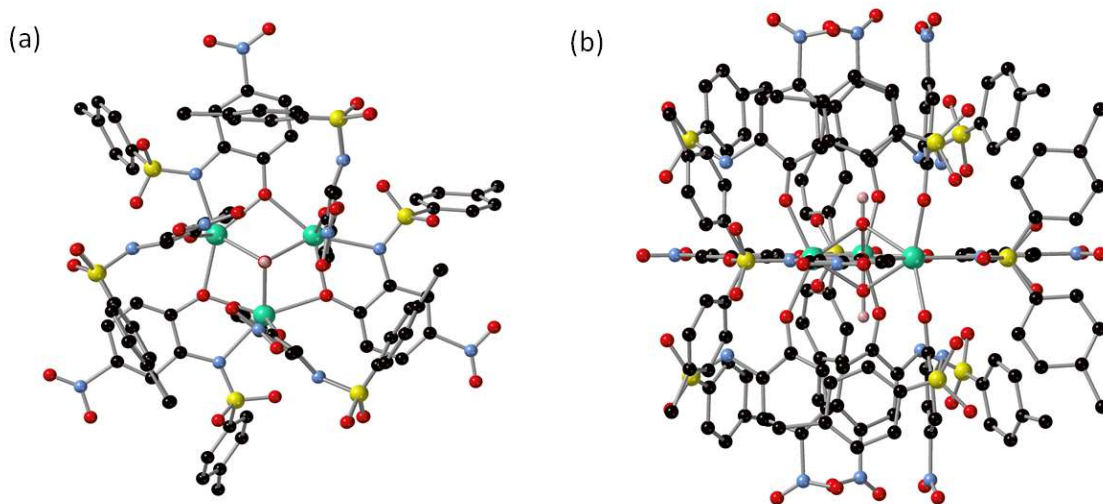


Figure 5.18. X-ray structure of the anionic $[Lu_3(\mu_3-OH)_2(LH)_6(\mu-L)_3]^{3-}$ (ball-and-stick diagram - five Et_3NH^+ are not shown). (a) view down the threefold axis, showing three equatorial L^{2-} bridging three Lu(III) (b) Projected view perpendicular to the 3-fold axis with hydrogens omitted for clarity. Color code: teal = Lu, red = O, yellow = S, blue = N, and black = C.

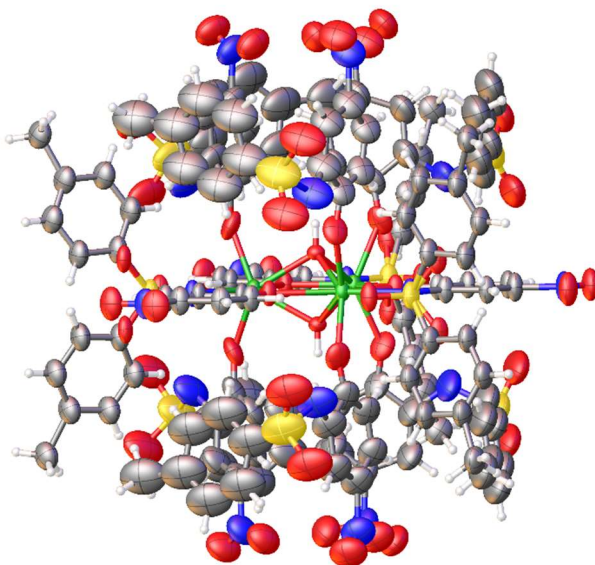


Figure 5.19. ORTEP representation of the anionic $[Lu_3(\mu_3-OH)_2(LH)_6(L)_3]^{3-}$ (30% probability ellipsoids) Projected view perpendicular to the 3-fold axis (five Et_3NH^+ are not shown).

Table 5.3: X-ray Crystallography data for (Et₃NH)₅[Lu₃(μ₃-OH)₂(LH)₆(μ-L)₃]Experimental details

Crystal data

Chemical formula	C ₁₁₇ H ₉₂ Lu ₃ N ₁₈ O ₄₇ S ₉
<i>Mr</i>	3315.46
Crystal system, space group	Hexagonal, <i>P6₃/m</i>
Temperature (K)	150
<i>a</i> , <i>c</i> (Å)	18.3364(9), 28.888(2)
<i>V</i> (Å ³)	8412(1)
<i>Z</i>	2.0
Radiation type	Mo <i>K</i> α
<i>μ</i> (mm ⁻¹)	1.93
Crystal size (mm)	0.18 × 0.07 × 0.03
Data collection	
Diffractometer	Bruker D8 Quest PHOTON II
Absorption correction	<i>SADABS</i> 2016/2: Krause, L., Herbst-Irmer, R., Sheldrick G.M. & Stalke D., <i>J. Appl. Cryst.</i> 48 (2015)3-10.
<i>T</i> _{min} , <i>T</i> _{max}	0.652, 0.745
No. of measured, independent and observed [<i>I</i> > 2σ(<i>I</i>)] reflections	91749, 5275, 3545
<i>R</i> _{int}	0.127
(sin θ/λ) _{max} (Å ⁻¹)	0.604
Refinement	
R[<i>F</i> ² > 2σ(<i>F</i> ²)], wR(<i>F</i> ²), <i>S</i>	0.157, 0.401, 1.21

No. of reflections	5275
No. of parameters	328
No. of restraints	605
H-atom treatment	H atoms treated by a mixture of independent and constrained refinement
	$w = 1/[\sigma^2(F^2) + (0.1311P)^2 + 149.4661P]$
	where $P = (F^2 + 2F^2)/3$
$(\Delta/\sigma)_{\max}$	0.522
$\Delta\rho_{\max}, \Delta\rho_{\min}$ (e Å ⁻³)	1.83, -5.94

Fractional atomic coordinates and isotropic or equivalent isotropic displacement parameters (Å²)

	<i>x</i>	<i>y</i>	<i>z</i>	<i>U</i> _{iso} */ <i>U</i> _{eq}	<i>Occ.</i> (<1)
Lu1	0.30246 (7)	0.54574 (7)	0.250000	0.0749 (5)	
S1	0.0567 (6)	0.6876 (6)	0.250000	0.116 (3)	
S2	0.0510 (12)	0.3124 (14)	0.1099 (8)	0.329 (9)	
O1	0.333333	0.666667	0.2893 (8)	0.076 (5)	
O2	0.1807 (13)	0.5544 (12)	0.250000	0.099 (5)	
O3	-0.193 (2)	0.272 (2)	0.250000	0.184 (9)	
O4	-0.1996 (19)	0.385 (2)	0.250000	0.178 (9)	
O6	0.1243 (14)	0.7698 (13)	0.250000	0.128 (6)	
O7	0.2588 (16)	0.4915 (14)	0.1810 (10)	0.163 (6)	
O8	0.374 (3)	0.580 (3)	-0.0209 (14)	0.264 (13)	
O9	0.254 (3)	0.465 (3)	-0.0329 (14)	0.274 (13)	
O10	0.028 (3)	0.258 (3)	0.1533 (16)	0.342 (14)	
O11	0.059 (3)	0.255 (3)	0.0719 (16)	0.350 (13)	
N1	-0.164 (2)	0.345 (2)	0.250000	0.154 (6)	
N2	0.0939 (16)	0.6291 (15)	0.250000	0.106 (4)	

N3	0.304 (3)	0.517 (3)	-0.0128 (19)	0.241 (9)
N4	0.148 (3)	0.374 (3)	0.1356 (17)	0.286 (9)
C1	0.0973 (18)	0.4962 (17)	0.250000	0.095 (4)
C2	0.063 (2)	0.4154 (18)	0.250000	0.105 (5)
H2	0.097365	0.390505	0.250000	0.126*
C3	-0.020 (2)	0.367 (2)	0.250000	0.121 (5)
H3	-0.046560	0.306884	0.250000	0.145*
C4	-0.065 (2)	0.409 (2)	0.250000	0.129 (5)
C5	-0.038 (2)	0.493 (2)	0.250000	0.117 (5)
H5	-0.073979	0.516795	0.250000	0.141*
C6	0.0496 (19)	0.5396 (19)	0.250000	0.105 (4)
C14	0.274 (3)	0.497 (3)	0.1379 (19)	0.189 (7)
C15	0.346 (3)	0.555 (3)	0.1182 (18)	0.188 (7)
H15	0.390382	0.593441	0.137663	0.225*
C16	0.359 (3)	0.561 (3)	0.0731 (19)	0.203 (8)
H16	0.412134	0.602090	0.061817	0.244*
C17	0.302 (4)	0.514 (3)	0.044 (2)	0.223 (8)
C18	0.219 (3)	0.443 (3)	0.0606 (19)	0.229 (8)
H18	0.177090	0.402843	0.040864	0.275*
C19	0.212 (4)	0.444 (3)	0.109 (2)	0.234 (7)
C20	0.0268 (13)	0.367 (3)	0.096 (3)	0.344 (10)
C21	0.012 (2)	0.368 (3)	0.048 (2)	0.355 (12)
H21	0.019447	0.330664	0.028305	0.426*
C22	-0.013 (3)	0.422 (4)	0.0306 (13)	0.362 (12)
H22	-0.022637	0.422419	-0.001696	0.434*
C23	-0.023 (2)	0.476 (3)	0.060 (3)	0.363 (12)
C24	-0.009 (3)	0.476 (3)	0.107 (2)	0.359 (12)
H24	-0.015943	0.512753	0.127228	0.430*
C25	0.016 (2)	0.421 (4)	0.1250 (13)	0.352 (12)
H25	0.026141	0.420999	0.157230	0.423*

C26	-0.050 (3)	0.546 (3)	0.054 (2)	0.376 (15)	
H26A	-0.049580	0.570142	0.083663	0.565*	
H26B	-0.009745	0.589815	0.032777	0.565*	
H26C	-0.106396	0.519634	0.040112	0.565*	
O5	-0.004 (2)	0.662 (2)	0.2113 (14)	0.114 (6)	0.5
C7	0.003 (2)	0.6898 (14)	0.2980 (14)	0.134 (6)	0.5
C8	-0.083 (2)	0.661 (2)	0.2954 (14)	0.145 (8)	0.5
H8	-0.111996	0.640061	0.266936	0.174*	0.5
C9	-0.1262	0.663 (2)	0.3344 (17)	0.153 (8)	0.5
	(17)				
H9	-0.184897	0.643299	0.332668	0.184*	0.5
C10	-0.084 (3)	0.694 (2)	0.3760 (14)	0.158 (8)	0.5
C11	0.002 (3)	0.722 (2)	0.3786 (14)	0.155 (8)	0.5
H11	0.031286	0.743354	0.407072	0.187*	0.5
C12	0.0455 (17)	0.720 (2)	0.3396 (17)	0.147 (8)	0.5
H12	0.104189	0.740116	0.341340	0.177*	0.5
C13	-0.121 (4)	0.702 (3)	0.426 (3)	0.168 (13)	0.5
H13A	-0.161805	0.720543	0.421304	0.252*	0.5
H13B	-0.074463	0.742995	0.445436	0.252*	0.5
H13C	-0.148283	0.646972	0.441643	0.252*	0.5
H1	0.333333	0.666667	0.3204 (11)	0.00 (4)*	

Atomic displacement parameters (\AA^2)

	U^{11}	U^{22}	U^{33}	U^{12}	U^{13}	U^{23}
Lu1	0.0627 (8)	0.0620 (7)	0.1008 (10)	0.0317 (6)	0.000	0.000
S1	0.071 (4)	0.088 (5)	0.189 (8)	0.040 (4)	0.000	0.000
S2	0.285 (12)	0.234 (13)	0.273 (13)	-0.016 (10)	-0.019 (11)	-0.092 (10)
O1	0.084 (9)	0.084 (9)	0.061 (13)	0.042 (4)	0.000	0.000
O2	0.068 (7)	0.063 (8)	0.169 (12)	0.036 (6)	0.000	0.000

O3	0.113 (15)	0.099 (11)	0.27 (2)	0.005 (11)	0.000	0.000
O4	0.092 (13)	0.129 (15)	0.29 (2)	0.035 (11)	0.000	0.000
O6	0.080 (10)	0.069 (9)	0.230 (17)	0.034 (9)	0.000	0.000
O7	0.177 (13)	0.115 (10)	0.210 (13)	0.082 (9)	-0.025 (12)	-0.068 (11)
O8	0.25 (2)	0.22 (2)	0.249 (19)	0.063 (15)	-0.001 (18)	-0.048 (17)
O9	0.26 (2)	0.24 (2)	0.234 (19)	0.058 (17)	-0.038 (18)	-0.070 (17)
O10	0.30 (2)	0.23 (2)	0.29 (2)	-0.026 (17)	-0.016 (19)	-0.084 (17)
O11	0.30 (2)	0.25 (2)	0.29 (2)	-0.014 (17)	-0.013 (19)	-0.097 (17)
N1	0.085 (9)	0.101 (10)	0.240 (14)	0.019 (8)	0.000	0.000
N2	0.070 (7)	0.071 (6)	0.185 (10)	0.041 (6)	0.000	0.000
N3	0.232 (16)	0.197 (15)	0.232 (14)	0.061 (12)	-0.019 (13)	-0.064 (13)
N4	0.257 (13)	0.205 (13)	0.251 (13)	0.006 (10)	-0.013 (12)	-0.083 (11)
C1	0.065 (7)	0.058 (6)	0.174 (11)	0.040 (5)	0.000	0.000
C2	0.074 (8)	0.054 (7)	0.185 (12)	0.029 (6)	0.000	0.000
C3	0.078 (8)	0.066 (8)	0.199 (12)	0.021 (7)	0.000	0.000
C4	0.078 (8)	0.079 (8)	0.212 (12)	0.026 (6)	0.000	0.000
C5	0.071 (7)	0.078 (8)	0.198 (12)	0.034 (7)	0.000	0.000
C6	0.068 (7)	0.068 (6)	0.185 (10)	0.040 (6)	0.000	0.000
C14	0.195 (12)	0.140 (11)	0.217 (13)	0.073 (9)	-0.020 (11)	-0.073 (11)
C15	0.194 (13)	0.144 (12)	0.218 (14)	0.080 (10)	-0.018 (12)	-0.070 (12)
C16	0.204 (14)	0.159 (13)	0.222 (14)	0.073 (11)	-0.016 (13)	-0.067 (12)
C17	0.219 (14)	0.177 (13)	0.226 (13)	0.063 (10)	-0.020 (12)	-0.068 (12)
C18	0.221 (14)	0.178 (13)	0.226 (13)	0.052 (11)	-0.022 (12)	-0.076 (12)
C19	0.223 (12)	0.175 (11)	0.228 (13)	0.043 (9)	-0.020 (11)	-0.078 (11)
C20	0.298 (14)	0.253 (16)	0.291 (15)	-0.004 (12)	-0.032 (13)	-0.079 (13)
C21	0.310 (16)	0.263 (18)	0.299 (16)	-0.001 (14)	-0.032 (15)	-0.073 (15)
C22	0.318 (17)	0.269 (19)	0.307 (17)	0.003 (15)	-0.033 (16)	-0.070 (16)
C23	0.321 (17)	0.270 (19)	0.311 (18)	0.007 (15)	-0.032 (17)	-0.069 (16)
C24	0.316 (17)	0.267 (18)	0.307 (18)	0.006 (15)	-0.032 (16)	-0.069 (16)
C25	0.309 (16)	0.262 (18)	0.301 (17)	0.003 (14)	-0.030 (15)	-0.075 (15)

C26	0.33 (3)	0.28 (2)	0.34 (3)	0.01 (2)	-0.03 (2)	-0.05 (2)
O5	0.075 (12)	0.089 (14)	0.193 (14)	0.053 (10)	0.001 (12)	0.010 (13)
C7	0.081 (9)	0.119 (10)	0.198 (11)	0.046 (8)	0.000 (8)	-0.009 (9)
C8	0.082 (10)	0.135 (13)	0.203 (14)	0.044 (10)	0.000 (10)	-0.010 (12)
C9	0.089 (11)	0.146 (14)	0.204 (15)	0.042 (11)	0.003 (11)	-0.014 (13)
C10	0.093 (12)	0.151 (14)	0.204 (14)	0.042 (12)	0.003 (11)	-0.015 (13)
C11	0.093 (12)	0.147 (14)	0.202 (14)	0.041 (12)	0.000 (11)	-0.014 (13)
C12	0.088 (11)	0.136 (13)	0.201 (13)	0.043 (11)	-0.002 (10)	-0.011 (11)
C13	0.106 (19)	0.17 (2)	0.206 (19)	0.051 (19)	0.007 (17)	-0.01 (2)

Geometric parameters (Å, °)

Lu1—O1 ⁱ	2.295 (11)	C14—C19	1.35 (6)
Lu1—O1	2.295 (11)	C15—H15	0.9500
Lu1—O2 ⁱⁱ	2.280 (19)	C15—C16	1.32 (6)
Lu1—O2	2.315 (19)	C16—H16	0.9500
Lu1—O7 ⁱⁱⁱ	2.19 (3)	C16—C17	1.28 (6)
Lu1—O7	2.19 (3)	C17—C18	1.50 (6)
Lu1—N2 ⁱⁱ	2.37 (2)	C18—H18	0.9500
S1—O6	1.39 (2)	C18—C19	1.41 (6)
S1—N2	1.53 (3)	C20—C21	1.3900
S1—O5	1.48 (4)	C20—C25	1.3900
S1—C7	1.71 (3)	C21—H21	0.9500
S2—O10	1.52 (5)	C21—C22	1.3900
S2—O11	1.58 (5)	C22—H22	0.9500
S2—N4	1.73 (5)	C22—C23	1.3900
S2—C20	1.35 (5)	C23—C24	1.3900
O1—H1	0.90 (2)	C23—C26	1.58 (2)
O2—C1	1.36 (3)	C24—H24	0.9500
O3—N1	1.17 (4)	C24—C25	1.3900
O4—N1	1.20 (5)	C25—H25	0.9500
O7—C14	1.27 (5)	C26—H26A	0.9800

O8—N3	1.24 (5)	C26—H26B	0.9800
O9—N3	1.10 (4)	C26—H26C	0.9800
N1—C4	1.59 (5)	C7—C8	1.3900
N2—C6	1.42 (4)	C7—C12	1.3900
N3—C17	1.63 (7)	C8—H8	0.9500
N4—C19	1.45 (6)	C8—C9	1.3900
C1—C2	1.29 (4)	C9—H9	0.9500
C1—C6	1.45 (4)	C9—C10	1.3900
C2—H2	0.9500	C10—C11	1.3900
C2—C3	1.32 (4)	C10—C13	1.64 (7)
C3—H3	0.9500	C11—H11	0.9500
C3—C4	1.40 (5)	C11—C12	1.3900
C4—C5	1.36 (5)	C12—H12	0.9500
C5—H5	0.9500	C13—H13A	0.9800
C5—C6	1.39 (4)	C13—H13B	0.9800
C14—C15	1.35 (6)	C13—H13C	0.9800
O1 ⁱ —Lu1—O1	59.2 (10)	C4—C3—H3	122.6
O1—Lu1—O2	73.4 (4)	C3—C4—N1	111 (3)
O1 ⁱ —Lu1—O2	73.4 (4)	C5—C4—N1	118 (4)
O1—Lu1—N2 ⁱⁱ	130.6 (5)	C5—C4—C3	131 (3)
O1 ⁱ —Lu1—N2 ⁱ	130.6 (5)	C4—C5—H5	124.9
O2 ⁱⁱ —Lu1—O1 ⁱ	74.1 (4)	C4—C5—C6	110 (3)
O2 ⁱⁱ —Lu1—O1	74.1 (4)	C6—C5—H5	124.9
O2 ⁱⁱ —Lu1—O2	142.4 (8)	N2—C6—C1	119 (3)
O2 ⁱⁱ —Lu1—N2 ⁱⁱ	66.9 (7)	C5—C6—N2	122 (3)
O2—Lu1—N2 ⁱⁱ	150.6 (8)	C5—C6—C1	120 (3)
O7—Lu1—O1 ⁱ	81.2 (8)	O7—C14—C15	124 (5)
O7 ⁱⁱⁱ —Lu1—O1	81.2 (8)	O7—C14—C19	119 (6)
O7 ⁱⁱⁱ —Lu1—O1 ⁱ	138.2 (8)	C15—C14—C19	117 (6)
O7—Lu1—O1	138.2 (8)	C14—C15—H15	118.5

O7—Lu1—O2	83.4 (6)	C16—C15—C14	123 (5)
O7 ⁱⁱⁱ —Lu1—O2 ⁱⁱ	109.6 (7)	C16—C15—H15	118.5
O7 ⁱⁱⁱ —Lu1—O2	83.4 (6)	C15—C16—H16	118.2
O7—Lu1—O2 ⁱⁱ	109.6 (7)	C17—C16—C15	124 (6)
O7—Lu1—O7 ⁱⁱⁱ	130.8 (14)	C17—C16—H16	118.2
O7 ⁱⁱⁱ —Lu1—N2 ⁱⁱ	84.5 (6)	C16—C17—N3	130 (6)
O7—Lu1—N2 ⁱⁱ	84.5 (6)	C16—C17—C18	119 (6)
O6—S1—N2	106.9 (14)	C18—C17—N3	111 (5)
O6—S1—O5	117.4 (14)	C17—C18—H18	123.9
O6—S1—C7	100.7 (12)	C19—C18—C17	112 (5)
N2—S1—C7	118.7 (9)	C19—C18—H18	123.9
O5—S1—N2	108.3 (14)	C14—C19—N4	109 (5)
O5—S1—C7	105.2 (18)	C14—C19—C18	125 (6)
O10—S2—O11	103 (3)	C18—C19—N4	124 (5)
O10—S2—N4	86 (3)	S2—C20—C21	116 (7)
O11—S2—N4	109 (3)	S2—C20—C25	124 (7)
C20—S2—O10	131 (4)	C21—C20—C25	120.0
C20—S2—O11	117 (5)	C20—C21—H21	120.0
C20—S2—N4	105 (3)	C20—C21—C22	120.0
Lu1 ^{iv} —O1—Lu1 ^v	97.7 (6)	C22—C21—H21	120.0
Lu1 ^{iv} —O1—Lu1 ⁱⁱ	97.7 (6)	C21—C22—H22	120.0
Lu1 ⁱⁱ —O1—Lu1 ^v	0.00 (6)	C23—C22—C21	120.0
Lu1 ^{iv} —O1—Lu1	97.7 (6)	C23—C22—H22	120.0
Lu1 ⁱ —O1—Lu1	97.7 (6)	C22—C23—C24	120.0
Lu1 ^v —O1—Lu1	97.7 (6)	C22—C23—C26	135 (7)
Lu1 ⁱⁱ —O1—Lu1	97.7 (6)	C24—C23—C26	105 (7)
Lu1 ⁱ —O1—Lu1 ^{iv}	0.00 (4)	C23—C24—H24	120.0
Lu1 ⁱ —O1—Lu1 ⁱⁱ	97.7 (6)	C25—C24—C23	120.0
Lu1 ⁱ —O1—Lu1 ^v	97.7 (6)	C25—C24—H24	120.0
Lu1 ⁱ —O1—H1	119.6 (5)	C20—C25—H25	120.0

Lu1 ⁱⁱ —O1—H1	119.6 (5)	C24—C25—C20	120.0
Lu1—O1—H1	119.6 (5)	C24—C25—H25	120.0
Lu1 ^{iv} —O1—H1	119.6 (5)	C23—C26—H26A	109.5
Lu1 ^v —O1—H1	119.6 (5)	C23—C26—H26B	109.5
Lu1 ⁱ —O2—Lu1 ^{iv}	0.00 (6)	C23—C26—H26C	109.5
Lu1 ^{iv} —O2—Lu1	97.6 (8)	H26A—C26—H26B	109.5
Lu1 ⁱ —O2—Lu1	97.6 (8)	H26A—C26—H26C	109.5
C1—O2—Lu1	133.8 (16)	H26B—C26—H26C	109.5
C1—O2—Lu1 ⁱ	128.7 (16)	C8—C7—S1	120 (3)
C1—O2—Lu1 ^{iv}	128.7 (16)	C8—C7—C12	120.0
C14—O7—Lu1	148 (3)	C12—C7—S1	120 (3)
O3—N1—O4	128 (4)	C7—C8—H8	120.0
O3—N1—C4	124 (4)	C7—C8—C9	120.0
O4—N1—C4	109 (3)	C9—C8—H8	120.0
Lu1 ⁱ —N2—Lu1 ^{iv}	0.00 (6)	C8—C9—H9	120.0
S1—N2—Lu1 ^{iv}	115.4 (14)	C10—C9—C8	120.0
S1—N2—Lu1 ⁱ	115.4 (14)	C10—C9—H9	120.0
C6—N2—Lu1 ⁱ	116.9 (18)	C9—C10—C13	129 (4)
C6—N2—Lu1 ^{iv}	116.9 (18)	C11—C10—C9	120.0
C6—N2—S1	128 (2)	C11—C10—C13	111 (4)
O8—N3—C17	102 (4)	C10—C11—H11	120.0
O9—N3—O8	136 (7)	C12—C11—C10	120.0
O9—N3—C17	120 (6)	C12—C11—H11	120.0
C19—N4—S2	117 (4)	C7—C12—H12	120.0
O2—C1—C6	109 (2)	C11—C12—C7	120.0
C2—C1—O2	128 (3)	C11—C12—H12	120.0
C2—C1—C6	123 (3)	C10—C13—H13A	109.5
C1—C2—H2	119.3	C10—C13—H13B	109.5
C1—C2—C3	121 (3)	C10—C13—H13C	109.5
C3—C2—H2	119.3	H13A—C13—H13B	109.5

C2—C3—H3	122.6	H13A—C13—H13C	109.5
C2—C3—C4	115 (3)	H13B—C13—H13C	109.5
Lu1 ⁱ —O2—C1—C2	180.0	N2—S1—C7—C12	66 (2)
Lu1 ^{iv} —O2—C1—C2	180.0	N3—C17—C18—C19	-173 (5)
Lu1—O2—C1—C2	0.000 (1)	N4—S2—C20—C21	120 (3)
Lu1 ⁱ —O2—C1—C6	0.0	N4—S2—C20—C25	-59 (3)
Lu1 ^{iv} —O2—C1—C6	0.0	C1—C2—C3—C4	0.0
Lu1—O2—C1—C6	180.0	C2—C1—C6—N2	180.0
Lu1—O7—C14—C15	5 (9)	C2—C1—C6—C5	0.0
Lu1—O7—C14—C19	-171 (4)	C2—C3—C4—N1	180.0
Lu1 ^{iv} —N2—C6—C1	0.0	C2—C3—C4—C5	0.0
Lu1 ⁱ —N2—C6—C1	0.0	C3—C4—C5—C6	0.0
Lu1 ⁱ —N2—C6—C5	180.0	C4—C5—C6—N2	180.0
Lu1 ^{iv} —N2—C6—C5	180.0	C4—C5—C6—C1	0.0
S1—N2—C6—C1	180.0	C6—C1—C2—C3	0.0
S1—N2—C6—C5	0.0	C14—C15—C16—C17	2 (9)
S1—C7—C8—C9	180.0 (7)	C15—C14—C19—N4	165 (5)
S1—C7—C12—C11	-180.0 (7)	C15—C14—C19—C18	4 (9)
S2—N4—C19—C14	164 (4)	C15—C16—C17—N3	174 (5)
S2—N4—C19—C18	-34 (8)	C15—C16—C17—C18	-5 (9)
S2—C20—C21—C22	-179.9 (8)	C16—C17—C18—C19	6 (9)
S2—C20—C25—C24	179.9 (9)	C17—C18—C19—N4	-165 (6)
O2—C1—C2—C3	180.0	C17—C18—C19—C14	-6 (9)
O2—C1—C6—N2	0.0	C19—C14—C15—C16	-1 (8)
O2—C1—C6—C5	180.0	C20—S2—N4—C19	-52 (6)
O3—N1—C4—C3	0.0	C20—C21—C22—C23	0.0
O3—N1—C4—C5	180.0	C21—C20—C25—C24	0.0
O4—N1—C4—C3	180.0	C21—C22—C23—C24	0.0
O4—N1—C4—C5	0.0	C21—C22—C23—C26	180 (3)

O6—S1—N2—Lu1 ^{iv}	0.0	C22—C23—C24—C25	0.0
O6—S1—N2—Lu1 ⁱ	0.0	C23—C24—C25—C20	0.0
O6—S1—N2—C6	180.0	C25—C20—C21—C22	0.0
O6—S1—C7—C8	129.8 (17)	C26—C23—C24—C25	-180 (2)
O6—S1—C7—C12	-50.2 (17)	O5—S1—N2—Lu1 ^{iv}	127.4 (15)
O7—C14—C15—C16	-177 (4)	O5—S1—N2—Lu1 ⁱ	127.4 (15)
O7—C14—C19—N4	-18 (7)	O5—S1—N2—C6	-52.6 (15)
O7—C14—C19—C18	180 (5)	O5—S1—C7—C8	7 (2)
O8—N3—C17—C16	-2 (9)	O5—S1—C7—C12	-173 (2)
O8—N3—C17—C18	177 (5)	C7—S1—N2—Lu1 ⁱ	-112.8 (17)
O9—N3—C17—C16	169 (6)	C7—S1—N2—Lu1 ^{iv}	-112.8 (17)
O9—N3—C17—C18	-12 (9)	C7—S1—N2—C6	67.2 (17)
O10—S2—N4—C19	177 (5)	C7—C8—C9—C10	0.0
O10—S2—C20—C21	-141 (3)	C8—C7—C12—C11	0.0
O10—S2—C20—C25	39 (4)	C8—C9—C10—C11	0.0
O11—S2—N4—C19	75 (5)	C8—C9—C10—C13	-180 (3)
O11—S2—C20—C21	0 (2)	C9—C10—C11—C12	0.0
O11—S2—C20—C25	180 (2)	C10—C11—C12—C7	0.0
N1—C4—C5—C6	180.0	C12—C7—C8—C9	0.0
N2-S1-C7-C8	-114(2)	C13-C10-C11-C12	-180 (2)

5.4.4.3 X-ray crystallography for $(\text{Et}_3\text{NH})_3[\text{Lu}(\text{LH})_6]$

Crystal data, data collection, and structure refinement details are summarized in Table 5.4. The complex bearing three triethylammonium counterion and the anionic $[\text{Lu}(\text{LH})_6]^{3-}$ crystallized in a monoclinic $C2/c$ space group with half a molecule within the asymmetric unit and the other half is symmetry generated. Therefore, the coordination geometry around the central Lu is perfectly octahedral (figure 5.20). Though LH_2 could potentially bind the Lu ion through both O and N atoms, in $(\text{Et}_3\text{NH})_3[\text{Lu}(\text{LH})_6]$ the six ligands uniformly bind the metal center in a monodentate fashion through the O atom. The uncoordinated N atom of the ligand disposed in a manner that is significantly distant from the central metal ion. The dihedral angle between the two aryl rings of LH is 87.5 deg. Both the aryl rings of the ligand are highly planar (with mean deviation, 0.006 Å). A careful examination revealed no intermolecular π - π stacking interactions, however the extended structure is consolidated through moderate intermolecular hydrogen bonding interactions. Among other few such notable interactions involve one of the O atoms of the NO_2 substituent on LH and N-H of group of the triethylammonium ion (O---H-N, with an O---N distance of 2.930 Å), one of the O atoms of the SO_2 fragment of LH and the N-H group of the triethylammonium ion (O---H-N with an O---N distance of 2.782 Å). A rather weak intramolecular hydrogen bonding interaction involving the coordinated O atoms of one of the ligands with an uncoordinated N-H moiety of a proximal ligand was also noted (O---H-N with an O---N distance of 3.058 Å).

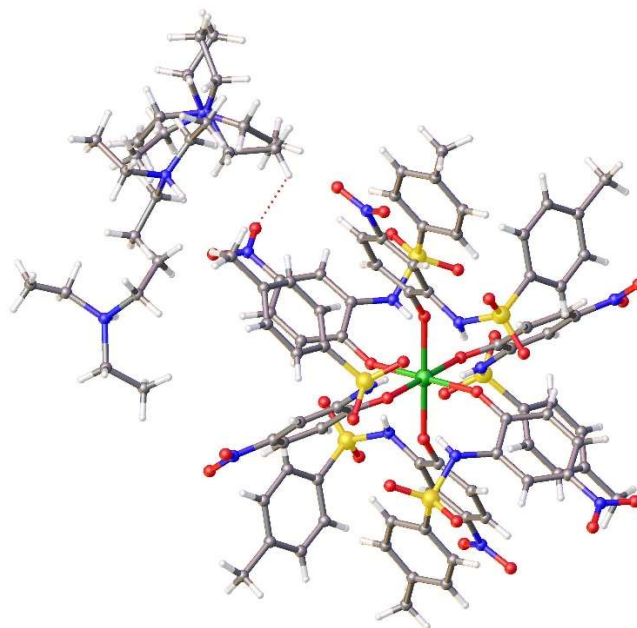


Figure 5.20. Ball and stick representation of $(\text{Et}_3\text{NH})_3[\text{Lu}(\text{LH})_6]$ showing three triethylammonium counteranions and an O---H intermolecular hydrogen bond interaction.

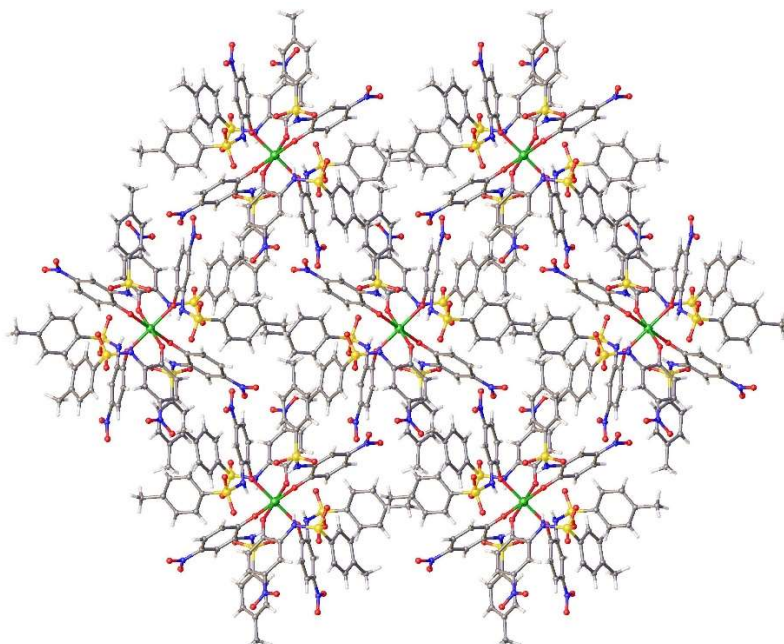


Figure 5.21. Packing pattern of $(\text{Et}_3\text{NH})_3[\text{Lu}(\text{LH})_6]$

Table 5.4: X-ray crystallography data for (Et₃NH)₃[Lu(LH)₆]

Experimental details

Crystal data

Chemical formula	C ₉₆ H ₁₁₄ LuN ₁₅ O ₃₀ S ₆
<i>M_r</i>	2325.35
Crystal system, space group	Monoclinic, <i>C2/c</i>
Temperature (K)	298
<i>a</i> , <i>b</i> , <i>c</i> (Å)	29.8877 (19), 16.0434 (11), 22.3585 (15)
<i>β</i> (°)	92.101 (1)
<i>V</i> (Å ³)	10713.7 (12)
<i>Z</i>	4
Radiation type	Mo <i>Kα</i>
<i>μ</i> (mm ⁻¹)	1.12
Crystal size (mm)	0.35 × 0.32 × 0.25
Data collection	
Diffractometer	Bruker D8 Quest PHOTON II
Absorption correction	Multi-scan <i>SADABS</i> 2016/2: Krause, L., Herbst-Irmer, R., Sheldrick G.M. & Stalke D., <i>J. Appl. Cryst.</i> 48 (2015)3-10.
<i>T_{min}</i> , <i>T_{max}</i>	0.704, 0.745
No. of measured, independent and observed [<i>I</i> >	60566, 9831, 8387

$2\sigma(I)$

reflections

R_{int} 0.038

$(\sin \theta/\lambda)_{max}$ (\AA^{-1}) 0.603

Refinement

$R[F^2 > 2\sigma(F^2)]$, $wR(F^2)$, S 0.033, 0.077, 1.05

No. of reflections 9831

No. of parameters 839

No. of restraints 552

H atoms treated by a mixture of independent and constrained

H-atom treatment refinement

$$w = 1/[\sigma^2(F_o^2) + (0.0303P)^2 + 17.4052P]$$

$$\text{where } P = (F_o^2 + 2F_c^2)/3$$

ρ_{max} , ρ_{min} ($e \text{\AA}^{-3}$) 0.49, -0.55

Table 5.5: Fractional atomic coordinates and isotropic or equivalent isotropic displacement parameters (\AA^2)

	x	y	z	U_{iso}^*/U_{eq}	Occ. (<1)
Lu1	0.250000	0.250000	0.500000	0.04117 (2)	
S1	0.38999 (2)	0.05671 (3)	0.47170 (2)	0.05996 (13)	
S2	0.11909 (2)	0.07393 (3)	0.42360 (2)	0.05891 (13)	
S3	0.07775 (2)	0.16365 (4)	0.63057 (3)	0.08032 (17)	
O1	0.26485 (4)	0.15740 (8)	0.43413 (5)	0.0575 (3)	
O2	0.33225 (7)	0.07811 (12)	0.18101 (7)	0.1034 (6)	
O3	0.39217 (6)	0.05491 (12)	0.23497 (7)	0.1043 (6)	
O4	0.42390 (4)	0.04875 (10)	0.42881 (7)	0.0837 (5)	
O5	0.40161 (5)	0.08482 (9)	0.53100 (7)	0.0782 (4)	
O6	0.19245 (4)	0.29729 (7)	0.44792 (5)	0.0540 (3)	
O7	0.09767 (6)	0.33780 (13)	0.19644 (7)	0.1176 (7)	
O8	0.05797 (7)	0.24285 (14)	0.23415 (9)	0.1329 (8)	
O9	0.07849 (4)	0.07278 (9)	0.38717 (6)	0.0720 (4)	
O10	0.11884 (5)	0.04007 (8)	0.48262 (6)	0.0706 (4)	
O11	0.19970 (4)	0.17017 (7)	0.54130 (5)	0.0575 (3)	
O12	0.20376 (7)	-0.17348 (9)	0.67020 (8)	0.1109 (6)	
O13	0.13892 (7)	-0.12838 (10)	0.69384 (8)	0.1181 (7)	

O14	0.06092 (6)	0.24331 (11)	0.61257 (8)	0.1246 (6)	
O15	0.05228 (5)	0.09097 (13)	0.61632 (7)	0.1069 (6)	
N1	0.35250 (6)	0.07509 (11)	0.22969 (7)	0.0760 (5)	
N2	0.35251 (5)	0.12243 (10)	0.44573 (7)	0.0567 (4)	
H2	0.3376 (7)	0.1374 (13)	0.4719 (9)	0.085*	
N3	0.08984 (6)	0.28909 (15)	0.23677 (8)	0.0901 (6)	
N4	0.13405 (5)	0.17121 (9)	0.43199 (6)	0.0567 (4)	
H4	0.1505 (7)	0.1751 (13)	0.4604 (9)	0.085*	
N5	0.17447 (7)	-0.11993 (10)	0.66930 (8)	0.0791 (6)	
N6	0.12659 (5)	0.15748 (10)	0.60288 (7)	0.0628 (4)	
H6	0.1339 (7)	0.1932 (14)	0.5874 (9)	0.094*	
N7	-0.02038 (17)	0.5757 (2)	0.18179 (17)	0.1366 (14)	0.5
H7	-0.047216	0.558055	0.202273	0.164*	0.5
C40	-0.0043 (3)	0.6486 (3)	0.2257 (3)	0.154 (2)	0.5
H40A	0.026856	0.660829	0.218811	0.184*	0.5
H40B	-0.021536	0.698331	0.215985	0.184*	0.5
C41	-0.0090 (3)	0.6292 (5)	0.2911 (3)	0.221 (4)	0.5
H41A	0.001311	0.675838	0.314742	0.332*	0.5
H41B	-0.039870	0.618468	0.298752	0.332*	0.5
H41C	0.008586	0.580917	0.301581	0.332*	0.5
C42	0.0054 (2)	0.4965 (3)	0.1855 (4)	0.144 (2)	0.5
H42A	0.024971	0.498132	0.221105	0.173*	0.5
H42B	0.024213	0.493015	0.151176	0.173*	0.5
C43	-0.0230 (2)	0.4184 (3)	0.1876 (3)	0.147 (2)	0.5
H43A	-0.003850	0.370336	0.190018	0.220*	0.5
H43B	-0.041137	0.420244	0.222141	0.220*	0.5
H43C	-0.041897	0.415118	0.152092	0.220*	0.5
C44	-0.0406 (3)	0.5865 (5)	0.1196 (3)	0.189 (2)	0.5
H44A	-0.043116	0.528792	0.107062	0.227*	0.5
H44B	-0.070907	0.602312	0.128761	0.227*	0.5
C45	-0.0371 (3)	0.6212 (5)	0.0703 (3)	0.202 (3)	0.5
H45A	-0.061571	0.604529	0.043905	0.303*	0.5
H45B	-0.037779	0.680600	0.075509	0.303*	0.5
H45C	-0.009335	0.605353	0.053300	0.303*	0.5
N8	0.02483 (13)	0.2813 (2)	0.09223 (17)	0.1099 (11)	0.5
H8A	0.049138	0.290346	0.122140	0.132*	0.5
C46	-0.01574 (18)	0.3221 (4)	0.1180 (3)	0.1289 (18)	0.5
H46A	-0.040932	0.313598	0.090057	0.155*	0.5
H46B	-0.022473	0.293150	0.154653	0.155*	0.5
C47	-0.0127 (2)	0.4121 (4)	0.1314 (3)	0.142 (2)	0.5
H47A	-0.040371	0.430689	0.147459	0.213*	0.5
H47B	0.011332	0.421758	0.160228	0.213*	0.5
H47C	-0.007196	0.442282	0.095392	0.213*	0.5
C48	0.0392 (2)	0.3252 (4)	0.0376 (2)	0.1248 (18)	0.5
H48A	0.067948	0.302888	0.026675	0.150*	0.5
H48B	0.043549	0.383686	0.047200	0.150*	0.5
C49	0.0076 (2)	0.3190 (5)	-0.0155 (2)	0.160 (2)	0.5
H49A	0.019507	0.348992	-0.048415	0.241*	0.5
H49B	0.003634	0.261477	-0.026322	0.241*	0.5
H49C	-0.020817	0.342445	-0.005753	0.241*	0.5
C50	0.02103 (19)	0.1928 (3)	0.0867 (3)	0.1180 (11)	0.5

H50A	-0.001591	0.179984	0.055899	0.142*	0.5
H50B	0.010940	0.170246	0.124181	0.142*	0.5
C51	0.0659 (2)	0.1486 (4)	0.0708 (3)	0.142 (2)	0.5
H51A	0.061099	0.089580	0.067822	0.212*	0.5
H51B	0.075818	0.169489	0.033304	0.212*	0.5
H51C	0.088359	0.159743	0.101643	0.212*	0.5
N9	0.0057 (2)	0.1301 (3)	0.08346 (19)	0.1047 (11)	0.280 (2)
H9A	-0.024357	0.107259	0.087866	0.126*	0.280 (2)
C52	0.0243 (3)	0.1629 (5)	0.1417 (3)	0.1097 (15)	0.280 (2)
H52A	0.007691	0.212156	0.152814	0.132*	0.280 (2)
H52B	0.055309	0.178798	0.137507	0.132*	0.280 (2)
C53	0.0212 (3)	0.0956 (5)	0.1923 (3)	0.108 (3)	0.280 (2)
H53A	0.033275	0.117945	0.229288	0.162*	0.280 (2)
H53B	-0.009563	0.080435	0.196905	0.162*	0.280 (2)
H53C	0.037987	0.047125	0.181621	0.162*	0.280 (2)
C54	0.0054 (3)	0.1995 (5)	0.0353 (4)	0.1153 (13)	0.280 (2)
H54A	0.035005	0.224143	0.033977	0.138*	0.280 (2)
H54B	-0.001721	0.175168	-0.003663	0.138*	0.280 (2)
C55	-0.0275 (3)	0.2649 (4)	0.0479 (5)	0.117 (2)	0.280 (2)
H55A	-0.026958	0.306870	0.017315	0.176*	0.280 (2)
H55B	-0.056913	0.240763	0.048479	0.176*	0.280 (2)
H55C	-0.020225	0.289687	0.086079	0.176*	0.280 (2)
C56	0.0349 (3)	0.0696 (5)	0.0527 (4)	0.1081 (15)	0.280 (2)
H56A	0.045831	0.028362	0.081361	0.130*	0.280 (2)
H56B	0.060580	0.098864	0.037691	0.130*	0.280 (2)
C57	0.0100 (3)	0.0248 (5)	0.0000 (4)	0.109 (3)	0.280 (2)
H57A	0.030020	-0.013471	-0.018390	0.164*	0.280 (2)
H57B	-0.015111	-0.005292	0.014712	0.164*	0.280 (2)
H57C	-0.000365	0.065196	-0.028949	0.164*	0.280 (2)
N10	0.0055 (3)	0.1369 (3)	0.0803 (2)	0.1068 (12)	0.220 (2)
H10	-0.020003	0.100578	0.087960	0.128*	0.220 (2)
C58	0.0378 (3)	0.1035 (8)	0.1281 (4)	0.1123 (14)	0.220 (2)
H58A	0.062020	0.143083	0.135002	0.135*	0.220 (2)
H58B	0.050656	0.051589	0.114652	0.135*	0.220 (2)
C59	0.0134 (4)	0.0884 (7)	0.1878 (3)	0.111 (3)	0.220 (2)
H59A	0.034423	0.067327	0.217628	0.167*	0.220 (2)
H59B	0.001098	0.140048	0.201450	0.167*	0.220 (2)
H59C	-0.010247	0.048705	0.181134	0.167*	0.220 (2)
C60	-0.0201 (3)	0.2168 (5)	0.0661 (6)	0.1120 (14)	0.220 (2)
H60A	-0.042377	0.203791	0.034899	0.134*	0.220 (2)
H60B	-0.036232	0.231430	0.101491	0.134*	0.220 (2)
C61	0.0033 (4)	0.2908 (5)	0.0475 (6)	0.127 (2)	0.220 (2)
H61A	-0.017832	0.335108	0.040473	0.191*	0.220 (2)
H61B	0.024705	0.307101	0.078383	0.191*	0.220 (2)
H61C	0.018522	0.279289	0.011375	0.191*	0.220 (2)
C62	0.0186 (4)	0.1000 (5)	0.0210 (4)	0.1112 (15)	0.220 (2)
H62A	0.050555	0.106903	0.016690	0.133*	0.220 (2)
H62B	0.003351	0.130218	-0.011342	0.133*	0.220 (2)
C63	0.0068 (4)	0.0066 (5)	0.0155 (4)	0.100 (3)	0.220 (2)
H63A	0.015634	-0.013917	-0.022641	0.150*	0.220 (2)
H63B	0.022277	-0.023875	0.046868	0.150*	0.220 (2)

H63C	-0.024920	-0.000564	0.018840	0.150*	0.220 (2)
C1	0.28492 (6)	0.14013 (10)	0.38524 (8)	0.0498 (5)	
C2	0.26337 (6)	0.14218 (13)	0.32850 (9)	0.0661 (6)	
H2A	0.233580	0.158841	0.325217	0.079*	
C3	0.28476 (7)	0.12050 (13)	0.27801 (9)	0.0654 (6)	
H3	0.269741	0.121714	0.240848	0.079*	
C4	0.32914 (6)	0.09667 (11)	0.28305 (8)	0.0573 (5)	
C5	0.35267 (6)	0.09570 (11)	0.33741 (8)	0.0557 (5)	
H5	0.382752	0.080754	0.339648	0.067*	
C6	0.33070 (6)	0.11729 (10)	0.38816 (8)	0.0483 (4)	
C7	0.36406 (6)	-0.04102 (11)	0.47647 (8)	0.0541 (5)	
C8	0.34522 (7)	-0.06568 (13)	0.52844 (9)	0.0708 (6)	
H8	0.344885	-0.029959	0.561178	0.085*	
C9	0.32671 (9)	-0.14427 (15)	0.53161 (11)	0.0892 (8)	
H9	0.314178	-0.161137	0.567099	0.107*	
C10	0.32621 (8)	-0.19826 (14)	0.48409 (11)	0.0813 (7)	
C11	0.34441 (10)	-0.17183 (14)	0.43242 (10)	0.0933 (9)	
H11	0.344138	-0.207159	0.399427	0.112*	
C12	0.36302 (9)	-0.09450 (14)	0.42818 (9)	0.0840 (8)	
H12	0.375107	-0.077713	0.392381	0.101*	
C13	0.30684 (11)	-0.28591 (18)	0.48881 (17)	0.1308 (13)	
H13A	0.282813	-0.292675	0.459531	0.196*	
H13B	0.295710	-0.294018	0.528122	0.196*	
H13C	0.329812	-0.326177	0.481747	0.196*	
C14	0.16963 (5)	0.29445 (11)	0.39681 (8)	0.0501 (5)	
C15	0.17403 (7)	0.35519 (13)	0.35248 (9)	0.0703 (6)	
H15	0.194560	0.398156	0.358723	0.084*	
C16	0.14857 (7)	0.35282 (14)	0.29965 (9)	0.0758 (6)	
H16	0.152108	0.393373	0.270484	0.091*	
C17	0.11826 (6)	0.29037 (14)	0.29089 (8)	0.0649 (6)	
C18	0.11284 (6)	0.22818 (13)	0.33274 (8)	0.0604 (5)	
H18	0.092140	0.185743	0.325543	0.072*	
C19	0.13839 (6)	0.22970 (10)	0.38517 (8)	0.0490 (5)	
C20	0.16038 (6)	0.02198 (11)	0.38415 (8)	0.0587 (5)	
C21	0.15614 (7)	0.01168 (13)	0.32285 (9)	0.0688 (6)	
H21	0.131890	0.034356	0.301270	0.083*	
C22	0.18841 (8)	-0.03269 (14)	0.29439 (10)	0.0793 (7)	
H22	0.185548	-0.039882	0.253154	0.095*	
C23	0.22488 (8)	-0.06690 (14)	0.32488 (11)	0.0834 (7)	
C24	0.22844 (8)	-0.05432 (15)	0.38605 (11)	0.0843 (8)	
H24	0.252885	-0.076381	0.407571	0.101*	
C25	0.19705 (7)	-0.01041 (13)	0.41567 (9)	0.0720 (6)	
H25	0.200296	-0.002321	0.456784	0.086*	
C26	0.25956 (11)	-0.1158 (2)	0.29238 (14)	0.1296 (12)	
H26A	0.250235	-0.121460	0.251038	0.194*	
H26B	0.262818	-0.170007	0.310137	0.194*	
H26C	0.287701	-0.086942	0.295274	0.194*	
C27	0.19588 (5)	0.10173 (10)	0.57289 (7)	0.0473 (4)	
C28	0.22797 (6)	0.03889 (11)	0.57549 (9)	0.0579 (5)	
H28	0.254318	0.045508	0.555121	0.070*	
C29	0.22137 (6)	-0.03314 (11)	0.60780 (9)	0.0616 (5)	

H29	0.243187	-0.074478	0.609744	0.074*
C30	0.18225 (6)	-0.04277 (11)	0.63691 (8)	0.0564 (5)
C31	0.14959 (6)	0.01793 (11)	0.63656 (7)	0.0545 (5)
H31	0.123307	0.009898	0.656812	0.065*
C32	0.15665 (5)	0.09038 (10)	0.60577 (7)	0.0472 (4)
C33	0.08662 (7)	0.16321 (12)	0.70857 (9)	0.0681 (6)
C34	0.05908 (7)	0.11585 (16)	0.74326 (10)	0.0868 (8)
H34	0.037994	0.080381	0.725238	0.104*
C35	0.06298 (9)	0.12136 (16)	0.80502 (11)	0.0968 (8)
H35	0.044174	0.089770	0.828281	0.116*
C36	0.09376 (10)	0.17206 (14)	0.83204 (11)	0.0999 (9)
C37	0.12270 (12)	0.21609 (16)	0.79705 (13)	0.1161 (11)
H37	0.144808	0.249169	0.815298	0.139*
C38	0.11927 (10)	0.21168 (15)	0.73544 (11)	0.0956 (8)
H38	0.138988	0.241418	0.712309	0.115*
C39	0.09756 (15)	0.1769 (2)	0.89959 (12)	0.1564 (17)
H39A	0.092680	0.233308	0.912123	0.235*
H39B	0.126904	0.159230	0.913102	0.235*
H39C	0.075498	0.141255	0.916419	0.235*

Atomic displacement Parameter (\AA^2)

	U_{11}	U_{22}	U_{33}	U_{12}	U_{13}	U_{23}
Lu1	0.02989 (4)	0.04127 (4)	0.05295 (5)	-0.00070 (4)	0.00952 (4)	0.00823 (4)
S1	0.0433 (2)	0.0637 (3)	0.0727 (3)	0.0080 (2)	-0.0002 (2)	-0.0021 (2)
S2	0.0582 (2)	0.0618 (2)	0.0566 (2)	-0.0210 (2)	-0.0005 (2)	0.0077 (2)
S3	0.0477 (2)	0.1121 (4)	0.0825 (3)	0.0138 (3)	0.0202 (2)	0.0393 (3)
O1	0.0452 (6)	0.0616 (7)	0.0666 (7)	-0.0004 (6)	0.0133 (6)	-0.0068 (6)
O2	0.1387 (15)	0.1126 (13)	0.0599 (8)	-0.0032 (12)	0.0177 (9)	-0.0101 (9)
O3	0.0922 (10)	0.1270 (14)	0.0966 (10)	0.0095 (10)	0.0438 (8)	-0.0157 (10)
O4	0.0511 (7)	0.0939 (10)	0.1075 (10)	0.0196 (7)	0.0224 (7)	0.0123 (9)
O5	0.0651 (8)	0.0781 (9)	0.0893 (9)	0.0052 (7)	-0.0271 (7)	-0.0185 (8)
O6	0.0412 (6)	0.0520 (6)	0.0684 (7)	0.0009 (5)	-0.0023 (5)	0.0118 (6)
O7	0.1151 (14)	0.1634 (16)	0.0740 (9)	0.0071 (13)	-0.0007 (9)	0.0539 (10)
O8	0.0886 (11)	0.209 (2)	0.0981 (11)	-0.0309 (13)	-0.0326 (9)	0.0527 (12)
O9	0.0551 (7)	0.0815 (9)	0.0787 (8)	-0.0218 (7)	-0.0071 (7)	0.0011 (7)
O10	0.0849 (9)	0.0690 (8)	0.0583 (7)	-0.0283 (7)	0.0079 (7)	0.0120 (6)
O11	0.0453 (6)	0.0544 (6)	0.0738 (7)	-0.0062 (5)	0.0146 (6)	0.0209 (6)
O12	0.1476 (15)	0.0543 (8)	0.1271 (13)	0.0009 (10)	-0.0441 (11)	0.0265 (8)
O13	0.1529 (16)	0.0821 (10)	0.1205 (12)	-0.0243 (10)	0.0226 (11)	0.0491 (8)
O14	0.0895 (10)	0.1571 (13)	0.1303 (12)	0.0666 (9)	0.0446 (9)	0.0829 (9)
O15	0.0615 (8)	0.1688 (16)	0.0907 (10)	-0.0305 (10)	0.0058 (8)	0.0319 (11)
N1	0.0992 (12)	0.0637 (10)	0.0670 (9)	-0.0111 (9)	0.0269 (9)	-0.0035 (8)
N2	0.0478 (8)	0.0609 (9)	0.0618 (8)	0.0105 (7)	0.0049 (7)	-0.0023 (7)
N3	0.0719 (11)	0.1349 (15)	0.0632 (10)	0.0153 (12)	-0.0002 (9)	0.0297 (11)
N4	0.0591 (8)	0.0576 (8)	0.0528 (8)	-0.0149 (7)	-0.0040 (7)	0.0092 (7)
N5	0.1112 (13)	0.0531 (9)	0.0710 (10)	-0.0161 (9)	-0.0232 (10)	0.0184 (8)
N6	0.0537 (8)	0.0651 (9)	0.0713 (9)	0.0037 (7)	0.0255 (7)	0.0251 (7)
N7	0.123 (3)	0.109 (2)	0.179 (3)	0.029 (2)	0.017 (3)	0.050 (2)
C40	0.119 (3)	0.116 (3)	0.228 (5)	0.026 (4)	0.031 (4)	0.053 (3)

C41	0.131 (6)	0.184 (7)	0.351 (9)	0.051 (5)	0.043 (7)	-0.004 (7)
C42	0.119 (3)	0.132 (4)	0.184 (4)	0.020 (3)	0.029 (3)	0.015 (4)
C43	0.126 (4)	0.130 (4)	0.186 (5)	0.005 (4)	0.026 (4)	0.039 (4)
C44	0.205 (5)	0.165 (4)	0.199 (4)	0.013 (4)	0.012 (4)	0.062 (4)
C45	0.208 (7)	0.170 (6)	0.220 (6)	-0.046 (6)	-0.088 (5)	0.075 (5)
N8	0.0914 (19)	0.137 (2)	0.1001 (19)	-0.0178 (19)	-0.0123 (18)	0.0160 (19)
C46	0.091 (3)	0.182 (4)	0.113 (3)	-0.009 (3)	-0.004 (3)	0.030 (3)
C47	0.110 (4)	0.181 (5)	0.135 (4)	0.015 (4)	0.004 (4)	0.002 (4)
C48	0.105 (3)	0.161 (4)	0.109 (3)	-0.001 (3)	0.001 (3)	0.006 (3)
C49	0.138 (4)	0.211 (5)	0.129 (4)	0.047 (4)	-0.033 (4)	0.016 (4)
C50	0.116 (2)	0.123 (2)	0.1128 (19)	-0.0268 (19)	-0.0269 (19)	0.0155 (19)
C51	0.154 (4)	0.129 (4)	0.139 (4)	-0.003 (3)	-0.031 (3)	0.005 (3)
N9	0.105 (2)	0.102 (2)	0.105 (2)	-0.0175 (19)	-0.0242 (19)	0.0129 (19)
C52	0.113 (3)	0.106 (3)	0.107 (3)	-0.020 (3)	-0.038 (3)	0.013 (3)
C53	0.115 (5)	0.082 (4)	0.122 (5)	-0.013 (4)	-0.057 (4)	0.012 (4)
C54	0.114 (2)	0.121 (2)	0.110 (2)	-0.019 (2)	-0.013 (2)	0.020 (2)
C55	0.098 (4)	0.148 (4)	0.104 (4)	-0.001 (4)	-0.005 (4)	0.034 (4)
C56	0.101 (3)	0.112 (3)	0.109 (3)	-0.007 (3)	-0.018 (3)	0.009 (3)
C57	0.094 (5)	0.127 (6)	0.107 (5)	0.022 (4)	0.006 (4)	0.002 (5)
N10	0.107 (2)	0.106 (2)	0.106 (2)	-0.017 (2)	-0.025 (2)	0.013 (2)
C58	0.111 (2)	0.112 (2)	0.112 (2)	-0.014 (2)	-0.029 (2)	0.008 (2)
C59	0.120 (5)	0.093 (5)	0.116 (5)	-0.008 (5)	-0.060 (5)	0.011 (5)
C60	0.103 (2)	0.119 (2)	0.112 (2)	-0.015 (2)	-0.012 (2)	0.014 (2)
C61	0.115 (4)	0.157 (4)	0.107 (4)	-0.018 (4)	-0.015 (4)	0.020 (4)
C62	0.110 (3)	0.113 (3)	0.110 (3)	-0.011 (3)	-0.013 (3)	0.014 (3)
C63	0.089 (5)	0.117 (5)	0.094 (6)	0.007 (5)	0.004 (5)	0.007 (5)
C1	0.0456 (8)	0.0407 (8)	0.0636 (10)	-0.0047 (7)	0.0098 (8)	0.0019 (8)
C2	0.0484 (10)	0.0766 (12)	0.0733 (12)	-0.0008 (10)	0.0023 (9)	0.0044 (10)
C3	0.0654 (11)	0.0715 (12)	0.0595 (10)	-0.0088 (10)	0.0037 (9)	0.0027 (10)
C4	0.0681 (11)	0.0476 (9)	0.0576 (9)	-0.0079 (8)	0.0190 (8)	0.0016 (8)
C5	0.0508 (9)	0.0507 (9)	0.0665 (10)	0.0022 (8)	0.0138 (8)	0.0033 (8)
C6	0.0468 (9)	0.0389 (8)	0.0595 (9)	0.0000 (7)	0.0069 (8)	0.0037 (7)
C7	0.0511 (9)	0.0587 (10)	0.0519 (9)	0.0112 (8)	-0.0044 (8)	-0.0039 (8)
C8	0.0777 (13)	0.0728 (12)	0.0626 (11)	0.0053 (11)	0.0130 (10)	-0.0099 (10)
C9	0.0980 (16)	0.0806 (15)	0.0910 (15)	-0.0041 (13)	0.0317 (13)	0.0013 (13)
C10	0.0748 (13)	0.0669 (13)	0.1011 (16)	-0.0014 (11)	-0.0133 (12)	-0.0032 (12)
C11	0.147 (2)	0.0625 (13)	0.0681 (13)	0.0047 (14)	-0.0249 (14)	-0.0101 (11)
C12	0.134 (2)	0.0678 (12)	0.0496 (10)	0.0093 (14)	0.0010 (12)	-0.0012 (10)
C13	0.127 (2)	0.0776 (16)	0.187 (3)	-0.0246 (18)	0.001 (2)	-0.004 (2)
C14	0.0360 (8)	0.0505 (9)	0.0643 (10)	0.0101 (7)	0.0095 (7)	0.0110 (8)
C15	0.0570 (11)	0.0640 (11)	0.0901 (13)	-0.0043 (9)	0.0044 (10)	0.0284 (10)
C16	0.0667 (12)	0.0853 (13)	0.0762 (12)	0.0127 (11)	0.0111 (10)	0.0398 (10)
C17	0.0504 (10)	0.0860 (12)	0.0588 (10)	0.0127 (10)	0.0085 (8)	0.0203 (10)
C18	0.0514 (10)	0.0725 (12)	0.0572 (10)	-0.0025 (9)	0.0027 (8)	0.0067 (9)
C19	0.0414 (8)	0.0533 (9)	0.0529 (9)	0.0038 (7)	0.0083 (7)	0.0086 (7)
C20	0.0650 (11)	0.0560 (10)	0.0550 (9)	-0.0142 (9)	0.0006 (9)	0.0099 (8)
C21	0.0738 (12)	0.0712 (12)	0.0610 (11)	-0.0084 (11)	-0.0036 (10)	0.0115 (10)
C22	0.0994 (16)	0.0775 (13)	0.0618 (11)	-0.0082 (13)	0.0116 (11)	0.0020 (11)
C23	0.0911 (15)	0.0684 (13)	0.0919 (15)	0.0007 (12)	0.0184 (13)	0.0116 (12)
C24	0.0780 (14)	0.0801 (14)	0.0947 (15)	0.0079 (12)	0.0014 (13)	0.0182 (12)
C25	0.0803 (13)	0.0707 (12)	0.0644 (11)	-0.0074 (11)	-0.0060 (10)	0.0107 (10)

C26	0.137 (2)	0.119 (2)	0.136 (2)	0.0348 (19)	0.0440 (19)	-0.0009 (19)
C27	0.0398 (8)	0.0497 (9)	0.0521 (9)	-0.0081 (7)	-0.0011 (7)	0.0069 (7)
C28	0.0398 (8)	0.0576 (10)	0.0764 (11)	-0.0049 (8)	0.0006 (8)	0.0034 (9)
C29	0.0588 (10)	0.0477 (9)	0.0765 (11)	0.0044 (8)	-0.0205 (9)	0.0000 (9)
C30	0.0706 (11)	0.0449 (9)	0.0524 (9)	-0.0125 (8)	-0.0132 (9)	0.0090 (8)
C31	0.0595 (10)	0.0562 (10)	0.0480 (9)	-0.0134 (8)	0.0037 (8)	0.0121 (8)
C32	0.0435 (8)	0.0497 (9)	0.0483 (8)	-0.0072 (7)	0.0020 (7)	0.0108 (7)
C33	0.0613 (10)	0.0648 (11)	0.0803 (12)	0.0147 (9)	0.0291 (9)	0.0197 (10)
C34	0.0649 (12)	0.1136 (18)	0.0837 (13)	-0.0023 (13)	0.0271 (11)	0.0218 (13)
C35	0.1020 (16)	0.1011 (17)	0.0905 (14)	0.0157 (14)	0.0455 (12)	0.0260 (13)
C36	0.157 (2)	0.0587 (12)	0.0864 (15)	0.0235 (14)	0.0365 (15)	0.0010 (11)
C37	0.179 (3)	0.0621 (13)	0.1080 (19)	-0.0218 (18)	0.020 (2)	-0.0135 (14)
C38	0.134 (2)	0.0586 (12)	0.0967 (15)	-0.0112 (14)	0.0360 (15)	0.0121 (12)
C39	0.284 (5)	0.103 (2)	0.0843 (18)	0.010 (3)	0.037 (2)	-0.0153 (17)

Geometric Paramter (Å, °)

Lu1—O1 ⁱ	2.1497 (12)	C56—H56B	0.9700
Lu1—O1	2.1497 (12)	C56—C57	1.547 (10)
Lu1—O6	2.1779 (11)	C57—H57A	0.9600
Lu1—O6 ¹	2.1778 (11)	C57—H57B	0.9600
Lu1—O11 ⁱ	2.2034 (11)	C57—H57C	0.9600
Lu1—O11	2.2034 (11)	N10—H10	0.9800
S1—O4	1.4262 (15)	N10—C58	1.511 (9)
S1—O5	1.4311 (15)	N10—C60	1.521 (9)
S1—N2	1.6297 (15)	N10—C62	1.517 (9)
S1—C7	1.7540 (19)	C58—H58A	0.9700
S2—O9	1.4367 (14)	C58—H58B	0.9700
S2—O10	1.4273 (13)	C58—C59	1.564 (11)
S2—N4	1.6325 (15)	C59—H59A	0.9600
S2—C20	1.754 (2)	C59—H59B	0.9600
S3—O14	1.4258 (18)	C59—H59C	0.9600
S3—O15	1.422 (2)	C60—H60A	0.9700
S3—N6	1.6095 (16)	C60—H60B	0.9700
S3—C33	1.755 (2)	C60—C61	1.446 (11)
O1—C1	1.296 (2)	C61—H61A	0.9600
O2—N1	1.227 (2)	C61—H61B	0.9600
O3—N1	1.230 (2)	C61—H61C	0.9600
O6—C14	1.310 (2)	C62—H62A	0.9700
O7—N3	1.222 (3)	C62—H62B	0.9700
O8—N3	1.207 (3)	C62—C63	1.543 (11)
O11—C27	1.313 (2)	C63—H63A	0.9600
O12—N5	1.226 (2)	C63—H63B	0.9600
O13—N5	1.221 (3)	C63—H63C	0.9600
N1—C4	1.446 (2)	C1—C2	1.402 (3)
N2—H2	0.79 (2)	C1—C6	1.416 (2)
N2—C6	1.424 (2)	C2—H2A	0.9300
N3—C17	1.453 (3)	C2—C3	1.363 (3)
N4—H4	0.79 (2)	C3—H3	0.9300
N4—C19	1.415 (2)	C3—C4	1.381 (3)

N5—C30	1.457 (2)	C4—C5	1.382 (3)
N6—H6	0.71 (2)	C5—H5	0.9300
N6—C32	1.402 (2)	C5—C6	1.376 (2)
N7—H7	0.9800	C7—C8	1.368 (3)
N7—C40	1.590 (6)	C7—C12	1.379 (3)
N7—C42	1.487 (6)	C8—H8	0.9300
N7—C44	1.506 (7)	C8—C9	1.380 (3)
C40—H40A	0.9700	C9—H9	0.9300
C40—H40B	0.9700	C9—C10	1.370 (3)
C40—C41	1.507 (8)	C10—C11	1.363 (3)
C41—H41A	0.9600	C10—C13	1.526 (4)
C41—H41B	0.9600	C11—H11	0.9300
C41—H41C	0.9600	C11—C12	1.364 (3)
C42—H42A	0.9700	C12—H12	0.9300
C42—H42B	0.9700	C13—H13A	0.9600
C42—C43	1.514 (7)	C13—H13B	0.9600
C43—H43A	0.9600	C13—H13C	0.9600
C43—H43B	0.9600	C14—C15	1.400 (3)
C43—H43C	0.9600	C14—C19	1.415 (2)
C44—H44A	0.9700	C15—H15	0.9300
C44—H44B	0.9700	C15—C16	1.382 (3)
C44—C45	1.242 (8)	C16—H16	0.9300
C45—H45A	0.9600	C16—C17	1.360 (3)
C45—H45B	0.9600	C17—C18	1.381 (3)
C45—H45C	0.9600	C18—H18	0.9300
N8—H8A	0.9800	C18—C19	1.376 (2)
N8—C46	1.511 (6)	C20—C21	1.382 (3)
N8—C48	1.488 (6)	C20—C25	1.382 (3)
N8—C50	1.429 (6)	C21—H21	0.9300
C46—H46A	0.9700	C21—C22	1.374 (3)
C46—H46B	0.9700	C22—H22	0.9300
C46—C47	1.477 (8)	C22—C23	1.378 (3)
C47—H47A	0.9600	C23—C24	1.383 (3)
C47—H47B	0.9600	C23—C26	1.507 (4)
C47—H47C	0.9600	C24—H24	0.9300
C48—H48A	0.9700	C24—C25	1.364 (3)
C48—H48B	0.9700	C25—H25	0.9300
C48—C49	1.493 (7)	C26—H26A	0.9600
C49—H49A	0.9600	C26—H26B	0.9600
C49—H49B	0.9600	C26—H26C	0.9600
<hr/>			
C49—H49C	0.9600	C27—C28	1.391 (2)
C50—H50A	0.9700	C27—C32	1.418 (2)
C50—H50B	0.9700	C28—H28	0.9300
C50—C51	1.570 (8)	C28—C29	1.381 (3)
C51—H51A	0.9600	C29—H29	0.9300
C51—H51B	0.9600	C29—C30	1.367 (3)
C51—H51C	0.9600	C30—C31	1.378 (3)
N9—H9A	0.9800	C31—H31	0.9300
N9—C52	1.492 (8)	C31—C32	1.371 (2)
N9—C54	1.549 (8)	C33—C34	1.380 (3)

N9—C56	1.490 (9)	C33—C38	1.369 (3)
C52—H52A	0.9700	C34—H34	0.9300
C52—H52B	0.9700	C34—C35	1.384 (3)
C52—C53	1.568 (9)	C35—H35	0.9300
C53—H53A	0.9600	C35—C36	1.354 (4)
C53—H53B	0.9600	C36—C37	1.382 (4)
C53—H53C	0.9600	C36—C39	1.512 (4)
C54—H54A	0.9700	C37—H37	0.9300
C54—H54B	0.9700	C37—C38	1.380 (4)
C54—C55	1.474 (10)	C38—H38	0.9300
C55—H55A	0.9600	C39—H39A	0.9600
C55—H55B	0.9600	C39—H39B	0.9600
C55—H55C	0.9600	C39—H39C	0.9600
C56—H56A	0.9700		
O1 ⁱ —Lu1—O1	180.0	C56—C57—H57A	109.5
O1—Lu1—O6 ⁱ	86.94 (4)	C56—C57—H57B	109.5
O1—Lu1—O6	93.06 (5)	C56—C57—H57C	109.5
O1 ¹ —Lu1—O6 ¹	93.05 (5)	H57A—C57—H57B	109.5
O1 ⁱ —Lu1—O6	86.95 (4)	H57A—C57—H57C	109.5
O1 ¹ —Lu1—O11	87.33 (5)	H57B—C57—H57C	109.5
O1 ⁱ —Lu1—O11 ⁱ	92.67 (5)	C58—N10—H10	98.5
O1—Lu1—O11	92.67 (5)	C58—N10—C60	138.5 (7)
O1—Lu1—O11 ¹	87.33 (5)	C58—N10—C62	107.6 (7)
O6 ¹ —Lu1—O6	180.0	C60—N10—H10	98.5
O6—Lu1—O11 ¹	96.38 (4)	C62—N10—H10	98.5
O6—Lu1—O11	83.62 (4)	C62—N10—C60	106.9 (7)
O6 ⁱ —Lu1—O11	96.38 (4)	N10—C58—H58A	109.5
O6 ¹ —Lu1—O11 ¹	83.62 (4)	N10—C58—H58B	109.5
O11—Lu1—O11 ⁱ	180.00 (4)	N10—C58—C59	110.7 (7)
O4—S1—O5	119.79 (9)	H58A—C58—H58B	108.1
O4—S1—N2	108.34 (9)	C59—C58—H58A	109.5
O4—S1—C7	106.70 (9)	C59—C58—H58B	109.5
O5—S1—N2	105.44 (8)	C58—C59—H59A	109.5
O5—S1—C7	108.55 (9)	C58—C59—H59B	109.5
N2—S1—C7	107.49 (8)	C58—C59—H59C	109.5
O9—S2—N4	107.43 (8)	H59A—C59—H59B	109.5
O9—S2—C20	107.71 (9)	H59A—C59—H59C	109.5
O10—S2—O9	119.10 (9)	H59B—C59—H59C	109.5
O10—S2—N4	105.56 (8)	N10—C60—H60A	107.2
O10—S2—C20	108.16 (9)	N10—C60—H60B	107.2
N4—S2—C20	108.50 (8)	H60A—C60—H60B	106.8

O14—S3—N6	105.19 (10)	C61—C60—N10	120.5 (8)
O14—S3—C33	108.84 (11)	C61—C60—H60A	107.2
O15—S3—O14	119.43 (11)	C61—C60—H60B	107.2
O15—S3—N6	110.42 (10)	C60—C61—H61A	109.5
O15—S3—C33	106.23 (10)	C60—C61—H61B	109.5
N6—S3—C33	106.01 (9)	C60—C61—H61C	109.5
C1—O1—Lu1	147.05 (11)	H61A—C61—H61B	109.5
C14—O6—Lu1	146.10 (11)	H61A—C61—H61C	109.5

C27—O11—Lu1	141.80 (10)	H61B—C61—H61C	109.5
O2—N1—O3	122.53 (18)	N10—C62—H62A	109.1
O2—N1—C4	119.02 (19)	N10—C62—H62B	109.1
O3—N1—C4	118.44 (17)	N10—C62—C63	112.5 (7)
S1—N2—H2	109.5 (15)	H62A—C62—H62B	107.8
C6—N2—S1	124.79 (12)	C63—C62—H62A	109.1
C6—N2—H2	115.9 (15)	C63—C62—H62B	109.1
O7—N3—C17	118.9 (2)	C62—C63—H63A	109.5
O8—N3—O7	122.0 (2)	C62—C63—H63B	109.5
O8—N3—C17	119.04 (19)	C62—C63—H63C	109.5
S2—N4—H4	109.1 (15)	H63A—C63—H63B	109.5
C19—N4—S2	125.52 (12)	H63A—C63—H63C	109.5
C19—N4—H4	118.1 (15)	H63B—C63—H63C	109.5
O12—N5—C30	118.46 (19)	O1—C1—C2	123.15 (16)
O13—N5—O12	123.18 (18)	O1—C1—C6	119.53 (15)
O13—N5—C30	118.36 (18)	C2—C1—C6	117.33 (16)
S3—N6—H6	116.1 (18)	C1—C2—H2A	119.0
C32—N6—S3	128.18 (12)	C3—C2—C1	121.99 (18)
C32—N6—H6	115.7 (18)	C3—C2—H2A	119.0
C40—N7—H7	99.1	C2—C3—H3	120.6
C42—N7—H7	99.1	C2—C3—C4	118.78 (18)
C42—N7—C40	116.7 (5)	C4—C3—H3	120.6
C42—N7—C44	109.9 (5)	C3—C4—N1	119.35 (17)
C44—N7—H7	99.1	C3—C4—C5	122.08 (17)
C44—N7—C40	126.0 (5)	C5—C4—N1	118.52 (17)
N7—C40—H40A	108.7	C4—C5—H5	120.7
N7—C40—H40B	108.7	C6—C5—C4	118.66 (17)
H40A—C40—H40B	107.6	C6—C5—H5	120.7
C41—C40—N7	114.3 (5)	C1—C6—N2	115.88 (15)
C41—C40—H40A	108.7	C5—C6—N2	122.93 (15)
C41—C40—H40B	108.7	C5—C6—C1	121.11 (16)
C40—C41—H41A	109.5	C8—C7—S1	120.44 (15)
C40—C41—H41B	109.5	C8—C7—C12	119.15 (19)
C40—C41—H41C	109.5	C12—C7—S1	120.40 (15)
H41A—C41—H41B	109.5	C7—C8—H8	120.5
H41A—C41—H41C	109.5	C7—C8—C9	119.1 (2)
H41B—C41—H41C	109.5	C9—C8—H8	120.5
N7—C42—H42A	108.6	C8—C9—H9	119.0
N7—C42—H42B	108.6	C10—C9—C8	122.1 (2)
N7—C42—C43	114.8 (5)	C10—C9—H9	119.0
H42A—C42—H42B	107.5	C9—C10—C13	121.5 (2)
C43—C42—H42A	108.6	C11—C10—C9	117.9 (2)
C43—C42—H42B	108.6	C11—C10—C13	120.6 (2)
C42—C43—H43A	109.5	C10—C11—H11	119.4

C42—C43—H43B	109.5	C10—C11—C12	121.2 (2)
C42—C43—H43C	109.5	C12—C11—H11	119.4
H43A—C43—H43B	109.5	C7—C12—H12	119.7
H43A—C43—H43C	109.5	C11—C12—C7	120.6 (2)
H43B—C43—H43C	109.5	C11—C12—H12	119.7

N7—C44—H44A	100.4	C10—C13—H13A	109.5
N7—C44—H44B	100.4	C10—C13—H13B	109.5
H44A—C44—H44B	104.3	C10—C13—H13C	109.5
C45—C44—N7	145.8 (8)	H13A—C13—H13B	109.5
C45—C44—H44A	100.4	H13A—C13—H13C	109.5
C45—C44—H44B	100.4	H13B—C13—H13C	109.5
C44—C45—H45A	109.5	O6—C14—C15	122.29 (16)
C44—C45—H45B	109.5	O6—C14—C19	120.34 (15)
C44—C45—H45C	109.5	C15—C14—C19	117.35 (16)
H45A—C45—H45B	109.5	C14—C15—H15	119.2
H45A—C45—H45C	109.5	C16—C15—C14	121.54 (19)
H45B—C45—H45C	109.5	C16—C15—H15	119.2
C46—N8—H8A	105.1	C15—C16—H16	120.4
C48—N8—H8A	105.1	C17—C16—C15	119.10 (19)
C48—N8—C46	111.6 (4)	C17—C16—H16	120.4
C50—N8—H8A	105.1	C16—C17—N3	119.76 (19)
C50—N8—C46	113.7 (4)	C16—C17—C18	121.91 (18)
C50—N8—C48	115.1 (4)	C18—C17—N3	118.32 (19)
N8—C46—H46A	108.0	C17—C18—H18	120.4
N8—C46—H46B	108.0	C19—C18—C17	119.29 (18)
H46A—C46—H46B	107.2	C19—C18—H18	120.4
C47—C46—N8	117.3 (5)	C14—C19—N4	115.37 (15)
C47—C46—H46A	108.0	C18—C19—N4	123.75 (16)
C47—C46—H46B	108.0	C18—C19—C14	120.79 (16)
C46—C47—H47A	109.5	C21—C20—S2	121.00 (15)
C46—C47—H47B	109.5	C21—C20—C25	120.19 (19)
C46—C47—H47C	109.5	C25—C20—S2	118.79 (15)
H47A—C47—H47B	109.5	C20—C21—H21	120.6
H47A—C47—H47C	109.5	C22—C21—C20	118.76 (19)
H47B—C47—H47C	109.5	C22—C21—H21	120.6
N8—C48—H48A	108.5	C21—C22—H22	118.9
N8—C48—H48B	108.5	C21—C22—C23	122.2 (2)
N8—C48—C49	115.3 (5)	C23—C22—H22	118.9
H48A—C48—H48B	107.5	C22—C23—C24	117.5 (2)
C49—C48—H48A	108.5	C22—C23—C26	120.9 (2)
C49—C48—H48B	108.5	C24—C23—C26	121.6 (2)
C48—C49—H49A	109.5	C23—C24—H24	119.1
C48—C49—H49B	109.5	C25—C24—C23	121.8 (2)
C48—C49—H49C	109.5	C25—C24—H24	119.1
H49A—C49—H49B	109.5	C20—C25—H25	120.2
H49A—C49—H49C	109.5	C24—C25—C20	119.6 (2)
H49B—C49—H49C	109.5	C24—C25—H25	120.2
N8—C50—H50A	108.8	C23—C26—H26A	109.5
N8—C50—H50B	108.8	C23—C26—H26B	109.5
N8—C50—C51	113.7 (4)	C23—C26—H26C	109.5
H50A—C50—H50B	107.7	H26A—C26—H26B	109.5
C51—C50—H50A	108.8	H26A—C26—H26C	109.5

C51—C50—H50B	108.8	H26B—C26—H26C	109.5
C50—C51—H51A	109.5	O11—C27—C28	123.71 (15)

C50—C51—H51B	109.5	O11—C27—C32	118.44 (15)
C50—C51—H51C	109.5	C28—C27—C32	117.85 (15)
H51A—C51—H51B	109.5	C27—C28—H28	119.4
H51A—C51—H51C	109.5	C29—C28—C27	121.10 (17)
H51B—C51—H51C	109.5	C29—C28—H28	119.4
C52—N9—H9A	110.9	C28—C29—H29	120.5
C52—N9—C54	110.3 (5)	C30—C29—C28	118.99 (17)
C54—N9—H9A	110.9	C30—C29—H29	120.5
C56—N9—H9A	110.9	C29—C30—N5	119.16 (17)
C56—N9—C52	115.4 (6)	C29—C30—C31	122.35 (16)
C56—N9—C54	97.8 (5)	C31—C30—N5	118.49 (17)
N9—C52—H52A	109.5	C30—C31—H31	120.7
N9—C52—H52B	109.5	C32—C31—C30	118.66 (17)
N9—C52—C53	110.9 (6)	C32—C31—H31	120.7
H52A—C52—H52B	108.0	N6—C32—C27	114.71 (14)
C53—C52—H52A	109.5	C31—C32—N6	124.32 (15)
C53—C52—H52B	109.5	C31—C32—C27	120.96 (16)
C52—C53—H53A	109.5	C34—C33—S3	119.31 (17)
C52—C53—H53B	109.5	C38—C33—S3	120.88 (17)
C52—C53—H53C	109.5	C38—C33—C34	119.8 (2)
H53A—C53—H53B	109.5	C33—C34—H34	120.1
H53A—C53—H53C	109.5	C33—C34—C35	119.7 (2)
H53B—C53—H53C	109.5	C35—C34—H34	120.1
N9—C54—H54A	109.3	C34—C35—H35	119.5
N9—C54—H54B	109.3	C36—C35—C34	121.0 (2)
H54A—C54—H54B	108.0	C36—C35—H35	119.5
C55—C54—N9	111.4 (7)	C35—C36—C37	118.9 (2)
C55—C54—H54A	109.3	C35—C36—C39	120.1 (3)
C55—C54—H54B	109.3	C37—C36—C39	120.9 (3)
C54—C55—H55A	109.5	C36—C37—H37	119.5
C54—C55—H55B	109.5	C38—C37—C36	120.9 (3)
C54—C55—H55C	109.5	C38—C37—H37	119.5
H55A—C55—H55B	109.5	C33—C38—C37	119.5 (2)
H55A—C55—H55C	109.5	C33—C38—H38	120.2
H55B—C55—H55C	109.5	C37—C38—H38	120.2
N9—C56—H56A	109.1	C36—C39—H39A	109.5
N9—C56—H56B	109.1	C36—C39—H39B	109.5
N9—C56—C57	112.4 (6)	C36—C39—H39C	109.5
H56A—C56—H56B	107.8	H39A—C39—H39B	109.5
C57—C56—H56A	109.1	H39A—C39—H39C	109.5
C57—C56—H56B	109.1	H39B—C39—H39C	109.5
Lu1—O1—C1—C2	-95.7 (2)	C46—N8—C48—C49	-67.7 (7)
Lu1—O1—C1—C6	84.8 (2)	C46—N8—C50—C51	-169.8 (5)
Lu1—O6—C14—C15	-100.4 (2)	C48—N8—C46—C47	-54.4 (7)
Lu1—O6—C14—C19	81.2 (2)	C48—N8—C50—C51	59.7 (6)
Lu1—O11—C27—C28	-21.9 (3)	C50—N8—C46—C47	173.4 (5)
Lu1—O11—C27—C32	158.91 (13)	C50—N8—C48—C49	63.7 (7)
S1—N2—C6—C1	142.40 (13)	C52—N9—C54—C55	-68.8 (9)
S1—N2—C6—C5	-40.8 (2)	C52—N9—C56—C57	168.1 (7)

S1—C7—C8—C9	-177.33 (17)	C54—N9—C52—C53	175.4 (7)
S1—C7—C12—C11	177.47 (19)	C54—N9—C56—C57	-74.9 (8)
S2—N4—C19—C14	-152.20 (13)	C56—N9—C52—C53	-75.0 (9)
S2—N4—C19—C18	31.2 (2)	C56—N9—C54—C55	170.4 (7)
S2—C20—C21—C22	-177.13 (16)	C58—N10—C60—C61	70.7 (16)
S2—C20—C25—C24	176.99 (17)	C58—N10—C62—C63	72.5 (11)
S3—N6—C32—C27	175.42 (13)	C60—N10—C58—C59	70.9 (14)
S3—N6—C32—C31	-3.5 (3)	C60—N10—C62—C63	-130.9 (9)
S3—C33—C34—C35	-173.72 (19)	C62—N10—C58—C59	-144.1 (9)
S3—C33—C38—C37	173.9 (2)	C62—N10—C60—C61	-74.5 (12)
O1—C1—C2—C3	-177.29 (18)	C1—C2—C3—C4	-0.7 (3)
O1—C1—C6—N2	-5.5 (2)	C2—C1—C6—N2	175.04 (16)
O1—C1—C6—C5	177.68 (15)	C2—C1—C6—C5	-1.8 (2)
O2—N1—C4—C3	-0.3 (3)	C2—C3—C4—N1	-178.78 (18)
O2—N1—C4—C5	-177.90 (18)	C2—C3—C4—C5	-1.3 (3)
O3—N1—C4—C3	179.20 (19)	C3—C4—C5—C6	1.6 (3)
O3—N1—C4—C5	1.6 (3)	C4—C5—C6—N2	-176.63 (16)
O4—S1—N2—C6	52.06 (17)	C4—C5—C6—C1	0.0 (3)
O4—S1—C7—C8	151.29 (16)	C6—C1—C2—C3	2.2 (3)
O4—S1—C7—C12	-27.70 (19)	C7—S1—N2—C6	-62.89 (16)
O5—S1—N2—C6	-178.55 (14)	C7—C8—C9—C10	-0.6 (4)
O5—S1—C7—C8	20.92 (18)	C8—C7—C12—C11	-1.5 (3)
O5—S1—C7—C12	-158.08 (17)	C8—C9—C10—C11	-0.6 (4)
O6—C14—C15—C16	-177.73 (18)	C8—C9—C10—C13	178.2 (2)
O6—C14—C19—N4	0.4 (2)	C9—C10—C11—C12	0.7 (4)
O6—C14—C19—C18	177.11 (16)	C10—C11—C12—C7	0.3 (4)
O7—N3—C17—C16	9.6 (3)	C12—C7—C8—C9	1.7 (3)
O7—N3—C17—C18	-171.7 (2)	C13—C10—C11—C12	-178.1 (3)
O8—N3—C17—C16	-166.8 (2)	C14—C15—C16—C17	0.6 (3)
O8—N3—C17—C18	11.9 (3)	C15—C14—C19—N4	-178.07 (16)
O9—S2—N4—C19	-51.21 (16)	C15—C14—C19—C18	-1.4 (3)
O9—S2—C20—C21	20.37 (19)	C15—C16—C17—N3	177.25 (19)
O9—S2—C20—C25	-158.19 (16)	C15—C16—C17—C18	-1.4 (3)
O10—S2—N4—C19	-179.28 (14)	C16—C17—C18—C19	0.8 (3)
O10—S2—C20—C21	150.32 (16)	C17—C18—C19—N4	177.08 (17)
O10—S2—C20—C25	-28.24 (18)	C17—C18—C19—C14	0.7 (3)
O11—C27—C28—C29	-177.63 (17)	C19—C14—C15—C16	0.7 (3)
O11—C27—C32—N6	-3.0 (2)	C20—S2—N4—C19	64.97 (16)
O11—C27—C32—C31	175.95 (15)	C20—C21—C22—C23	-0.3 (3)
O12—N5—C30—C29	1.2 (3)	C21—C20—C25—C24	-1.6 (3)
O12—N5—C30—C31	-179.12 (18)	C21—C22—C23—C24	-0.7 (4)
O13—N5—C30—C29	-178.26 (18)	C21—C22—C23—C26	179.6 (2)
O13—N5—C30—C31	1.4 (3)	C22—C23—C24—C25	0.5 (4)
O14—S3—N6—C32	-177.57 (16)	C23—C24—C25—C20	0.6 (3)
O14—S3—C33—C34	110.03 (19)	C25—C20—C21—C22	1.4 (3)
O14—S3—C33—C38	-67.4 (2)	C26—C23—C24—C25	-179.7 (2)
O15—S3—N6—C32	-47.45 (19)	C27—C28—C29—C30	0.9 (3)
O15—S3—C33—C34	-19.8 (2)	C28—C27—C32—N6	177.72 (15)
O15—S3—C33—C38	162.85 (19)	C28—C27—C32—C31	-3.3 (2)
N1—C4—C5—C6	179.13 (16)	C28—C29—C30—N5	177.84 (17)
N2—S1—C7—C8	-92.67 (17)	C28—C29—C30—C31	-1.9 (3)
N2—S1—C7—C12	88.33 (18)	C29—C30—C31—C32	0.2 (3)

N3—C17—C18—C19	-177.92 (18)	C30—C31—C32—N6	-178.68 (16)
N4—S2—C20—C21	-95.63 (17)	C30—C31—C32—C27	2.5 (3)
N4—S2—C20—C25	85.81 (17)	C32—C27—C28—C29	1.6 (3)
N5—C30—C31—C32	-179.52 (16)	C33—S3—N6—C32	67.21 (18)
N6—S3—C33—C34	-137.26 (18)	C33—C34—C35—C36	-0.6 (4)
N6—S3—C33—C38	45.3 (2)	C34—C33—C38—C37	-3.5 (4)
C40—N7—C42—C43	133.4 (6)	C34—C35—C36—C37	-2.6 (4)
C40—N7—C44—C45	48.6 (17)	C34—C35—C36—C39	-179.8 (3)
C42—N7—C40—C41	-64.6 (8)	C35—C36—C37—C38	2.8 (4)
C42—N7—C44—C45	-100.0 (14)	C36—C37—C38—C33	0.2 (4)
C44—N7—C40—C41	148.7 (7)	C38—C33—C34—C35	3.7 (3)
C44—N7—C42—C43	-74.8 (8)	C39—C36—C37—C38	180.0 (3)

5.5 Conclusions

In conclusion, we have demonstrated μM level optical sensing of Lu(III) with a *p*-nitrophenol-sulfonamide under alkaline conditions even in the presence of high concentrations of other metals present in HLW, such as Na(I), K(I) and Sr(II). Nonlinear regression analysis from UV-Vis titrations of **LH**₂ and 2.5 equivalents of DIPEA gave a binding constant of $K_{11} = 5.8 (\pm 0.4) \times 10^6 \text{ M}^{-1}$ for Lu(III) for 1:1 complexation in acetonitrile. Lu(III) sensing with LOD as low as 0.207 μM was achieved within a linear range of 0 – 4.93 μM in the presence of higher concentrations of competing metals present in alkaline HLW. Complex formation was confirmed by electrochemistry, with redox changes due to the formation of a Lu(III) complex consistent with CVs which were very different from those of **LH**₂ and Lu(III) measured independently. The X-ray structure of two separately isolated complexes showed a monomeric Lu(III) complex $(\text{Et}_3\text{NH})_3[\text{Lu}(\text{LH})_6]$ and a unique Lu(III) trimeric cluster $(\text{Et}_3\text{NH})_5[\text{Lu}_3(\mu_3\text{-OH})_2(\text{LH})_6(\text{L})_3]$. We anticipate that such simple sensors could find application in detecting Lu(III) for biomedical applications and for detection of Ln(III) fission products in HLW.

5.6 Acknowledgments

This work was supported by the U.S. Department of Energy Office of Environmental Management MSIP Program managed by the Savannah River National Laboratory under SRNS contracts BOA 541, TOAs 0000403071 and 0000525181 to FIU. We also appreciate the support received from the Florida International University Dissertation Year Fellowship for Oluwaseun William Adedoyin (DYF Summer/Fall 2021 Fellow).

5.7 References

1. Gupta, C. K.; Krishnamurthy, N. Extractive metallurgy of rare earths. *International Materials Reviews* **1992**, *37*, 197-248.
2. Aime, S.; Barge, A.; Delli Castelli, D.; Fedeli, F.; Mortillaro, A.; Nielsen, F. U.; Terreno, E. Paramagnetic lanthanide (III) complexes as pH-sensitive chemical exchange saturation transfer (CEST) contrast agents for MRI applications. *Magnetic Resonance in Medicine: An Official Journal of the International Society for Magnetic Resonance in Medicine* **2002**, *47*, 639-648.
3. Sherry, A. D.; Caravan, P.; Lenkinski, R. E. Primer on gadolinium chemistry. *Journal of Magnetic Resonance Imaging: An Official Journal of the International Society for Magnetic Resonance in Medicine* **2009**, *30*, 1240-1248.
4. Clough, T. J.; Jiang, L.; Wong, K.; Long, N. J. Ligand design strategies to increase stability of gadolinium-based magnetic resonance imaging contrast agents. *Nature Communications* **2019**, *10*, 1-14.
5. Bottrill, M.; Kwok, L.; Long, N. J. Lanthanides in magnetic resonance imaging. *Chemical Society Reviews* **2006**, *35*, 557-571.
6. Peters, C.; Braekers, D.; Kroupa, J.; Kasyan, O.; Miroshnichenko, S.; Rudzevich, V.; Böhmer, V.; Desreux, J. CMPO-calix[4]arenes and the influence of structural modifications on the Eu(III), Am(III), Cm(III) separation. *Radiochimica Acta* **2008**, *96*, 203-210.
7. Dam, H. H.; Reinhoudt, D. N.; Verboom, W. Multicoordinate ligands for actinide/lanthanide separations. *Chemical Society Reviews* **2007**, *36*, 367-377.
8. Kolarik, Z. Complexation and separation of lanthanides (III) and actinides (III) by heterocyclic N-donors in solutions. *Chemical Reviews* **2008**, *108*, 4208-4252.

9. Nash, K. L. A review of the basic chemistry and recent developments in trivalent f-elements separations. *Solvent Extraction and Ion Exchange* **1993**, *11*, 729-768.
10. Hudson, M. J.; Harwood, L. M.; Laventine, D. M.; Lewis, F. W. Use of soft heterocyclic N-donor ligands to separate actinides and lanthanides. *Inorganic Chemistry* **2013**, *52*, 3414-3428.
11. Lewis, F. W.; Hudson, M. J.; Harwood, L. M. Development of highly selective ligands for separations of actinides from lanthanides in the nuclear fuel cycle. *Synlett*. **2011**, *18*, 2609-2632.
12. Modolo, G.; Wilden, A.; Geist, A.; Magnusson, D.; Malmbeck, R. A review of the demonstration of innovative solvent extraction processes for the recovery of trivalent minor actinides from PUREX raffinate. *Radiochimica Acta* **2012**, *100*, 715-725.
13. Paiva, A. P.; Malik, P. Recent advances on the chemistry of solvent extraction applied to the reprocessing of spent nuclear fuels and radioactive wastes. *Journal of Radioanalytical and Nuclear Chemistry* **2004**, *261*, 485-496.
14. Lehman-Andino, I.; Su, J.; Papathanasiou, K. E.; Eaton, T. M.; Jian, J.; Dan, D.; Albrecht-Schmitt, T. E.; Dares, C. J.; Batista, E. R.; Yang, P. Soft-donor dipicolinamide derivatives for selective actinide (III) / lanthanide (III) separation: the role of S- vs. O-donor sites. *Chemical Communications* **2019**, *55*, 2441-2444.
15. Sartain, H. T.; McGraw, S. N.; Lawrence, C. L.; Werner, E. J.; Biros, S. M. A novel tripodal CMPO ligand: Affinity for f-elements, computational investigations, and luminescence properties. *Inorganica Chimica Acta* **2015**, *426*, 126-135.
16. Grimes, T. S.; Tillotson, R. D.; Martin, L. R. Trivalent lanthanide/actinide separation using aqueous-modified TALSPEAK chemistry. *Solvent Extraction and Ion Exchange* **2014**, *32*, 378-390.
17. Veliscek-Carolan, J. Separation of actinides from spent nuclear fuel: A review. *Journal of Hazardous Materials* **2016**, *318*, 266-281.
18. MR Pillai, A.; F Russ Knapp, F. Evolving important role of lutetium-177 for therapeutic nuclear medicine. *Current radiopharmaceuticals* **2015**, *8*, 78-85.
19. Banerjee, S.; Pillai, M.; Knapp, F. F. Lutetium-177 therapeutic radiopharmaceuticals: linking chemistry, radiochemistry, and practical applications. *Chemical Reviews* **2015**, *115*, 2934-2974.
20. Sanders, J. K.; Williams, D. H. A shift reagent for use in nuclear magnetic resonance spectroscopy. A first-order spectrum of *n*-hexanol. *Journal of the Chemical Society D: Chemical Communications* **1970**, 422-423.
21. Sanders, J. K.; Hanson, S. W.; Williams, D. H. Paramagnetic shift reagents. Nature of the interactions. *Journal of the American Chemical Society* **1972**, *94*, 5325-5335.

22. Park, J. K.; Choi, K. J.; Kim, C. H.; Park, H. D.; Choi, S. Y. Optical properties of Eu(II) - activated Sr₂SiO₄ phosphor for light-emitting diodes. *Electrochemical and Solid-State Letters* **2004**, *7*, H15.
23. Yoo, J. S.; Kim, S. H.; Yoo, W. T.; Hong, G. Y.; Kim, K. P.; Rowland, J.; Holloway, P. H. Control of spectral properties of strontium-alkaline earth-silicate-europium phosphors for LED applications. *Journal of the Electrochemical Society* **2005**, *152*, G382.
24. Kaur, B.; Kaur, N.; Kumar, S. Colorimetric metal ion sensors—a comprehensive review of the years 2011–2016. *Coordination Chemistry Reviews* **2018**, *358*, 13-69.
25. Bonnesen, P. V.; Delmau, L. H.; Moyer, B. A.; Leonard, R. A. A robust alkaline-side CSEX solvent suitable for removing cesium from Savannah River high-level waste. *Solvent Extraction and Ion Exchange* **2000**, *18*, 1079-1107.
26. Bonnesen, P. V.; Delmau, L. H.; Haverlock, T. J.; Moyer, B. A. Alkaline-Side Extraction of Cesium from Savannah River Tank Waste Using a Calixarene-Crown Ether Extractant. Alkaline-Side Extraction of Cesium from Savannah River Tank Waste Using a Calixarene-Crown Ether Extractant Oak Ridge National Lab., TN (US), No. ORNL/TM-13704, **1998**.
27. Choppin, G. R. Lanthanide complexation in aqueous solutions. *Journal of the Less Common Metals* **1984**, *100*, 141-151.
28. Neidig, M. L.; Clark, D. L.; Martin, R. L. Covalency in f-element complexes. *Coordination Chemistry Reviews* **2013**, *257*, 394-406.
29. Habenschuss, A.; Spedding, F. H. The coordination (hydration) of rare earth ions in aqueous chloride solutions from X-ray diffraction. II. LaCl₃, PrCl₃, and NdCl₃. *Journal of Chemical Physics* **1979**, *70*, 3758-3763.
30. Kanno, H.; Akama, Y. Evidence for the change of inner-sphere hydration number or rare earth ions in the middle of the series. *Chemical Physics Letters* **1980**, *72*, 181-183.
31. Morozov, A. N.; Govor, E. V.; Anagnostopoulos, V. A.; Kavallieratos, K.; Mebel, A. M. 1, 3, 5-Tris-(4-(iso-propyl)-phenylsulfamoylmethyl) benzene as a potential Am(III) extractant: experimental and theoretical study of Sm(III) complexation and extraction and theoretical correlation with Am(III). *Molecular Physics* **2018**, *116*, 2719-2727.
32. Fedosseev, A. M.; Grigoriev, M. S.; Budantseva, N. A.; Guillaumont, D.; Le Naour, C.; Simoni, É; Den Auwer, C.; Moisy, P. Americium (III) coordination chemistry: An unexplored diversity of structure and bonding. *Comptes Rendus Chimie* **2010**, *13*, 839-848.
33. Liang, Z.; Liu, Z.; Gao, Y. A selective colorimetric chemosensor based on calixarene framework for lanthanide ions Dy(III) and Er(III). *Tetrahedron Letters* **2007**, *48*, 3587-3590.

34. Kaur, N.; Kumar, S. Colorimetric metal ion sensors. *Tetrahedron* **2011**, *67*, 9233-9264.
35. Liu, Z.; Jiang, L.; Liang, Z.; Gao, Y. A selective colorimetric chemosensor for lanthanide ions. *Tetrahedron* **2006**, *62*, 3214-3220.
36. Rouis, A.; Mlika, R.; Dridi, C.; Davenas, J.; Ben Ouada, H.; Halouani, H.; Bonnamour, I.; Jaffrezic, N. Optical spectroscopy studies of the complexation of chromogenic azo-calix[4]arene with Eu(III), Ag(I) and Cu(II) ions. *Materials Science and Engineering: C* **2006**, *26*, 247-252.
37. Lisowski, C. E.; Hutchison, J. E. Malonamide-functionalized gold nanoparticles for selective, colorimetric sensing of trivalent lanthanide ions. *Analytical Chemistry* **2009**, *81*, 10246-10253.
38. Bekiari, V.; Judeinstein, P.; Lianos, P. A sensitive fluorescent sensor of lanthanide ions. *Journal of Luminescence* **2003**, *104*, 13-15.
39. Das, P.; Ghosh, A.; Das, A. Unusual specificity of a receptor for Nd(III) among other lanthanide ions for selective colorimetric recognition. *Inorganic Chemistry* **2010**, *49*, 6909-6916.
40. Wang, S.; Ding, L.; Fan, J.; Wang, Z.; Fang, Y. Bispyrene/surfactant-assembly-based fluorescent sensor array for discriminating lanthanide ions in aqueous solution. *ACS Applied Materials & Interfaces* **2014**, *6*, 16156-16165.
41. Hosseini, M.; Ganjali, M. R.; Aboufazeli, F.; Faridbod, F.; Goldooz, H.; Badiiei, A.; Norouzi, P. A selective fluorescent bulk sensor for lutetium based on hexagonal mesoporous structures. *Sensors Actuators B: Chem* **2013**, *184*, 93-99.
42. Kumar, R. S.; Kumar, S. A.; Vijayakrishna, K.; Sivaramakrishna, A.; Rao, C. B.; Sivaraman, N.; Sahoo, S. K. Highly selective CHEF-type chemosensor for lutetium (III) recognition in semi-aqueous media. *Spectrochimica Acta Part A: Molecular and Biomolecular Spectroscopy* **2019**, *214*, 32-39.
43. Faridbod, F.; Sedaghat, M.; Hosseini, M. E.; Ganjali, M. R.; Khoobi, M.; Shafiee, A.; Norouzi, P. Turn-on fluorescent chemosensor for determination of lutetium ion. *Spectrochimica Acta Part A: Molecular and Biomolecular Spectroscopy* **2015**, *137*, 1231-1234.
44. Alvarado, R. J.; Rosenberg, J. M.; Andreu, A.; Bryan, J. C.; Chen, W.; Ren, T.; Kavallieratos, K. Structural insights into the coordination and extraction of Pb(II) by disulfonamide ligands derived from *o*-phenylenediamine. *Inorganic Chemistry* **2005**, *44*, 7951-7959.
45. Govor, E. V.; Morozov, A. N.; Rains, A. A.; Mebel, A. M.; Kavallieratos, K. Spectroscopic and theoretical insights into surprisingly effective Sm(III) extraction

- from alkaline aqueous media by *o*-phenylenediamine-derived sulfonamides. *Inorganic Chemistry* **2020**, *59*, 6884-6894.
46. Myasoedov, B. F.; Karalova, Z. K.; Nekrasova, V. V.; Rodionova, L. M. Extraction of actinides and lanthanides from alkaline solutions by quaternary ammonium bases and alkylpyrocatechols. *Journal of Inorganic and Nuclear Chemistry* **1980**, *42*, 1495-1499.
 47. Smirnov, I. V.; Stepanova, E. S.; Drapailo, A. B.; Kalchenko, V. I. Extraction of americium and europium with functionalized calixarenes from alkaline solutions. *Radiochemistry* **2016**, *58*, 42-51.
 48. Gale, P.; Twyman, L.; Handlin, C.; Sessler, J. A colourimetric calix[4]pyrrole-4-nitrophenolate based anion sensor. *Chemical Communications* **1999**, 1851-1852.
 49. Bartsch, R. A.; Chapoteau, E.; Czech, B. P.; Krzykawski, J.; Kumar, A.; Robison, T. W. A novel 12-membered triazaoxamacrocyclic-N, N', N''-triacetic acid indicator for colorimetric determination of calcium. *Journal of Organic Chemistry* **1993**, *58*, 4681-4684.
 50. KumaraBoominathan, S. S.; ChandruSenadi, G; KishoreaVandavasi, J. A one-pot hypiodite catalysed oxidative cycloetherification approach to benzoxazoles. *Chemical Communications* **2014**, *51*, 6726 – 6728.
 51. Connors, K. A. Binding constants: the measurement of molecular complex stability; Wiley-Interscience: **1987**.
 52. Shrivastava, A.; Gupta, V. B. Methods for the determination of limit of detection and limit of quantitation of the analytical methods. *Chronicles of young scientists* **2011**, *2*, 21-25.
 53. Lee, C.; Yang, W. and Parr, R. G. Development of the ColleSalvetti correlation-energy formula into a functional of the electron density. *Physical Review B* **1988**, *37*, 785-789.
 54. Becke, A. D. Density-functional thermochemistry. The role of exact exchange. *The Journal of Chemical Physics* **1993**, *98*, 5648-5652.
 55. Hariharan, P. C., & Pople, J. A. The influence of polarization functions on molecular orbital hydrogenation energies. *Theoretica Chimica Acta* **1973**, *28*, 213-222.

56. Francl, M. M.; Pietro, W. J.; Hehre, W. J.; Binkley, J. S.; Gordon, M. S.; DeFrees, D. J.; & Pople, J. A. Self-consistent molecular orbital methods. XXIII. A polarization-type basis set for second-row elements. *The Journal of Chemical Physics* **1982**, *77*, 3654-3665.
57. Dolg, M.; Stoll, H.; & Preuss, H. Energy-adjusted abinitio pseudopotentials for the rare earth elements. *The Journal of Chemical Physics* **1989**, *90*, 1730-1734.
58. Tomasi, J.; Mennucci, B.; & Cammi, R. Quantum mechanical continuum solvation models. *Chemical Reviews* **2005**, *105*, 2999-3094.
59. Adamo, C.; & Jacquemin, D. The calculations of excited-state properties with Time-Dependent Density Functional Theory. *Chemical Society Reviews* **2013**, *42*, 845-856.
60. Bhattacharyya, A; Mohapatra, P. K. Separation of trivalent actinides and lanthanides using various 'N', 'S' and mixed 'N', 'O' donor ligands: a review. *Radiochimica Acta* **2019**, *107*, 931 – 949.
61. Perrin, D. D.; Dempsey, B.; Serjeant, E. P. pKa prediction for organic acids and bases; Springer: **1981**; Vol. 1.
62. Schultz, W, T. Relative toxicity of para-substituted phenols: log kow and pKa-dependent structure-activity relationships. *Bulletin of Environmental Contamination and Toxicology* **1987**, *38*, 994 – 999.
63. Liptak, M. D.; Gross, K. C.; Seybold, P. G.; Feldgus, S.; Shields, G. C. Absolute pKa determination for substituted phenols. *Journal of the American Chemical Society* **2002**. *124*, 6421 – 6427.
64. Dauphin, G.; Kergomard, A. Etude de la dissociation acide de quelques sulfonamides. *Bulletin de la Societe Chimique de France* **1961**, 486-492.
65. Paluch, M.; Ślepokura, K.; Lis, T.; Lisowski, J. Enantiopure trinuclear lanthanide (III) complexes: Cooperative formation of Ln₃(μ₃-OH)₂ core within the macrocycle. *Inorganic Chemistry Communications* **2011**, *14*, 92-95.
66. Calvez, G.; Le Natur, F.; Daiguebonne, C.; Bernot, K.; Suffren, Y.; Guillou, O. Lanthanide-based hexa-nuclear complexes and their use as molecular precursors. *Coordination Chemistry Reviews* **2017**, *340*, 134-153.
67. Beckett, R.; Colton, R.; Hoskins, B. F.; Martin, R. L.; Vince, D. G. Magnetism and structure of a novel trinuclear cluster compound of divalent copper. *Australian Journal of Chemistry* **1969**, *22*, 2527-2533.

68. Costes, J.; Dahan, F.; Nicodeme, F. A trinuclear gadolinium complex: structure and magnetic properties. *Inorganic Chemistry* **2001**, *40*, 5285-5287.
69. Wong, K.; Zhu, Y.; Yang, Y.; Law, G.; Fan, H.; Tanner, P. A.; Wong, W. Structure and photophysical properties of new trinuclear lanthanide complexes (Ln= Eu and Tb) with 1, 10-phenanthroline. *Inorganic Chemistry Communications* **2009**, *12*, 52-54.

Chapter VI: General Conclusions

During the nuclear arms race between the US and the former Soviet Union, reprocessing of spent nuclear fuel for weapons production using the PUREX process led to the accumulation of a large volume of radioactive HLW which was made alkaline to facilitate prolonged storage. Treatment of this waste has therefore become paramount to mitigate environmental exposure and radioactive contamination. In the literature, relatively less research effort has been expended towards extraction of actinides in alkaline HLW compared to acidic spent fuel An / Ln separations. Our work helps to bridge this gap by developing efficient f-element extractants and sensors for alkaline HLW and facilitating understanding of f-element chemistry and complexation under highly alkaline conditions.

In this dissertation we studied the complexation, extraction, and spectrophotometric sensing of f-elements - especially lanthanides (which are used as experimental surrogates for actinides) in alkaline media, using several *o*-sulfonamidophenol derivatives. Insights into the stoichiometric ratio, binding constants and sensing behavior were obtained through spectroscopic methods (UV-Vis absorption, fluorescence), FT-IR, and NMR studies. Theoretical studies gave useful data relating to spectral changes and thermodynamic stability, while X-ray crystallography was used to determine some new and unique Ln(III) complexation patterns.

Chapter I provides a brief background into the origin, quantity, and radioactivity of legacy waste in the US, as well as the composition of typical tank waste at the SRS due to speciation in high alkalinity. It also discusses important factors leading to the solubility in

such waste of actinides and other metal cations of interest due to the presence of highly coordination anions and high ionic strength. Other methods which have been adopted or proposed for treating radioactive actinides, Sr and Cs at the SRS were discussed, with emphasis on the Caustic Side Solvent extraction (CSSX) and the Actinide Removal Process (ARP). This chapter also summarizes some of the recent extractants used in the former Soviet Union and in Russia, along with their extraction efficiency for actinides. Chapter I ends by giving useful design parameters needed for the synthesis of efficient ligands for extraction of f-elements from alkaline environments.

In Chapter II, four lipophilic *o*-sulfonamidophenol derived ligands bearing *tert*-butyl and isopropyl groups exhibited good extraction of Ln(III) from alkaline aqueous phases into organic diluents (dichloromethane or *n*-dodecane:octanol (80:20, v/v)). High efficiency in extraction and recovery of Sm(III) after stripping was achieved for all the studied ligands after just one extraction / stripping contact at high alkalinity with 96.1 (± 4.4)% at pH 13.0 and 93.3 (± 5.2)% at pH 14.0. Even when extraction conditions were modified to include several lanthanides together in the same aqueous phase and *n*-dodecane:octanol (80:20, v/v) was used as diluent instead of chlorinated organic solvents, relatively high metal recoveries were still obtained. Reaction stoichiometry were obtained using extraction studies, Job plots, UV-Vis titration and DFT calculations, all confirming a 1:2 binding between metal and the ligand. Binding constants with Sm(III) for all the ligands in CH₃CN:CH₃OH, 96:4 (v/v) were in the range $\beta_2 = 10^{10} - 10^{12} \text{ M}^{-2}$ after non-linear regression analysis using the 1:2 isotherm.

Chapter III extends the study of sulfonamide derived ligands to even more lipophilic analogues bearing long alkyl substituents for f-element extraction under process conditions used in CSSX. The two synthesized ligands studied were lipophilic derivatives of an *o*-sulfonamidophenol, **msa** and an *o*-phenylenediamine sulfonamide, **dsa**. Both ligands displayed excellent solubility in *n*-dodecane, which has similar properties to the diluent used in CSSX. Sm(III) recovery of 40.9 (± 7.7)% for **msa** and 56.8 (± 14.9)% for **dsa** at pH 12.0 and 12.5 respectively were obtained after stripping the loaded organic phase (*n*-dodecane) in the presence of trioctylamine - which was added to further simulate the organic base used in CSSX for improved stripping. Job plots and slope analysis showed 1:1 complexation stoichiometry, while UV-Vis titrations gave useful information on the 1:1 binding constants in solution.

In Chapter IV an *o*-sulfonamidophenol analog bearing a dansyl sensing moiety was synthesized to study the extraction and fluorescence sensing of lanthanides in high alkaline pH. Similar to the results in Chapter II, a very high Sm(III) recovery efficiency of 92.2 (± 13.5)% at pH 13.0 was achieved after just one contact and subsequent stripping of the loaded organic phase. Fluorescence titrations of the ligand and 2.2 equivalents of NaOH with Sm(III) and Yb(III) gave turn-on fluorescence responses in CH₃CN:CH₃OH, 96:4 (v/v). This fluorescence responses was unaffected even when the titrations were performed in the presence of other metals like Na(I), K(I) Cs(I), and Sr(II) already in solution. Job plots and UV-Vis titrations for the ligand in the presence of 2.2 equivalents of NaOH confirmed 1:2 metal-ligand stoichiometry in CH₃CN:CH₃OH, 96:4 (v/v) for both Sm(III) and Yb(III).

Chapter V focused on the optical sensing of Lu(III) using a *p*-nitro substituted *o*-sulfonamidophenol ligand, **LH₂**. In the presence of 2.5 equivalents of DIPEA, **LH₂** gave visible color change from bright yellow to colorless when titrated with Lu(III), and to a lesser extent with other lanthanides, but not for the other metals studied in acetonitrile. Analysis of the spectra from the UV-Vis titration studies with Lu(III) showed a clear blue shift from $\lambda_{\text{max}} = 432$ nm to 398 nm along with distinct isosbestic points due to the 1:1 complexation of the ligand with Lu(III) in the presence of DIPEA. **LH₂** in the presence of DIPEA proved to be an efficient sensor for Lu(III) at micromolar level, even in the presence of excess concentrations of other metals, such as Na(I), K(I), Cs(I) and Sr(II). Theoretical studies for the formed Lu(III) complexes suggested a bis-deprotonated ligand bound via -O and -N to a Lu(III) metal center while redox changes in solution was used to further confirm the complexation of Lu(III) by **LH₂**, but only in the presence of DIPEA. Furthermore, two crystal structures from isolated complexes confirmed the formation of both a monomeric octahedral Lu(III) complex and a rare trinuclear Lu(III) cluster.

Appendices A, B and C are respectively dedicated to: 1) The regioselectivity in the synthesis of sulfonamides *vs.* sulfonic esters from *o*-aminophenol frameworks; 2) the synthesis and characterization of a Zn(II) complex and lastly 3) the study of three trisulfonamide analogs, which failed to show effective complexation with lanthanides.

Overall, this work has demonstrated that *o*-sulfonamidophenol ligands with electron-rich O- and N- donor sites are efficient extractants and sensors for f-elements in highly alkaline solutions, such as those at SRS. Therefore, the way is paved for future

studies into the synthesis and application of sulfonamide-based ligands with improved lipophilicity and denticity for actinide separation, extraction and sensing from alkaline HLW.

APPENDICES

APPENDIX A: Regioselectivity of Reaction Of Aminophenols with Sulfonyl Chlorides: X-Ray Characterization of an Aminophenol-derived Sulfonic Ester and Attempts for Ln(III) Coordination and Extraction.

Oluwaseun W. Adedoyin, Indranil Chakraborty, Raphael G. Raptis

and Konstantinos Kavallieratos

A.1 Abstract

As part of our effort to gain understanding in the ability of sulfonamidophenols vs. sulfonic esters to complex and extract Ln(III), the regioselectivity for the reaction of *p*-(*tert*-butyl)-2-amino-phenol, with *p*-tolylchloride was explored. It was found that, depending on the conditions employed, either the sulfonamidophenol N-(5-(*tert*-butyl)-2-hydroxyphenyl)-4-methylbenzenesulfonamide (**1**) or the sulfonic ester, 2-amino-4-(*tert*-butyl)phenyl-4-methylbenzenesulfonate (**2**) could be synthesized and characterized. While **1** is a known compound, **2** is newly synthesized. Good yields from both reactions were obtained, and the products were characterized by NMR, FT-IR and X-ray crystallography. Sulfonamidophenols, such as **1**, have demonstrated excellent coordination and extraction for Ln(III), as has been demonstrated within the main part of this dissertation (Chapters 2-5). The sulfonic ester analog, however, showed no such ability, pointing to the importance of a 5-member chelate ring formation during complexation.

A.2 Introduction

Since the early 30s sulfonamides or sulfa drugs as they became popularly known came to be seen as miracle drugs¹ because of their vast chemotherapeutic properties for the treatment of bacterial infections like gonorrhea, pneumonia, urinary tract and intestinal tract infections.² They also demonstrated veterinary and herbicidal benefits.^{3,4} Secondary sulfonamides typically bear the $R_1-SO_2NH-R_2$ group and apart from being bioactive compounds they have been very useful as sensors⁵ and chelators for metal cations⁵⁻⁷ due to the presence of electron rich O- and N- donor sites, when deprotonated, which act as binding sites for metal cations. Synthetic pathways for sulfonamides vary⁸⁻¹⁰ but common ones often rely on the reaction of sulfonyl chlorides with nucleophilic amino compounds, such as alkyl amines or anilines⁶ in the presence of a suitable organic base. Sulfonic esters or sulfonates on the other hand bear the general formula $R_1-SO_2O-R_2$. They find use also as compounds in pharmaceuticals and bioactive products in anti-malaria and cancer drugs.¹¹ Quinolone-derived scaffolds bearing sulfonic ester functional groups serve as anti-bacterial and antifungi therapeutics.¹² Sulfonic esters has also been known and used as intermediates in the synthesis of organic products mostly because their RSO_3^- groups serve as versatile leaving groups in many substitution reactions.^{12,13} They are also used in synthesizing intermediates which involves the protection of phenolic groups.^{14,15} Sulfonic esters can be made by reacting a hydroxyaniline derivative with a sulfonyl chloride in the presence of triethylamine.¹⁶ However due to simplicity and the need for high reaction efficiency, the choice of organic base becomes more significant in determining the kind of product formed during synthesis when an aminophenol is the nucleophilic template. This is because both the hydroxyl group and the amine group

when deprotonated can serve as nucleophiles, hence the need for regioselectivity when sulfonyl chloride derivatives are reacted with aminophenols during synthesis. Although, regioselectivity in this type of reactions has been previously reported.^{16,17} The focus of this study is to characterize the products N-(5-(*tert*-butyl)-2-hydroxyphenyl)-4-methylbenzenesulfonamide (**1**) and 2-amino-4-(*tert*-butyl)phenyl-4-methylbenzenesulfonate (**2**) obtained from the nucleophilic attack of 2-amino-4-(*tert*-butyl)phenol on *p*-toluenesulfonyl chloride in presence of either pyridine or triethylamine respectively with the aim of using the synthesized compounds for the complexation of f-elements.

A.3 Experimental section

Materials and methods

All reagents were purchased from ACROS Organics or Fisher Scientific and were used without further purification. Solvents used for titrations were spectroscopic grade. ¹H- and ¹³C-NMR Spectra were recorded on a 600 MHz Bruker NMR spectrometer and referenced to the residual solvent resonance. All chemical shifts, δ , are reported in ppm. **1** was synthesized according to modification of known procedures in the literature^{17,18} and was found to be spectroscopically identical to the reported compound, however we now include an X-ray crystal structure for full characterization. FT-IR spectra were recorded on an Agilent Technologies Cary 670 FTIR Spectrometer using the ATR (attenuation total reflectance) technique. X-ray diffraction studies were carried out on a Bruker D8 Quest with PHOTON 100 detector.

A.4 Synthetic details

Both compounds were synthesized from 2-amino-4-*tert*-butylphenol and *p*-toluenesulfonyl chloride. **1** is a known compound but is now fully characterized using X-ray crystallography. **2** is a new compound and was synthesized based on modifications of known procedures in the literature.^{17,18}

A.4.1 Synthesis 2-amino-4-(*tert*-butyl)phenyl-4-methylbenzenesulfonate (**2**)

2-Amino-4-*tert*-butylphenol (80.0 mg; 0.5 mmol) together with triethylamine (48.6 mg; 0.5 mmol) in 10 mL CH₂Cl₂ was added dropwise to a solution of *p*-toluenesulfonyl chloride (92.3 mg; 0.5 mmol) previously dissolved in 10 mL of CH₂Cl₂. The reaction was stirred for 5 h at 35 °C and monitored by TLC (Hexanes:EtOAc ; 2:1) to ensure completion of the reaction. When judged to be complete, the reaction solution was washed with 1.0 M HCl, 1.0 M NaHCO₃ and DI water (3 × 25 mL each). The crude organic layer was then collected and dried using Na₂SO₄ and the volatiles were removed under pressure using a rotary evaporator. The yellow-brown oil obtained was dissolved in CH₂Cl₂ and purified by column chromatography using hexanes / EtOAc (7:1). The volatiles were then removed, and the product was recrystallized from CH₂Cl₂ using hexanes. The resulting solid was dried overnight under vacuum giving the pure C₁₇H₂₁NO₃S (**2**) as a yellow powder (112.0 mg, 73.4% yield); ¹H-NMR (DMSO-d₆; 25°C) δ 7.83 (d; 2H); 7.45 (d; 2H); 6.75 (s; 1H); 6.74 (d; 1H); 6.50 (dd; 1H); 4.86 (s; 1H); 2.42 (s; 3H); 1.18 (s; 9H). ¹³C-NMR (DMSO-d₆; 25°C) δ 150.5, 145.9, 140.6, 133.9, 132.9, 130.5, 128.7, 121.9, 113.9, 113.6, 34.5, 31.5, 21.6. FT-IR (cm⁻¹ ; ATR) 3470 (m; N-H); 3392 (m; N-H); 2963 (m; C-H); 2923 (w); 2867 (w); 2113 (w); 1623 (m); 1502

(m); 1424 (m); 1362 (vs; S=O); 1166 (vs; S=O); 1136 (m); 1089 (s); 936 (m); 843 (s); 807 (s); 748 (m); 719 (m); 678 (m); 657 (m). Elemental Analysis calculated / found (%): C 63.92/63.64, H 6.63/6.45, N 4.39/4.24.

A.4.2 UV-Vis titrations

UV-Vis titrations were carried out at constant concentration of ligand (**2**) and two equivalents of diisopropylethylamine (DIPEA), with sole variable the concentration of Sm(III), as follows: A solution of **2** (1.0×10^{-5} M) and DIPEA (2.0×10^{-5} M) was prepared in acetonitrile (Solution A). Using Solution A, a solution of Sm(NO₃)₃·6H₂O (1.0×10^{-3} M) of was prepared by weighing appropriate amount of Sm(NO₃)₃·6H₂O and dissolving in Solution A (Solution B). Solution A (2.70 mL) was placed in a 1.00 cm cuvette cell and was titrated with Solution B in small additions. Control experiments were conducted in a similar fashion in the absence of **2**, and the response of Sm(III) addition was monitored.

A.4.3 X-ray crystallography

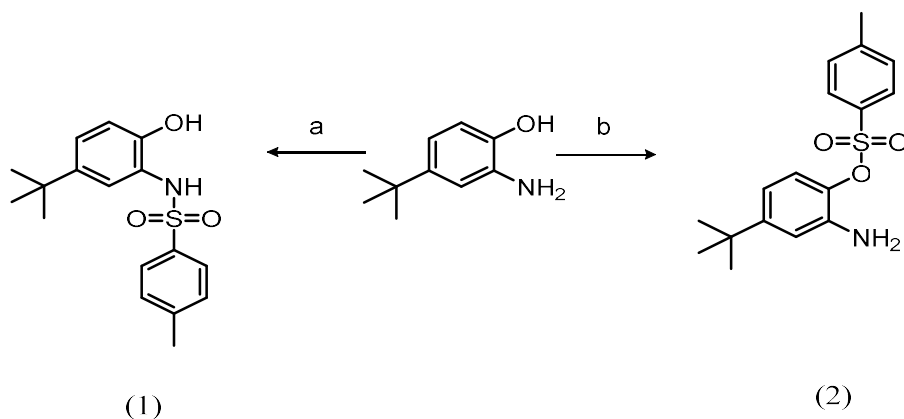
Transparent crystals of **1** were obtained by slow evaporation from CHCl₃, while golden-brown crystals of **2** suitable for single-crystal X-ray diffraction were grown by slow evaporation of a concentrated solution of **2** in CH₂Cl₂ layered with excess hexanes at ambient temperature. Data collection and structure refinement details are summarized in Table A.1 and A.2. Suitable crystals were selected and mounted on a Bruker D8 Quest diffractometer equipped with Photon 100 detector operating at T = 298K. The structures were solved into their respective space groups determined by *ShelXS*^{19,20} structure

solution program. Calculations and molecular graphics were performed using *SHELXTL 2014* and *Olex 2* programs.

A.5 Results and discussion

A.5.1 Synthesis

When 2-amino-4-*tert*-butylphenol was reacted with *p*-toluenesulfonyl chloride in the presence of pyridine at reduced temperature regioselectivity was in favor of the sulfonation of the amine (Figure A.1 - 1). On the other hand, reaction of 2-Amino-4-*tert*-butylphenol with *p*-toluenesulfonyl chloride in the presence of triethylamine gave exclusively the sulfonic ester, instead (Figure A.1 - 2).



a : Pyridine, 0°C, *p*-TsCl, DCM, 5hrs

b : Et₃N, *p*-TsCl, DCM, 5hrs

Figure A.1. Synthesis of sulfonamide (1) and sulfonic ester (2)

Reactions leading to the formation of N-(5-(*tert*-butyl)-2-hydroxyphenyl)-4-methylbenzenesulfonamide (1) and 2-amino-4-(*tert*-butyl)phenyl-4-

methylbenzenesulfonate (**2**) are based on nucleophilic substitution, a schematic representation of these reactions is presented in Figures A.2 and A.3 below.

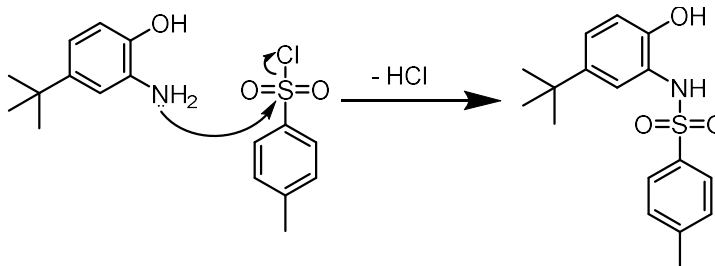


Figure A.2. Synthetic scheme for *N*-(5-(*tert*-butyl)-2-hydroxyphenyl)-4-methylbenzenesulfonamide (**1**)

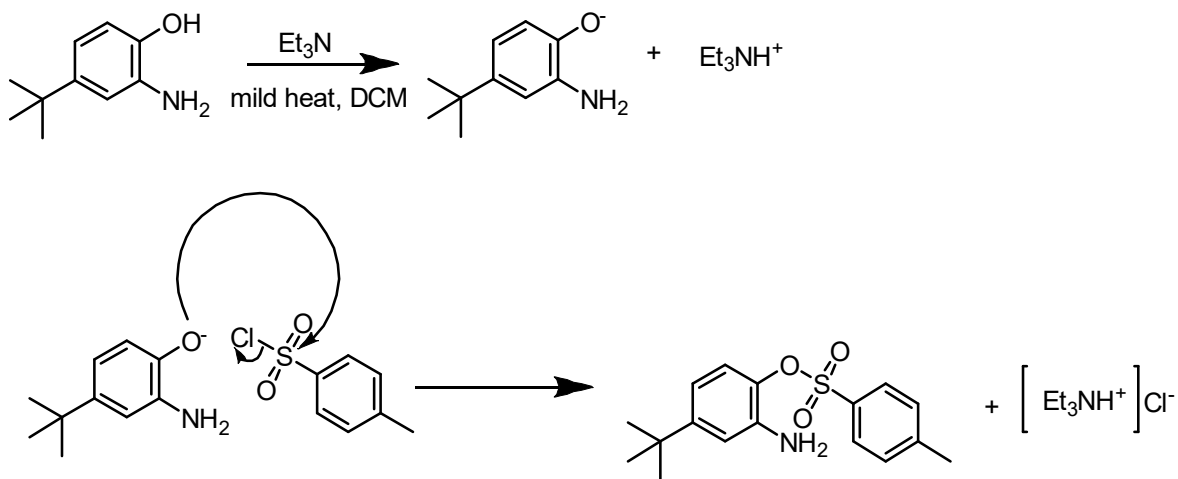


Figure A.3. Synthetic scheme for 2-amino-4-(*tert*-butyl)phenyl-4-methylbenzenesulfonate (**2**)

A.5.2 UV-Vis titrations

Addition of Sm(III) to **2** in the presence of DIPEA in acetonitrile did not give any notable changes other than a linear increase in absorbance at 219 nm (Figure A.4 - a), due to excess Sm(NO₃)₃. The absence of any saturation or an isosbestic point further

suggested that there was no notable interaction between **2** and Sm(III). This was confirmed by a control experiment (Figure A.4 - b) which indicated that the increase in absorbance at 219 nm was only caused by the increasing concentration of Sm(III) in solution and not due to any interaction with **2**. Indeed, the lack of effective binding site on the sulfonic ester makes it unsuitable for Ln(III) complexation. **1** on the other hand was used for efficient complexation of Zn(II) (Appendix B) and analogs of **1** have demonstrated efficient binding throughout the course of this dissertation

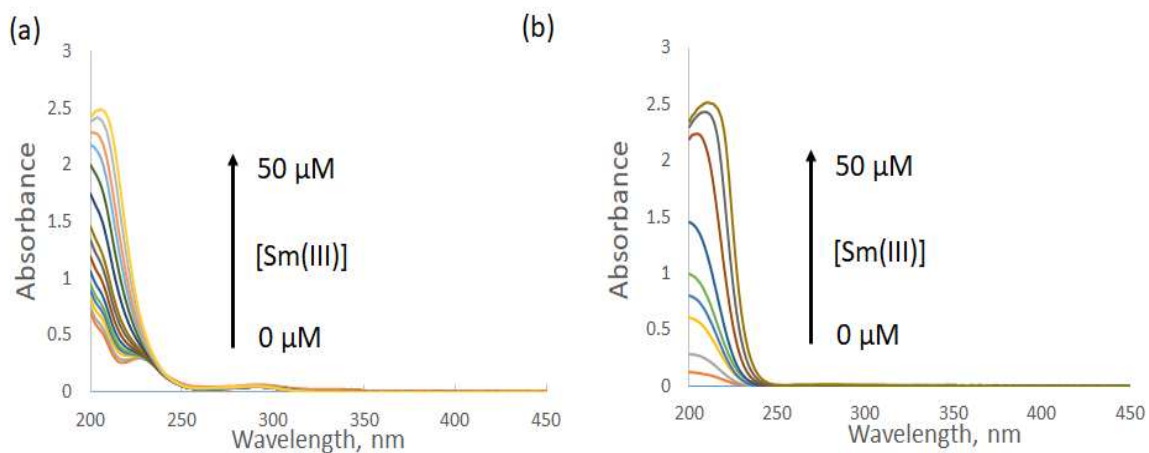


Figure A.4. UV-Vis spectra showing absorbance changes due to addition of $\text{Sm}(\text{NO}_3)_3 \cdot 6\text{H}_2\text{O}$ ($1.0 \times 10^{-3} \text{ M}$) to (a) **2** ($1.0 \times 10^{-5} \text{ M}$) with 2 equivalents of DIPEA in acetonitrile, (b) DIPEA in acetonitrile ($2.0 \times 10^{-5} \text{ M}$).

A.5.3 X-ray crystallography

Crystallographic data for **1** and **2** confirmed the formation of a sulfonamide and a sulfonic ester, respectively.

For the sulfonamide **1**, crystal data, data collection and structure refinement details are summarized in Table A.1. Compound **1** was solved and refined in a Triclinic *P-1* space group. Both phenyl groups appear planar as expected, the dihedral angle

between both aryl rings were 82.96 deg (Figure A.5). In the extended crystal structure of **1**, π - π stacking was observed, and C-H \cdots O hydrogen bond interactions were found to consolidate the structure (Figure A.6).

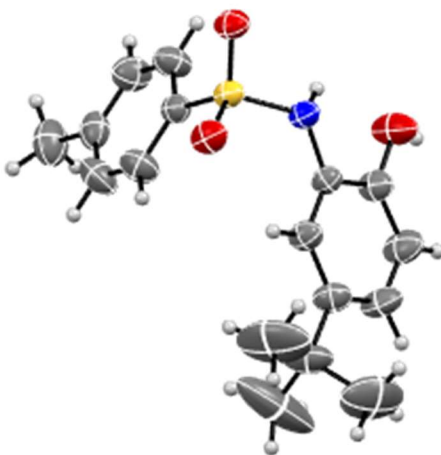


Figure A.5. ORTEP representation of the X-ray crystal structure of **1** (50% probability ellipsoids).

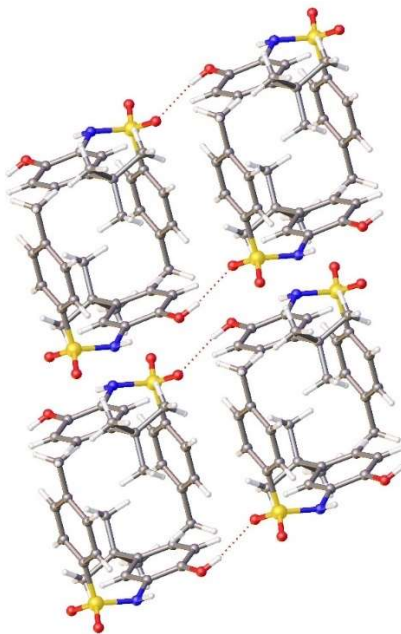


Figure A.6. Ball and stick representation of **1** showing π - π stacking interaction and C-H \cdots O intermolecular hydrogen bonding interactions of **1**.

Table A.1: Crystal data for **1**

Crystal Data	
Chemical formula	C ₁₇ H ₂₁ NO ₃ S
Mr	319.41
Crystal system, space group	Triclinic, P-1
Temperature (K)	298
a, b, c (Å)	7.6534 (3), 9.8916 (4), 12.2797 (5)
α, β, γ (°)	97.048 (1), 95.115 (1), 112.249 (1)
V (Å ³)	844.55 (6)
Z	2
Radiation type	Mo Kα
μ (mm ⁻¹)	0.20
Crystal size (mm)	0.30 x 0.25 x 0.20

For the sulfonic ester **2**, crystal data, data collection and structure refinement details are summarized in Table A.2. Compound **2** was solved and refined in a monoclinic *P2₁/c* space group. Both phenyl groups appear planar as expected, and the dihedral angle between both aryl rings was 51.73 deg (Figure A.7). In the extended crystal structure of **2**, slipped π–π stacking was observed, and weak non classical C–H⋯O intermolecular hydrogen bond interactions were found to consolidate the structure (Figure A.8).

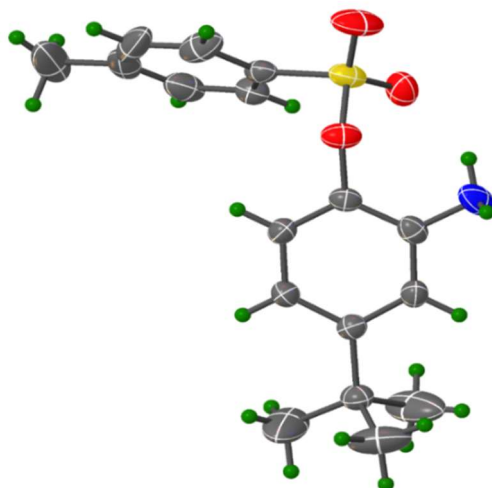


Figure A.7. ORTEP representation of the X-ray crystal structure of **2** (50% probability ellipsoids).

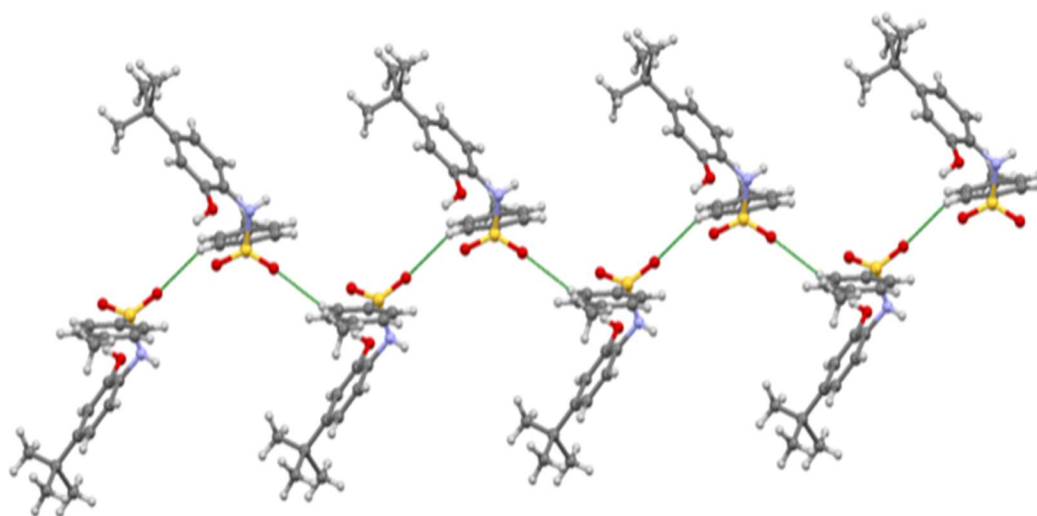


Figure A.8. Ball and stick representation of **2**, showing slipped π - π stacking interaction and weak non classical C-H...O intermolecular hydrogen bonding interactions

Table A.2: Crystal data for **2**

Crystal Data	
Chemical formula	C ₁₇ H ₂₁ NO ₃ S
Mr	319.41
Crystal system, space group	Monoclinic, P2 ₁ /c
Temperature (K)	298
a, b, c (Å)	13.792 (3), 10.785 (2), 12.583 (3)
β (°)	113.381 (4)
V (Å ³)	1718.0 (7)
Z	4
Radiation type	Mo Kα
μ (mm ⁻¹)	0.20
Crystal size (mm)	0.22 x 0.17 x 0.11

A.6. Conclusion

The efficient synthesis of N-(5-(*tert*-butyl)-2-hydroxyphenyl)-4-methylbenzenesulfonamide (**1**) or 2-amino-4-(*tert*-butyl)phenyl-4-methylbenzenesulfonate (**2**) starting with an *o*-aminophenol and tosyl chloride was used to demonstrate the regioselectivity of the nucleophilic substitution, depending on the reaction conditions. *o*-Aminophenol-derived sulfonamides have been efficient in coordinating, complexing and extracting Ln(III) (Chapters 2 – 5) and Zn(II) (Appendix

B), while sulfonic esters have gave no interaction with Ln(III) due to lack of an effective binding site.

A.7 References

1. Lesch, J. E. *The first miracle drugs: how the sulfa drugs transformed medicine*; Oxford University Press, USA: **2007**.
2. Kivelä, A. J.; Kivelä, J.; Saarnio, J.; Parkkila, S. Carbonic anhydrases in normal gastrointestinal tract and gastrointestinal tumours. *World journal of gastroenterology* **2005**, *11*, 155.
3. Battaglin, W. A.; Furlong, E. T.; Burkhardt, M. R.; Peter, C. J. Occurrence of sulfonylurea, sulfonamide, imidazolinone, and other herbicides in rivers, reservoirs and ground water in the Midwestern United States. *Science of the Total Environment* **2000**, *248*, 123-133.
4. Sukul, P.; Spiteller, M. Sulfonamides in the environment as veterinary drugs. *Review of Environmental Contamination and Toxicology* **2006**, 67-101.
5. Kavallieratos, K.; Rosenberg, J. M.; Chen, W.; Ren, T. Fluorescent sensing and selective Pb (II) extraction by a dansylamide ion-exchanger. *Journal of the American Chemical Society* **2005**, *127*, 6514-6515.
6. Alvarado, R. J.; Rosenberg, J. M.; Andreu, A.; Bryan, J. C.; Chen, W.; Ren, T.; Kavallieratos, K. Structural insights into the coordination and extraction of Pb (II) by disulfonamide ligands derived from *o*-phenylenediamine. *Inorganic Chemistry* **2005**, *44*, 7951-7959.
7. Morozov, A. N.; Govor, E. V.; Anagnostopoulos, V. A.; Kavallieratos, K.; Mebel, A. M. 1, 3, 5-Tris-(4-(iso-propyl)-phenylsulfamoylmethyl) benzene as a potential Am(III) extractant: experimental and theoretical study of Sm(III) complexation and extraction and theoretical correlation with Am(III). *Molecular Physics* **2018**, *116*, 2719-2727.
8. Pandya, R.; Murashima, T.; Tedeschi, L.; Barrett, A. G. Facile one-pot synthesis of aromatic and heteroaromatic sulfonamides. *Journal of Organic Chemistry* **2003**, *68*, 8274-8276.
9. Caddick, S.; Wilden, J. D.; Judd, D. B. Direct synthesis of sulfonamides and activated sulfonate esters from sulfonic acids. *Journal of the American Chemical Society* **2004**, *126*, 1024-1025.

10. Wright, S. W.; Hallstrom, K. N. A Convenient preparation of heteroaryl sulfonamides and sulfonyl fluorides from heteroaryl thiols. *Journal Organic Chemistry* **2006**, *71*, 1080-1084.
11. Betts, L. M.; Tam, N. C.; Kabir, S. H.; Langler, R. F.; Crandall, I. Ether aryl sulfonic acid esters with improved antimalarial/anticancer activities. *Australian Journal of Chemistry* **2006**, *59*, 277-282.
12. Krishna, P. Chemoselective synthesis of 5-amino-7-bromoquinolin-8-yl sulfonate derivatives and their antimicrobial evaluation. *Phosphorus, Sulfur, and Silicon and the Related Elements* **2018**, *193*, 685-690.
13. Reddy, L. V.; Nakka, M.; Suman, A.; Ghosh, S.; Helliwell, M.; Mukkanti, K.; Mukherjee, A. K.; Pal, S. Synthesis of novel quinoline analogues of nimesulide: An unusual observation. *Journal of Heterocyclic Chemistry* **2011**, *48*, 555-562.
14. Andersen, K. K.; Gowda, G.; Jewell, L.; McGraw, P.; Phillips, B. T. Substitution at tetracoordinate sulfur (VI). Rearrangement of 2-aminoaryl arenesulfonates to N-(2-hydroxyaryl) arenesulfonamides. *Journal of Organic Chemistry* **1982**, *47*, 1884-1889.
15. Greene, T. W. *Greene's protective groups in organic synthesis*; Wiley-Interscience: **2007**.
16. Bae, S. J.; Ha, Y. M.; Kim, J.; Park, J. Y.; Ha, T. K.; Park, D.; Chun, P.; Park, N. H.; Moon, H. R.; Chung, H. Y. A novel synthesized tyrosinase inhibitor:(E)-2-((2, 4-dihydroxyphenyl) diazenyl) phenyl 4-methylbenzenesulfonate as an azo-resveratrol analog. *Bioscience, Biotechnology and Biochemistry* **2013**, *77*, 65-72.
17. KumaraBoominathan, S. S.; ChandruSenadi, G; KishoreaVandavasi, J. A one-pot hypiodite catalysed oxidative cycloetherification approach to benzoxazoles. *Chemical Communications* **2014**, *51*, 6726 – 6728.
18. Wen, K.; Wu, Z.; Huang, B.; Ling, Z.; Gridnev, I. D.; Zhang, W. Solvent-Controlled Pd(II)-Catalyzed Aerobic Chemoselective Intermolecular 1, 2-Aminooxygenation and 1, 2-Oxyamination of Conjugated Dienes for the Synthesis of Functionalized 1, 4-Benzoxazines. *Organic Letters* **2018**, *20*, 1608-1612.
19. Sheldrick, G. M. A short history of SHELX. *Acta Crystallographica Section A: Foundations of Crystallography* **2008**, *64*, 112-122.
20. Sheldrick, G. M. Crystal structure refinement with SHELXL. *Acta Crystallographica Section C: Structural Chemistry* **2015**, *71*, 3-8.

APPENDIX B: Zinc (II) Complexation with a *p-tert*-Butyl Substituted *o*-Sulfonamidophenol

Oluwaseun W. Adedoyin, Indranil Chakraborty, Raphael G. Raptis and

Konstantinos Kavallieratos

B.1 Abstract

Complexation of Zn(II) was demonstrated by the *o*-sulfonamidophenol derivative N-(5-(*tert*-butyl)-2-hydroxyphenyl)-4-methylbenzenesulfonamide via its O- and N-binding sites. The tetrahedrally-coordinated Zn(II) complex in methanol was characterized by ¹H-NMR, FT-IR and X-ray crystallography.

B.2 Introduction

Several transition and d-block metals are products of the environment, existing as ores and minerals, but anthropogenic activities like mining, smelting and other mineral processing activities tend to deposit them in high concentrations. In addition, leaching and percolation can cause such metals to seep through the soil or get into our natural waterways during run offs and can bioaccumulate over a long period.¹ Some metals, like zinc and iron are beneficial to human health, but only at tolerable limits. Zinc for instance is important for male reproductive function,² and its deficiency can lead to delayed growth and bodily development.³ However, in spite of the many benefits of zinc, at high concentration it can cause neurological disorders, including conditions like epilepsy and Alzheimer's disease. Zinc in excess of 50 μ M has been associated with toxicity^{3,4} as it inhibits the ability of cells to generate Adenosine Triphosphate ATP, which keeps cells

alive by providing the energy needed for them to thrive.⁵ Other health problems associated with overconsumption of zinc include stomach cramps, vomiting, skin irritations, anemia and nausea.⁶

Methods used for separation and sensing of metals, including zinc, from drinking water and effluents include membrane sorption,⁷⁻⁹ filtration,¹⁰ ion-exchange, precipitation and complexation.¹¹ Zhang et al. reported Zn(II) fluorescence sensing by the bis-9-anthryldiamine ligand - N,N'-bis(anthrylmethyl)-propylene diamine, and isolated a Zn(II) complex.¹² Matlock et al. reported a pyridine-based thiol ligand that forms insoluble complexes with several metals, including Zn(II).¹³ We recently pioneered novel *o*-sulfonamidophenol ligands, for effective extraction (Chapters 2, 3 and 4) and sensing (Chapters 4 and 5) of lanthanides. As an extension of this work we report herein the synthesis of a Zn(II) complex isolated as (Et₃NH)₂[ZnL₂], using the *o*-sulfonamidophenol ligand, N-(5-(*tert*-butyl)-2-hydroxyphenyl)-4-methylbenzenesulfonamide (**LH₂**) (Figure B.1).

B.3 Experimental section

B.3.1 Materials and methods

Commercial reagents and solvents were purchased from Fisher Scientific or Sigma Aldrich and were used without further purification. NMR spectra were recorded on a 600 MHz Bruker NMR spectrometer and referenced to the residual solvent resonances. All ¹H-NMR chemical shifts δ are recorded in ppm. FT-IR spectra were recorded on a Cary 600 series FT-IR spectrometer. X-ray diffraction studies were carried out on a Bruker D8 Quest with PHOTON 100 detector. **LH₂** was synthesized based on

modifications of previously reported methods^{14,15} and was found spectroscopically identical to the reported compound.

B.3.2 Synthesis of complex (Et₃NH)₂[ZnL₂]

LH₂ (60.0 mg, 0.19 mmol) along with 2.5 equivalents of triethylamine (66.20 μL, 0.48 mmol) was allowed to stir in 5 mL of methanol. To this clear solution Zn(NO₃)₂ (18.0 mg, 0.09 mmol) dissolved in 5 mL of methanol was added dropwise, and the reaction was left to stir for 10 h. The clear solution was then concentrated under vacuum and dropwise addition of diethyl ether gave a white precipitate which was filtered out. The filtrate was left to slowly evaporate which gave clear crystals within a week. Analytical Data for (Et₃NH)₂[ZnL₂]; ¹H-NMR (600 MHz, CDCl₃): δ 1.09 (s, 9H), 2.36 (s, 3H), 6.69 (d, 1H), 6.82 (d, 1H), 7.02 (dd, 1H), 7.19 (d, 2H), 7.59 (d, 2H). FT-IR (cm⁻¹; ATR) 3056 (w); 2949 (w; C-H); 1623 (w); 1496 (m); 1460 (w); 1397 (w); 1300(m) 1258 (s; S=O); 1130 (vs; S=O); 1085 (m); 1085 (s); 993 (m); 913 (m); 827 (m); 807 (m) 732 (w).

B.4 X-ray crystallography

Crystals were obtained by slow evaporation of a solution of (Et₃NH)₂[ZnL₂] in methanol. Data collection and structure refinement details are summarized in Table B.1. A suitable crystal was selected and mounted on a Bruker D8 Quest diffractometer equipped with Photon 100 detector operating at T = 298K. The structure was solved in

space group *P-1* determined by *ShelXS*^{16,17} structure solution program. Calculations and molecular graphics were performed using *SHELXTL 2014* and *Olex 2* programs.

B.5 Results and Discussion

B.5.1 Synthesis of $(\text{Et}_3\text{NH})_2[\text{ZnL}_2]$

Synthesis of $(\text{Et}_3\text{NH})_2[\text{ZnL}_2]$ was carried out by reacting a methanolic solution of $\text{Zn}(\text{NO}_3)_2$ with **LH₂** in the presence of 2.5 equivalents of Et_3N in methanol (Figure B.1). $(\text{Et}_3\text{NH})_2[\text{ZnL}_2]$ was isolated as the anionic $[\text{ZnL}_2]^{2-}$ with two triethylammonium counterocations forming the neutral complex $(\text{Et}_3\text{NH})_2[\text{ZnL}_2]$, as confirmed by FT-IR, ¹H-NMR and X-ray crystallography.

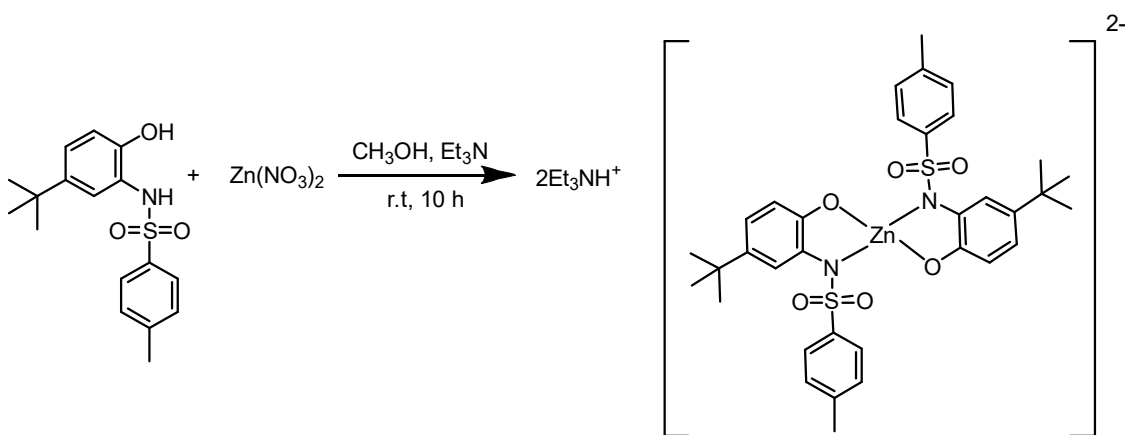


Figure B.1. Synthesis of $(\text{Et}_3\text{NH})_2[\text{ZnL}_2]$

B.5.2 FT-IR Spectroscopy

By comparing the FT-IR spectra of the ligand (**LH₂**) and $(\text{Et}_3\text{NH})_2[\text{ZnL}_2]$, there is the absence of any prominent signal above 3000 cm^{-1} for the complex, indicating that

both the OH and NH groups are fully deprotonated, and the ligand binds to Zn(II) in its dianionic form L^{2-} . Another evidence of complexation is the low energy shifts of the $\nu_{\text{asym}}(\text{SO}_2)$ and $\nu_{\text{sym}}(\text{SO}_2)$, at 1322 cm^{-1} and 1154 cm^{-1} , to 1258 cm^{-1} and 1130 cm^{-1} , respectively (Figure B.2), while the $\nu(\text{S-N})$ band for LH_2 at 885 cm^{-1} shifts to higher frequency at 913 cm^{-1} (Figure B.2). Shifts of the $\nu(\text{S-N})$ band are attributed to the resonance exhibited by the deprotonated ligand during complexation as electron density is directed to the S-N bond, which is shortened upon complexation.¹⁹

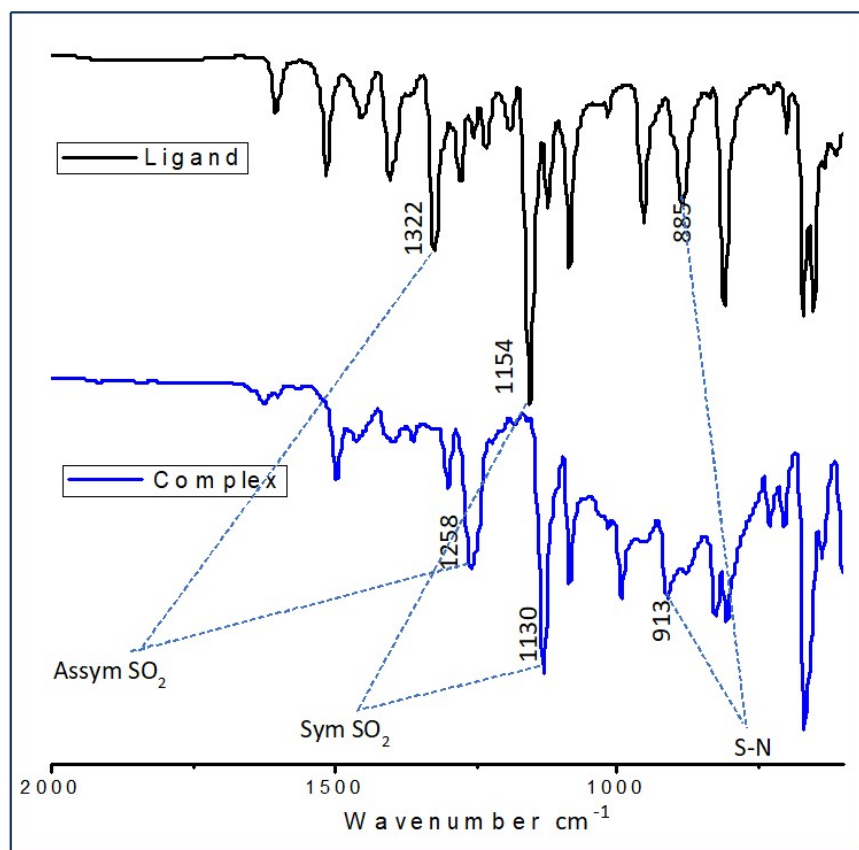


Figure B.2. FT-IR spectra of LH_2 and $(Et_3NH)_2[ZnL_2]$ ($2000 - 600\text{ cm}^{-1}$ range).

B.5.3 ¹H-NMR studies

The ¹H-NMR spectra of **LH₂** and the complex (Et₃NH)₂[ZnL₂] were obtained in CDCl₃. On comparing the spectra for **LH₂** vs. (Et₃NH)₂[ZnL₂], the -OH and -NH signals are noticeably absent in (Et₃NH)₂[ZnL₂] (Figure B.3 – iii) compared to the spectrum of **LH₂** in which these signals are present at δ 6.13 and 6.19 respectively (Figure B.3 - i). These signals are also absent for both the spectrum of **LH₂** + triethylamine (Figure B.3 - ii), and (Et₃NH)₂[ZnL₂] (Figure B.3 - iii). This could be attributed to the deprotonation of the ligand in the presence of the base, and agrees with the spectrum obtained from the FT-IR. The signals at “e”, “f” and “d” also seem to be the most affected due to their proximity to the binding site. “e” and “f” become more shielded in the presence of the organic base due to the formation of the phenolate anion (Figure B.3 - ii), while upon complexation (Figure B.3 - iii) they both become deshielded, once again, due to coordination with the metal which shares electron density with the ligand.

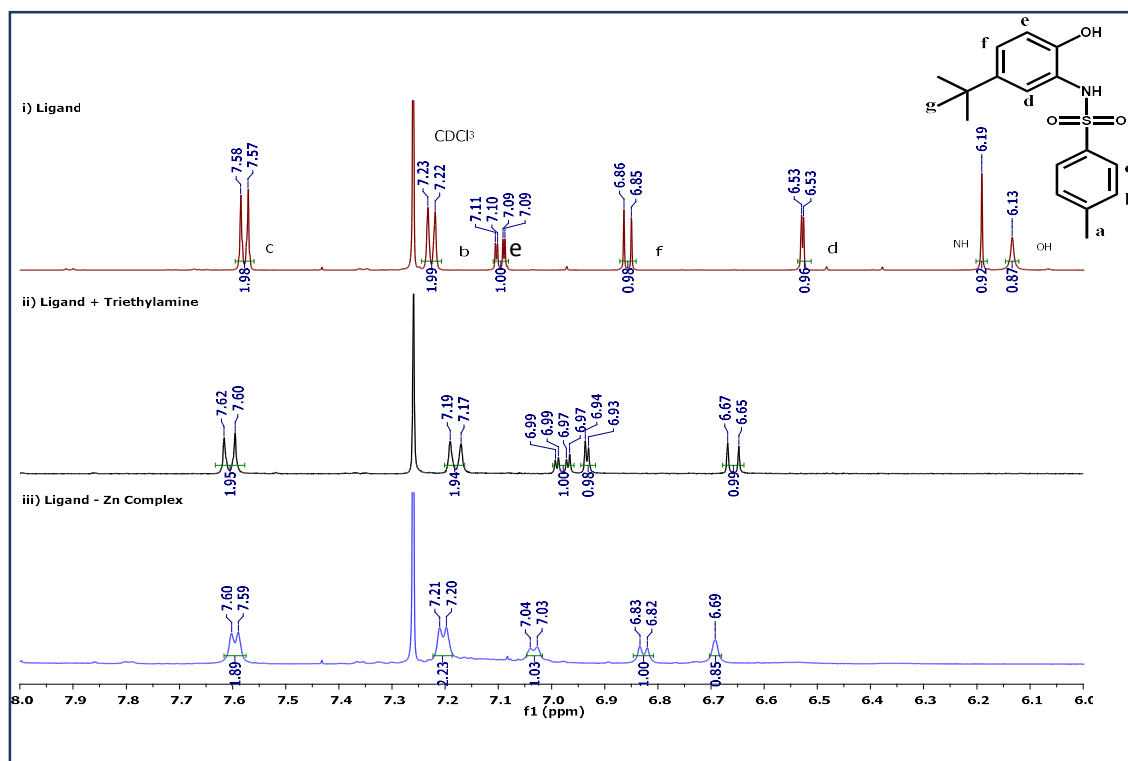


Figure B.3. $^1\text{H-NMR}$ in CDCl_3 of: (i) LH_2 (ii) LH_2 in presence of triethylamine, (iii) Isolated $(\text{Et}_3\text{NH})_2[\text{ZnL}_2]$

B.6 Single crystal X-ray crystallography

The molecular structure of $(\text{Et}_3\text{NH})_2[\text{ZnL}_2]$ revealed a dianionic complex with two triethylammonium countercations. The $\text{Zn}(\text{II})$ center in the complex resides in a distorted tetrahedral coordination environment. The two ligands are coordinated to $\text{Zn}(\text{II})$ in a bidentate (N,O) fashion. The two chelate rings thus formed are noticeably deviated from planarity (0.067 and 0.037 Å). The dihedral angles between the two aryl rings within the same ligand are 80.4° and 76.6° , also indicating a slightly different disposition of the two ligands around the central metal. All the aryl rings in the two bidentate ligands

are highly planar, with mean deviation of 0.004 Å (average). The extended structure is consolidated by moderate intermolecular hydrogen bonding interactions involving an O atom of one of the ligand and N-H moiety of the triethyl ammonium ion (O \cdots H-N, with O \cdots N distance of 2.619 Å). In addition, a noticeable non-bonding interaction involving one of the O atoms of a ligand with a proximal O atom from a neighboring ligand (O \cdots O distance of 2.471 Å) is also noted. No π - π stacking interactions have been detected upon a careful scrutiny of the packing pattern.

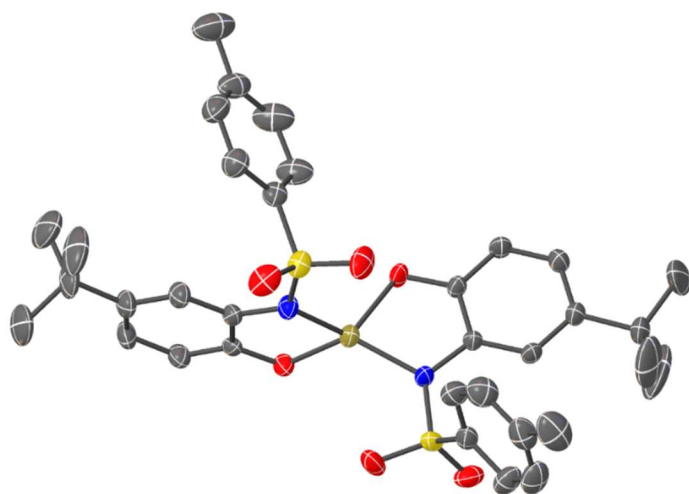


Figure B.4. ORTEP representation of the structure of $[ZnL_2]^{2-}$ (showing 50% probability ellipsoids). Hydrogens and triethylammonium counterions have been omitted for clarity.

Table B.1: Crystal data of $(\text{Et}_3\text{NH})_2[\text{ZnL}_2]$

Crystal Data	
Chemical Formula	$\text{C}_{38}\text{H}_{50}\text{N}_2\text{O}_6\text{S}_2\text{Zn}$
M_r	1676.83
Crystal System, Space group	Triclinic, <i>P-1</i>
Temperature (K)	298
a, b, c (Å)	12.447 (4), 14.768 (5), 14.996 (5)
α, β, γ (°)	117.063 (5), 108.097 (5), 97.449 (6)
V (Å ³)	2210.6 (12)
Z	2
Radiation type	Mo $K\alpha$
μ (mm ⁻¹)	0.70
Crystal size (mm)	0.22 x 0.18 x 0.15

B.7. Conclusion

Complexation of Zn(II) has been demonstrated with an *o*-sulfonamidophenol derivative bearing O- and N- chelating sites in alkaline conditions, with the formation and isolation of a tetrahedrally coordinated $(\text{Et}_3\text{NH})_2[\text{ZnL}_2]$ complex, which was

characterized by FT-IR, ¹H-NMR and X-ray crystallography. Future ligand designs based on this framework could be modified for effective sensing or sequestration of toxic heavy metals from aqueous environments.

B.8 References

1. Duruibe, J. O.; Ogwuegbu, M.; Egwurugwu, J. N. Heavy metal pollution and human biotoxic effects. *International Journal of Physical sciences* **2007**, *2*, 112-118.
2. El-Tawil, A. M. Zinc deficiency in men with Crohn's disease may contribute to poor sperm function and male infertility. *Andrologia* **2003**, *35*, 337-341.
3. Black, M. M. The evidence linking zinc deficiency with children's cognitive and motor functioning. *Journal of Nutrition* **2003**, *133*, 1473-1476.
4. Steinebach, O. M.; Wolterbeek, H. Effects of zinc on rat hepatoma HTC cells and primary cultured rat hepatocytes. *Toxicology and Applied Pharmacology* **1993**, *118*, 245-254.
5. Walsh, C. T.; Sandstead, H. H.; Prasad, A. d. S.; Newberne, P. M.; Fraker, P. J. Zinc: health effects and research priorities for the 1990s. *Environmental Health Perspective* **1994**, *102*, 5-46.
6. Plum, L. M.; Rink, L.; Haase, H. The essential toxin: impact of zinc on human health. *International journal of environmental research and public health* **2010**, *7*, 1342-1365.
7. Zwain, H. M.; Vakili, M.; Dahlan, I. Waste material adsorbents for zinc removal from wastewater: a comprehensive review. *International Journal of Chemical Engineering* **2014**. 1- 13
8. Balköse, D.; Baltacioğlu, H. Adsorption of heavy metal cations from aqueous solutions by wool fibers. *Journal of Chemical Technology & Biotechnology* **1992**, *54*, 393-397.
9. Dahlan, I.; Zwain, H. M. A study on the removal characteristic of zinc ion (Zn(II)) from synthetic wastewater using a novel waste-derived siliceous sorbent. *Caspian Journal of Applied Sciences Research* **2013**, *2*, 10-17.

10. Gardea-Torresdey, J. L.; Gonzalez, J. H.; Tiemann, K. J.; Rodriguez, O.; Gamez, G. Phytofiltration of hazardous cadmium, chromium, lead and zinc ions by biomass of *Medicago sativa* (Alfalfa). *Journal of Hazardous Materials* **1998**, *57*, 29-39.
11. Fu, F.; Wang, Q. Removal of heavy metal ions from wastewaters: a review. *Journal of Environmental Management* **2011**, *92*, 407-418.
12. Zhang, G.; Yang, G.; Zhu, L.; Chen, Q.; Ma, J. A potential fluorescent sensor for Zn²⁺ based on a selective bis-9-anthryldiamine ligand operating in buffer. *Sensors Actuators B: Chem* **2006**, *114*, 995-1000.
13. Matlock, M. M.; Howerton, B. S.; Henke, K. R.; Atwood, D. A. A pyridine-thiol ligand with multiple bonding sites for heavy metal precipitation. *Journal of Hazardous Materials* **2001**, *82*, 55-63.
14. Wen, K.; Wu, Z.; Huang, B.; Ling, Z.; Gridnev, I. D.; Zhang, W. Solvent-Controlled Pd (II)-Catalyzed Aerobic Chemoselective Intermolecular 1, 2-Aminooxygenation and 1, 2-Oxyamination of Conjugated Dienes for the Synthesis of Functionalized 1, 4-Benzoxazines. *Organic Letters* **2018**, *20*, 1608-1612.
15. Andersen, K. K.; Gowda, G.; Jewell, L.; McGraw, P.; Phillips, B. T. Substitution at tetracoordinate sulfur (VI). Rearrangement of 2-aminoaryl arenesulfonates to N-(2-hydroxyaryl) arenesulfonamides. *Journal of Organic Chemistry* **1982**, *47*, 1884-1889.
16. Sheldrick, G. M. Crystal structure refinement with SHELXL. *Acta Crystallographica Section C: Structural Chemistry* **2015**, *71*, 3-8.
17. Sheldrick, G. M. A short history of SHELX. *Acta Crystallographica Section A: Foundations of Crystallography* **2008**, *64*, 112-122.
18. Govor, E. V.; Morozov, A. N.; Rains, A. A.; Mebel, A. M.; Kavallieratos, K. Spectroscopic and theoretical Insights into surprisingly effective Sm(III) extraction from alkaline aqueous media by *o*-Phenylenediamine-derived sulfonamides. *Inorganic Chemistry* **2020**, *59*, 6884-6894.

APPENDIX C: Trisulfonamide Ligands for f-Element Extraction from
Alkaline High-level waste

Oluwaseun W. Adedoyin, Maria Lucia Masferrer Bertoli, Konstantinos Kavallieratos*

(Reproduced in part from a portion of a published peer-reviewed proceedings paper entitled: Sulfonamide Ligand Frameworks for Sm(III) Extraction From Alkaline High Level Waste. Xinrui Zhang, Oluwaseun W. Adedoyin, Maria L. Masferrer Bertoli, Evgen V. Govor and Konstantinos Kavallieratos. *RAD Conference 2020 Proceedings*, **2020**, 4, 173-178. DOI: 10.21175/RadProc.2020.35)

C.1. Abstract

A new trisulfonamide ligand, N,Nⁱ,Nⁱⁱ-(2,4,6-triethylbenzene-1,3,5-triyl)tris(methylene)tris-4-methylbenzene sulfonamide (**1**) was studied for complexation and extraction of lanthanides, and showed no Ln(III) complexation. Two analogous tripodal ligands, N,N',N''-(nitrilotris(ethane-2,1-diyl))tris-4-(methyl)benzenesulfonamide (**2**) and N,N',N''-(nitrilotris(ethane-2,1-diyl))tris-4-(*tert*-butyl)benzenesulfonamide (**3**), were successfully synthesized in order to provide a preorganized framework for Ln(III) complexation and extraction. Several complexation and extraction experiments performed using the more lipophilic ligand **3** and La(III) or Sm(III) were conducted. ¹H-NMR and UV-Vis results from spectrometry suggest that just like for **1**, no complexation or extraction of Ln(III) occurred. Evidence from ¹H-NMR spectroscopy suggests that the primary reason for lack of Ln(III) complexation under the current experimental conditions, is difficulty in deprotonation.

C.2 Introduction

During the cold war, large amounts of HLW was generated from the production of nuclear weapons. This waste was mostly stored in large tanks kept in nuclear facilities.¹ Recently, a concerted effort has begun in a bid to address the threat of environmental radioactive exposure and integrated HLW processing.² In the United States, the two main sites for storage of such waste are the Savannah River Site (SRS) and the Hanford Site (HS).³ To this end, chemists have been working to design organic ligands that selectively bind with actinides and are compatible with the caustic side solvent extraction (CSSX) solvents, to improve efficiency in terms of time and cost. Under acidic conditions, ligands mimicking siderophores, which are naturally produced by bacteria, have been studied and proved to be efficient at extracting radioactive elements such as plutonium.⁴ Complexation by siderophores have shown that chelation is made possible by electronegative atoms present in groups like hydroxypyridinones, catecholamides and hydroxamic acids.⁴ Such groups have over the years formed the basis for ligand design for the extraction and separation of f-elements. Previous ligands that have been studied for this purpose under alkaline conditions include thiacalix analogs⁵ and calix[4]arenes.⁶ Prior investigation in our group has demonstrated the ability of trisulfonamides based on tripodal benzene framework to complex and extract f-elements.⁷ Theoretical studies has also suggested the presence of weak cation- π interactions in some of these complexes, which influences their stability.^{7,8} In this work the synthetic routes for three tripodal sulfonamide ligand derivatives (Figure C.1) are described. The design of N,N^i,N^{ii} - (2,4,6-triethylbenzene-1,3,5-triyl)tris(methylene) tris-4-methylbenzene sulfonamide (**1**) seemed particularly promising in complexation of trivalent f-elements

due to the anticipated stability offered by the cation- π interaction between the central benzene ring and a complexed metal.⁸ In addition to **1**, two other ligands N,N',N''-(nitrilotris(ethane-2,1-diyl))tris-4-(methyl)benzenesulfonamide (**2**) and N,N',N''-(nitrilotris(ethane-2,1-diyl))tris-4-(*tert*-butyl)benzenesulfonamide (**3**) were synthesized and studied in detail to evaluate their performance in complexation and extraction of lanthanides and by extension actinides⁹ under alkaline conditions. Experimental data obtained from UV-Vis, ¹H-NMR spectroscopy, and extraction studies indicated that this ligand framework is not suitable for complexation of Ln(III) under the studied conditions. Evidence from ¹H-NMR spectroscopy suggests that the primary reason for lack of Ln(III) complexation under the current experimental conditions, is difficulty in deprotonation, thus more basic conditions for studying these ligands are warranted.

C.3 Experimental section

Methods and Materials

All chemical reagents and solvents were purchased from Fischer Scientific or Alfa Aesar and were used without further purification. All solvents were spectroscopic grade. ¹H- and ¹³C-NMR spectra were recorded on a 400 MHz Bruker Avance NMR spectrometer and were referenced using the residual solvent resonances. All chemical shifts (δ) were measured in ppm. UV-Vis absorption spectra were recorded on a Varian Cary 100 Bio UV-Visible spectrophotometer. FT-IR spectra were recorded with a Perkin Elmer Spectrum 100 FT-IR Spectrophotometer. Compounds **A**, **B**, **C** and **1** are known compounds, which were synthesized and found to be spectroscopically identical to the previously synthesized compounds.

C.3.1 Synthesis of 1,3,5-triethyl-2,4,6-trischloro(methyl)benzene (A)

Synthesis was based on previously reported procedure by Kilway and co-workers,¹⁰ and was found to be spectroscopically identical to the previously synthesized product. (7.21 g, 38%, yield). ¹H-NMR (600 MHz, CDCl₃): δ4.69 (s, 6H, CH₂ adjacent to Cl), δ2.95 (q, 6H, CH₂), δ1.31 (t, 9H, CH₃).

C.3.2 Synthesis of 1,3,5-tris(azidomethyl)-2,4,6-triethylbenzene (B)

Synthesis was based on previously reported procedure by Kilway and co-workers,¹⁰ and was found to be spectroscopically identical to the previously synthesized product. (1.48 g, 80% yield). ¹H-NMR (600 MHz, CDCl₃): δ4.49 (s, 6H, CH₂ adjacent to N₂), δ2.86 (q, 6H, CH₂), δ1.24 (t, 9H, CH₃).

C.3.3 Synthesis of 1,3,5-Tris(aminomethyl)-2,4,6-triethylbenzene (C)

Synthesis was based on previously reported procedure by Kilway and co-workers,¹⁰ and was found to be spectroscopically identical to the previously synthesized product. (0.35 g, 79% yield). ¹H-NMR (CDCl₃) δ 3.86 (s; 6H, CH₂ adjacent to NH₂); 2.84 (q; 6H, CH₂); 1.26 (t; 9H, CH₃).

C.3.4 Synthesis of N,Nⁱ,Nⁱⁱ- (2,4,6-triethylbenzene-1,3,5-triyl)tris(methylene) tris-4-methylbenzene sulfonamide (1)

A solution of 1,3,5-Tris(aminomethyl)-2,4,6-triethylbenzene (60.0 mg; 0.241 mmol) and triethylamine (73.0 mg; 0.721mmol) together in 5 mL of dichloroethane (DCE) was added dropwise to a solution of *p*-tosyl chloride (137.8 mg; 0.723mmol) in 10 mL of DCE at room temperature. The reaction was conducted under N₂ and left to stir for 12 h. The reaction progress was monitored using TLC (Hexanes:EtOAc, 2:1). Work up was done by washing the reaction solution with 1.0 M HCl and 1.0 M brine solution (each 3 × 25 mL). The organic layer was collected and dried using Na₂SO₄, while DCE was evaporated under reduced pressure and the resulting white solid was dried overnight under reduced pressure (138.0 mg, 80% yield). ¹H-NMR (CDCl₃; 20°C) δ 4.47 (s; 3H); 3.88 (s; 6H); 7.77 (d; 6H); 7.34 (d; 6H); 2.49 (s; 9H); 2.22 (q; 6H); 0.80 (t; 9H). ¹³C-NMR (CDCl₃; 20°C) δ 143.7, 141.7, 135.4, 130.2, 129.8, 127.5, 40.8, 21.6, 22.2, 16.1. FT-IR (cm⁻¹; ATR) 3284 (m; N-H) 3261 (m); 3207 (m); 2970 (w; C-H); 1597 (w); 1496 (w); 1420 (s); 1345 (s); 1307 (s; S=O); 1238 (w; C-N); 1162 (vs; S=O); 1093 (s); 1046(s); 950 (m); 902 (s); 876 (m); 812 (s); 669 (s); 630 (w). Elemental analysis calcd (C₃₆H₄₅N₃O₆S₃): C, 59.24%; H, 6.49%; N, 5.76%; found C, 59.72%; H, 6.25%; N, 5.63%.

C.3.5 Synthesis of N,N',N''-(nitrilotris(ethane-2,1-diyl))tris-4-(methyl)benzenesulfonamide (2)

Using a modification of the synthetic approach adopted by Zhou and co-workers,¹¹ a THF solution containing dry triethylamine (7.47 mL, 53.6 mmol) and *p*-toluenesulfonyl chloride (8.2 g, 42.8 mmol) was stirred under N₂. To this stirring solution tris(2-aminoethyl)amine (2.00 mL, 13.4 mmol) was added slowly turning the clear solution cloudy. The solution was left to stir for 24 h at room temperature. Saturated ammonium chloride solution was added and extraction of the product into organic phase was carried out using dichloromethane. The combined organic phase was washed with a 1.0 M brine solution (3 × 25 mL) and dried using Na₂SO₄. The filtrate was concentrated under reduced pressure and recrystallized from dichloromethane using hexanes to give a whitish solid which was dried under vacuum (6.65 g, 81.6% yield). ¹H-NMR (400 MHz, CDCl₃): δ 7.79 (d, 6H, Hs at ortho positions in benzene ring), δ 7.29 (d, 6H, Hs at methyl positions in benzene ring), δ 6.01 (t, 3H, H bonded with N), δ 2.92 (q, 6H, CH₂ bonded to central N), δ 2.49 (t, 6H, CH₂ bonded to 2° amine), δ 2.41 (s, 9H, CH₃ at the ends). ¹³C-NMR (101 MHz, CDCl₃): 143.4, 136.8, 129.8, 127.2, 54.1, 40.7, 21.5. FT-IR (cm⁻¹): 3517 (w), 3289(m), 2968(w), 2857(w), 1653(w), 1596(w), 1493(w), 1451(m), 1414(m), 1318(s), 1288(m), 1153(vs), 1120(m), 1090(s), 1044(m), 950(m), 915(m), 852(m), 814(s), 730(m).

C.3.6 Synthesis of N,N',N''-(nitrilotris(ethane-2,1-diyl))tris-4-(*tert*-butyl)benzenesulfonamide (**3**)

Synthetic procedure for **3** was similar to **2** except, a THF solution containing dry triethylamine (7.47 mL, 53.6 mmol) and 4-*tert*-butylbenzenesulfonyl chloride (9.98 g, 42.9 mmol) was stirred under N₂. To this stirring solution was added slowly tris(2-aminoethyl)amine (2.00 mL, 0.0134 mmol). Yield: 8.11 g, 82.4%. ¹H-NMR (400 MHz, CDCl₃): δ7.83 (d, 6H, Hs at ortho positions in benzene ring), δ7.50 (d, 6H, Hs at methyl positions in benzene ring), δ6.02 (t, 3H, H bonded with N), δ2.94 (q, 6H, CH₂ bonded to central N), δ2.50 (t, 6H, CH₂ bonded to 2° amine), δ1.30 (s, 27H, CH₃ at the ends). ¹³C-NMR (101 MHz, CDCl₃): 156.3, 136.9, 126.9, 126.2, 54.4, 40.9, 35.1, 31.1. FT-IR (cm⁻¹): 3304(s), 3259(m), 2957(m), 2867(w), 2815(w), 1595(w), 1460(w), 1398(m), 1322(s), 1292(m), 1270(w), 1198(w), 1157(vs), 1112(s), 1087(s), 1049(m), 1015(w), 944(m), 924(w), 894(w), 837(m), 812(w), 754(m), 664(m).

C.3.7 UV-Vis studies

UV-Vis titrations were carried out by preparing solutions of ligands (0.01 mM) and 2.5 eq. of DIPEA (0.025 mM) in acetonitrile (Solution A). Solution A was then used to prepare a 0.10 mM solution of Sm(NO₃)₃·6H₂O (Solution B), thus keeping the ligand concentration constant. Solution A (2.70 mL) placed in a 1 cm quartz cuvette cell was titrated with solution B, UV-Vis absorption changes were monitored by gradual addition of 0 - 640.00 μL of Solution B.

C.3.8 ¹H-NMR studies

¹H-NMR studies were performed by comparing the spectra of; (a) ligand, (b) ligand with pyridine, and (c) ligand with DIPEA. In addition, the spectra of the solid obtained from a complexation attempt between ligand **3** in the presence of 3 eq. of DIPEA and La(III) was compared to the spectrum of **3** alone. All ¹H-NMR studies were performed using CDCl₃.

C.3.9 pH-dependent extraction and stripping of Sm(III) using CH₂Cl₂ as diluent and spectrophotometric determination of [Sm(III)]_t

pH dependent extraction studies were performed using ligand **3**. Aqueous phases containing a constant concentration of Sm(III) (2.0 mM) in 5.00 mL of DI water and increasing concentrations of NaOH (1.0×10^{-4} – 1.0 M) were contacted with 5.00 mL of ligand solution (30.0 mM) in CH₂Cl₂. Both phases were brought into contact and rotated on a wheel (70 rpm, 20 h). After 20 h, the samples were centrifuged for 5 min, and the two layers were carefully separated and filtered in preparation for stripping. Stripping was done by adding 4.00 mL of 0.1 M HNO₃ to 4.00 mL of filtered organic phases. The two phases were brought once again into contact by rotating on a wheel (70 rpm; 20 h). The samples were then centrifuged for 5 min and the aqueous phase was analyzed for Sm(III) using the Arsenazo-III method, as previously described in this dissertation.

C.4 Results and discussion

Ligands **1**, **2** and **3** were synthesized as tripodal ligands for complexation and extraction of f-elements. **1** was based on the 1,3,5-triethylbenzene framework while **2** and **3** were based on the tris(2-aminoethyl)amine (tren) framework, with **3**, being more lipophilic by having a *tert*-butyl group instead of a methyl group at the para position of the benzene ring in the pendant arms. Complexation experiments were carried out with **1** and **3**. Studies were performed using UV-Vis spectroscopy, ¹H-NMR spectroscopy, and pH-dependent extractions.

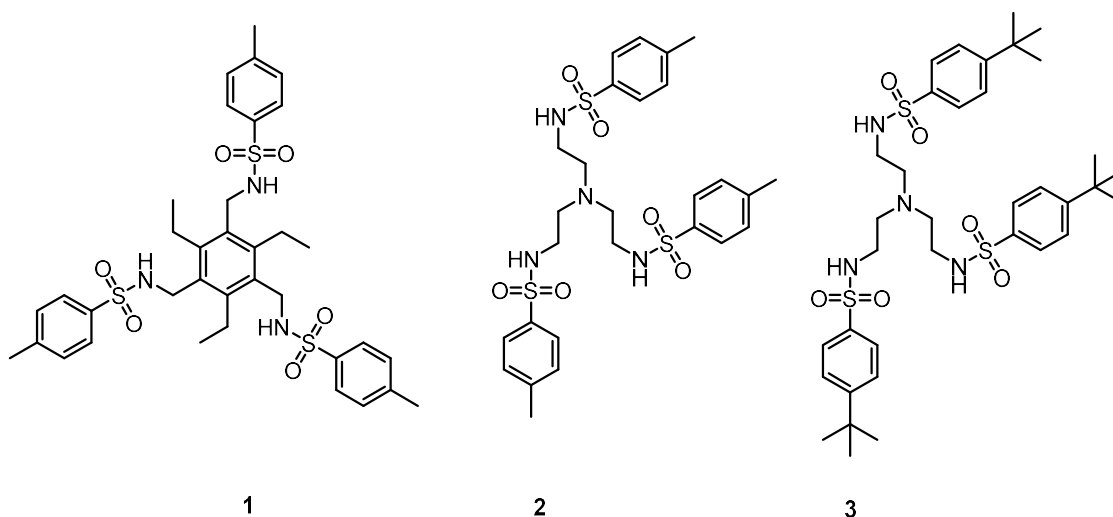


Figure C.1. Structure of synthesized ligands **1**, **2**, **3**

C.4.1 UV-Vis titrations

When Sm(III) was added to solutions of **1**, there were no observed changes in the spectra other than the expected increase in absorbance at 220 nm due solely to the Sm(III) salt. (Figure C.2). There were also no isosbestic points or the formation of any new absorbance bands that would have indicated signs of complexation.

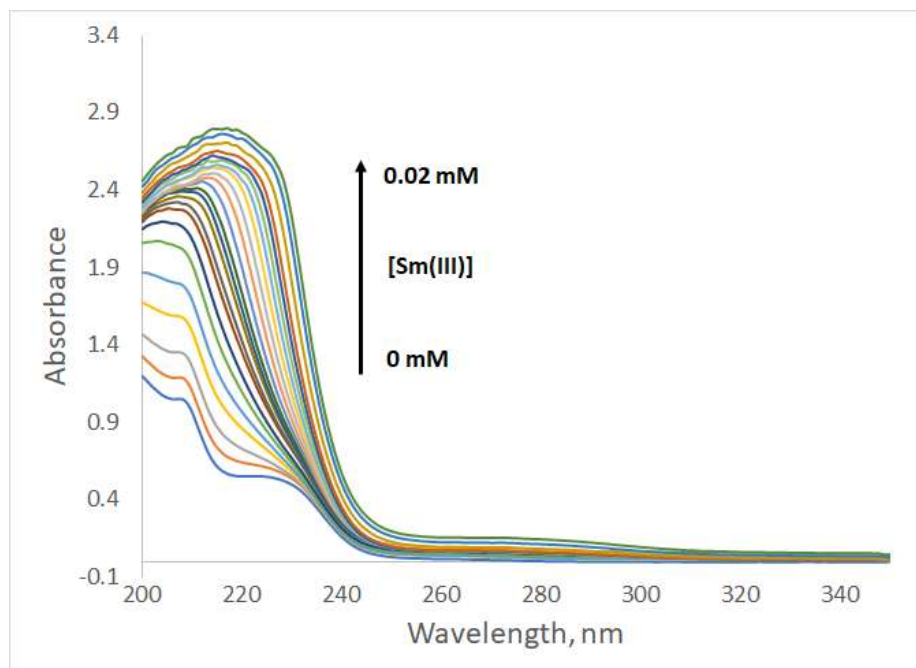


Figure C.2. UV-Vis titration of a solution of **1** (1.0×10^{-5} M) and 2.5 eq. of DIPEA in CH_3CN with Sm(III) (1.0×10^{-4} M)

Similar experiments were conducted separately for ligands **2** and **3**, with similar results, (no complexation) as it can be seen in Figures C.3 and C.4, with the only noticeable change in the spectra of both ligands in presence of DIPEA being due to Sm(III) addition (0 – 0.02 mM). The absence of a new absorbance peak other than the growing intensity of the Sm(III) absorbance, at 220 nm along with the absence of an isosbestic point, was indicative of no complexation occurring between these ligands and Sm(III) under the studied conditions (Figures C.3 and C.4).

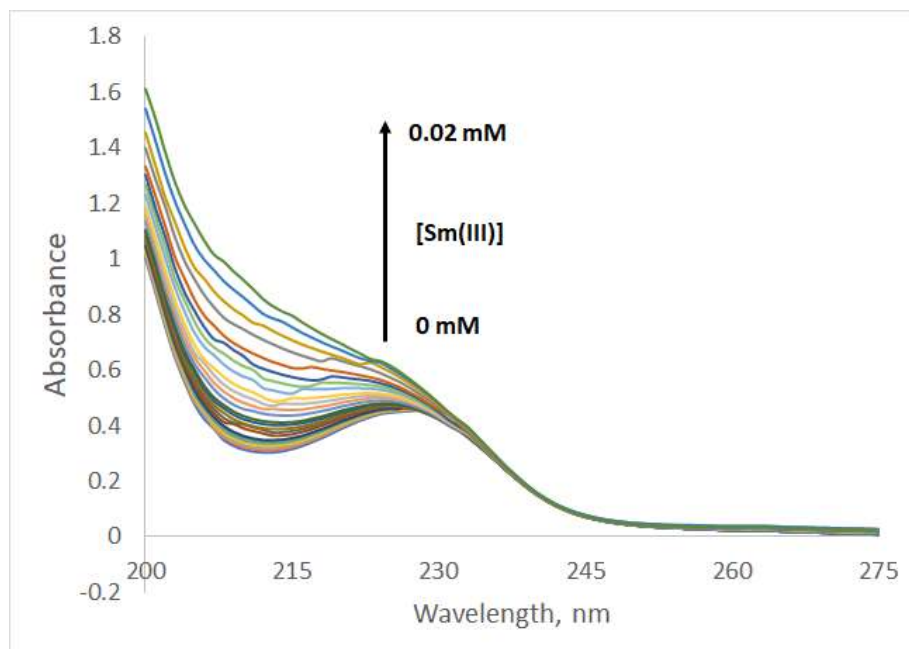


Figure C.3. UV-Vis titration of a solution of **2** ($1.0 \times 10^{-5} M$) and 2.5 eq. of DIPEA in CH_3CN with $Sm(III)$ ($1.0 \times 10^{-4} M$)

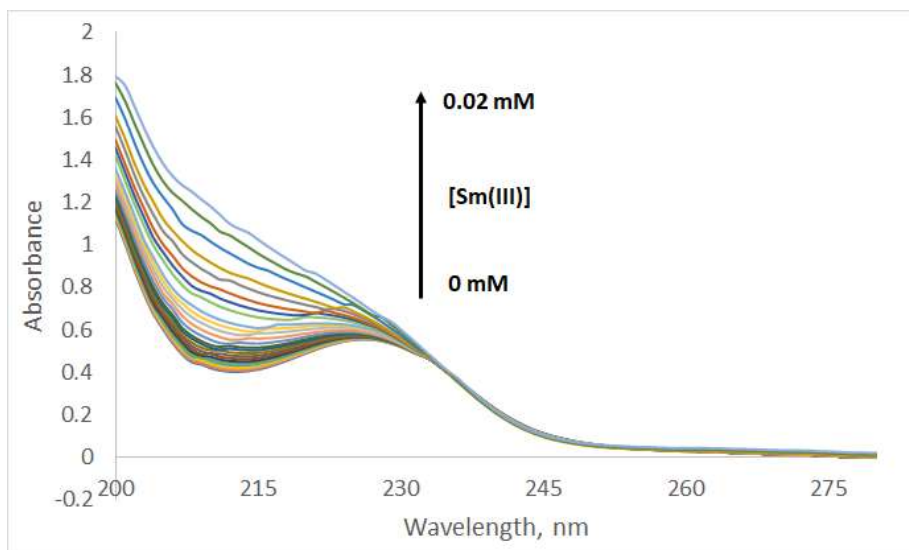


Figure C.4. UV-Vis titration of a solution of **3** ($1.0 \times 10^{-5} M$) and 2.5 eq. of DIPEA in CH_3CN with $Sm(III)$ ($1.0 \times 10^{-4} M$)

C.4.2 ¹H-NMR studies

In the framework of **3**, the sulfonamide proton “d”, as shown in Figure C.5a, is expected to be the most acidic proton. The ligand was therefore expected to be deprotonated in alkaline conditions. Such deprotonation of the ligand would make available electron rich sites for complexation with the acidic lanthanide cation. To investigate this premise, ¹H-NMR studies were conducted. All three spectra were compared to observe any spectral changes. It was observed that there was little to no change in the proton signals of the ligand in presence of both bases (DIPEA and pyridine). New signals found in spectrum b and spectrum c are solely due to the non-interacting organic base, pyridine and DIPEA, respectively. In Spectrum a, the signal at δ 6.02 ppm is a triplet which integrates to 3 protons and is assigned to the 3 protons of the N-H present on each sulfonamide arm. This signal is still present in spectrum b at δ 6.20 ppm (also integrating to 3 protons) even in the presence of pyridine. In spectrum c, although we do not see the N-H proton signal when we use DIPEA as an organic base, we still do not observe any change in the protons close to the sulfonamide nitrogen on the ligand structure. This could also suggest the absence of deprotonation despite the alkaline environment caused by DIPEA. Likewise comparing the ¹H-NMR spectrum of **3** with the attempted complexation reaction of **3** with La(III) did not yield any noticeable spectral difference. All this evidence suggests that the architecture of this ligand did not favor the complexation of La(III) under the current experimental conditions, primarily due to difficulty in deprotonation.

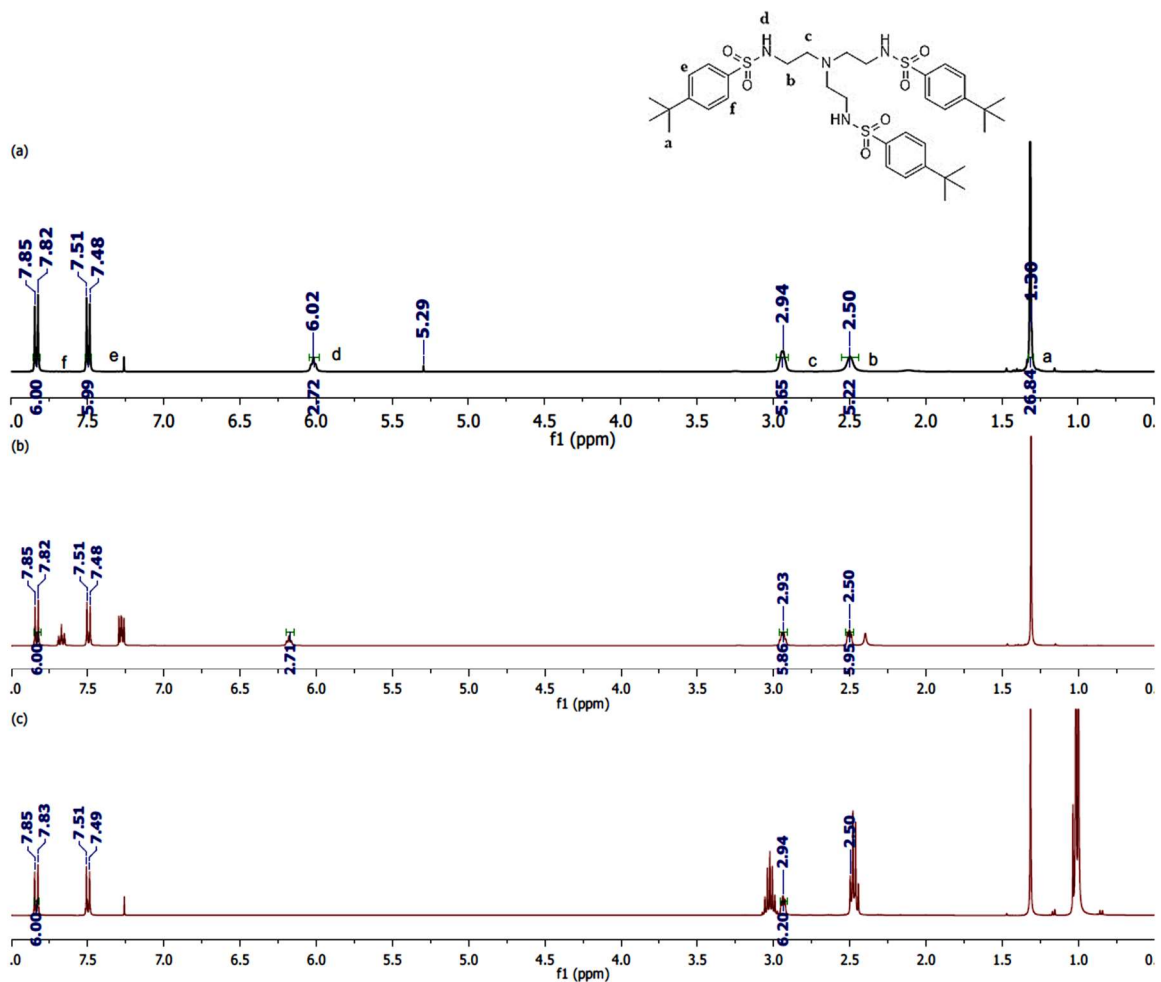


Figure C.5. Comparison of $^1\text{H-NMR}$ spectra in deuterated chloroform of (a) **3**, (b) **3** with 3.2 eq. of py, (c) **3** with 3.2 eq. of DIPEA.

C.4.3 pH-dependent extraction studies

Extraction of Sm(III) using **3** was carried out and after quantification, the acidic aqueous phases obtained after stripping were found to contain no Sm(III) in any of the pH range tested. Furthermore, when the alkaline aqueous phase left after the extraction experiment was analyzed, a significant amount of Sm(III) was found unextracted, especially at lower alkalinity (Figure C.6). Having Sm(III) present in the aqueous phase after extraction suggests that **3** is not a good extractant due to poor deprotonation at such

low alkalinity (pH 10.0 – pH 12.0). Although no Sm(III) is detected in the left over aqueous phase from extraction at higher pH range (12.0-14.0), this could be due to either weak binding of Sm(III) as a result of poor deprotonation even at these higher NaOH concentrations or very low solubility of a presumed Sm(III)-sulfonamide complex that makes stripping very difficult.

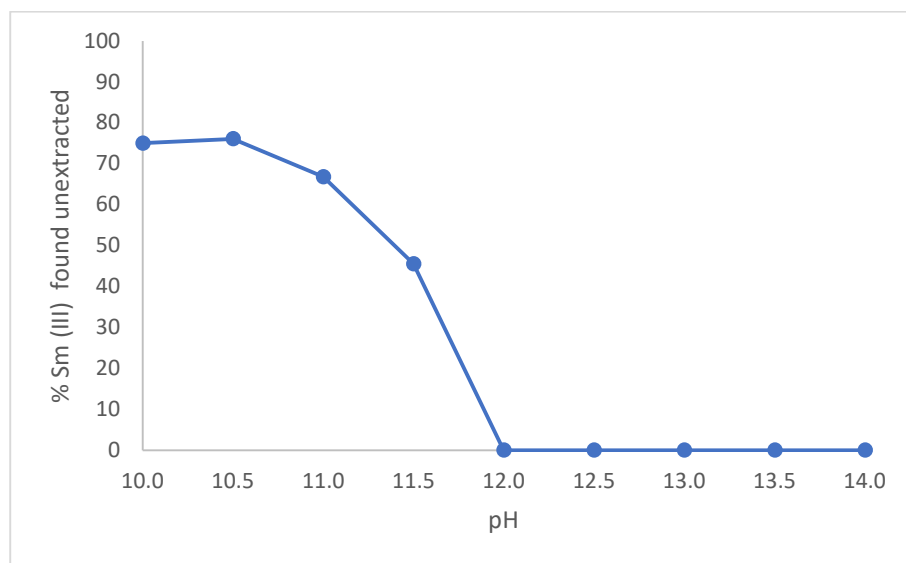


Figure C.6. Percent unextracted Sm(III) in the alkaline aqueous phase when using **3** (30.0 mM) in CH₂Cl₂. [Sm(III)]_t = 2.0 mM

C.5 Conclusion

Three tripodal sulfonamides were successfully synthesized and characterized. UV-Vis titrations with Sm(III), as well as ¹H-NMR studies with addition of La(III), showed that these ligands were unable to complex Ln(III) under the studied conditions due to lack of effective deprotonation - since deprotonation is a prerequisite for

complexation for this ligand architecture. Likewise, for extraction studies, no Sm(III) was recovered after stripping.

While there could be several reasons for this negative results, studies elsewhere¹² have suggested that sulfonamides with the architecture in this study might have a pKa > 12.0, as -NH groups directly attached to aryl groups have shown much higher acidity¹² as opposed to -NH groups that are adjacent to alkyl groups like the current ligands possess, thus deprotonation of the ligands in this study could be difficult under the studied pH range.

C.6 References

1. Wiersma, B. J. The performance of underground radioactive waste storage tanks at the Savannah River Site: A 60-year historical perspective. *Journal of the Minerals, Metals & Materials Society* **2014**, *66*, 471-490.
2. Craig, J.R.; Vaughan, D.J.; Skinner, B.J. *Earth Resources and the Environment*. 4th edition, Pearson: Essex, **2014**, 120-121.
3. Wilmarth, W.R.; Lumetta, G. J.; Johnson, M.E.; Poirier, M.R.; Thompson, M.C.; Suggs, P.C. Machara, N.P. Review: Waste pretreatment technologies for remediation of legacy defense nuclear wastes. *Solvent Extraction & Ion Exchange* **2011**, *29*, 1 - 48.
4. Zhao, P.; Romanovski, V.; Whisenhunt, D.W.; Hoffman, T.R.M.; Xu, J.; Raymond, K.N. Extraction of plutonium by chelating hydroxypyridone and catecholamide resins. *Solvent Extraction & Ion Exchange* **1999**, *17*, 1328-1329.
5. Kuzovkina, I.V.; Lavrinovich, E.A.; Novikov, A.P.; Stepanova, E.S.; Karavan, M.D.; Smirnov, I.V. *Journal of Radioanalytical and Nuclear Chemistry* **2017**, *311*, 1983.
6. Smirnov, I.V.; Stepanova, E.S. Extraction of americium with substituted Calix[4]arenes from alkaline solutions. *Procedia Chemistry* **2016**, *21*, 203.

7. Morozov, A. N.; Govor, E. V.; Anagnostopoulos, V. A.; Kavallieratos, K.; Mebel, A. M. 1, 3, 5-Tris-(4-(iso-propyl)-phenylsulfamoylmethyl) benzene as a potential Am(III) extractant: experimental and theoretical study of Sm(III) complexation and extraction and theoretical correlation with Am(III). *Molecular Physics* **2018**, *116*, 2719-2727.
8. Bart, S.C.; Heinemann, F.W.; Anthon, C.; Hauser, C.; Meyer, K. A new tripodal ligand system with steric and electronic modularity for uranium coordination chemistry. *Inorganic Chemistry* **2009**, *48*, 9419.
9. Fedosseev, A.M.; Grigoriev, M.S.; Budantseva, N.A.; Guillaumont, D.; Le Naour, C.; Simoni, E.; Den Auwer, C.; Moisy, P. Americium (III) coordination chemistry: An unexplored diversity of structure and bonding. *Compendus Rendus Chimie* **2010**, *13*, 839.
10. Kilway, K. V. and Siegel, J. S. Control of functional group proximity and direction by conformational networks: Synthesis and stereodynamics of persubstituted arenes *Tetrahedron* **2001**, *57*, 3615-3627.
11. Zhou, J.R.; Liu, D.P.; He, X.J.; Kong, Z.M.; Zhang, Y.P.; Ren, L.S.; Long, R.B.; Huang, L.S.; Zheng, L.S. A highly selective colorimetric chemosensor for cobalt (II) ions based on a tripodal amide ligand. *Dalton Transactions* **2014**, *43*, 11579-11586.
12. Dauphin, G., and Kergomard, A. Étude de la dissociation acide de quelques sulfonamides. *Bulletin de la société chimique de France* **1961**, *3*, 486 – 492.

VITA

OLUWASEUN W. ADEDOYIN

Born, Ilorin, Kwara State, Nigeria

2003 - 2007	Bachelor of Science (BSc.) – Industrial Chemistry Nnamdi Azikiwe University Awka, Nigeria.
2017 - 2020	Master of Science (MSc.) – Chemistry Florida International University, Miami, Florida.
2017 - current	Doctoral Candidate – Chemistry Radiochemistry Track Florida International University, Miami, Florida.

PUBLICATIONS AND PRESENTATIONS:

- Highly-Lipophilic Sulfonamide Chelators and Analogs for Actinide Separation from Caustic High-Level Waste. Rene Panzer, Oluwaseun W. Adedoyin, Xinrui Zhang, Evgen V. Govor, Alexander N. Morozov, Alexander M. Mebel, and Konstantinos Kavallieratos. WM2022 Conference, Proceedings. (Accepted for publication)
- Sulfonamide Ligand Frameworks for Sm(III) Extraction From Alkaline High Level Waste. Xinrui Zhang, Oluwaseun W. Adedoyin, Maria L. Masferrer Bertoli, Evgen V. Govor and Konstantinos Kavallieratos. *RAD Conference 2020 Proceedings*, **2020**, 4, 173-178.
- Extraction of Ln(III) and An(III) from Alkaline Solutions by Sulfonamide Ligands and Analogs. Konstantinos Kavallieratos, Evgen V. Govor, Alexander N. Morozov, Oluwaseun W. Adedoyin, April A. Rains, Raphael G. Raptis, Alexander M. Mebel. Waste Management Symposium 2020, Phoenix Arizona, USA. Proceedings of the WM2020 Conference, Phoenix, Arizona USA, March 8 – 12, 2020. P20216 (6 pages).

- Sulfonamide Ligands for Extraction of Ln(III) and An(III) from Alkaline Aqueous Media. Evgen V. Govor, Oluwaseun W. Adedoyin, Alexander N. Morozov, April A. Rains, B. Nabi Ajoff, Alexander M. Mebel, Konstantinos Kavallieratos. Proceedings of Global-Topfuel 2019 International Fuel Cycle Conference, Seattle Washington, USA, September 22-27, **2019**. P 118-119.
- Radio-Assay of Plant Samples at the Proposed Nuclear Reactor Site in Geregu, North – Central Nigeria. Ngbede Awodi, Abiodun Ayodeji, Oluwaseun Adedoyin. Journal of Nuclear Engineering and Technology. **2015**; 5, 6-13.
- Measurement Of Shielding Effectiveness of Building Blocks Against 662 Kev Photons. Oluwaseun Adedoyin, and Abiodun Ayodeji. *Journal of Physical Science*. **2016**, 27, 55.
- Porous and non-porous electrospun fibres from discarded expanded polystyrene. Oluwagbemiga Alayande, Oluwaseun Adedoyin, Samuel Olatubosun, Olayinka Sanda, Oluwagbenga Dare, Gabriel Osinkolu, John Ajao, Olalekan Deborah, Adeniyi Fasasi and David Pelemo. (International Journal of Physical Science) Vol. 7(11). pp 1832-1836, 9 March 2012. DOI:10.5897/IJPS11.1783.